2022

Progress Towards Next Generation Modulators of CtBP's Oncogenic Effects

Jacqueline L. West
Virginia Commonwealth University

PROGRESS TOWARDS NEXT GENERATION MODULATORS OF CTBP'S ONCOGENIC EFFECTS

A dissertation submitted in partial fulfillment of the requirements for the degree of Doctor of Philosophy at Virginia Commonwealth University

by

Jacqueline Louise West

Bachelor of Science, University of North Carolina Wilmington, May 2015

Master of Science, University of North Carolina Wilmington, July 2018

Director: Keith C. Ellis

Associate Professor, Department of Medicinal Chemistry

Acknowledgements

First, I'd like to thank my husband Sam for his unwavering support in me in all of my academic endeavors. Without you cheering me on, I would not have made it through graduate school, or even had the courage to apply. I would also like to thank my family for being so understanding with me throughout my graduate school journey, and for encouraging me along the way.

I would like to thank my advisor and mentor, Dr. Keith C. Ellis for all the assistance and knowledge he has given me over the last 5 years. I am so grateful that you allowed me to volunteer in your laboratory prior to joining the PhD program, as I truly believe that the skills that I learned during that year really prepared me for the graduate program, and helped me immensely when it came to starting my research at VCU.

Next, I would like to thank my committee members: Dr. Aaron May, Dr. Jiong Li, Dr. John Hackett, and Dr. Douglas Sweet for all of their support and attending all of my committee meetings. I especially want to thank you all for sitting through some very long presentations, and giving me guidance along the way. A special thank you to our collaborators Dr. Steven Grossman, Dr. Martin M. Dcona, and Dr. Boxiao Ding at University of Southern California for their assistance with biological assays.

I would like to thank all of my friends at VCU. Thank you to Nicole Luzi for teaching me all of the basics, and for helping me with even the smallest tasks. Thank you to Dr. John Saathoff and Dr. Yam Timsina for all of the conversation and guidance. And a special thank you to Mohammad Al Mughram for all of the assistance with the ITC.

Finally, I'd like to thank my friend Alexandra Carroll. Without you, I would never have made it this far. Thank you for seeing in me all that I couldn't see in myself.

Table of Contents

List of Tables

List of Figures

List of Schemes

Abstract

PROGRESS TOWARDS NEXT GENERATION MODULATORS OF CTBP'S ONCOGENIC EFFECTS

By Jacqueline L. West, M.S.

A dissertation submitted in partial fulfillment of the requirements for the degree of Doctor of Philosophy at Virginia Commonwealth University

Virginia Commonwealth University, 2022

Major Director: Keith C. Ellis

Associate Professor, Department of Medicinal Chemistry

Human C-terminal binding proteins (CtBP1 and CtBP2) are transcriptional coregulators of multiple genes in the human genome, including tumor suppressor genes (e.g., Bik, PTEN, BRCA1, and E-cadherin) as well as oncogenes (e.g. MDR1 and Tiam1). Both homologues of CtBP are overexpressed in many types of cancer, including breast cancer (92%), ovarian cancer (83%), colorectal cancer (64%), hepatocellular carcinoma (60%), gastric cancer, prostate cancer, and pancreatic adenocarcinoma. Further, expression levels of CtBP correlate with worse prognostic outcomes and more aggressive tumor features because it promotes proliferation, epithelial-mesenchymal transition, and cancer stem cell self-renewal activity.

Our laboratory has identified a lead inhibitor of CtBP, 2-hydroxyimino-3-phenyl propanoic acid (HIPP), with a binding affinity of 370 nM for CtBP1. Data from the co-crystal structure of CtBP1 complexed with HIPP and NADH (PDBID: 4U6Q) revealed essential interactions between HIPP and residues Arg97, Arg266, His315, and Trp318. Importantly, the aromatic ring of HIPP forms a π-stacking interaction with Trp318. HIPP has been shown to displace CtBP from transcriptional promoter regions, restore expression of tumor suppressing genes, and induce apoptosis. However, high doses of HIPP are required to induce these anti-oncogenic effects in cell and animal models.

The first part of this work describes the rational design and computational evaluation of new, heteroaromatic HIPP analogues. A small library of compounds (36 total) was constructed *in silico* and docked into the co-crystal structure of HIPP-CtBP. The best scoring compounds were synthesized and the binding affinity of these compounds was measured utilizing isothermal titration calorimetry (ITC). We identified 2 analogues that bind to CtBP with higher affinity than HIPP. We found that replacement of the carboxylic acid on 4-Cl HIPP with an ethyl ester increases its potency in A2780 cells 50-fold, and the same substitution increases the potency of HIPP in HCT116 cells 15-fold. We also discovered 5 analogues that were more potent than the HIPP ester in cells.

The second part of this work describes the design and development of HIPP-based CtBP PROteolysis TArgeting Chimeras (PROTACs) for *in vivo* degradation of CtBP using the endogenous Ubiquitin/Proteasome System. The PROTACs were synthesized in a 9-step synthetic route, and the degradation of CtBP was quantified by western blot. We found that CtBP1/2 can be successfully and effectively degraded in cells with HIPP-based PROTACs.

List of Abbreviations

◦ C	Degrees Celcius
Ala (A)	Alanine
ALK	anaplastic lymphoma kinase
Alloc	allyloxycarbonyl
APC/C	anaphase-promoting complex/cyclosome
AR	Androgen Receptor
Arg (R)	Arginine
Asn (N)	Asparagine
Asp (D)	Aspartic Acid
ATRA	all-trans retinoic acid
B3LYP/SVP	Becke, 3-parameter, Lee-Yang-Parr/Split-Valence Polarized
BARS	Brefeldin A-ADP Ribosylated Substrate
BCL-2	B-cell lymphoma 2
BCL-X_L	B-cell lymphoma-extra large
BCR-ABL	breakpoint cluster region-Abelson
BH3	Bcl-2 homology domain 3
Bik	BCL-2 interacting killer
Boc	tert-butyloxycarbonyl
BRCA1	BReast Cancer gene 1
BRD	bromodomain containing protein
BRK	baby rat kidney
BTK	Bruton tyrosine kinase

Cbz	carboxybenzyl
CCC	cadherin-catenin-cytoskeleton
CD	catalytic domain
CDH1	E-cadherin
CDK9	cyclin-dependent kinase 9
CHARMM	Chemistry at Harvard Macromolecular Mechanics
cIAP1	cellular inhibitor of apoptosis protein 1
Cl	chlorine
c-Met	mesenchymal-epithelial transition factor
CoREST	REST corepressor 1
CPP	cell-permeating peptide
CRABP	cellular retinoic acid binding protein
CRBN	cereblon
CRL	cullin-RING E3 ligase
CtBP	C-terminal Binding Protein
Cys (C)	Cysteine
DBU	1,8-Diazabicyclo[5.4.0]undec-7-ene
dCtBP	Drosophilia CtBP
DDB1	damaged DNA binding protein 1
DFT	Density Functional Theory
DHT	dihydroxytestosterone
DIABLE	direct IAP-binding protein with low isoelectric point
DIBAL	diisobutylaluminum hydride

DMBA	1,3-dimethylbarbituric acid
DMSO	dimethyl sulfoxide
DSB	double-strand DNA break
DTT	dithiothreitol
E2	estradiol
E2F7	E2F Transcription Factor 7
EC50	Effective concentration to kill 50% of cells
EDCI	1-Ethyl-3-(3-dimethylaminopropyl)carbodiimide
EGFP	enhance green fluorescent protein
EGFR	epidermal growth factor receptor
Elk4	ETS domain-containing protein
EMT	Epithelial Mesenchymal Transition
eq	equivalents
ER	estrogen receptor
ERRα	estrogen-related receptor alpha
EtOAc	ethyl acetate
Ey	Eyeless
FKBP12	FK506-binding protein 12
FLT3	fms-like tyrosine kinase 3
Fmoc-7-AHP-OH	Fmoc-amino heptanoic acid
GDP	guanine diphosphate
GFP	green fluorescent protein

Gln (Q)	Glutamine
Glu (E)	Glutamic Acid
Gly (G)	Glycine
GNEF	Guanine Nucleotide Exchange Factor
GTP	guanine triphosphate
GTPase	guanine triphosphatase
HATU	Hexafluorophosphate Azabenzotriazole Tetramethyl Uronium
HBV	hepatitis B virus
hCtBP	human CtBP
HDAC	histone deacetylase
HECT	homologous to E6-AP carboxy terminus
HER2	human epidermal growth factor receptor 2
HGSOC	high grade serous ovarian cancer
HIA	hydroxyimino acid
HINT	Hydropatic INTeractions
HIPP	2-hydroxyimino-3-phenylpropanoic acid
His (H)	Histidine
HMT	histone methyltransferase
HOBt	Hydroxybenzotriazole
HPC2	Histone promoter control protein 2
HRMS	High resolution mass spectrometry
HWE	Horner Wadsworth Emmons
IAP	Inhibitors of Apoptosis Protein

Ile (I)	Isoleucine
IRAK4	Interleukin 1 Receptor Associated Kinase 4
ITC	isothermal tritration calorimetry
Kd	Binding constant
kDa	kiloDaltons
KLF8	Kruppel-like factor 8
LAH	lithium aluminum hydride
LDA	lithium diisopropylamide
LDH	lactate dehydrogenase
Leu (L)	Leucine
LiHMDS	lithium bis(trimethylsilyl)amide
LSD1	lysine-specific demethylase 1
Lys (K)	Lysine
MCL-1	induced myeloid leukemia cell differentiation protein 1
mCtBP	mouse CtBP
MDM2	murine double minute gene 2
MeBS	methyl bestatin
Met (M)	Methionine
MetAP2	methionine aminopeptidase-2
MTD	maximum tolerable dose
MTOB	4-Methylthio-2-oxobutyric acid
MTT	3-(4,5-dimethylthiazol-2-yl)-2,5-diphenyltetrazolium bromide
NAD+	nicotinamide adenine dinucleotide

NBD	nucleotide binding domain
NLS	nuclear localization signal
NMC	NUT midline carcinoma
nNOS	neuronal nitric acid synthase
NUT	NUclear protein in Testes
Pak1	p21-activated kinase
Pc2	Polycomb 2
PEG	polyethylene glycol
P-gp	P-glycoprotein
Phe (F)	Phenylalanine
PI3K	phosphoinositide-3-kinase
PIAS1	Protein inhibitor of Activated STAT 1
PIP3	phosphatidylinositol (3,4,5)-triphosphate
POI	protein of interest
Pom-Gly-OH	pomalidomide-glycine
PPI	protein protein interaction
PR	Progesterone Receptor
Pro (P)	Proline
PROTAC	PROteolysis TArgeting Chimera
PTEN	phosphatase and tensin homolog
PVDF	polyvinyl difluoride
PyBOP	benzotriazol-1-yloxytripyrrolidinophosphonium hexafluorophosphate

RAR	retinoic acid receptor
RBR	RING-Between-RING-RING
RING	really interesting new gene
RIPK2	Receptor Interacting Serine/Threonine Kinase 2
RTK	receptor tyrosine kinase
SAR	structure activity relationships
SARM	selective androgen receptor modulator
SCF	Skp1-Cul1-F-box
SDS-PAGE	Sodium dodecyl-sulfate polyacrylamide gel electrophoresis
Ser (S)	Serine
Sirt2	sirtuin 2
SMAC	second mitochondrial activator of caspases
SMILES	Simplified Molecular Input Line Entry System
SNIPER	Specific and Nongenetic IAPs-dependent Protein ERaser
SRS	Substrate recognition subunit
STAT3	Signal Transducer and Activator of Transcription 3
SUMO	small ubiquitin-like modifier
TBK1	TANK Binding Kinase 1
TEA	triethyl amine
TGIF	TG-interacting factor
Thr (T)	Threonine
TRIM24	Tripartite Motif Containing 24
TRK	tropomyosin receptor kinase

Trp (W)	Tryptophan
TSG	tumor suppressor gene
Tyr (Y)	Tyrosine
Ub	Ubiquitin
UPS	Ubiquitin/proteasome system
Val (V)	Valine
VanH	vancomycin resistance protein
VHL	von Hippel-Lindau
ZEB1/2	Zing finger E-box-binding homeobox 1/2

Chapter 1: Introduction

1.1: C-terminal Binding Protein

1.1.1: Discovery

CtBP was first discovered in 1993 when it was found to bind to the C-terminal region of E1A human adenovirus oncoprotein.[1] Specifically, CtBP was found to associate with a 14-amino acid region (amino acids 225-238) of E1A that is critical for negative modulation of tumorigenesis and metastasis; deletion of these residues increases the tumorigenic and metastatic potential in primary baby rat kidney (BRK) cells.[1] This deletion mutant also fails to bind to CtBP. In further studies where CtBP was molecularly cloned, it was discovered that CtBP actually binds to a 9-amino acid region (amino acids 229-238), which contains a PLDLS motif that is well-conserved in adenovirus serotypes.[2]

Researchers were able to show that CtBP is a phosphoprotein with phosphorylation levels varying in different stages of the cell cycle. This caused researchers to believe that CtBP plays a regulatory role in cell proliferation.[1,2]

1.1.2: Isoforms and Localization

In the human genome, there are two CtBP genes, known as *CTBP1* and *CTBP2*.[3] Each gene produces a CtBP isoform (CtBP1 or CtBP2) that has a molecular weight of 48-kDa. The two *ctbp* genes share 76% sequence identity at the nucleotide level and the two CtBP protein isoforms share 72% sequence identity at the amino acid level.[3] CtBP1 is a 441-amino acid protein and CtBP2 is a 445-amino acid protein.[2,3] CtBP1 has been mapped onto chromosome 4p16, while CtBP2 has been mapped onto chromosome 21q21.3.[3]

Both vertebrate genes, CtBP1 and CtBP2, code for multiple splice variants of CtBP. CtBP isoforms are localized based on post-translational modifications as well as the presence/absence of a nuclear localization signal (NLS).[4] However, localization data is not consistent throughout the literature. CtBP1 codes for two splice variants – CtBP1-L (long) and CtBP1-S (short), in which exon 1 is spliced out so that the first 15 amino acids of the N-terminus are not encoded.[5] CtBP1 splice variants do not possess the NLS sequence, KRQR, which corresponds to the residues 10-13 of hCtBP2, but both CtBP1-L and CtBP1-S have been observed in the nucleus and the cytoplasm as heterodimers with CtBP2.[4] There is some evidence that phosphorylation of CtBP1 at Ser158 by p21-activated kinase (Pak1) facilitates localization to the cytoplasm.[6] CtBP1 has also been shown to associate with the enzyme neuronal nitric acid synthase (nNOS) which allows it to translocate from the nucleus to the cytoplasm.[7] CtBP1-S is also known as CtBP1/BARS (Brefeldin A-ADP Ribosylated Substrate), and is localized predominantly in the cytoplasm where it aids in regulation of lipid storage and golgi membrane fission.[8]

CtBP2 codes for three splice variants – CtBP2-L, CtBP2-S, and RIBEYE.[5,9] Like CtBP1-S, CtBP2-S differs from CtBP2-L in that it does not possess the first 25 amino acids of the N-terminal domain.[4] CtBP2-S does not contain the NLS sequence, and is therefore localized to the cytoplasm.[4] The RIBEYE protein (120 kDa) is expressed in the retina by an alternative promoter, and has an extended N-terminus fused to CtBP2.[5,9] RIBEYE is a structural component of synaptic ribbons and aids in transmission of sensory signals.[10,11] RIBEYE is also localized in the cytoplasm.[4]

1.1.3: Structure

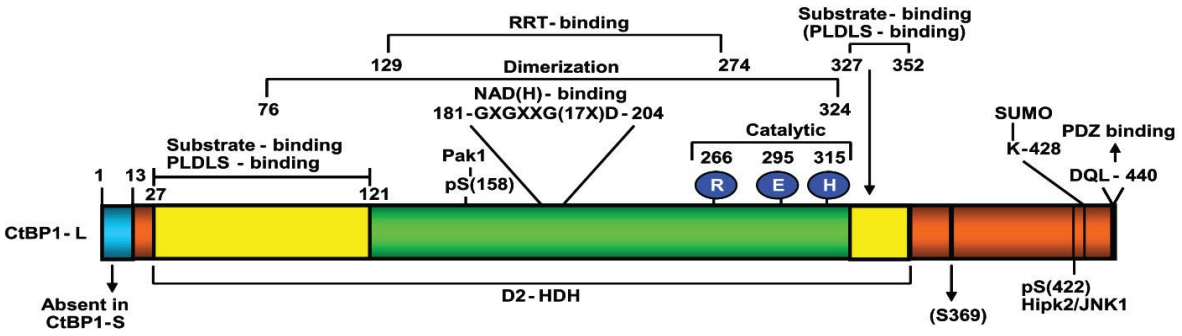

Figure 1.1: The Structure of CtBP1. *Adapted from reference 35.*

CtBPs are highly conserved proteins in both invertebrates and vertebrates.[12] CtBP has three functional domains: an N-terminal domain, a dehydrogenase domain, and a C-terminal domain.[5] A detailed structure of CtBP1 is depicted in **Figure 1.1**. The N-terminal domain is responsible for its recognition of the consensus PxDLS domain of E1A and other proteins including transcription factors and corepressor partners like histone deacetylases (HDACs) and histone methyltransferases (HMTs).[5]

The dehydrogenase domain is responsible for CtBP's enzymatic activity and oligomerization. It can be further divided into an NADH or nucleotide-binding domain (NBD), a catalytic domain (CD), and an RRT motif. The NBD contains the classic "Rossman Fold" topology that is seen in other D-isomer-specific 2-hydroxy acid dehydrogenases (D2-HDHs). This aids in nucleotide binding and contains a catalytic triad (CtBP1/2: His315/321-Glu295/301-Arg266/272) that is responsible for substrate binding.[5,13] CtBP undergoes a conformational change in the presence of NADH, in which the NBD is in close proximity to the bound substrate. This conformational change is a critical step in the formation of oligomers. Further, mutations in the NBD lead to diminished ability of the protein to oligomerize.[13]

The C-terminal domain (90 residues) is largely unstructured due to its proline/glycine-rich sequence.[5] It contains the site for phosphorylation by Homeodomain Interacting Protein Kinase 2 (HIPK2). HIPK2 phosphorylates CtBP1 at Ser422 and CtBP2 at Ser428. This domain also contains a SUMOylation motif, identified as ^{427}VKPE^{430} in CtBP1. CtBP1 is SUMOylated by the E3 ligases PIAS1 and PIASxβ.[5] Mutation of Lys428 to Arg blocks SUMOylation, and results in relocalization of CtBP1 from the nucleus to the cytoplasm.[7] The C-terminus also forms a negative regulatory interaction with the p14/p19 Alternative Reading Frame (ARF) tumor suppressor, which leads to proteasome-dependent degradation.[14] At the distal C-terminus, CtBP1 has a PDZ-binding site (^{438}DQL^{440}) where the protein binds to nNOS to be retained in the cytoplasm; this site is not present in CtBP2.[15]

1.1.4: Dehydrogenase Activity

CtBP shares significant homology (67%) with the vancomycin resistance protein VanH, which is a D2-HDH that is dependent on nicotinamide adenine dinucleotide (NAD^+) for its dehydrogenase activity.[2] In fact, most of the structure of CtBP1 can be aligned with this subfamily of dehydrogenases, except a 90-amino acid sequence at the C-terminus.[13] Despite this, it was originally thought that CtBP did not possess dehydrogenase activity.[1,2] In 2002, however, it was discovered that CtBPs are in fact D2-HDHs that bind to NAD^+.[13] In an assay that couples the reduction of pyruvate to lactic acid with the oxidation of NADH to NAD^+, CtBP is able to catalyze this reaction in a dose-dependent manner.[13]

1.1.5: Oligomerization

CtBP1/2 are able to form hetero- and homodimers through the dehydrogenase domain, similar to other D2-HDH family members. This has been observed in the bacterial D2-HDHs D-Lactate Dehydrogenase,[16,17] Hydroxyisocaproate Dehydrogenase,[18] Formate Dehydrogenase,[19] and D-Glycerate Dehydrogenase,[20] as well as the Human D2-HDHs Glyoxylate Reductase/Hydroxypyruvate Reductase and D-3 Phosphoglycerate Dehydrogenase.[21]

The activity of CtBP is dependent on the metabolic status of the cell (i.e. the NADH/NAD^+ ratio); CtBP1 binds to NADH with 9-fold higher affinity than NAD^+ while CtBP2 binds to NADH with 2-fold higher affinity than NAD^+.[22] Recruitment of NADH induces tetramerization and nuclear localization of CtBP, which is essential for CtBP's transcriptional repressor activity.[22,23] It was long believed that CtBP acts as a redox sensor: when NADH levels increase due to hypoxia or high extracellular glucose levels, the activity of CtBP also increases.[24,25] However, recent data suggests that under normal cellular conditions, CtBP would be fully saturated by NAD^+ and unable to monitor the changes in NADH concentration.[22]

Each monomer of CtBP contains a single PxDLS-binding motif, which interacts with a number of repressor proteins and chromatin-modifying enzymes. When CtBP exists as a monomer there is only one PxDLS-binding motif; this results in competition between the different proteins that associate with CtBP and disruption of CtBP's activity as a transcriptional corepressor.[26] NADH-mediated tetramerization enhances the activity of CtBP because this increases the number of PxDLS-binding sites, which allows more

than one co-repressing partner to bind. Further, mutants of CtBP2 that are unable to dimerize cannot interact with most cellular factors, including the E1A oncoprotein.[26]

CtBP tetramerizes in an NADH-dependent manner, proceeding through a dimeric intermediate.[23] CtBP differs from other D2-HDHs in that it contains a tryptophan residue within the active site, Trp318/324 in CtBP1/2 respectively, which is able to further interact with the bound substrate.[5,27] This Trp residue is critical for tetramer formation, as it forms a hydrogen bond with bound NAD^+ and directs contact with the αC helix of the opposite monomer in the dimeric pair (**Figure 1.2**).[23]

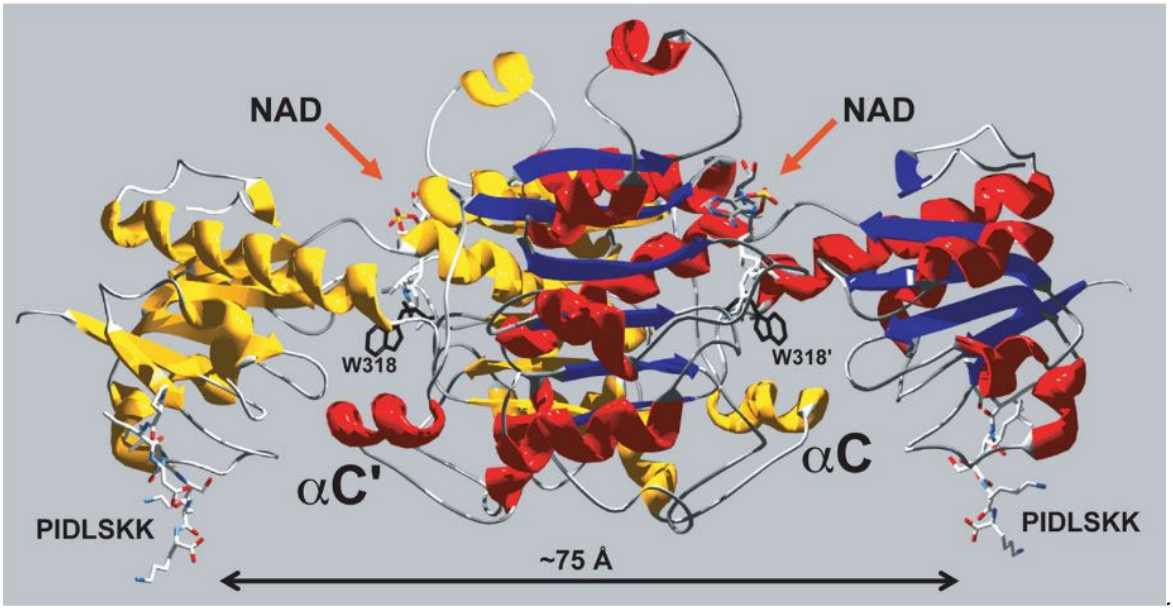

Figure 1.2: A model of CtBP1 dimer with a bound NAD^+ and PIDLSKK peptide *Adapted from reference 23.*

In an analytical ultracentrifuge experiment, it was shown via gel filtration that in the absence of NAD^+ or NADH, CtBP1 elutes primarily as a monomer (48 kDa). In the presence of NAD^+ or NADH, the elution pattern shifts so that CtBP1 elutes primarily as a tetramer (192 kDa) with some dimeric species (96 kDa).[23] When Trp318 is mutated to a Phenylalanine (Phe), gel filtration analysis shows that CtBP1 fails to tetramerize and only

minimally dimerizes, even in the presence of NAD^+.[23] This provides evidence that Trp318 acts as a dimerization/tetramerization switch in CtBP1.

1.1.6: Transcriptional Repression Activity and Mechanism

The E1A human adenovirus protein is a known tumor suppressor in human cells, and functions by transcriptionally inducing epithelial cell adhesion genes and repressing other genes.[28] In the E1A protein, transcriptional repression was found to correlate with presence of the CtBP binding site.[29] Further, removal of the CtBP binding site in E1A is sufficient to attenuate the transcriptional repression, and it is thought that this repression is mediated by binding of CtBP.[29] It was also found that the E1A-CtBP interaction is necessary for induction of epithelial gene expression.[28]

CtBP family proteins are not able to bind directly to DNA, and must be recruited to active transcription sites by DNA-binding transcription repressors such as ZEB1/2,[30] human Krüppel-like factors,[31] Elk4,[32] and E2F7.[33] CtBPs then regulate transcription by associating with chromatin remodeling proteins, such as HDACs and HMTs, as well as DNA-bound transcription factors to block transcriptional activity at the sequence-specific gene promotors recognized by the DNA-bound transcriptional repressors.[32,34] This forms a corepressor complex, shown in **Figure 1.3**, which can catalyze three different types of histone modifications: histone deacetylation (HDAC1/2), histone methylation (G9a and GLP), and histone lysine-specific demethylation (LSD1).[35]

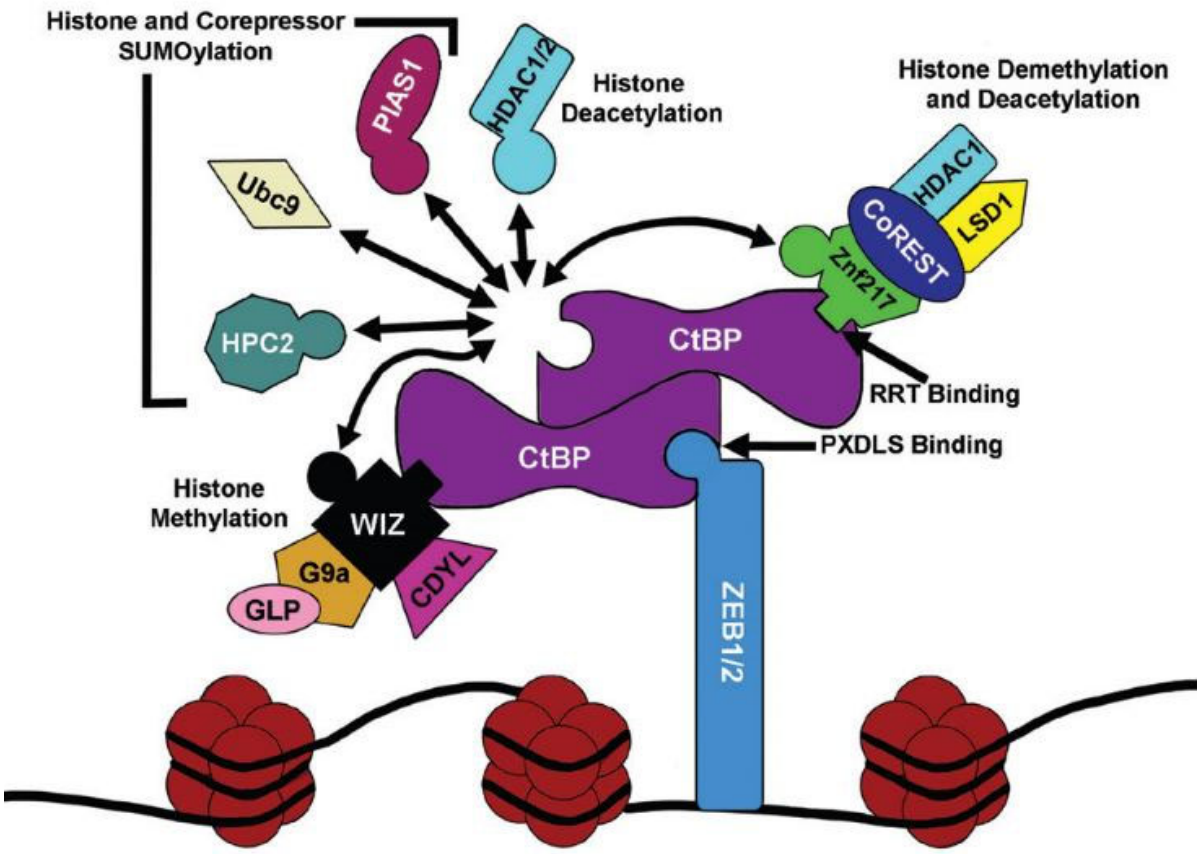

Figure 1.3: CtBP's corepressor complex. *Adapted from reference 32.*

CtBPs are also able to interact with three SUMO E3 ligases, HPC2, PIAS1, and Pc2, which enhance gene repression.[35,36] CtBPs bind to members of the corepressor complex at both the PxDLS domain binding site in the N-terminus, and the RRT binding cleft in the dehydrogenase domain.[35,37] CtBPs have been reported for recruitment at more than 30 different transcription factors.[12] CtBP's activity as a transcriptional corepressor plays an important role in development and oncogenesis.

1.1.7: CtBP as a Transcriptional Corepressor in Development

Transcriptional repression is an important part of gene expression and regulation.[12] Proper gene expression in embryogenesis relies on the coordination of both

transcriptional activators and repressors because certain genes are required at different stages of embryo development. For example dCtBP acts as a transcriptional corepressor during embryo development of *Drosophila*.[38–40] Hairy is a transcriptional repressor necessary for proper embryonic segmentation. CtBP interacts with a PLSLV domain on the C-terminus of Hairy; deletion of these five amino acids eradicates the interaction between Hairy and dCtBP. Further, embryos lacking maternal dCtBP fail to segment properly.[38] Knirps, a nuclear receptor protein involved in segmentation of the abdomen, also relies on its association with dCtBP in *Drosophila* embryogenesis.[39] It has also been shown that dCtBP interacts with the Eyeless (Ey) gene in *Drosophilia* to prevent overproliferation of eye precursors.[40] Zygotic mutations of dCtBP are lethal mutations to the developing embryo.[41,42]

Analysis of mice harboring mutations in the genes *CTBP1* and/or *CTBP2* showed that the two protein isoforms play unique and redundant roles in mouse embryogenesis.[43] Mice that are mCtBP1$^{-/-}$ are small in size compared to wildtype (wt) mice, and have a reduced survival rate. mCtBP2$^{-/-}$ knockout mice fail to develop due to delayed neural tube development, axial truncations, and defects in heart morphogenesis. Mice that were null for both CtBP1 and CtBP2 exacerbated both phenotypes, with the embryos experiencing minimal heart morphogenesis and earlier embryonic death.[43]

In humans, hCtBP1/2 are expressed in most tissues.[12,44] In development, it interacts with the transcriptional repressor TGIF (TG-interacting factor) via a PLDLS motif. A mutation in TGIF that results in a single amino acid substitution within the PLDLS motif abolishes the interaction between the two proteins. This leads to holoprosencephaly (HPE), which causes defected craniofacial development and brain malformation.[45]

1.2: CtBP and its Role in Cancer

1.2.1: Hallmarks of Cancer

Cancer is among the most common causes of death in the United States. In 2021, there were approximately 1.9 million new cancer diagnoses in the US, equivalent to roughly 5200 new cases every day. There were approximately 600,000 American deaths due to cancer, corresponding to 1600 deaths per day.[46] There are more than 100 different distinct types of cancer, not including specific subtypes of tumors. However, there are six characteristics that all tumors are believed to have in common: self-sufficiency in growth signals, insensitivity to growth inhibitory signals, evasion of apoptosis, limitless replicative potential, sustained angiogenesis, and tissue invasion and metastasis.[47]

Most cancer treatments employ radiation and chemotherapy that are not specific to tumor type and instead target parts of the cell cycle, as cancer cells divide and proliferate more rapidly than normal cells. These types of chemotherapy are known as kinetic poisons.[48] However, other types of cells also divide rapidly, such as hair follicles and cells of the stomach lining. This is why most cancer treatments are harsh and rife with off-target side effects. However, there has been a recent push for targeted cancer therapy. This can be thought of in terms of infectious diseases. When developing drugs for a bacteria or virus-borne illness, drugs are developed that target cell components (i.e. proteins) that are present in bacterial or virus-infected cells, but not present in normal cells. In targeted cancer therapy, researchers look to target proteins that are present in tumor cells but not in normal cells to minimize the risk of off-target side effects. Specifically, this sort of targeted therapeutic is able to block cell proliferation of cancer cells, promote cell cycle regulation, or induce apoptosis.[48]

CtBP family proteins are ideal targets for cancer therapeutics, because while CtBPs are ubiquitously expressed in most tissue types, they are overexpressed in a broad range of solid human tumors.[5]

1.2.2: Overexpression of CtBP in Human Cancers

Both homologues of CtBP are overexpressed in many types of cancer, including breast cancer (92%),[49–51] ovarian cancer (83%),[52–54] colorectal cancer (64%),[5,14] hepatocellular carcinoma (60%),[55] gastric cancer,[56] prostate cancer,[57,58] and pancreatic adenocarcinoma.[59] Expression levels of CtBP correlate with worse prognostic outcomes and more aggressive tumor features because it promotes proliferation, epithelial-mesenchymal transition, and cancer stem cell self-renewal activity.[5]

The overexpression of CtBP in tumors is in part due to a phenomenon in cancer known as the "Warburg effect," in which tumors are dependent on aerobic glycolysis for the production of ATP as opposed to oxidative phosphorylation.[60,61] Cells that are utilizing aerobic glycolysis have higher ratios of NADH/NAD^+ compared to normal cells.[62–64] Elevated levels of NADH facilitate activation and recruitment of CtBP, which leads to genome-wide changes in chromatin through CtBP's activity as a transcriptional corepressor.[51] Further, CtBP is able to affect the expression of cancer-related genes: tumor suppressor genes and proto-oncogenes, which contribute to many of the hallmarks of cancer such as metastasis and resistance to programmed cell death.[5]

1.2.3: CtBP and Tumor Suppressor Genes

Tumor suppressor genes (TSGs) are genes that are involved in repair of damaged DNA, induction of apoptosis, inhibition of cell division/proliferation, and suppression of metastasis. As one might expect, loss of function of TSGs results in tumor formation and

progression.[65] Through transcriptional repression, CtBP is able to cause loss of function of several TSGs including *BIK*, *PTEN*, E-Cadherin (*CDH1*), and *BRCA1*.[5]

Apoptosis is largely controlled by the BCL-2 (B-cell lymphoma 2) family of proteins. *BIK* (BCL-2 interacting killer) is a pro-apoptotic, Bcl-2 homology domain 3 (BH3)-only gene. It acts by antagonizing the antiapoptotic proteins BCL-X_L (B-cell lymphoma-extra large) and MCL-1 (induced myeloid leukemia cell differentiation protein 1), which causes the release of the multidomain proapoptotic protein Bak and induces Bak-dependent apoptosis.[66] In this way, Bik coordinates with other BCL-2 family proteins to sensitize cells to apoptosis. CtBP is recruited to the Bik promoter by BKLF (Basic Krüppel-like Factor) and is able to repress expression of Bik. Further, CtBP2 depletion or ARF overexpression results in the upregulation of Bik.[67] Inhibition of CtBP with a small molecule inhibitor has been shown to displace CtBP from the Bik promoter and induce apoptosis.[68]

PTEN (phosphatase and tensin homolog) is a gene that encodes for a phosphatase, which dephosphorylates and inactivates the intracellular second messenger PIP3 (phosphatidylinositol (3,4,5)-triphosphate).[69,70] PIP3 is phosphorylated by the lipid kinase PI3K (phosphoinositide-3-kinase). When PIP3 is activated (i.e. phosphorylated), it recruits the Akt family of kinases to the plasma membrane, which then are able to phosphorylate a number of downstream targets that play important roles in cellular proliferation and apoptosis. Inactivation of PTEN leads to the PI3K/Akt pathway being constitutively active, which has implications in cell growth, signaling, migration and apoptosis.[69–72] CtBP2 overexpression in cancer cells has been shown to repress PTEN expression as CtBP2 is recruited to the PTEN promoter.[72,73] Repression of PTEN by

CtBP2 leads to activation of PI3K/Akt signaling, which increases the rate of cancer cell migration.[72–74]

Epithelial-mesenchymal transition (EMT) is a process in cancer where cells lose their epithelial status and acquire mesenchymal traits, which leads to cell migration and metastasis.[5] E-cadherin is expressed in all mammalian epithelia and is involved in the maintenance of epithelial status of cells.[75] It is coded for by the *CDH1* gene, and is the key molecule in forming a cadherin-catenin-cytoskeleton complex (CCC) with β-catenin and αE-catenin. The CCC exists in the cell junction and helps execute cell adhesion by connecting to actin molecules in the cytoskeleton. In epithelial tumors, E-cadherin expression is often downregulated or repressed. In hypoxia conditions, NADH levels are increased, which in turn recruits CtBP to the E-cadherin promoter via ZEB1.[24] Overexpression of CtBP2 has been shown to decrease E-cadherin expression, which increases tumor cell migration.[55] In hepatocellular carcinoma (HCC) cells, knockdown of CtBP1 leads to the upregulation of E-cadherin, and inhibits the invasive abilities of cancer cells.[76]

The role of CtBP in breast cancer has been well studied. The *BRCA1* (BReast CAncer gene 1) gene is involved in DNA repair, transcription, and regulation of the cell cycle.[77] Inherited mutations in *BRCA1* make one predisposed to breast cancer.[78] The *BRCA1* gene encodes the BRCA1 protein, which is involved in the cellular response at double-strand DNA breaks (DSBs).[78] BRCA1 expression is regulated by environmental stimuli such as estrogen stimulation and hypoxia.[77] It has been shown that BRCA1 expression is downregulated as a result of CtBP1 expression.[79] Specifically, CtBP1 forms a corepressor complex with p130 and HDAC1 at the BRCA1 promoter, and represses

histone acetylation at the BRCA1 promoter, repressing *BRCA1* transcription. Further, loss of CtBP from the BRCA1 promoter results when the NAD^+/NADH ratio increases, which increases BRCA1 transcription.[77]

1.2.4: CtBP and Oncogenes

In contrast to tumor suppressor genes, proto-oncogenes are genes that are involved in pathways that promote the cell cycle and cellular growth. Activating mutations in proto-oncogenes can cause normal cells to become cancer cells as they lead to unregulated cell growth and proliferation. Mutated proto-oncogenes are referred to as oncogenes.[65] CtBP has been shown to activate oncogenes such as Tiam1.

The protein coded for by the T-lymphoma and metastasis gene 1 (*TIAM1*) is a Guanine Nucleotide Exchange Factor (GNEF) that is involved in regulating the guanine triphosphatases (GTPases) of the Rho family by facilitating the exchange of GDP to GTP. Specifically, Tiam1 acts as an exchange factor for the proteins Rac1, Cdc42, and RhoA. Induction by Tiam1 or constitutive activation of Rac1 and Cdc42 lead to increased invasiveness of T-lymphoma cells. Tiam1 is also involved in breast cancer in that Tiam1-mediated activation of Rac has been shown to promote tumor cell migration.[80] Tiam1, when activated, is implicated in the promotion of cancer progression and metastasis, as it promotes cancer cell migration and enhances the invasiveness and metastatic properties of cancer cells.[27,71] CtBP2 is able to stimulate cell migration via regulation of Tiam1. Expression of CtBP2 is positively correlated with the expression of Tiam1. Further, CtBP2, when bound to NADH, is recruited by KLF8 to the Tiam1 promoter where it transcriptionally activates Tiam1. In this way, CtBP2 directly promotes cell migration and metastasis.[71]

1.2.5: CtBP and Drug Resistance

A major obstacle in cancer research is cancer cell resistance to chemotherapeutics. The multidrug resistance gene 1 (MDR1) codes for the protein product P-glycoprotein (P-gp), which can transport drug compounds such as paclitaxel, doxorubicin, and vinblastine resulting in lowered drug concentration in cells and lower efficacy.[81] In MDR cell lines, CtBP1 is overexpressed. Further, knockdown of CtBP1 decreases MDR1 expression and the cellular concentration of P-gp. CtBP1 interacts directly with the MDR1 promoter.[81]

1.3: Inhibition of CtBP

1.3.1: Peptide Inhibitors of CtBP

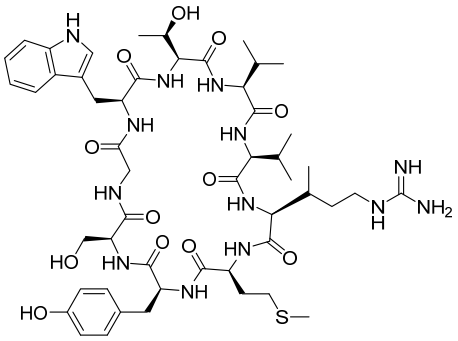

Figure 1.4: Structure of CP61

The first known inhibitor of CtBP is a cyclic peptide known as CP61 (**Figure 1.4**), and was discovered through a high-throughput screening that assessed 64 million genetically encoded cyclic peptides.[82] CP61 is a cyclic peptide with the sequence SGWTVVRMY. CP61 inhibits homodimerization of CtBP2 with an *in vitro* IC_{50} of 19 ± 4 μM, and inhibits both homo- and heterodimerization of CtBP1/2 in cells. CP61 has a binding affinity to dimeric CtBP1 of 3 μM and 11 μM; this suggests that CP61 may be able to bind to two different isoforms of CtBP1. Interestingly, though CP61 inhibits the interaction between CtBP1 and NADH, CP61 is an allosteric inhibitor in that it does not bind to CtBP in the nucleotide-binding pocket. Instead, CP61 indirectly inhibits CtBP by disrupting the protein-protein interaction (PPI) between the monomers of CtBP. Further, CP61 does not inhibit LDH and is therefore selective for CtBP over other dehydogenases.

In breast cancer cells, CP61 was shown to reduce mitotic fidelity, cellular proliferation and colony formation. However, this was only the case for cells with a high rate of glycolysis, providing evidence that the cell cycle is influenced by the glycolytic state of the cell.[82]

1.3.2: Small Molecule Inhibitors of CtBP

The first small molecule inhibitor of CtBP, NSC95397 (**Figure 1.5**), was identified in 2015 using an AlphaScreen assay for high throughput screening.[83] Like CP61, NSC95397 is an allosteric inhibitor of CtBP in that it is not a substrate for CtBP's NADH-dependent dehydrogenase activity and does not bind at the NBD. NSC95397 inhibits the interaction between CtBP and E1A with an IC_{50} of 2.9 μM. Further, NSC95397 is able to disrupt the complex between CtBP and the E-cadherin promoter and reverse transcriptional repression of E-cadherin.[83] The exact mechanism of NSC95397 is unknown. It is possible that NSC95397 binds at the PxDLS-binding motif, thereby inhibiting interaction of CtBP with its corepressor partners. While NSC95397 does not inhibit LDH,[83] it is not selective for CtBP because it is also a known inhibitor of cdc25 phosphatase activity[84] and spliceosome catalysis.[85]

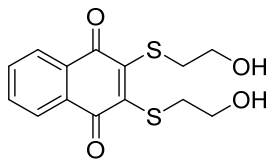

Figure 1.5: Structure of NSC95397

1.3.3: First-generation substrate-competitive CtBP inhibitors

A known substrate of CtBP is 4-methylthio-2-oxobutyic acid (MTOB).[86] A co-crystal structure of CtBP1 complexed with MTOB and NAD^+ has been reported, and it reveals that MTOB interacts with the catalytic triad (Arg97, Arg266 and His315) and forms a π interaction with Trp318 (**Figure 1.6**).[34] At low concentrations MTOB acts as a substrate

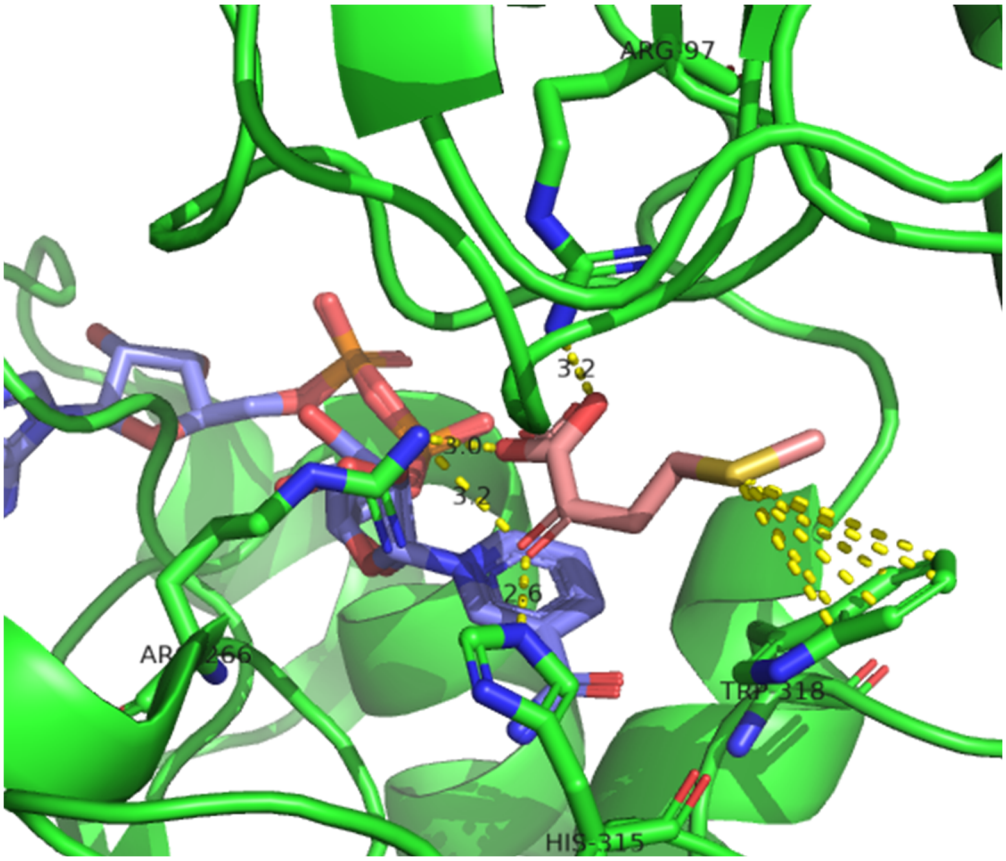

Figure 1.6: Crystal structure of CtBP1 (green) complexed with MTOB (pink) and NAD^+ (purple) (PDBID: 4LCE).

for CtBP; CtBP catalyzes the reduction of the ketone in MTOB to an alcohol to yield 4-methylthio-2-hydroxy-butyric acid (MTHB).[68] However, at high concentrations. MTOB inhibits the dehydrogenase activity of recombinant CtBP (IC_{50} = 300 μM) *in vitro* and disrupts transcriptional repression and activation of cancer-related genes.[86] MTOB has been shown to induce apoptosis in HCT116 colon carcinoma cells, and displace CtBP from the Bik promotor and induce Bik expression.[86]

Using MTOB as a starting point, our lab further investigated compounds that would inhibit the dehydrogenase activity of CtBP.[68] The first modification was replacement of the thioether in MTOB with a phenyl ring to increase the π interactions with Trp318, which lead to phenylpyruvic acid. Phenylpyruvic acid was found to be a 3-fold better inhibitor of CtBP (IC_{50} = 116 μM), however it acts as a substrate of CtBP as well as an inhibitor. The next step was to replace the ketone with nonreducible ketone isosteres (**Figure 1.7**) to find an inhibitor of CtBP that could not act as a substrate. Of these, the hydroxyimine analogue, also known as 2-hydroxyimino-3-phenyl propanoic acid (HIPP) was the only one found to be a more potent inhibitor than phenylpyruvic acid (IC_{50} = 240 nM).[68] A co-crystal structure of CtBP1 complexed with HIPP and NADH was solved (PDBID: 4U6Q) and revealed that HIPP binds to CtBP in the same binding site as MTOB (**Figure 1.8**).[87] Further, isothermal titration calorimetry (ITC) with CtBP1 provided a dissociation constant (K_d) of 370 nM.[87] HIPP has also been shown to displace CtBP from transcriptional promoters, restore expression of tumor suppressor genes in cells, and induce apoptosis.[68] Despite promising *in vitro* data with HIPP, when this compound was tested in an MTT assay for the ability to inhibit cancer cell growth and

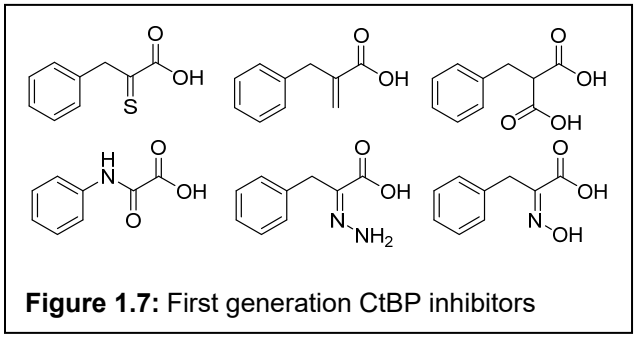

Figure 1.7: First generation CtBP inhibitors

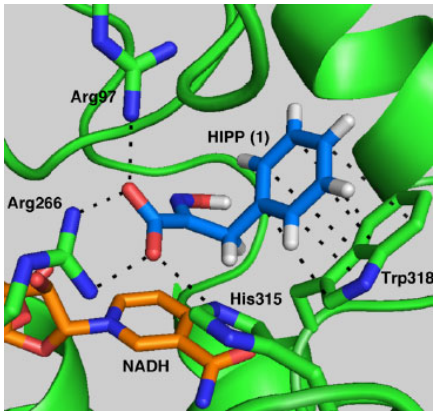

Figure 1.8: HIPP (blue)-CtBP1 (green)-NADH (orange) Crystal Structure

viability, the cellular IC_{50} was higher than expected (IC_{50} = 4.12 mM).[68] Further compounds were then designed to increase the potency in cells and *in vivo*.

1.3.4: Second generation substrate-competitive CtBP Inhibitors

A structure-activity relationship (SAR) study was performed on the phenyl ring of HIPP by synthesizing analogues with substituents that are electronically and sterically diverse. Specifically, this study explored the addition of substituents on the phenyl ring that were electron-donating, electron-withdrawing, and electron-neutral, and the position of the substitution on the phenyl ring compared to the rest of the molecule (ortho-, meta-, and para-). The structures of this set of compounds are shown in **Figure 1.9**. These analogues were tested for functional inhibition of CtBP using an NADH consumption assay.[68]

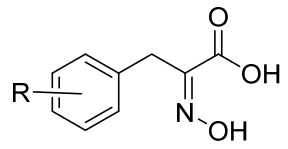

R = 4-Me 4-OMe 4-Cl 4-OH 4-F
3-Me 3-OMe 3-Cl 3-OH 4-CN
2-Me 2-OMe 2-Cl

Figure 1.9: Second generation CtBP inhibitors

In functional inhibition experiments, it was found that ortho-substitutions on the phenyl ring were unfavorable when compared to the parent compound HIPP. Para- and meta-substitution by electron-donating or electron-neutral substituents also resulted in a decrease in inhibitory activity. However, it was determined that para- and meta-substitution by a chlorine atom leads to more active inhibitors compared to HIPP. This did not prove true for other electron-withdrawing substituents at these positions.[68] 4-Cl HIPP and 3-Cl HIPP have functional IC_{50} values of 180 nM and 170 nM, respectively. These two compounds were also tested for inhibition of cancer cell viability and growth. While there is a marked improvement when compared to HIPP, with 4-Cl HIPP and 3-Cl HIPP exhibiting cellular IC_{50} values of 1.74 mM and 850 μM respectively, there is still a great

disparity between *in vitro* data and cellular data.[68] This dissertation focuses on finding new compounds that modulate CtBP's oncogenic effects in cells.

1.4: Scope of this dissertation

The first project in this dissertation focuses on design and development of heteroaromatic HIPP analogues that target CtBP for use as anti-cancer therapeutics. We have used computational techniques to prioritize synthesis of new analogues, which was followed by biological testing of the synthesized compounds. We synthesized nine new substrate-competitive inhibitors of CtBP, and obtained two compounds that had more affinity for CtBP2 than HIPP. We found that replacing the carboxylic acid on 4-Cl HIPP with an ethyl ester increases potency in cells 50-fold, and identified five novel compounds that were more potent than the HIPP ethyl ester in cells. The second part of this dissertation focuses on design and development of HIPP-based CtBP PROteolysis TArgeting Chimeras (PROTACs) to provoke degradation of CtBP by the endogenous ubiquitin/proteasome system. We have succeeded in synthesizing three PROTAC molecules in total, and one PROTAC molecule that degraded CtBP2 with a DC_{50} of 3.20 μM and degraded CtBP1 with a DC_{50} of 16.43 μM.

Chapter 2: Novel CtBP Inhibitor Design, Synthesis, and Evaluation

2.1: Background

2.1.1: Design rationale for in silico library

As previously discussed, the aromatic ring of HIPP forms a π-stacking interaction with Trp318 in CtBP1. Therefore, modulating the amount and nature of electron density in the aromatic ring system can either strengthen or weaken inhibitor binding. In this project, we designed a small library of compounds in which the phenyl ring of HIPP is substituted with either a monocyclic heteroaromatic ring or a bicyclic heteroaromatic ring to determine the optimal aromatic ring system to form a π-stacking interaction with Trp318. We also hypothesized that by correctly positioning the heteroatom(s) in these ring systems, a hydrogen-bonding interaction with the residue His315 can also be created to strengthen the overall binding affinity. In the compounds where a bicyclic ring was used, we also tested whether the methylene between the aromatic ring and oxime moieties should be cyclized or not (n = 1 vs n = 0). The 36 compounds tested are shown in **Figure 2.1**. Compounds at this stage were named using the following naming convention:

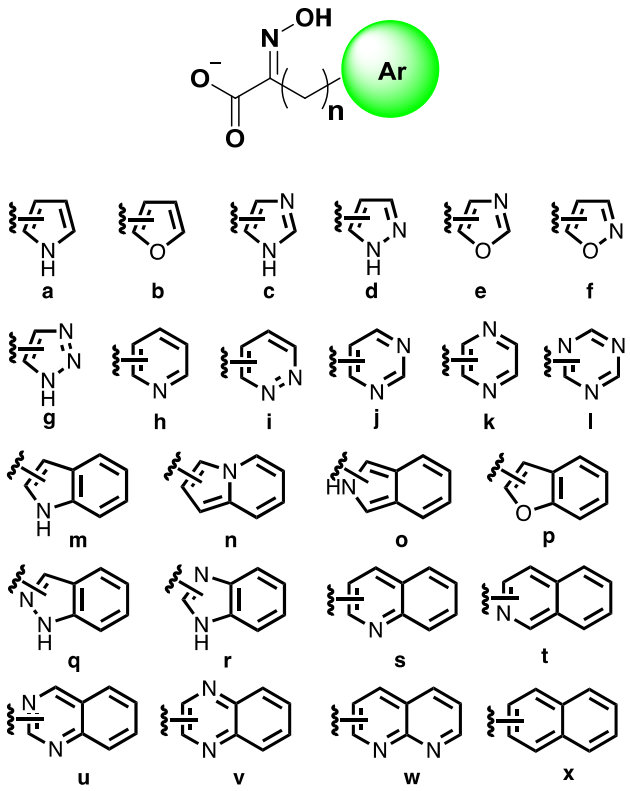

Figure 2.1: Heteroaromatic HIPP analogues for in silico library.

Heteroaromatic-#-(C*HIA), where the heteroaromatic is the name of the ring, # represents the substitution position of the hydroxyimino acid (HIA) on the ring system, and * being the number of carbon atoms between the acid hydrogen and the ring (2 or 3). As a note, these compounds were modeled as the conjugate base, as the acid would be deprotonated at physiological pH.

2.2: Experimental

2.2.1: Crystal structure and ligand preparation

The co-crystal structure for CtBP1 complexed with HIPP and NADH (PDBID: 4U6Q) was opened in WordPad, and the HIPP molecule was deleted manually. The CtBP1-NADH adduct was then imported into PDB2PQR, which was used to calculate the pKa of each histidine residue utilizing the PROPKA algorithm and the CHARMM forcefield. Each histidine (**Figure 2.2**) in the molecule was labeled as HIS (indicating no protonation), HSD (ND1 is protonated), HSE (NE2 is protonated), or HSP (dually protonated). With this data in hand, the CtBP1-NADH adduct was then imported into AutoDockTools v1.5.6, where the protonation of each histidine was set. The crystal structure was then saved as a .pdbqt file. In models where side chain flexibility was allowed, the residues His77, Arg97, Ser100, Arg266, His315, and Trp318 were saved as a separate “flex” .pdbqt file. These parameters were also applied in GoldSuite 5.3.

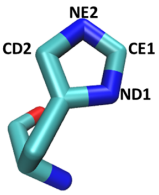

Figure 2.2: Histidine Protonation

The ligand files were initially drawn in ChemDraw v19.1, and the SMILES string of each ligand were imported into Avogadro v1.2.0. In Avogadro, each ligand was converted to a 3D structure with x, y, z coordinates and was saved as both a .xyz file and a .pdb file.

The 3D structures were energy minimized in Orca v4.2.1 with density functional theory (DFT) employing the B3LYP/SVP basis set.[88,89] Orca also predicted the CHELPG charges of each atom in a separate output file. The energy minimized structures were then imported into AutoDockTools v1.5.6, and saved as .pdbqt files for docking in AutoDock Vina. The energy minimized structures were also imported into SYBYLX2.1.1, and saved as .mol2 files for docking in GoldSuite 5.3. In Gold, AM1BCC charges were used for all atoms.

2.2.2: Docking and scoring of library against CtBP

AutoDock Vina was employed to perform automated docking tasks.[90] In order to effectively dock the HIPP analogues, the crystal structure of CtBP1 complexed with HIPP and NADH was used to determine the geometric location of the binding pocket by finding the median values of atoms of HIPP as x, y, z coordinates. The binding pocket was centered at 5.057, 30.011, -18.395 (x, y, z) and each direction was 20 Å in size. This was then fed into an input file containing the parameters to be used by the command line. 8 CPUs were used with an exhaustiveness of 256 to find a maximum of 20 different binding poses. Each pose predicted was scored using Vina's scoring function.

The first model was done with all histidine residues fully protonated and rigid side chains. Next the docking was repeated with rigid side chains and the histidine protonation as predicted by PDB2PQR. The third model kept the histidine protonation the same as in the second model, but side chain flexibility was allowed for His77, Arg97, Ser100, Arg266, His315, and Trp318. These side chains were selected based on studies done by our collaborators in Dr. Steven Grossman's laboratory, which determined the catalytically active residues in the active site.[27] Finally, the docking was repeated where the charges

on the ligand atoms were changed from the default AM1BCC charges to CHELPG charges manually in WordPad.

GoldSuite 5.3 was also employed to perform automated docking tasks. The default parameters were used except for the use of the CHEM-PLP scoring/fitness function. In order to effectively dock each compound, a 10 Å radius was set around the HIPP molecule in the crystal structure. The number of poses was set to 10 for each compound. Scoring with the CHEM-PLP scoring/fitness function was automatically performed for each fragment based on the docking poses.

Each model used the histidine protonation states predicted by PDB2PQR, with the exception of His315. Four models were tested in GOLD based around two variations: whether His315 was protonated on ND1 or NE2, and whether the six residues mentioned above were rigid or flexible. Three replicates were performed for each model.

2.2.3: Generation of HINT scores

The highest scoring CHEM-PLP solution for HIPP and the top 8 scoring analogues in each GOLD model were rescored with HINT. The complex for each ligand and protein were energy minimized in SYBYLX2.1.1. The HINT calculation was facilitated by in house SYBYL SPL scripts and default parameters were used. The results from all three scoring functions (*Section 2.3.1-2.3.3*) were analyzed together and used to prioritize choosing compounds for synthesis.

2.2.4: Synthesis of third generation substrate-competitive CtBP inhibitors

A Horner-Wadsworth-Emmons (HWE) reagent was synthesized (**Scheme 2.1**) by first coupling dimethyl phosphite (1 eq) and ethyl glyoxalate (1 eq) with triethylamine

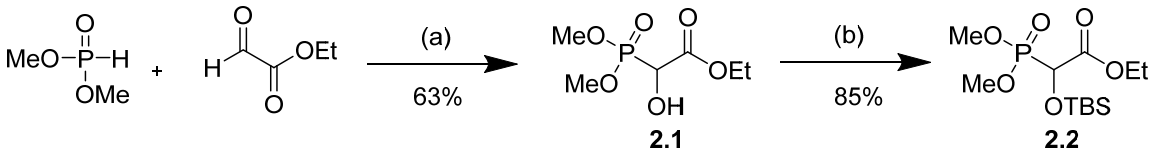

2.1 **2.2**

Scheme 2.1: Synthesis of compounds **2.1** and **2.2**. Reagents and conditions: (a) TEA, DCM, -78°C, 1h. (b) Imidazole, DMAP, TBS chloride, DCM, rt, 18h.

(TEA, 0.2 eq) to afford ethyl 2-(dimethoxyphosphoryl)-2-hydroxyacetate (**2.1**).[91] This was then TBS protected with *tert*-butyldimethylsilyl chloride (2 eq), imidazole (3 eq), and DMAP (0.15 eq) to yield the final HWE reagent, ethyl 2-((*tert*-butyldimethylsilyl)oxy)-2-(dimethoxyphosphoryl)acetate (**2.2**).

The heterocycle scaffolds were purchased as aldehydes, which were then subjected to an HWE reaction in the presence of LiHMDS (1.1 eq), where the aldehyde was used in excess (1.5 eq) relative to the HWE reagent (1 eq). Initially, we attempted the HWE reaction with LDA (1.1 eq) at -78°C.[92] However, we determined that because the aromatic ring systems of these analogues are more electron-rich, the synthesis required optimization (**Scheme 2.2**). This is why we opted to use a stronger base, LiHMDS, and reflux the

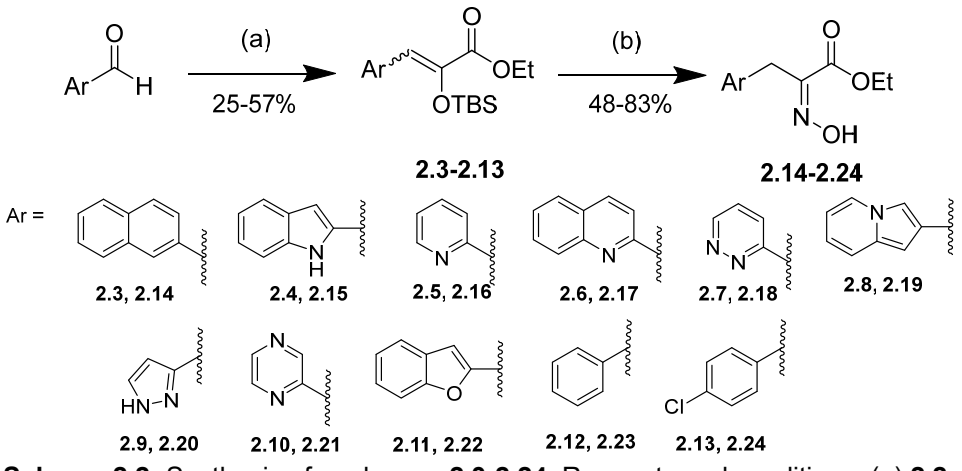

Scheme 2.2: Synthesis of analogues **2.3-2.24**. Reagents and conditions: (a) **2.2**, LiHMDS, THF, reflux, 15h. (b) $3HF•NEt_3$, $H_2NOH•HCl$, rt, 19h.

reaction at 60°C. After purification, the resulting silyl enol ethers (**2.3**-**2.11**) underwent a two-step, one-pot reaction in which the silyl enol ether is TBS de-protected using triethylamine trihydroflouride (1.7 eq), and the resulting enol is converted to an oxime with hydroxylamine hydrochloride (1.7 eq) to yield the final oxime product (**2.14-2.22**). These reactions were also repeated with benzaldehyde and 4-Cl-benzaldehyde to prepare the HIPP ester (**2.23**) and 4-Cl HIPP ester (**2.24**) to test in cells as controls.

Indolizine-2-carbaldehyde (**2.26**) was unable to be purchased due to high cost, so indolizine-2-carboxylic acid was purchased instead, which we reduced to an aldehyde in two steps. We first tried a reaction from the literature to synthesize indolizine-2-carbaldehyde (**Scheme 2.3**), where it was first converted to a Weinreb amide **2.25**, followed by a reduction to the aldehyde **2.26** with lithium aluminum hydride (LAH).[93] Indolizine-2-carboxylic acid (1 eq) was reacted with *N*-methoxymethanamine (1.5 eq), Hexafluorophosphate Azabenzotriazole Tetramethyl Uronium (HATU, 1.2 eq) and TEA (2 eq) to afford N-methoxy-N-methylindolizine-2-carboxamide (**2.25**). This was then reduced with LAH (1.5 eq) to yield indolizine-2-carbaldehyde (**2.26**).

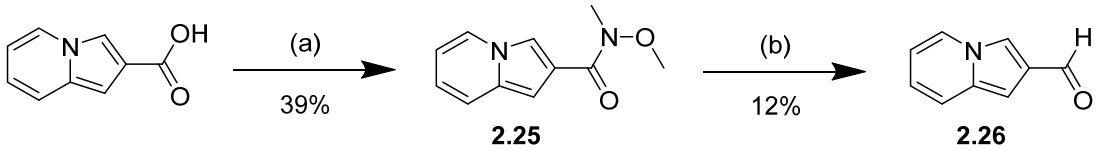

2.25 **2.26**

Scheme 2.3: Synthesis of compounds **2.25** and **2.26**. Reagents and conditions: (a) N-methoxymethanamine, HATU, TEA, DMF, 28°C, 12h. (b) LAH, THF rt, 2h.

However, while we were able to synthesize **2.25**, it was difficult to purify. Further, we were unable to perform the LAH reduction cleanly and incapable of effectively performing the subsequent HWE reaction with a viable yield. We next tried to reduce Weinreb amide **2.25** to the aldehyde **2.26** with either diisobutylaluminum hydride (DIBAL) or Dess-Martin periodinane, but these reactions were unsuccessful. Finally, we reduced

indolizine-2-carboxylic acid (1 eq) with LAH (4 eq) to yield indolizin-2-ylmethanol (**2.27**). This was then oxidized with Manganese (IV) oxide (MnO_2, 11 eq) to afford aldehyde **2.26** (**Scheme 2.4**).

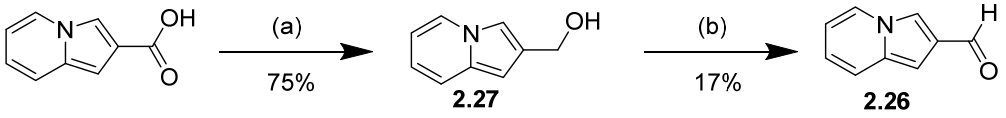

Scheme 2.4: Synthesis of compounds **2.27** and **2.26**. Reagents and conditions: (a) LAH, THF, 0°C→63°C, 16h. (b) MnO_2, THF, rt, 16h.

We had also planned on making ethyl 3-(1H-benzo[d]imidazol-2-yl)-2-(hydroxyimino)propanoate (**2.30**). However, when performing the above HWE reaction with 1H-benzimidazole-2-carboxaldehyde, the silyl enol ether product was not detected. Initially, we thought the issue might be with the amine hydrogen in the ring system, so we attempted to Boc protect that nitrogen, but were unsuccessful. Finally, we attempted to use the method to make HIPP and HIPP analogues outlined in Korwar et al. (2016, **Scheme 2.5**)[68] where benzimidazole-2-carbaldehyde is first reacted with hydantoin (1 eq) and ethanolamine (1.55 eq) to yield (Z)-5-((1H-benzo[d]imidazol-2-yl)methylene)imidazolidine-2,4-dione (**2.28**). However, we were unable to perform the reaction with hydantoin cleanly, and the following reaction to form 3-(1H-benzo[d]imidazol-2-yl)-2-hydroxyacrylic acid (**2.29**) was unsuccessful.

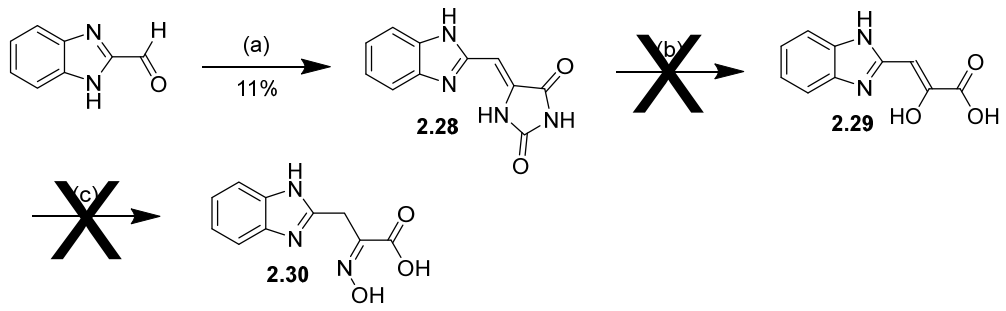

Scheme 2.5: Synthesis of compounds **2.28**-**2.30**. Reagents and conditions: (a) hydantoin, Na_2CO_3 (sat aq), ethanolamine, EtOH/H_2O (1:1), 120°C, 5-10h. (b) 20% NaOH (aq), 100°C, 3h. (c) NaOH, $H_2NOH{\cdot}HCl$, H_2O, rt, 16 h.

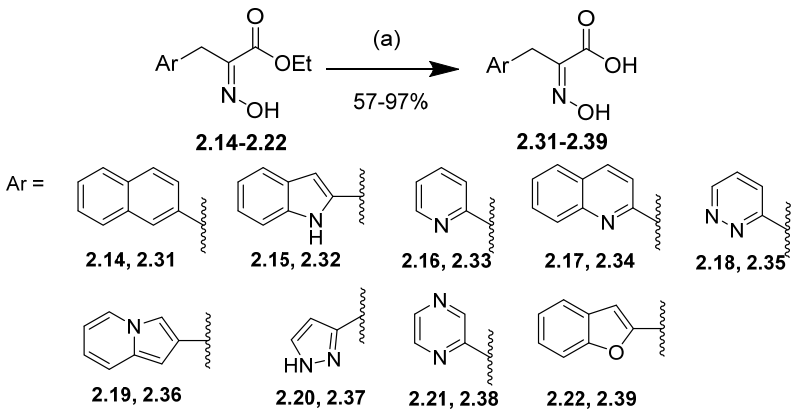

Scheme 2.6: Synthesis of compounds **2.31**-**2.39**. Reagents and conditions: (a) 1M NaOH (aq), EtOH, rt, 16 h.

As the esters of our heteroaromatic HIPP analogues will be hydrolyzed to carboxylic acids *in vivo*, we hydrolyzed these compounds to their acid derivatives (**Scheme 2.6**) for our ITC experiments to obtain an accurate binding constant for each compound. The hydrolysis was done by reacting the corresponding ester compound (**2.13**-**2.22**) with 1M aqueous sodium hydroxide (3 eq) to afford the acid product (**2.31**-**2.39**).[94]

We also synthesized HIPP (**2.40**) and 4-Cl HIPP (**2.41**) as the acid derivatives (**Scheme 2.7**) to measure binding affinity with CtBP2 utilizing ITC. We had phenylpyruvic acid and 4-chlorophenylpyruvic acid on hand, so these two reagents were used as starting materials as this allowed for conversion to the oxime products in one step. Phenylpyruvic acid and 4-chlorophenylpyruvic acid (1 eq) were reacted with sodium hydroxide (3 eq) and hydroxylamine hydrochloride (2 eq) to yield HIPP (**2.40**) and 4-Cl HIPP (**2.41**) respectively.

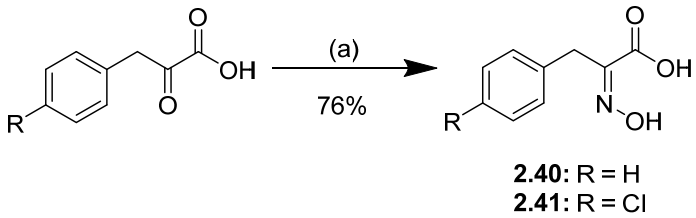

Scheme 2.7: Synthesis of compounds **2.40**-**2.41**. Reagents and conditions: (a) NaOH, H_2NOH•HCl, H_2O, rt, 16 h.

2.2.5: Evaluation of novel CtBP inhibitors in cells

A2780 ovarian cancer cells (~1000 cells) in 100 µL media were plated in a 96-well plate. After a 24-hour incubation period, inhibitors **2.14**-**2.24** and **2.41** in DMSO were further diluted in $NaHCO_3$ (0.8% diluted DMSO final volume/well) and added to plates at concentrations as shown in **Table 2.1**. 72 h after addition of inhibitor, 20 µL of MTT solution (Alfa Aesar) was added to each well and cells were incubated a further 4 h. Media was then aspirated and the MTT metabolic product formazan was resuspended in 200 µL DMSO. Optical density was measured at 560 nm (subtracting background at 670 nm) using a microplate reader. This MTT assay was repeated with inhibitors using HEY and Ovcar420 ovarian cancer cells, HCT116 colorectal cancer cells, and MCF-7 and MDA-MB-231 breast cancer cells.

Table 2.1: Inhibitor concentrations used in the MTT cell viability assay for compounds in each cell line

Concentration	HCT116	A2780	HEY	Ovcar420	MCF-7	MDA-MB-231
1024 µM to 1 µM, 2-fold dilutions	**2.14**	**2.14**-**2.16**, **2.41**	**2.14**-**2.16**, **2.41**	**2.14**-**2.16**, **2.41**	**2.14**	**2.14**
4 mM to 62.5 µM, 2-fold dilutions	**2.17**-**2.21**, **2.23**-**2.24**	**2.17**-**2.21**, **2.23**	**2.17**-**2.21**, **2.23**-**2.24**	**2.17**-**2.21**, **2.23**-**2.24**	N/A	N/A
16 mM to 250 µM, 2-fold dilutions	N/A	**2.22**	N/A	N/A	N/A	N/A
16 mM to 62.5 µM, 2-fold dilutions	N/A	**2.24**	N/A	N/A	N/A	N/A
16 mM to 62.5 µM, 2-fold dilutions	N/A	**2.24**	N/A	N/A	N/A	N/A

Inhibitors were also tested in a clonogenic assay. A2780 cells (~200 cells) in 100 µL media were plated in a 96-well plate. Inhibitors **2.14**, **2.15**, **2.17**-**2.24**, and **2.41** in DMSO were further diluted in $NaHCO_3$ (0.8% diluted DMSO final volume/well) and added to plates at 1000, 500, 250, 125, 62.5, and 0 µM concentrations. After addition of inhibitor, cells were incubated for a 72-h period. Colonies were then fixed and stained with a mixture of 6.0% glutaraldehyde and 0.5% crystal violet. Colonies were then counted using a stereomicroscope and an automatic counting colony counter pen. The plating efficiency

(PE) of control cells was determined as the fraction of colonies from untreated cells. This was then taken into account when calculating the surviving fraction (SF), or the number of colonies formed after treatment. This clonogenic assay was repeated with inhibitors using Patu8988T pancreatic cancer cells.

All cellular assays were performed by Dr. Martin M. Dcona at the University of Southern California. Percent cell/clone viability data were normalized to the no inhibitor control, converted to a percentage, and plotted against the log of the concentrations of the inhibitor. Curve fitting and the determination of the EC_{50} values were performed in Prism (Graphpad, Version 9) using non-linear regression to either the log(inhibitor) vs normalized response equation (MTT) or the [Inhibitor] vs normalized response equation (clonogenic). EC_{50} values represent the drug concentration that results in 50% of the cell/clone viability.

2.2.6: Isothermal titration calorimetry

ITC experiments were performed at 25°C with the Microcal PEAQ-ITC Automated System (Malvern). Purified CtBP2 wt (31-364) truncated[27] was stored in 50 mM Tris (base), 300 mM NaCl, 2 mM DTT and 14% glycerol. This was then concentrated by spin column (5000 RPM, 4°C, 30 min increments) and diluted into ITC buffer 50 mM HEPES at pH 7.5, 300 mM NaCl, 1 mM EDTA, 2 mM TCEP and 1-5% DMSO. The concentration of protein was determined utilizing a NanoDrop, which measured the absorbance at 280 nm. The absorbance was converted to a concentration in mg/mL utilizing the molecular weight 36873.1 kDa and the extinction coefficient 24410 M^{-1} cm^{-1}. Concentrated ligands in 49.35% DMSO were diluted to working concentrations in ITC buffer. Binding was measured by titrating 125-1000 μM inhibitor. CtBP2 concentration was 10-50 μM for all

experiments. Each measurement consisted of nineteen (19) 2.0 µL injections of inhibitor into the CtBP2 solutions. Data were fit in the MicroCal PEAQ-ITC analysis software to the single binding site model. Heats of ligand dilution were measured and subtracted for each type of binding experiment before curve fitting. Final results represent the average of at least 2 measurements. The K_d and ΔH of each binding experiment was calculated based on the ΔQ per injection. The thermodynamic data obtained was entered into Jamovi v2.2.5, where the average, standard deviation, and standard error of the mean was calculated.

2.3: Results and Discussion

2.3.1: Results from docking and scoring of library against CtBP in GOLD

Our compound library was docked in the co-crystal structure of CtBP1 using GoldSuite 5.3, which uses a genetic algorithm to find the best fit for each compound. Each pose in GOLD was scored with the CHEM-PLP scoring algorithm. The compounds were then rank-ordered based on their scores. Two parameters were varied to refine the model: the protonation state of His315, and whether the side chains of active site residues should be rigid or flexible. To account for this, there were four separate models in GOLD: two

Table 2.2: Top 15 scores from docking studies in GOLD. Model conditions: (a) Rigid side chains, HSD315; (b) Rigid side chains, HSE315; (c) Flexible side chains, HSD315; (d) Flexible side chains, HSE315.

	Compound			
Rank	(a)	(b)	(c)	(d)
1	Indolizine-2-(C3HIA)	Indolizine-2-(C3HIA)	Naphthalene-2-(C3HIA)	Indolizine-2-(C3HIA)
2	Naphthalene-2-(C3HIA)	Naphthalene-2-(C3HIA)	Indolizine-2-(C3HIA)	Naphthalene-2-(C3HIA)
3	Isoquinoline-3-(C3HIA)	Isoquinoline-3-(C3HIA)	Indole-2-(C3HIA)	Isoquinoline-3-(C3HIA)
4	Quinazoline-2-(C3HIA)	Quinoline-2-(C3HIA)	Isoquinoline-3-(C3HIA)	Quinoline-2-(C3HIA)
5	Quinoline-2-(C3HIA)	Quinazoline-2-(C3HIA)	Quinoline-2-(C3HIA)	Quinazoline-2-(C3HIA)
6	Benzofuran-2-(C3HIA)	Isoindole-1-(C3HIA)	Benzofuran-2-(C3HIA)	Naphthalene-2-(C2HIA)
7	Isoindole-1-(C3HIA)	Benzofuran-2-(C3HIA)	Naphthalene-2-(C2HIA)	Quinoline-2-(C2HIA)
8	Naphthyridine-2-(C3HIA)	Indole-2-(C3HIA)	Isoquinoline-3-(C2HIA)	Indolizine-2-(C2HIA)
9	Indole-2-(C3HIA)	Quinoxaline-2-(C3HIA)	Indolizine-2-(C2HIA)	Quinoxaline-2-(C3HIA)
10	Quinoxaline-2-(C3HIA)	Naphthyridine-2-(C3HIA)	Quinoxaline-2-(C3HIA)	Indole-2-(C3HIA)
11	Benzimidazole-2-(C3HIA)	Benzimidazole-2-(C3HIA)	Indole-2-(C2HIA)	Quinazoline-2-(C2HIA)
12	Indazole-3-(C3HIA)	Indazole-3-(C3HIA)	Benzimidazole-2-(C3HIA)	Naphthyridine-2-(C3HIA)
13	Indolizine-2-(C2HIA)	Pyridine-2-(C3HIA)	Indazole-3-(C3HIA)	Benzimidazole-2-(C3HIA)
14	Pyridine-2-(C3HIA)	Pyrrole-2-(C3HIA)	Quinazoline-2-(C3HIA)	Isoquinoline-3-(C2HIA)
15	HIPP	HIPP	HIPP	Benzimidazole-2-(C2HIA)

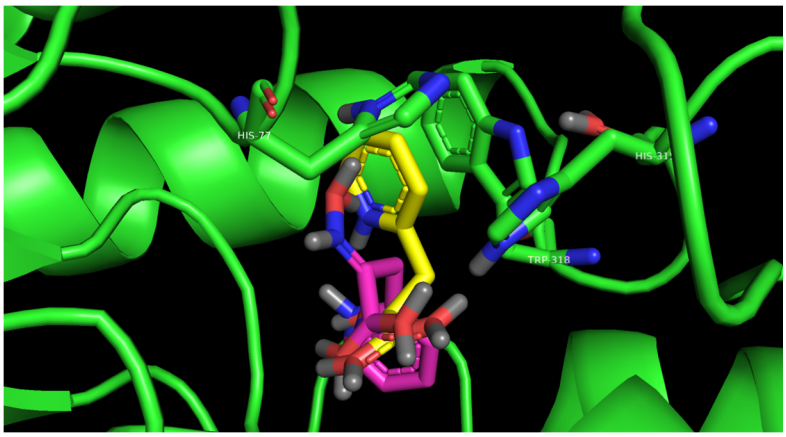

Figure 2.3: Compound **2.33** docked into the CtBP1-HIPP co-crystal structure with His315 protonated on the E-nitrogen (yellow) or the D-nitrogen (pink).

models with rigid active side chains where His315 was protonated on either ND1 or NE2, and two models with flexible active site side chains where His315 was protonated on either ND1 or NE2. The top 15 rank-ordered compounds from the GOLD docking sessions are shown in **Table 2.2**. All models in GOLD utilized AM1BCC atom charges. In terms of the protonation state of His315, we determined that the protonation state affects the poses generated in the docking sessions (**Figure 2.3**).

When allowing for side chain flexibility in GOLD models, the calculated PLP fitness scores did not differ greatly. Similarly to models with rigid side chains, bicyclic heterocycles had better PLP fitness scores than monocyclic heterocycles. Further, compounds with two atoms in the hydroxyimino acid (n = 0) did not score as well when compared to HIPP. It makes sense that PLP fitness scores would not differ between models with rigid or flexible side chains, because

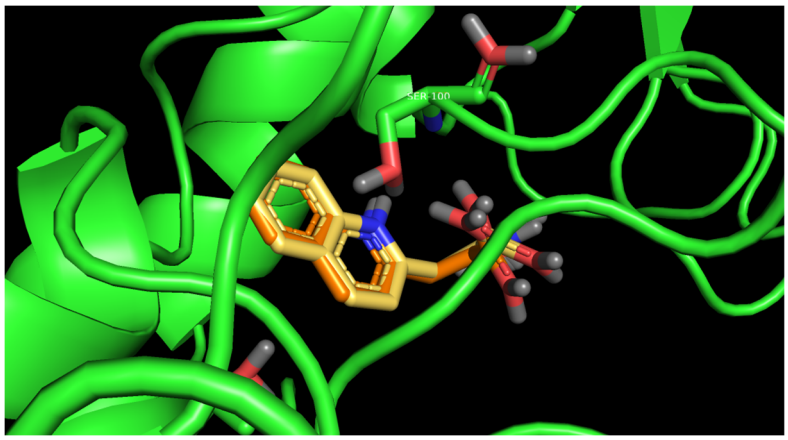

Figure 2.4: Compound **2.34** docked into the CtBP1-HIPP co-crystal structure with rigid side chains (orange) or flexible side chains (beige).

when one examines the poses generated in our GOLD models with flexible side chains, we see that the predicted poses do not differ greatly. (**Figure 2.4**).

When we took the average of the PLP fitness scores generated for each compound, we found that there were 8 compounds that exhibited higher scores than HIPP (**Table 2.3**). To test our model predictions, we chose to synthesize the two top-scoring compounds, Indolizine-2-(C3HIA) (**2.36**) and Naphthalene-2-(C3HIA) (**2.31**).

Table 2.3: Compounds that scored better than HIPP in GOLD models on average.

Compound	Average PLP Fitness Score
Indolizine-2-(C3HIA)	74.36583333
Naphthalene-2-(C3HIA)	73.15583333
Isoquinoline-3-(C3HIA)	72.89166667
Quinoline-2-(C3HIA)	71.06
Quinazoline-2-(C3HIA)	69.94333333
Indole-2-(C3HIA)	69.37833333
Quinoxaline-2-(C3HIA)	67.60166667
Benzimidazole-2-(C3HIA)	66.67166667
HIPP	59.89666667

Table 2.4: Rank-ordered scores from HINT scoring. Model conditions: (a) Rigid side chains, HSD315; (b) Rigid side chains, HSE315; (c) Flexible side chains, HSD315; (d) Flexible side chains, HSE315.

	Compound			
Rank	(a)	(b)	(c)	(d)
1	HIPP	HIPP	Quinoline-2-(C3HIA)	Indolizine-2-(C3HIA)
2	Quinoline-2-(C3HIA)	Quinoline-2-(C3HIA)	Indole-2-(C3HIA)	Quinoline-2-(C3HIA)
3	Naphthalene-2-(C3HIA)	Naphthalene-2-(C3HIA)	Naphthalene-2-(C3HIA)	Indole-2-(C3HIA)
4	Quinoxaline-2-(C3HIA)	Quinoxaline-2-(C3HIA)	Quinoxaline-2-(C3HIA)	Naphthalene-2-(C3HIA)
5	Indolizine-2-(C3HIA)	Indolizine-2-(C3HIA)	Isoquinoline-3-(C3HIA)	HIPP
6	Quinazoline-2-(C3HIA)	Quinazoline-2-(C3HIA)	Benzimidazole-2-(C3HIA)	Quinoxaline-2-(C3HIA)
7	Isoquinoline-3-(C3HIA)	Isoquinoline-3-(C3HIA)	HIPP	Quinazoline-2-(C3HIA)
8	Indole-2-(C3HIA)	Indole-2-(C3HIA)	Quinazoline-2-(C3HIA)	Benzimidazole-2-(C3HIA)
9	Benzimidazole-2-(C3HIA)	Benzimidazole-2-(C3HIA)	Indolizine-2-(C3HIA)	Isoquinoline-2-(C3HIA)
9	Benzimidazole-2-(C3HIA)	Benzimidazole-2-(C3HIA)	Indolizine-2-(C3HIA)	Isoquinoline-2-(C3HIA)
9	Benzimidazole-2-(C3HIA)	Benzimidazole-2-(C3HIA)	Indolizine-2-(C3HIA)	Isoquinoline-2-(C3HIA)

2.3.2: Results from generation of HINT scores

The top-scoring compounds (**Table 2.3**) using the CHEM-PLP scoring algorithm were also re-scored with the HINT scoring function. Only these 9 compounds were scored with HINT due to time constraints. The rank-ordered compounds from HINT scoring are shown in **Table 2.4**. In the models with rigid side chains, HIPP had the best HINT score overall. HINT scoring was inconsistent between replicates of some models, as several negative interactions were predicted. However, HINT did provide some insight in terms of potential interactions that are made between the docked compounds and residues in the active site. For example, Quinoline-2-(C3HIA) was predicted to have an acid/base interaction between its aromatic nitrogen and the hydroxyl moieties of residues Ser100 and Thr128 (**Figure 2.5**). Napthalene-2-(C3HIA) was predicted to have a stronger hydrophobic interaction with Met327 than HIPP, and Indolizine-2-(C3HIA) was predicted to form a hydrogen bond with Trp318, and an acid/base interaction with His315 in models where NE2 is protonated.

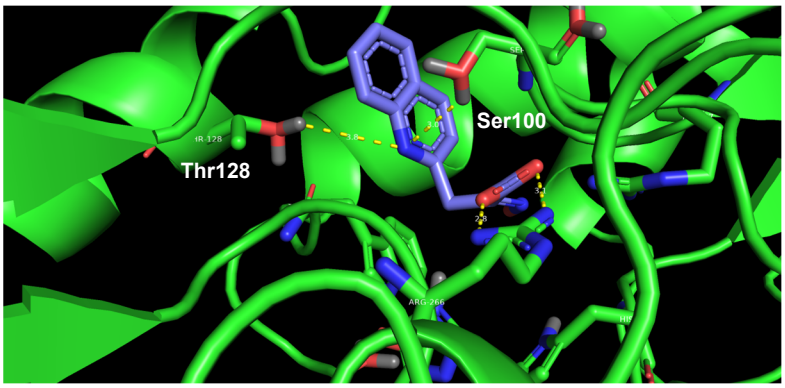

Figure 2.5: Compound **2.34** docked into the CtBP1-HIPP co-crystal structure is able to make acid/base interactions between its aromatic nitrogen and residues Thr128 and Ser100.

When we calculated the average HINT score for each compound across all models, we see that HIPP had the highest HINT score

Table 2.5*:* Average HINT Scores of each compound in models with flexible side chains.

Compound	Average HINT Score
Quinoline-2-(C3HIA)	1142.357
Indole-2-(C3HIA)	1128.879
Napthalene-2-(C3HIA)	1102.121
Quinoxaline-2-(C3HIA)	941.853
Benzimidazole-2-(C3HIA)	784.6862
HIPP	673.3669
Indolizine-2-(C3HIA)	607.114
Quinazoline-2-(C3HIA)	446.1478
Isoquinoline-3-(C3HIA)	212.8968

overall. However, if we only view the HINT scores from models with flexible side chains, there were 5 compounds that had higher HINT scores than HIPP (**Table 2.5**). Based on this data, we chose to synthesize Quinoline-2-(C3HIA) (**2.34**) and Indole-2-(C3HIA) (**2.32**) to test our model predictions.

2.3.3: Results from docking and scoring of library against CtBP in AutoDock Vina

Our compound library was docked in the co-crystal structure of CtBP1 using AutoDock Vina, which uses a gradient optimization algorithm to find the best fit for each compound. Each pose in AutoDock Vina was scored with Vina's scoring function, which

Table 2.6: Top 15 scores from docking studies in AutoDock Vina. Model conditions: (a) Rigid side chains, AM1BCC charges, His315 dually protonated; (b) Rigid side chains, AM1BCC charges, His315 D-nitrogen protonated; (c) Flexible side chains, AM1BCC charges, His315 D-nitrogen protonated; (d) Flexible side chains, CHELPG charges, His315 D-nitrogen protonated.

	Compound			
Rank	(a)	(b)	(c)	(d)
1	Pyridazine-3-(C3HIA)	Pyridazine-3-(C3HIA)	Quinoline-2-(C3HIA)	Naphthalene-2-(C3HIA)
2	HIPP	Pyridine-2-(C3HIA)	Naphthalene-2-(C3HIA)	Quinoline-2-(C3HIA)
3	Pyridine-2-(C3HIA)	Indole-2-(C2HIA)	Naphthyridine-2-(C3HIA)	Naphthyridine-2-(C3HIA)
4	Pyrrole-2-(C3HIA)	HIPP	Isoindole-1-(C3HIA)	Isoindole-1-(C3HIA)
5	Naphthalene-2-(C3HIA)	Furan-2-(C3HIA)	Quinazoline-2-(C3HIA)	HIPP
6	Quinoline-2-(C3HIA)	Pyrimidie-4-(C3HIA)	Pyridine-2-(C3HIA)	Quinazoline-2-(C3HIA)
7	Pyrazole-3-(C3HIA)	Isoxazole-5-(C3HIA)	HIPP	Pyridine-2-(C3HIA)
8	Pyrimidine-4-(C3HIA)	Naphthalene-2-(C2HIA)	Isoquinoline-3-(C3HIA)	Indole-2-(C3HIA)
9	Furan-2-(C3HIA)	Benzofuran-2-(C2HIA)	Indole-2-(C3HIA)	Isoquinoline-3-(C3HIA)
10	Triazine-2-(C3HIA)	Quinoline-2-(C3HIA)	Indazole-3-(C3HIA)	Indazole-3-(C3HIA)
11	Imidazole-4-(C4HIA)	Isoquinoline-3-(C2HIA)	Pyridazine-3-(C3HIA)	Pyridazine-3-(C3HIA)
12	Indole-2-(C3HIA)	Pyrrole-2-(C3HIA)	Naphthalene-2-(C2HIA)	Naphthalene-2-(C2HIA)
13	Isoxazole-5-(C3HIA)	Naphthalene-2-(C3HIA)	Isoquinoline-3-(C2HIA)	Isoquinoline-3-C2HIA)
14	Pyrazine-2-(C3HIA)	Pyrazine-2-(C3HIA)	Benzofuran-2-(C3HIA)	Quinoxaline-2-(C3HIA)
15	Triazole-4-(C3HIA)	Benzimidazole-2-(C2HIA)	Quinoxaline-2-(C3HIA)	Benzofuran-2-(C3HIA)

is physics-based and utilizes machine learning to predict the free energy of binding (kcal/mol).[90]

The top 15 rank-ordered compounds from the Autodock Vina docking sessions are shown in **Table 2.6**. Unlike the GOLD docking sessions, the docking scores varied greatly when comparing models with rigid versus flexible side chains. In models with rigid side chains, the top scoring compounds are monocyclic, heteroaromatic compounds. When accounting for flexible side chains in the active site, however, bicyclic heterocycles score better compared to HIPP. We also determined that compounds without the methylene group between the oxime moiety and the aromatic ring moiety do not score well in models with flexible side chains. We did not find a significant difference between models with AM1BCC charges compared to those with CHELPG charges, so we did not pursue this parameter further.

To test the accuracy of each model, we chose to synthesize Pyridazine-3-(C3HIA) (**2.35**) and Pyridine-2-(C3HIA) (**2.33**), which were the top compounds in models with rigid side chains (**Table 2.7**). The top scoring compounds in models with flexible side chains were Quinoline-2-(C3HIA) (**2.34**) and Naphthalene-2-(C3HIA) (**2.31**), which we had already planned to synthesize based on our results from GOLD and HINT.

Table 2.7: Average Vina Scores of select compounds in models with rigid side chains.

Compound	Average Vina Score
Pyridazine-3-(C3HIA)	-8.25
Pyridine-2-(C3HIA)	-8.05
HIPP	-8
Furan-2-(C3HIA)	-7.75
Pyrimidine-4-(C3HIA)	-7.75
Pyrrole-2-(C3HIA)	-7.75
Quinoline-2-(C3HIA)	-7.75
Napthalene-2-(C3HIA)	-7.7
Isoxazole-5-(C3HIA)	-7.65

In docking experiments with flexible side chains, the output files generated include not only the pose of the docked compound, but also how the side chains move to accommodate docking of the ligand. This provided us with insight for all of the catalytically active residues and how they might behave in the binding pocket. This feature seemed especially important for the residue Trp318, because it acts as a dimerization switch for CtBP that is dependent on its orientation.[23] In **Figure 2.6** it is evident that when Naphthalene-2-(C3HIA) is docked into the crystal structure, Trp318 flips its orientation to accommodate a π-stacking interaction with the naphthyl ring.

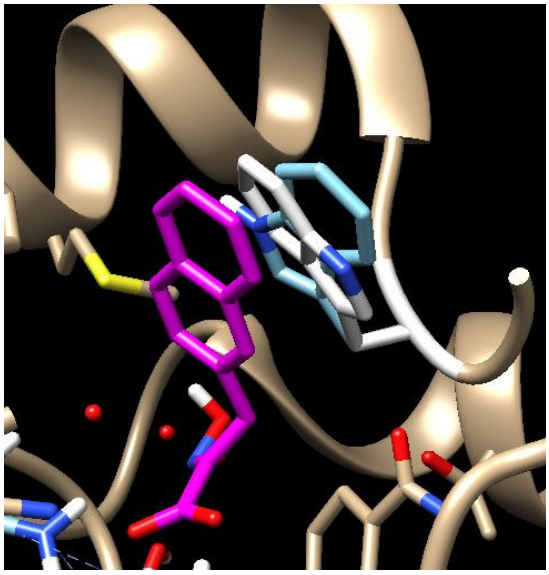

Figure 2.6: The orientation of Trp318 in the binding pocket when **2.31** (magenta) is docked into the CtBP1-HIPP co-crystal structure with rigid (white) or flexible (blue) side chains.

From this observation we made a prediction that compounds capable of flipping Trp318 would be more potent against CtBP in cells. Bicyclic heteroaromatic compounds scored better in docking sessions with flexible side chains, so we refined our hypothesis that bicyclic compounds capable of flipping Trp318 would be the most potent in cells. This gave us two factors to focus on – whether the compound was able to flip Trp318, and whether it was bicyclic or monocyclic. This provides four separate groups of compounds: bicyclic compounds that flip Trp318, bicyclic compounds that do not flip Trp318, monocyclic compounds that flip Trp318, and bicyclic compounds that do not flip Trp318. To test our hypothesis, we chose to synthesize a minimum of two compounds from each group. Of the compounds we had already selected to make based on the docking results,

Naphthalene-2-(C3HIA) (**2.31**), Indole-2-(C3HIA) (**2.32**), and Quinoline-2-(C3HIA) (**2.34**) are bicyclic compounds that flip Trp318, Pyridine-2-(C3HIA) (**2.33**) and Pyridazine-3-(C3HIA) (**2.35**) are monocyclic compounds that do not flip Trp318, and Indolizine-2-(C3HIA) (**2.36**) is bicyclic and does not flip Trp318. We decided to synthesize Pyrazole-3-(C3HIA) (**2.37**) and Pyrazine-2-(C3HIA) (**2.38**) as our two compounds that are monocyclic and do flip Trp318, and Benzofuran-2-(C3HIA) (**2.39**) as our second compound that is bicyclic but does not flip Trp318. This, along with the compound's rankings in Vina, GOLD, and HINT are shown in **Table 2.8**.

Table 2.8: Parameters of the 9 heteroaromatic HIPP analogues that were chosen for synthesis based on docking results. Docking ranks are all based on models with ND1 protonation of His315, flexible side chains, and AM1BCC charges.

Compound	Heteroaromatic Ring	Trp318 Flipped	Mono- vs Bicyclic	Vina Rank	GOLD Rank	HINT Rank
2.31	Naphthalene	Yes	Bicyclic	2	1	3
2.32	Indole	Yes	Bicyclic	9	3	2
2.33	Pyridine	No	Monocyclic	6	32	N/A
2.34	Quinoline	Yes	Bicyclic	1	5	1
2.35	Pyridazine	No	Monocyclic	11	24	N/A
2.36	Indolizine	No	Bicyclic	23	2	9
2.37	Pyrazole	Yes	Monocyclic	22	36	N/A
2.38	Pyrazine	Yes	Monocyclic	27	29	N/A
2.39	Benzofuran	No	Bicyclic	14	6	N/A

2.3.4: Results from evaluation of novel CtBP inhibitors in cells

The first compounds that were tested in cells were compounds **2.14-2.16** and **2.41**. EC_{50} values reported represent the concentration of drug compound necessary to kill 50% of the cells. In A2780 cells, or ovarian endometroid adenocarcinoma, compound **2.14** had an EC_{50} value of 139.6 μM, and **2.15** had an EC_{50} of 147.3 μM. Both of these values had a 10-fold improvement in potency compared to 4-Cl HIPP (**2.41**). These results are shown in **Figure 2.7**. Compound **2.16** did not show any improved cellular potency in comparison to 4-Cl HIPP.

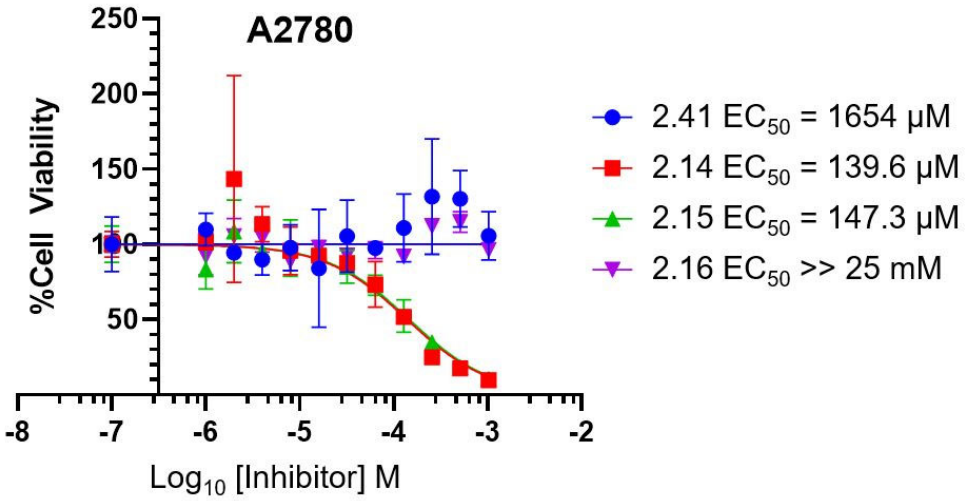

Figure 2.7: Comparisons of compounds **2.14-2.16** with 4-Cl HIPP in MTT Cell viability assay in A2780 cells.

Compounds **2.14-2.16** and **2.41** were then tested in HEY cells (**Figure 2.8**), or high grade ovarian serous adenocarcinoma. **2.14** had an EC_{50} value of 178.7 μM, while **2.15** had an EC_{50} value of 944.8 μM. Again **2.16** did not have improved cellular potency when compared to 4-Cl HIPP (**2.41**, EC_{50} = 2343 μM).

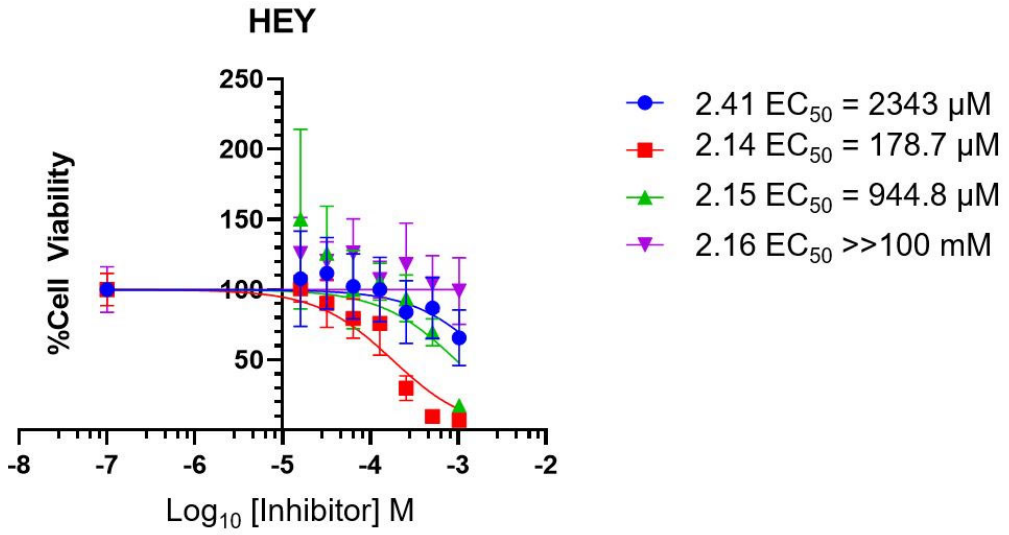

Figure 2.9: Comparisons of compounds **2.14-2.16** with 4-Cl HIPP in MTT Cell viability assay in HEY cells.

These four compounds were also tested for cell viability in Ovcar420 cells, or ovarian serous adenocarcinoma, though none of the compounds had an EC_{50} less than 1 mM (**Figure 2.9**).

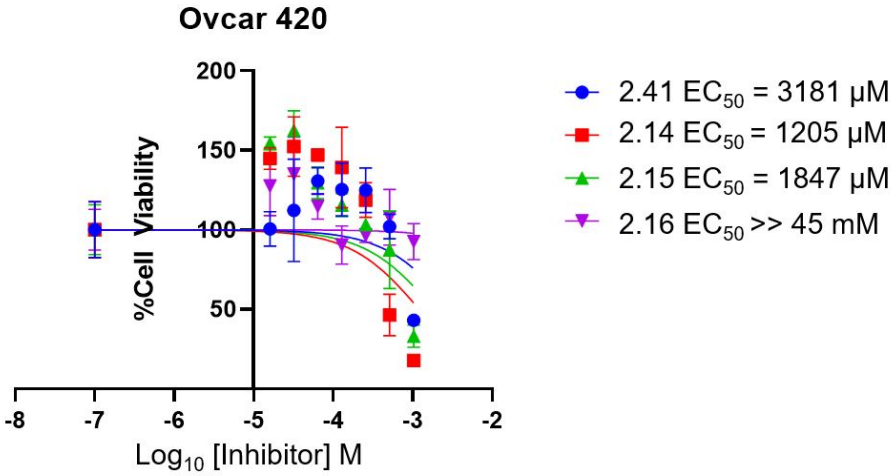

Figure 2.8: Comparisons of compounds **2.14-2.16** with 4-Cl HIPP in MTT Cell viability assay in Ovcar420 cells.

Given the initial success of **2.14** in two ovarian cancer cell lines, this compound was also tested in the MTT cell viability assay in breast and colorectal cancer cells. In HCT116 cells, **2.14** had an EC_{50} value of 65.03 µM (**Figure 2.10**). In breast cancer, **2.14**

was tested in the MTT assay in two cell lines, MCF-7 cells and MDA-MB-231 cells. MCF-7 cells are estrogen(+), progesterone(+), and HER2(-), and are used to represent hormone-dependent breast cancer. MDA-MB-231 cells are triple negative and are highly

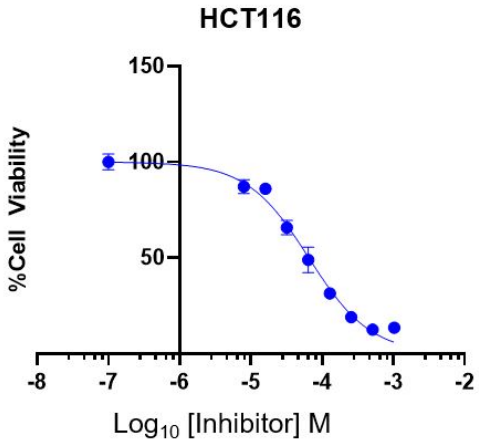

Figure 2.11: Compound **2.14** in the MTT Cell Viability assay in HCT116 cells.

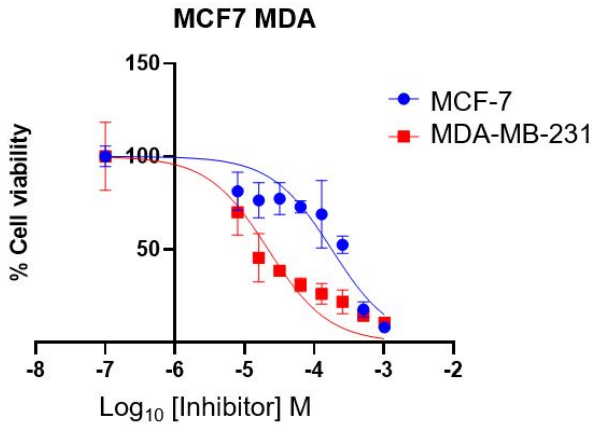

Figure 2.10: Compound **2.14** in the MTT Cell Viability assay in breast cancer cell lines.

invasive, hormone-independent breast cancer cells. **2.14** was more potent in MDA-MB-231 cells (EC_{50} = 21.88 μM) than in MCF-7 cells (EC_{50} = 179.5 μM) (**Figure 2.11**).

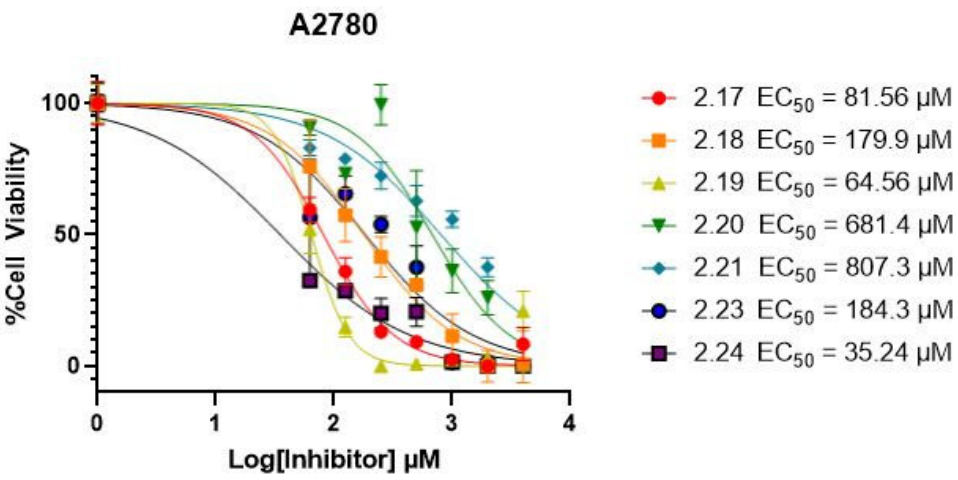

Figure 2.12: Comparisons of compounds **2.17-2.21** and **2.23-2.24** in MTT Cell viability assay in A2780 cells.

Next, compounds **2.17-2.21** and **2.23-2.24** were tested in the MTT cell viability assay in A2780, HEY, Ovcar420, and HCT116 cells. In A2780 cells (**Figure 2.12**)

compound **2.24** was the most potent, with an EC_{50} value of 35.24 μM. **2.19** demonstrated an EC_{50} of 64.56 μM and **2.17** demonstrated an EC_{50} of 81.56 μM.

In Ovcar420 cells (**Figure 2.13**), the most potent compound was **2.19**, which displayed an EC_{50} value of 92.90 μM. **2.17** exhibited an EC_{50} of 124.1 μM and **2.23** showed an EC_{50} of 117.8 μM. All of the compounds tested at EC_{50} values lower than 1 mM.

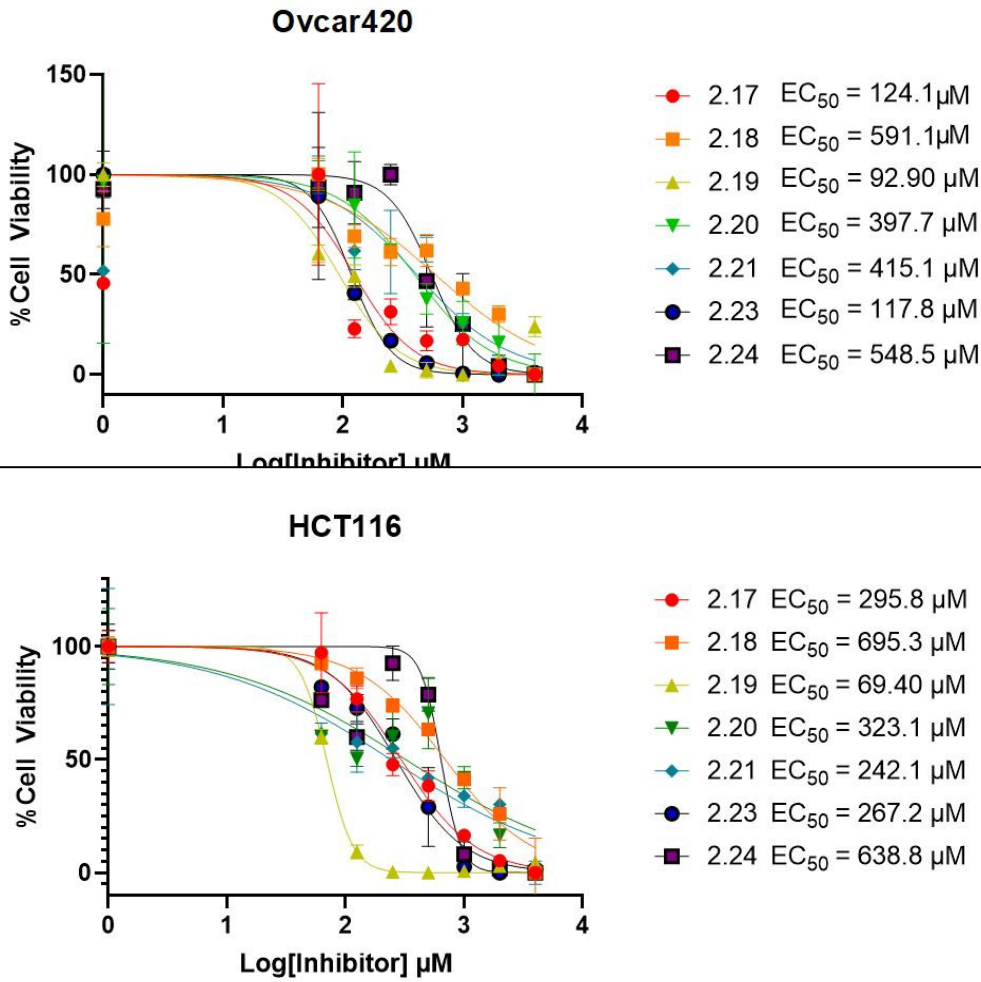

Figure 2.13: Comparisons of compounds **2.17-2.21** and **2.23-2.24** in in MTT Cell viability assay in HCT116 cells.

In HCT116 cells (**Figure 2.14**), the only compound that had an EC_{50} value less than 200 μM was **2.19**, which presented an EC_{50} of 69.40 μM.

Due to time constraints, compound **2.22** was tested in the MTT assay only in A2780 cells (**Figure 2.15**). **2.22** had an EC_{50} of 73.79 μM.

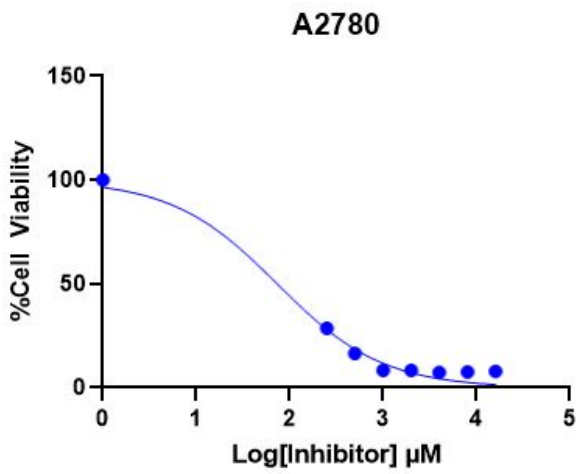

Figure 2.15: Compound **2.22** in the MTT Cell Viability assay in A2780 cells.

The MTT cell viability data for all tested compounds is summarized in **Table 2.9**.

Table 2.9: Cellular evaluation of HIPP heterocycle analogues in MTT cell viability assay. ND = not determined.

	EC_{50} (μM)					
Compound	**HCT116**	**A2780**	**HEY**	**Ovcar420**	**MCF-7**	**MDA-MB-231**
2.14	65.03	139.6	178.7	1205	179.5	21.88
2.15	ND	147.3	944.8	1847	ND	ND
2.16	ND	>>25 mM	>> 100 mM	>>45 mM	ND	ND
2.17	295.8	81.56	1279	124.1	ND	ND
2.18	695.3	179.9	3256	591.1	ND	ND
2.19	69.40	64.56	219.5	92.90	ND	ND
2.20	323.1	681.4	>>100 mM	397.7	ND	ND
2.21	242.1	807.3	>>100 mM	415.1	ND	ND
2.22	ND	73.79	ND	ND	ND	ND
2.23	267.2	184.3	1109	117.8	ND	ND
2.24	638.8	35.24	1042	548.5	ND	ND
2.41	2356	1654	2343	3181	ND	ND

Compounds **2.14**, **2.15**, and **2.17**-**2.24** were also tested in a clonogenic assay in both A2780 cells (**Figure 2.16**) and Patu8988T pancreatic cancer cells (**Figure 2.17**) to measure their ability to inhibit colony formation. The most potent compound in A2780 cells was **2.14**, which had an EC_{50} of 76.84 μM. Two other compounds demonstrated an EC_{50}

that was less than 100 μM: **2.23** (EC_{50} = 98.13 μM) and **2.24** (EC_{50} = 98.18 μM). **2.20** and **2.41** were inactive in this assay in A2780 cells.

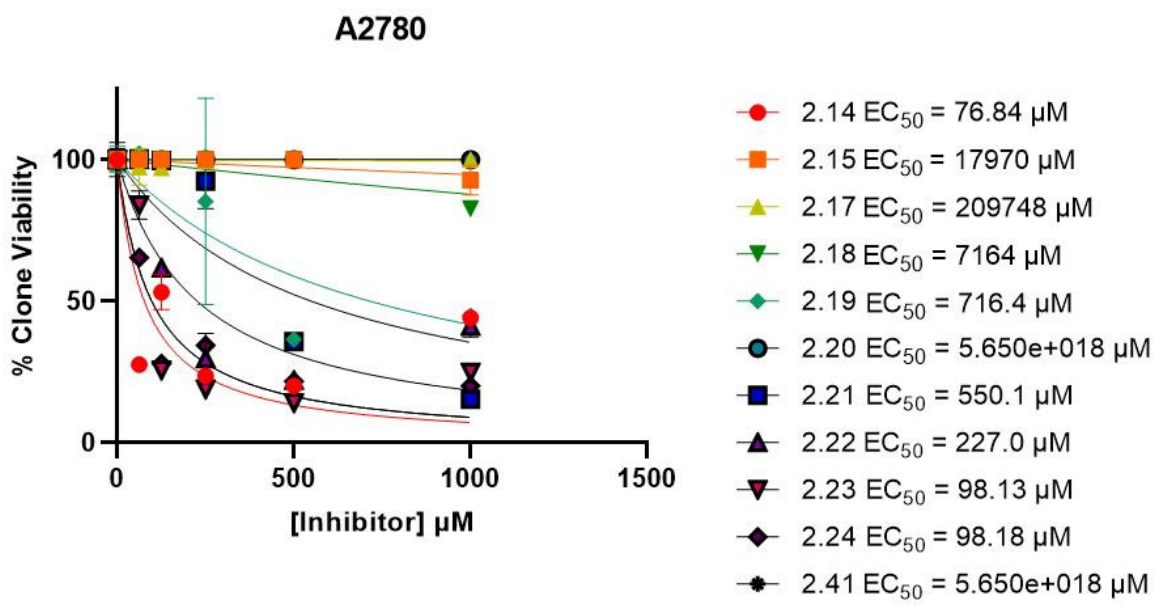

Figure 2.16: Comparisons of compounds **2.14**, **2.15**, and **2.17-2.24** with 4-Cl HIPP in clonogenic assay in A2780 cells.

The most potent compound in Patu8988T cells was **2.19**, which had an EC_{50} value of 135.6 μM. One other compound exhibited an EC_{50} less than 200 μM, **2.24** (EC_{50} = 199.4 μM). Compounds **2.15**, **2.16**, **2.20**, **2.21**, and **2.41** were inactive in Patu8988T cells. The clonogenic assay data for all compounds tested is shown in **Table 2.10**.

Table 2.10: Cellular evaluation of HIPP heterocycle analogues in clonogenic assays to determine their ability to inhibit colony formation.

	EC_{50} (μM)	
Compound	A2780	Patu8988T
2.14	76.84	269.1
2.15	17970	5.650e+018
2.17	209748	5.65e+018
2.18	7164	411.1
2.19	716.4	135.6
2.20	5.65e+018	5.650e+018
2.21	550.1	5.650e+018
2.22	227.0	249.5
2.23	98.13	1979
2.24	98.18	199.4
2.41	5.650e+018	5.650e+018

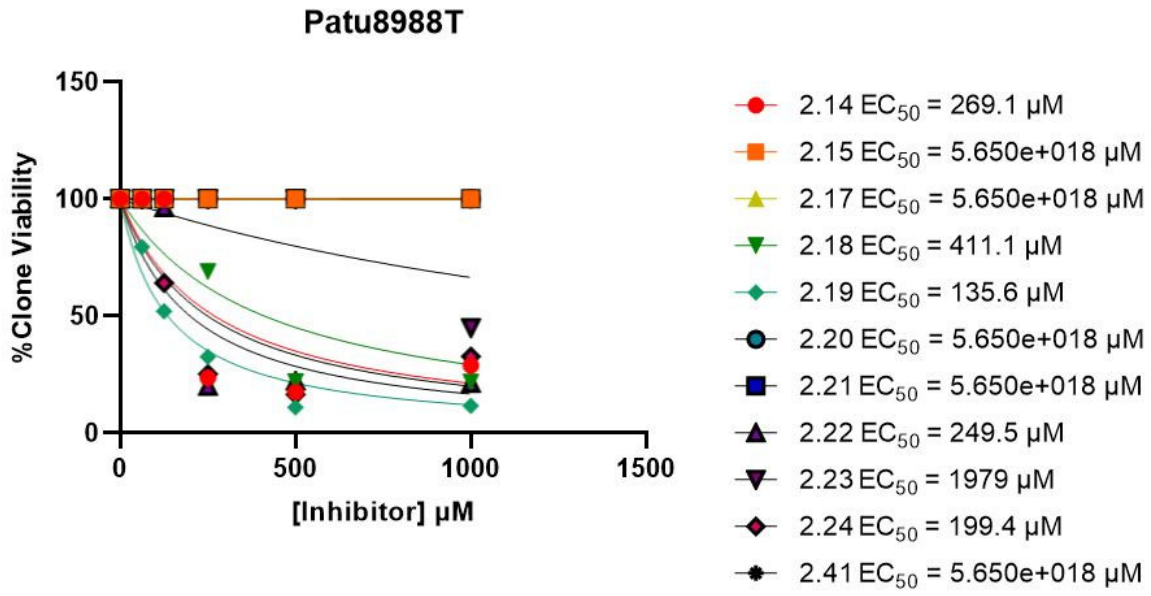

Figure 2.17: Comparisons of compounds **2.14**, **2.15**, and **2.17-2.24** with 4-Cl HIPP in clonogenic assay in Patu8988T cells.

2.3.5: Results from isothermal titration calorimetry

In order to investigate the validity of our modeling results and determine which model best predicts the binding affinity of the docked compounds, we employed ITC to measure the thermodynamics for binding of compounds **2.31**-**2.41** to CtBP2 at pH 7.5. We chose to perform the experiments at pH 7.5 because previously published work by our collaborators indicated that HIPP had greater affinity to CtBP1 at this pH, as opposed

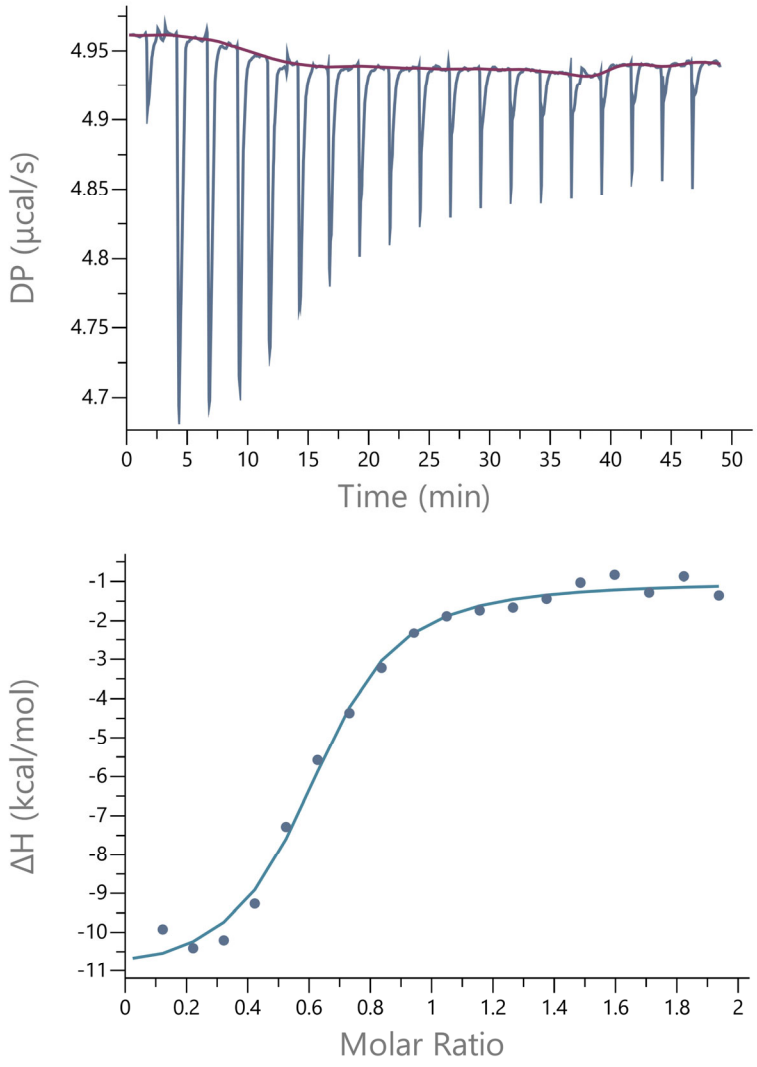

Figure 2.18: Example of a single ITC experiment utilizing HIPP (**2.40**) with CtBP2 wt (31-364) truncated at pH 7.5.

to pH 8.5.[87] Initial experiments measured the dissociation constant of HIPP (**2.40**) as 1.51 μM (**Figure 2.18**). This is comparable to the previously reported K_d of 1.30 μM.[87]

Utilizing the same conditions as when we measured the dissociation constant of HIPP (**2.40**), we next performed ITC experiments with **2.41** where the measured K_d was 310 nM (**Figure 2.19**). This is the first time that 4-Cl HIPP has undergone ITC with either CtBP1 or CtBP2.

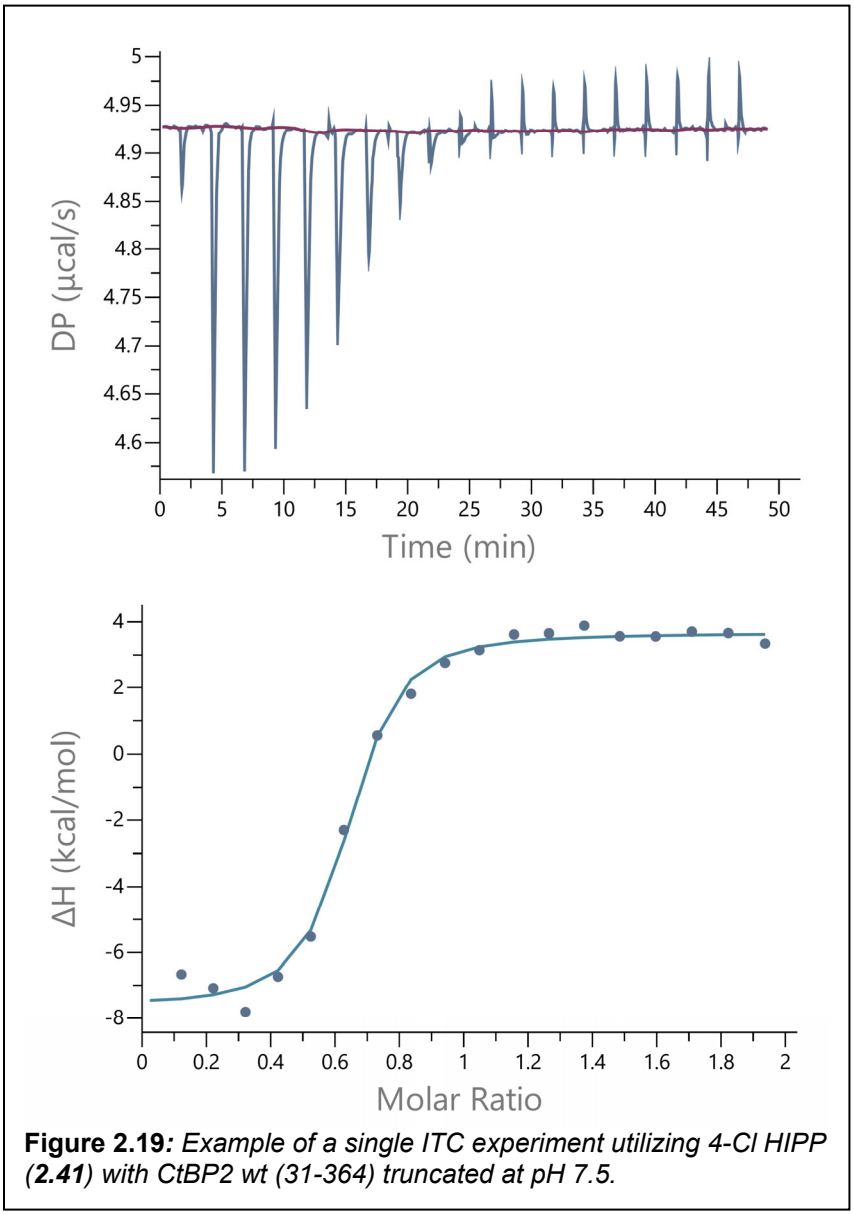

Figure 2.19*: Example of a single ITC experiment utilizing 4-Cl HIPP (**2.41**) with CtBP2 wt (31-364) truncated at pH 7.5.*

We next performed ITC experiments with our HIPP heteroaromatic analogues. The measured K_d of **2.31** binding to CtBP2 was 1.09 μM (**Figure 2.20**).

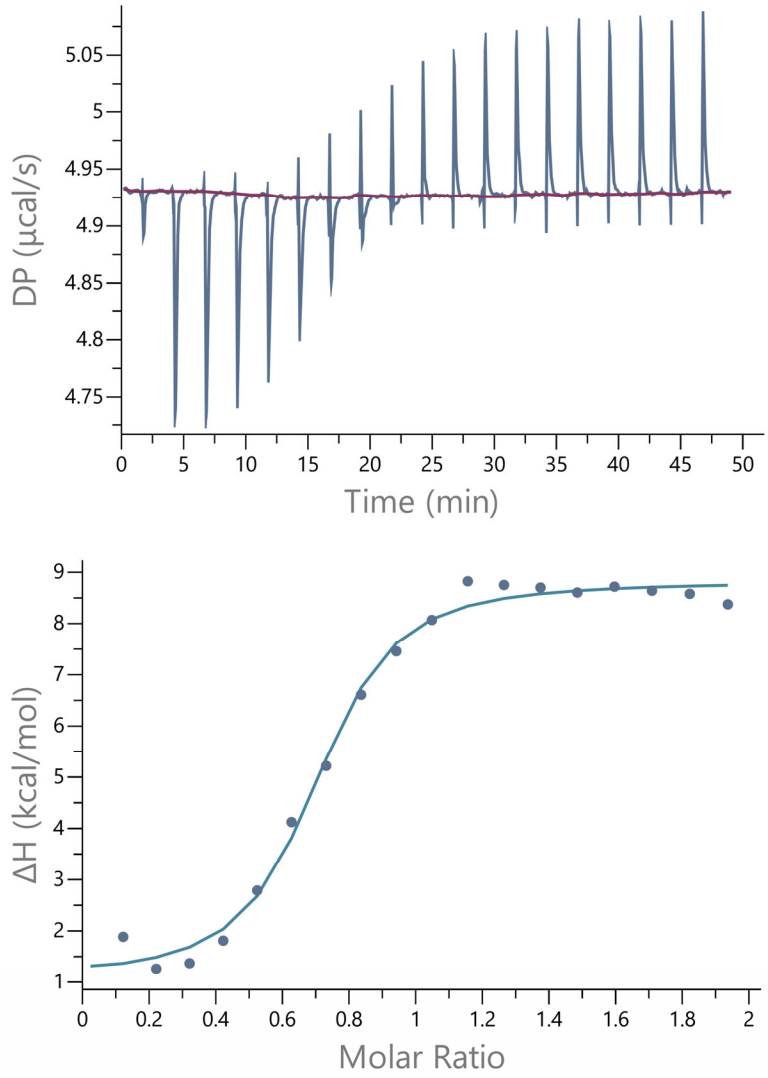

Figure 2.20: Example of a single ITC experiment utilizing Naphthalene-2-(C3HIA) (**2.31**) with CtBP2 wt (31-364) truncated at pH 7.5.

Compound **2.32** had a measured dissociation constant of 11.2 μM (**Figure 2.21**).

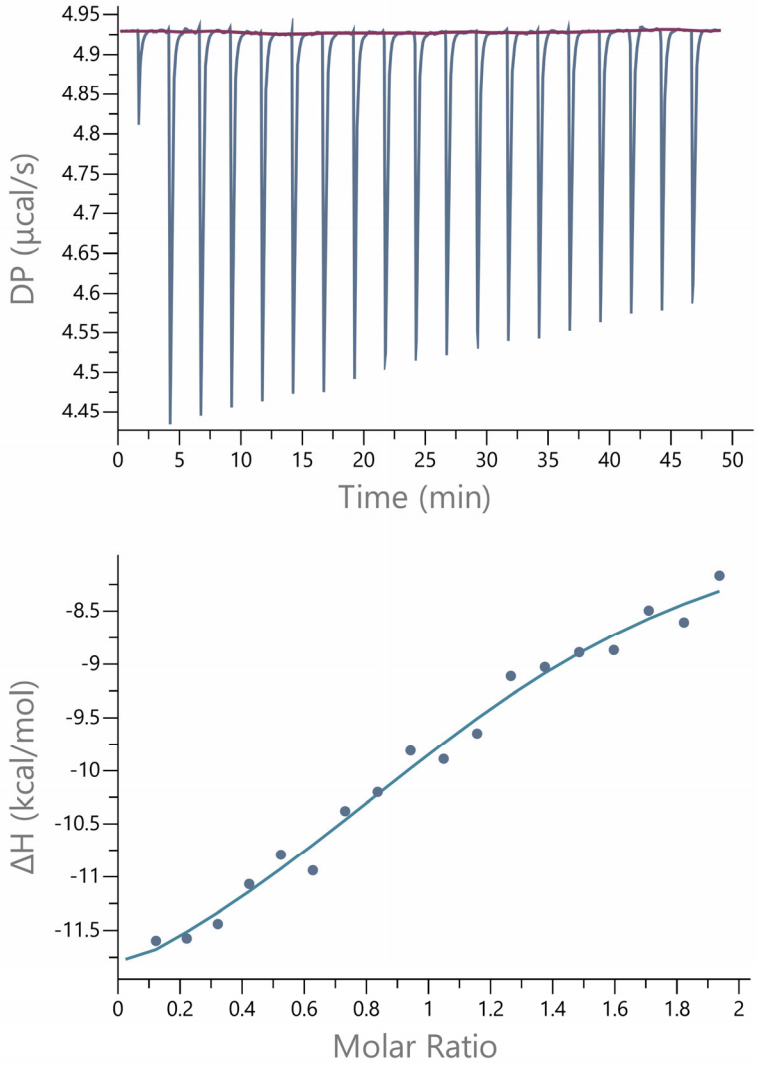

Figure 2.21: Example of a single ITC experiment utilizing Indole-2-(C3HIA) (**2.32**) with CtBP2 wt (31-364) truncated at pH 7.5.

Compound **2.33** had a measured dissociation constant of 204 μM (**Figure 2.22**).

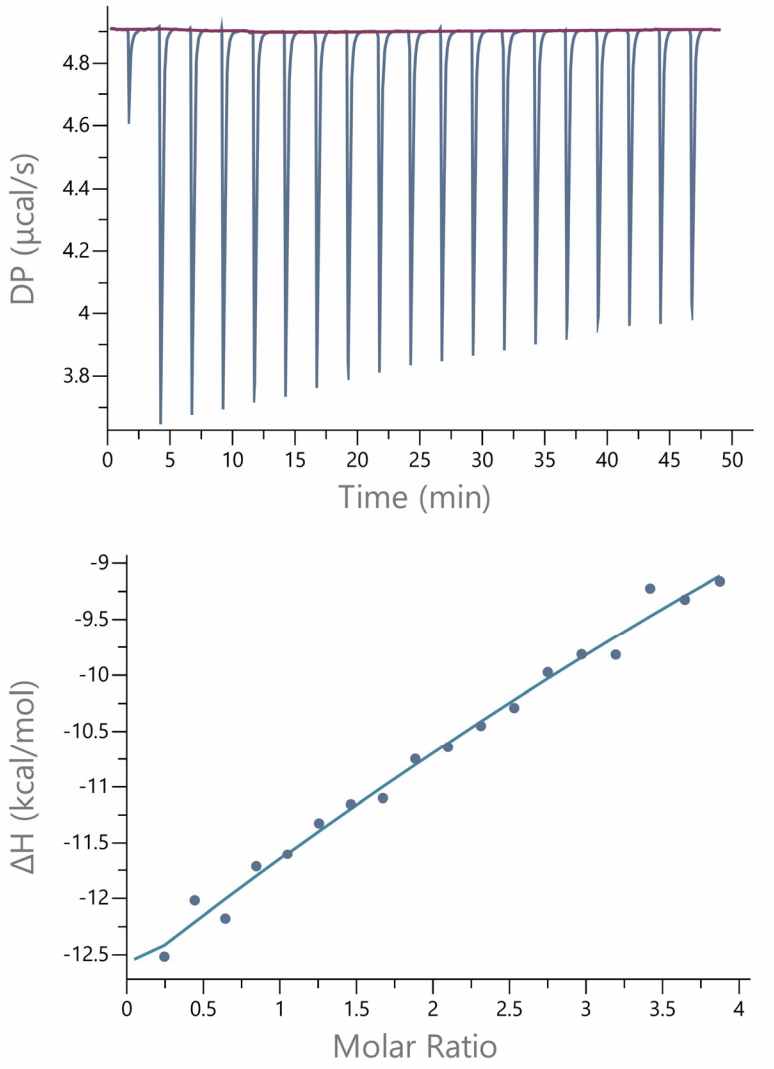

Figure 2.22: Example of a single ITC experiment utilizing Pyridine-2-(C3HIA) (2.33) with CtBP2 wt (31-364) truncated at pH 7.5.

Compound **2.34** had a measured dissociation constant of 46.0 μM (**Figure 2.23**).

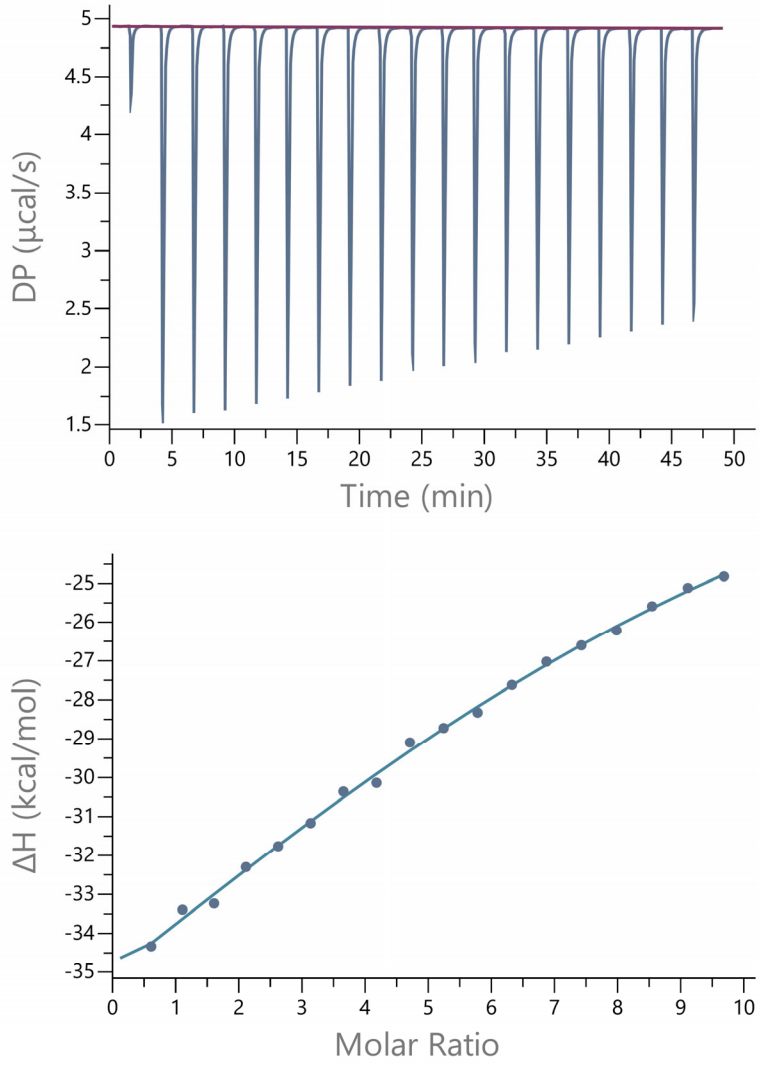

Figure 2.23: Example of a single ITC experiment utilizing Quinoline-2-(C3HIA) (2.34) with CtBP2 wt (31-364) truncated at pH 7.5.

Compound **2.35** had a measured dissociation constant of 439 μM (**Figure 2.24**).

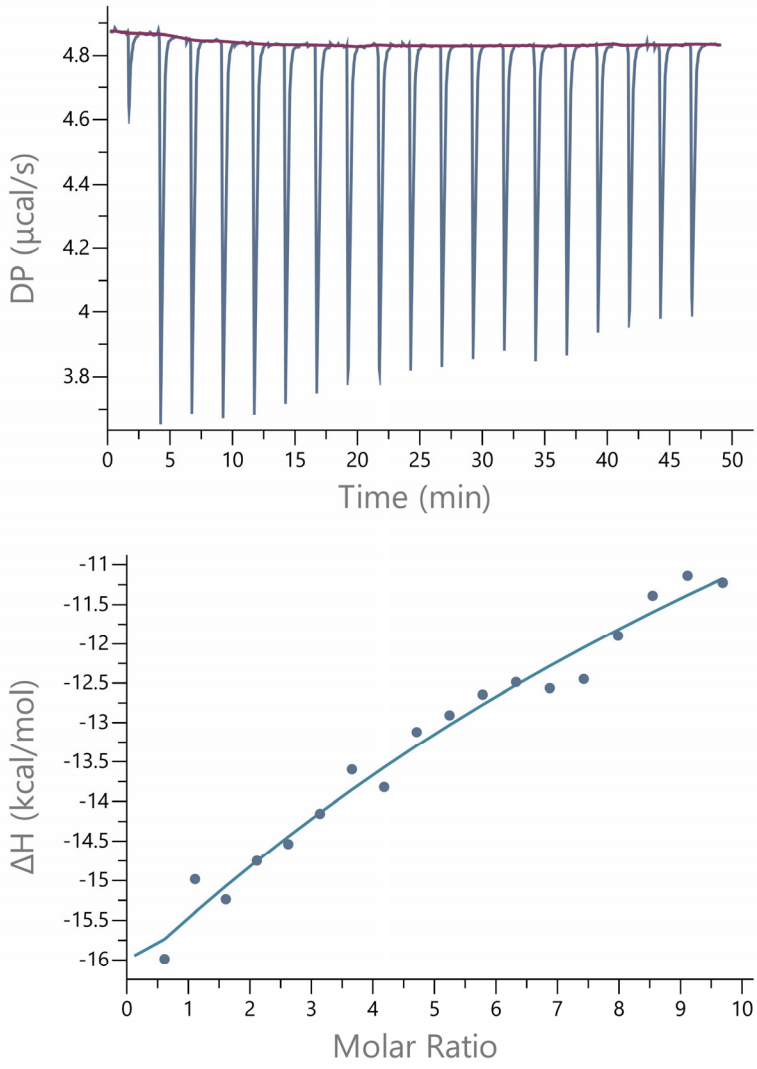

Figure 2.24: Example of a single ITC experiment utilizing Pyridazine-3-(C3HIA) (**2.35**) with CtBP2 wt (31-364) truncated at pH 7.5.

Compound **2.36** had a measured dissociation constant of 37.8 μM (**Figure 2.25**).

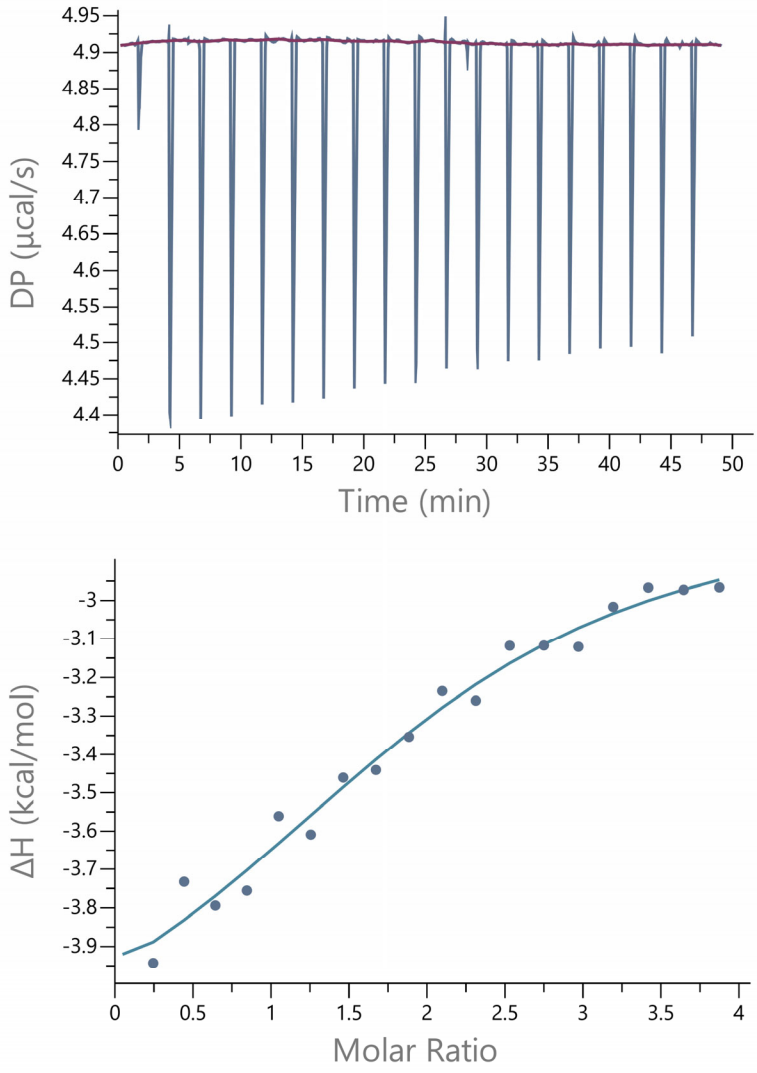

Figure 2.25: Example of a single ITC experiment utilizing Indolizine-2-(C3HIA) (**2.36**) with CtBP2 wt (31-364) truncated at pH 7.5.

Compound **2.37** had a measured dissociation constant of 60.0 μM (**Figure 2.26**).

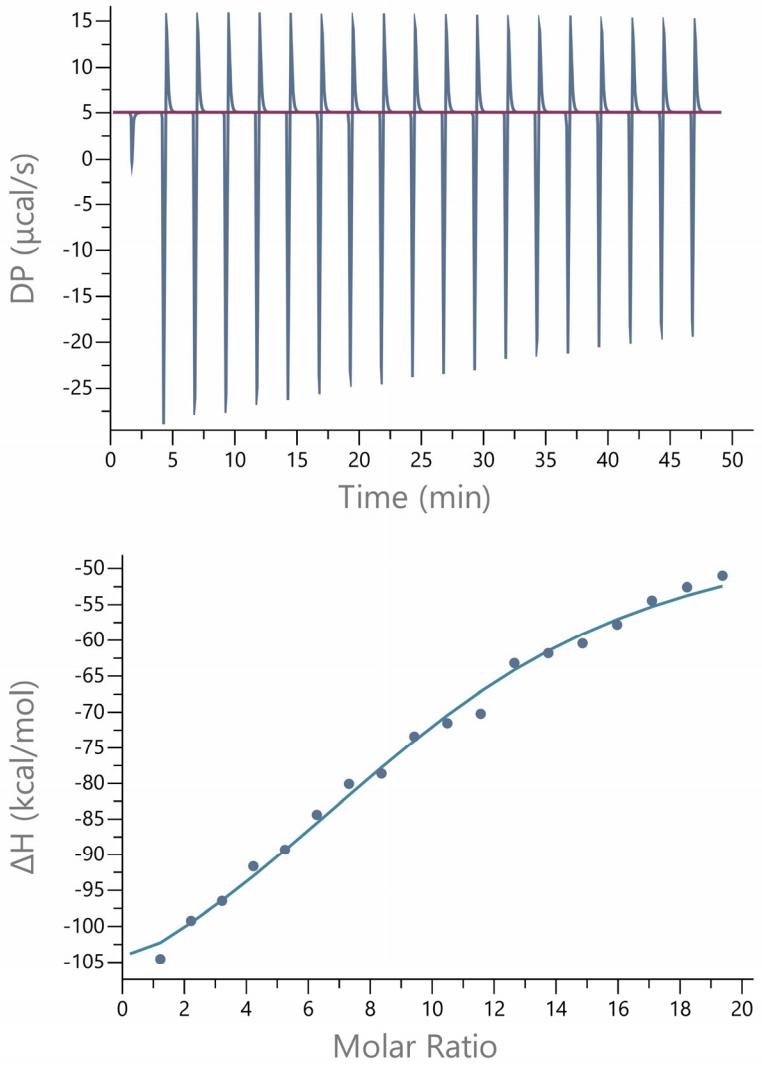

Figure 2.26: Example of a single ITC experiment utilizing Pyrazole-3-(C3HIA) (**2.37**) with CtBP2 wt (31-364) truncated at pH 7.5.

Compound **2.38** had a measured dissociation constant of 50.9 μM (**Figure 2.27**).

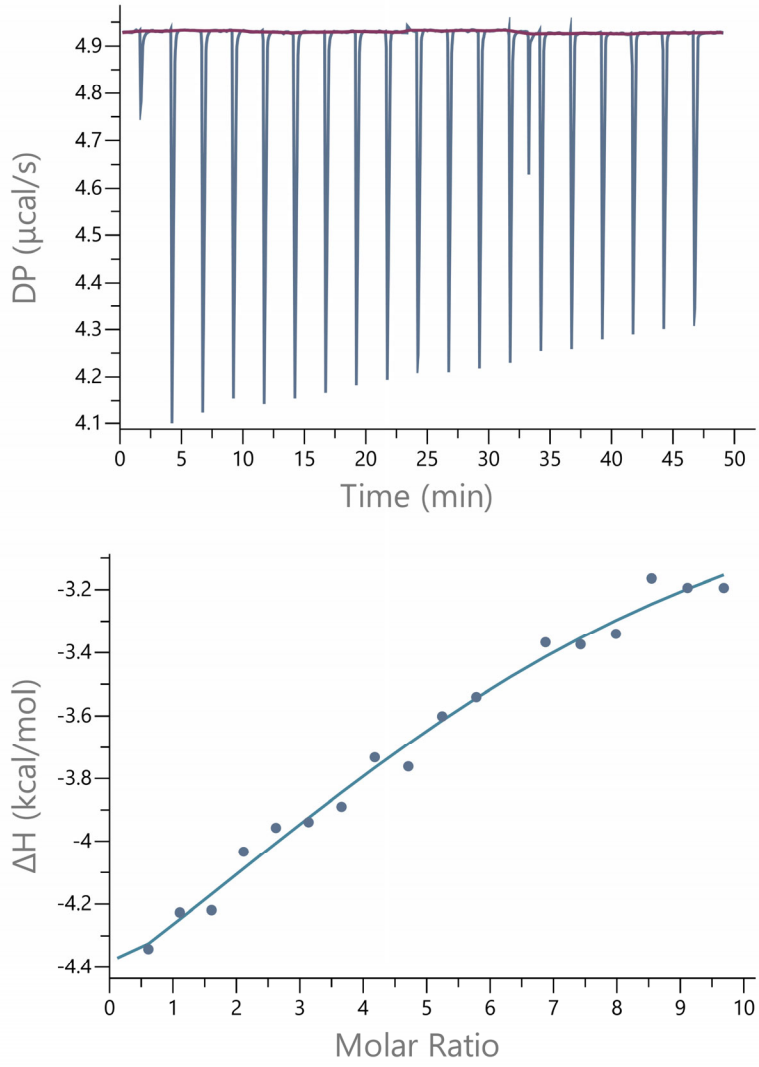

Figure 2.27*:* Example of a single ITC experiment utilizing Pyrazine-2-(C3HIA) (**2.38**) with CtBP2 wt (31-364) truncated at pH 7.5.

Of the heteroaromatic analogues, **2.39** had the most affinity for binding to CtBP2 with a K_d of 940 nM (**Figure 2.28**).

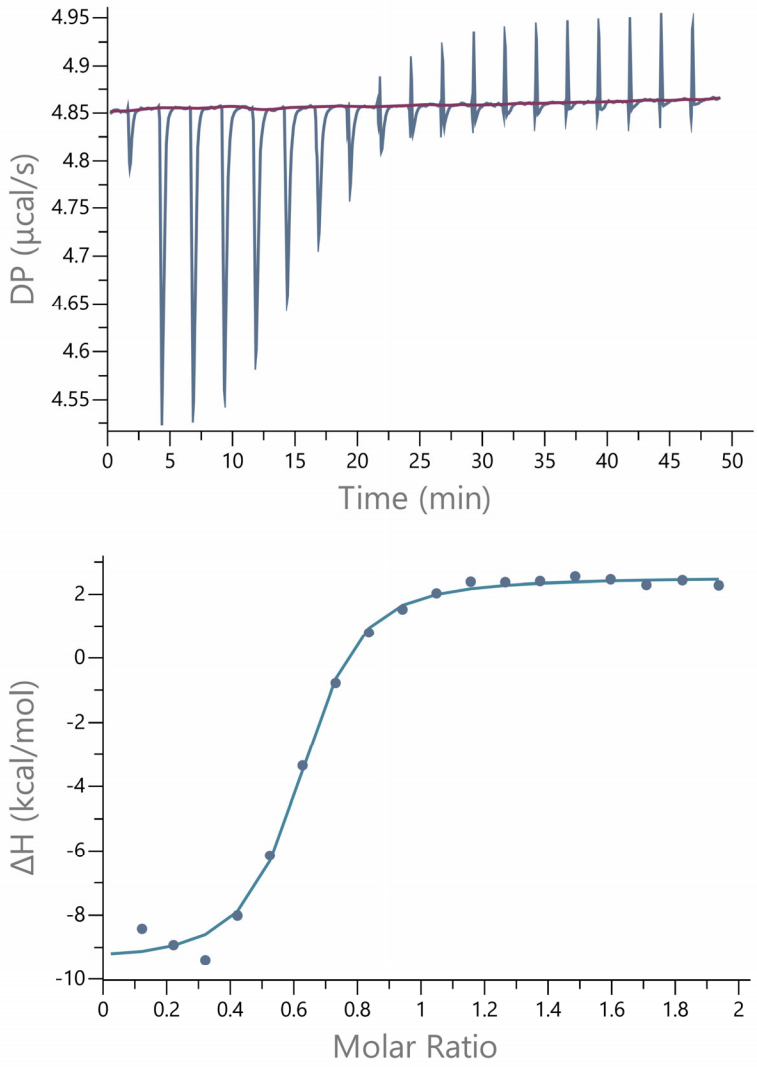

Figure 2.28: Example of a single ITC experiment utilizing Benzofuran-2-(C3HIA) (**2.39**) with CtBP2 wt (31-364) truncated at pH 7.5.

The full ITC results are provided in **Table 2.11**.

Table 2.11: Thermodynamic parameters for Ligand binding to CtBP2 Derived from ITC Measurements. Values reported represent the average of four measurements, unless otherwise noted.

Compound	pH	K_d	ΔG (kcal)	ΔH (kcal mol^{-1})	-TΔS (kcal mol^{-1})
2.31[a]	7.5	1.09 ± 0.63 μM	-8.42	-12.74 ± 3.35	4.3
2.32	7.5	11.2 ± 3.33 μM	-6.85	-1.28 ± 5.86	-5.6
2.33	7.5	204 ± 29.2 μM	-5.06	-6.3 ± 16.5	1.3
2.34	7.5	46.0 ± 7.90 μM	-5.94	-0.55 ± 10.7	-6.5
2.35	7.5	439 ± 25.8 μM	-4.59	4.08 ± 32.2	-8.7
2.36	7.5	37.9 ± 7.68 μM	-6.09	3.98 ± 9.34	-10
2.37[b]	7.5	60.0 ± 30.2 μM	-5.85	-49.8 ± 30.2	44
2.38	7.5	50.9 ± 14.8 μM	-5.93	1.63 ± 1.49	-7.6
2.39[a]	7.5	0.94 ± 0.34 μM	-8.50	-15.80 ± 1.85	7.3
2.40	7.5	1.51 ± 0.24 μM	-7.97	-12.00 ± 0.72	4.0
2.41	7.5	0.31 ± 0.07 μM	-8.93	-12.85 ± 0.87	3.9

[a]Five measurements. [b]Two Measurements.

2.3.6: Discussion

A small library (36 total) of substrate-competitive inhibitors of CtBP1/2 were designed *in silico*. These inhibitors involved replacement of the phenyl ring of HIPP with different heteroaromatic ring systems, with the goal of forming a stronger π-stacking interaction with Trp318 and a potential hydrogen bond interaction with His315. Each of these compounds was docked into the CtBP1-HIPP co-crystal structure utilizing AutoDock Vina and GOLD, and the docking interactions were scored in the corresponding scoring functions, as well as by HINT. From our docking results, 9 compounds were selected to be synthesized, both as a carboxylic acid for ITC (**2.31**-**2.39**), and as an ethyl ester for cellular assays (**2.14**-**2.22**). Each compound was synthesized as described in *Section 2.2.4*. Each compound was confirmed by HRMS, and purity was confirmed by analytical, reversed-phase HPLC.

The modeling serves to predict the binding affinity of the heteroaromatic HIPP analogues to CtBP. Logically, to test our model's predictions we measured the binding affinity (dissociation constant) of each compound with ITC. In our ITC experiments, the

compound that had the most affinity to CtBP2 was 4-Cl HIPP (**2.41**), which had an average K_d of 310 nM. This corresponds nicely with the cell viability data obtained, where its ester derivative **2.24** had an EC_{50} of 35.24 μM in the MTT assay in A2780 cells. Further, previous work done by our lab indicated that 4-Cl HIPP is able to inhibit CtBP's dehydrogenase activity with an IC_{50} of 180 nM.[68] However, it is interesting to note that **2.24** was not as potent in other cell lines.

Of the heteroaromatic HIPP analogues, two compounds had a better binding affinity than HIPP (**2.40**): **2.31** (Naphthalene-2-(C3HIA)) and **2.39** (Benzofuran-2-(C3HIA)). **2.31** had an average K_d of 1.09 μM. This corresponds well to the cell data reported, where the naphthyl ester derivative **2.14** (EC_{50} = 139.6 μM) had a 1.3-fold greater potency in the MTT assay in A2780 cells when compared to the HIPP ester (**2.23**, EC_{50} = 184.3 μM). Further, compound **2.39** had the most affinity for CtBP2 of all of the heteroaromatic analogues, with an average measured K_d of 940 nM. This also corresponds to the MTT cell viability assay in A2780 cells, where the benzofuranyl ester derivative **2.22** had an EC_{50} of 73.79 μM. All of the other compounds that underwent ITC experiments had higher dissociation constants than HIPP.

From the ITC experiments alone, one can infer that nitrogen-containing ring systems do not show affinity for CtBP when compared to HIPP, and bicyclic rings have higher affinity for CtBP than monocyclic rings. Further, bicyclic rings that do not contain nitrogen (i.e. naphthalene and benzofuran) have more affinity for CtBP than HIPP, but less affinity than 4-Cl HIPP. When we take into account the predicted binding affinity from our modeling data, all models with flexible side chains predicted that **2.31** would have greater affinity for CtBP than HIPP. However, only the models in GOLD predicted that

2.39 would have greater affinity than HIPP. However, the models in GOLD also predicted that compounds **2.32**, **2.34**, and **2.36** would have more affinity for CtBP than HIPP and this was not the case. 4-Cl HIPP was run through the models in AutoDock Vina as an exploratory study, and it was not predicted to have better affinity than HIPP in any of these models. This leads us to believe that the models in GOLD are more accurate, but should be further refined to better predict binding affinity.

However, we cannot make a definitive conclusion about whether the CHEM-PLP scoring function is more accurate than the HINT scoring function, because not all compound interactions were scored with HINT. Further, 4-Cl HIPP (**2.41**) was not modeled in GOLD, nor was its interaction scored with either the CHEM-PLP scoring function or the HINT scoring function. It would be interesting to see the HINT scores for CtBP's interactions with **2.39** and **2.41**, and which interactions are predicted to be stronger than those in HIPP. **2.31** was predicted by HINT to have a more hydrophobic interactions with Met327 than HIPP through the naphthalene ring; if the benzofuran ring was also predicted to have more hydrophobic interactions with this residue then perhaps this residue is more important for substrate binding to CtBP than was previously thought. Some studies have suggested that this methionine residue is implicated in substrate specificity of other D2-HDHs.[34]

In terms of the orientation of Trp318, **2.31** was predicted to flip Trp318 in AutoDock Vina, but **2.39** was not (**Table 2.12**). This leads us to believe that while this Trp residue is important for binding, perhaps AutoDock Vina is not equipped to predict its orientation. Though in the case of monocyclic heterocycles, the compounds that did flip Trp318, **2.37** and **2.38**, did have better affinity for CtBP2 than the two monocyclic compounds that did

not flip Trp318, **2.33** and **2.35**. Crystallography should be performed with **2.31**, **2.39**, and **2.41** to compare the orientation of Trp318 as well as other residues in CtBP's binding pocket with the HIPP-CtBP1 co-crystal structure.

Table 2.12: Parameters of the 9 heteroaromatic HIPP analogues that were chosen for synthesis based on docking results.

Compound (Ester/Acid)	Heteroaromatic Ring	Trp318 Flipped	Mono- vs Bicyclic	K_d (μM)	A2780 EC_{50} (μM)
2.14/2.31	Naphthalene	Yes	Bicyclic	1.09 ± 0.63	139.6
2.15/2.32	Indole	Yes	Bicyclic	11.2 ± 3.33	147.3
2.16/2.33	Pyridine	No	Monocyclic	204 ± 29.2	>>25 mM
2.17/2.34	Quinoline	Yes	Bicyclic	46.0 ± 7.90	81.56
2.18/2.35	Pyridazine	No	Monocyclic	439 ± 25.8	179.9
2.19/2.36	Indolizine	No	Bicyclic	37.9 ± 7.68	64.56
2.20/2.37	Pyrazole	Yes	Monocyclic	60.0 ± 30.2	681.4
2.21/2.38	Pyrazine	Yes	Monocyclic	50.9 ± 14.8	807.3
2.22/2.39	Benzofuran	No	Bicyclic	0.94 ± 0.34	73.79

One could make the assertion that because the ITC experiments were performed with CtBP2, while the docking studies were done with CtBP1, this could explain the disparity between docking results and ITC results. A K_d of HIPP binding to CtBP2 at pH 7.5 has not been reported, though at pH 8.5 HIPP has a reported dissociation constant of 1.30 μM. Further, HIPP has a lower reported dissociation constant with CtBP1 at pH 7.5 of 370 nM, but at pH 8.5 HIPP has more affinity for CtBP2 than CtBP1 (K_d at pH 8.5 = 2.77 μM).

Another limitation to the ITC experiments is that for compounds with higher K_d values than HIPP, saturation of protein was not reached. This means that the measured K_d values for compounds **2.32**-**2.38** are not as accurate, though it is clear that these compounds bind to CtBP with less affinity than HIPP. ITC experiments should be repeated with these compounds utilizing higher concentrations of protein and inhibitor to reach total saturation of CtBP. This was not performed because of time constraints and lack of protein necessary to repeat these experiments.

We showed that by changing the acid on 4-Cl HIPP to an ethyl ester (**2.24**), we can improve the cellular potency by almost 50-fold in A2780 cells with an EC_{50} of 35.24 μM. It was also shown that by replacing the carboxylic acid on HIPP with an ethyl ester in HCT116 cells increases its potency 15-fold. This shows that part of the previous disparity between *in vitro* inhibition and cellular inhibition of CtBP for HIPP, 4-Cl HIPP and 3-Cl HIPP is due to cell permeability (i.e., the ethyl ester is more cell permeable than the carboxylic acid).

Compounds **2.14**-**2.24** underwent an MTT cell viability assay in several cell lines to confirm activity of each compound. In A2780 cells, all of the compounds aside from **2.16** were found to be more potent than 4-Cl HIPP. When comparing these compounds to the 4-Cl HIPP ester **2.24**, however, none of the compounds had greater potency. The HIPP ethyl ester, **2.23** had an EC_{50} of 184.3 μM. Compounds **2.14**, **2.15**, **2.17**, **2.19**, and **2.22** were more active than **2.23**, but less active than **2.24**. Compound **2.18** had a similar EC_{50} to **2.23** at 179.9 μM, and compounds **2.20** and **2.21** were less active than **2.23**, but more active than 4-Cl HIPP. Only compound **2.16** was inactive in A2780 cells.

In HEY ovarian cancer cells, the most potent compound in the MTT assay was **2.14**, which displayed an EC_{50} of 178.7 μM. This is a 13-fold improvement in potency compared to 4-Cl HIPP. Compound **2.19** was the next most potent with an EC_{50} of 219.5 μM. Compounds **2.15**, **2.17**, **2.23**, and **2.24** had EC_{50} values of approximately 1 mM. Compound **2.18** had an EC_{50} of approximately 3 mM, and compounds **2.16**, **2.20**, and **2.21** were inactive in HEY cells. **2.22** was not tested in this cell line.

In Ovcar420 cells, the most potent compound was **2.19**, which demonstrated an EC_{50} in the MTT assay of 92.90 μM. All of the compounds performed better in this cell

line compared to **2.41**. Interestingly, **2.17**, **2.20**, **2.21** and **2.23** all had greater potency than **2.24** (EC_{50} = 548.5 μM). **2.18** had a comparable potency to **2.24** with an EC_{50} of 591.1 μM. Compounds **2.14** and **2.15** were less potent than **2.24** with EC_{50} values between 1-2 mM, and **2.16** was inactive in this cell line. **2.22** was not tested in this cell line.

In HCT116 cells, the most potent compounds were **2.14** (EC_{50} = 65.03 μM) and **2.19** (EC_{50} = 69.40 μM). All of the tested compounds were more potent than **2.41**. Compounds **2.17**, **2.20**, **2.21**, and **2.23** were more potent than the 4-Cl HIPP ester **2.24**. Compound **2.18** was slightly less potent than **2.24**, and compounds **2.15**, **2.16**, and **2.22** were not tested in this cell line.

We also found that **2.14** is more potent in MDA-MB-231 (triple negative) cells than in MCF-7 (ER+, PR+, HER2-) cells. This makes sense, because the MDA-MB-231 cell line expresses CtBP1/2 at slightly higher concentrations than the MCF-7 cell line.[49] Further, in a CtBP gene depletion study, it was found that depletion of CtBP derepresses a substantially larger portion of CtBP-targeted genes in MDA-MB-231 cells than MCF-7 cells.[51] Loss of CtBP has also been shown to have a greater effect on mitotic fidelity in MDA-MB-231 cells than in MCF-7 cells.[95]

From the MTT cell viability data collected, we can deduce that A2780 cells are the most sensitive to treatment with our compounds when compared with the other ovarian cancer cell lines. To date, the expression levels of CtBP in A2780, HEY, and Ovcar420 cells have not been compared, so one cannot say for certain if A2780 cells are more dependent on CtBP than other cells. However, there has been some evidence that

CtBP1/2 expression is more elevated in high grade serous ovarian cancer (HGSOC) than in other ovarian cancers.[52,54]

There are some limitations to the MTT assays performed. Not all of the compounds were tested in all of the cell lines; only A2780 cells were utilized with all of the inhibitors. **2.22** was only tested in A2780 cells but no other cell lines due to time constraints. Only **2.14** was tested in the two breast cancer cell lines. Further, MTT assays were performed at different concentrations as shown in **Table 2.1**. The MTT cell viability assay should be repeated with all of the compounds utilizing the same concentrations of inhibitor in at least two of the cell lines to see if these values correspond better to the ITC experimental data.

Compounds **2.14**, **2.15**, **2.17**-**2.24** and **2.41** were also tested in a clonogenic assay to measure their ability to inhibit colony formation in two cell lines. In A2780 cells, the most potent compounds were **2.14** (EC_{50} = 76.84 μM), **2.23** (EC_{50} = 98.13 μM), and **2.24** (EC_{50} = 98.18 μM). Compound **2.22** was less potent though it did inhibit some colony formation (EC_{50} = 227.0 μM). **2.19** and **2.21** displayed EC_{50} values less than 1 mM, and the rest of the compounds were inactive. In Patu8988T cells, the most potent compounds were **2.19** (EC_{50} = 135.6 μM), **2.24** (EC_{50} = 199.4 μM), **2.22** (EC_{50} = 249.5 μM), and **2.14** (EC_{50} = 269.1 μM). Compound **2.18** demonstrated an EC_{50} of 411.1 μM, and the rest of the compounds were inactive in this cell line. Compound **2.16** was not tested in either clonogenic assay.

One limitation to this project is that neither cell viability assay measures whether or not inhibition of CtBP is the reason for cell death. These compounds could be causing decreased cell viability for other reasons that are independent of CtBP. For instance, **2.17** and **2.19** showed much higher K_d values than **2.14** and **2.22** in ITC experiments, but

comparable or lower EC_{50} values in some of the cellular assays performed. To determine if these compounds are able to inhibit CtBP's dehydrogenase activity, *in vitro* assays with recombinant CtBP should be performed to measure on-target activity. These compounds should also be tested for their ability to inhibit recombinant lactate dehydrogenase (LDH) *in vitro* to measure off-target inhibition of other dehydrogenases. Further, these compounds should be tested in a noncancerous cell line, such as epithelial cells or fibroblasts, to determine whether they are toxic to all cells or only cancer cells.

Finally, we made the assumption that the binding pockets in CtBP1 and CtBP2 are equal. It is possible that **2.17** and **2.19** are selective for CtBP1 over CtBP2, and this would explain the discrepancy between the ITC results and the MTT cell viability assay results. For example, HIPP has a reported K_d with CtBP1 of 370 nM,[87] and we measured the K_d of HIPP with CtBP2 to be 1.51 μM. HIPP has greater affinity for CtBP1 than CtBP2 at both pH 7.5 and pH 8.5;[87] this could be the case for other compounds as well. ITC experiments should be repeated with CtBP1 to determine whether binding affinity is improved. This would also allow us to confirm our modeled predictions as all of our docking experiments utilized CtBP1.

2.3.7: Chemistry Experimental Data

General Chemical Methods

Reagents/chemicals, catalysts, solvents were purchased from Sigma-Aldrich, Fisher, Oakwood, AstaTech Inc., Alfa-Aesar and Enamine. Analytical Thin Layer Chromatography (TLC) was performed using silica gel GHLF plates (Analtech Inc.). Automated MPLC was performed on TELEDYNE ISCO CombiFlash® Rf instrument using RediSep Rf Normal-phase Flash Columns (4-gm, 12-gm, 24-gm, or 40-gm) with

gradients of either Hexanes/Ethyl Acetate or Dichloromethane/Methanol. ^{1}H NMR and ^{13}C NMR experiments were recorded on BRUKER 600MHz NMR instrument in deuterated solvents – chloroform ($CDCl_3$), dimethyl sulfoxide ($(CD_3)_2SO$) or deuterium oxide (D_2O). All chemical shifts are reported in parts per million (ppm) with reference to chloroform, DMSO, and H_2O residual peaks at 7.26, 2.50 and 4.80 respectively (^{1}H NMR spectra); 77.16 and 39.52 respectively (^{13}C NMR spectra). The data is reported as: chemical shifts (ppm), multiplicity (s = singlet, d = doublet, t = triplet, q = quartet, m = multiplet), coupling constant(s) (Hz) and integral values.

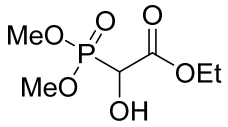

Ethyl 2-(dimethoxyphosphoryl)-2-hydroxyacetate (**2.1**): In an oven-dried, 100 mL round-bottom flask, dimethyl phosphite (1.38 mL, 15 mmol, 1 eq) was dissolved in anhydrous dichloromethane (12.5 mL, 1.2 M) under nitrogen at -78°C. Ethyl 2-oxoacetate (1.49 mL, 15 mmol, 1 eq) and triethylamine (0.42 mL, 3 mmol, 0.2 eq) were added dropwise sequentially. The reaction was stirred at -78°C for 1 h. The reaction mixture was then purified using an automated CombiFlash MPLC system (silica gel, 5% methanol/dichloromethane), followed by pumping down overnight on high-vac to yield the product as a white solid (2 g, 63% yield). ^{1}H NMR (600 MHz, $CDCl_3$) δ 4.59-4.56 (m, 1H), 4.40-4.34 (m, 2H), 3.89-3.86 (m, 6H), 1.35 (t, *J* = 7.14, 3H). ^{13}C NMR (150 MHz, $CDCl_3$) δ 169.24, 68.99, 67.95, 62.91, 54.24, 54.19, 53.88, 53.83, 13.95. HRMS ESI^{+} $C_6H_{13}O_6P$ $[M+Na]^{+}$ Expected: 235.0342, Found: 235.0338.

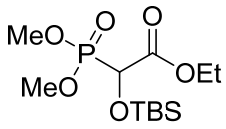

Ethyl 2-((tert-butyldimethylsilyl)oxy)-2-(dimethoxyphosphoryl)acetate (**2.2**): In an oven-dried, 100 mL round-bottom flask, ethyl 2-(dimethoxyphosphoryl)-2-hydroxyacetate (2 g, 9.4 mmol, 1 eq) was dissolved in anhydrous dichloromethane under nitrogen at room temperature. Imidazole (4.1 g, 28.2 mmol, 3 eq), 4-dimethylaminopyridine (172.26 mg, 1.41 mmol, 0.15 eq), and *tert*-butyldimethylsilyl chloride (2.83 g, 18.8 mmol, 2 eq) were added as solids sequentially. The reaction mixture was allowed to stir at room temperature for 18 h. The reaction was then washed with saturated sodium bicarbonate (38.3 mL). The organic layer was then dried with sodium sulfate and filtered. The filtrate was then concentrated *in vacuo* and purified using an automated CombiFlash MPLC system (silica gel, 50% ethyl acetate/hexanes), followed by pumping down overnight on high vac to yield the product as a colorless oil (2.6 g, 85% yield). ^{1}H NMR (600 MHz, $CDCl_3$) δ 4.62 (d, *J* = 18.06, 1H0, 4.31-4.24 (m, 2H), 3.84 (t, *J* = 10.44, 6H), 1.31 (t, J = 7.14, 3H), 0.93 (s, 9H), 0.12 (d, *J* = 6.36, 6H). ^{13}C NMR (150 MHz, $CDCl_3$) δ 168.43, 168.41, 71.15, 70.07, 61.85, 54.14, 54.10, 54.08, 54.03, 25.54, 18.37, 14.10, -5.34, -5.50. HRMS ESI$^+$ $C_{12}H_{27}O_6PSi$ $[M+H]^+$ Expected: 327.1387, Found: 327.1376.

Synthesis of Heterocyclic HIPP analogues intermediates:

General Procedure 1: In an oven-dried, 50-mL round bottom flask, ethyl 2-((tert-butyldimethylsilyl)oxy)-2-(dimethoxyphosphoryl)acetate (**2.2**, 326.4 mg, 1 mmol, 1 eq) was dissolved in tetrahydrofuran (0.39 M) and added dropwise to a stirring solution of lithium bis(trimethylsilyl)amide in THF (1.1 mL, 1M, 1.1 mmol, 1.1 eq) at 60°C. After

stirring for 30 minutes, the corresponding aldehyde (1.5 eq) was dissolved in tetrahydrofuran (0.59 M) and added dropwise to the reaction mixture. The reaction was then stirred under reflux for 15 h at 60°C. The reaction mixture was then quenched with saturated aqueous ammonium chloride and diluted with ethyl acetate. The quenched reaction mixture was washed with saturated ammonium chloride (3x), water (3x), and saturated sodium chloride (3x). The organic phase was then dried with sodium sulfate and filtered. The filtrate was then concentrated *in vacuo* and purified using an automated CombiFlash MPLC system (silica gel, ethyl acetate/hexanes), followed by pumping down overnight to yield the pure product.

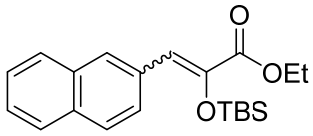

Ethyl 2-((tert-butyldimethylsilyl)oxy)-3-(naphthalen-2-yl)acrylate (**2.3**): Procedure 1 was followed using 2-naphthaldehyde (234.27 mg, 1.5 mmol) in THF (5.13 mL). Yield 57% (202.6 mg, 0.57 mmol). ^{1}H NMR (600 MHz, $CDCl_3$) δ 8.26 (s, 1H), 7.81-7.74 (m, 6H), 7.70 (s, 1H), 7.47-7.44 (m, 3H), 7.37 (d, *J* = 8.4, 1H), 7.02 (s, 1H), 6.56 (s, 1H), 4.31 (q, *J* = 7.14, 2H), 4.13 (q, *J* = 7.14, 1H), 1.54 (s, 1H), 1.39 (t, *J* = 7.14, 3H), 1.09 (t, *J* = 7.14, 2H), 1.02 (s, 5H), 0.99 (s, 9H), 0.27 (s, 4H), 0.16 (s, 6H). ^{13}C NMR (150 MHz, $CDCl_3$) δ 165.55, 165.12, 142.51, 140.95, 133.23, 133.16, 132.96, 132.47, 132.17, 131.75, 129.25, 128.17, 127.86, 127.61, 127.57, 127.55, 127.27, 126.99, 126.27, 126.14, 126.04, 125.85, 120.17, 118.83, 61.36, 60.97, 25.87, 25.62, 18.67, 18.33, 14.33, 13.80, -3.84, -4.69 HRMS ESI^{+} $C_{21}H_{28}O_3Si$ $[M+Na]^{+}$ Expected: 379.1700, Found: 379.1683.

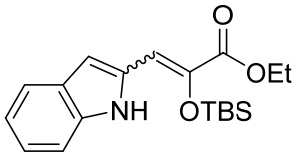

Ethyl 2-((tert-butyldimethylsilyl)oxy)-3-(1H-indol-2-yl)acrylate (**2.4**): Procedure 1 was followed using 1*H*-indole-2-carbaldehyde (217.74 mg, 1.5 mmol) in THF (5.13 mL). Yield 34% (117.6 mg, 0.34 mmol). ^{1}H NMR (600 MHz, $CDCl_3$) δ 11.33 (br s, 1H), 9.42 (br s, 1H), 7.60 (d, *J* = 7.92, 1H), 7.57 (d, *J* = 7.92, 1H), 7.40 (d, *J* = 8.16, 1H), 7.31 (d, *J* = 8.04, 1H), 7.23-7.19 (m, 2H), 7.11-7.06 (m, 2H), 6.96 (s, 1H), 6.63-6.56 (m, 3H), 4.36 (q, *J* = 7.14, 2H), 4.30 (q, *J* = 7.14, 2H), 1.12-1.37 (m, 6H), 1.07 (s, 9H), 1.01 (s, 8H), 0.31 (s, 6H), 0.21 (s, 5H). ^{13}C NMR (150 MHz, $CDCl_3$) δ 166.08, 164.71, 138.86, 136.96, 136.91, 136.55, 132.67, 131.33, 127.82, 127.75, 123.23, 123.08, 120.69, 120.36, 119.95, 119.70, 117.93, 111.32, 110.47, 110.13, 108.51, 105.78, 61.48, 61.32, 25.95, 25.49, 18.70, 18.12, 14.19, 14.01, -3.79, -4.86. HRMS ESI$^+$ $C_{19}H_{27}NO_3Si$ $[M+Na]^+$ Expected: 368.1652, Found: 368.1638.

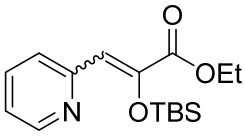

Ethyl 2-((tert-butyldimethylsilyl)oxy)-3-(pyridin-2-yl)acrylate (**2.5**): Procedure 1 was followed using 2-pyridine carboxaldehyde (500 mg, 4.67 mmol) in THF (15.95 mL). Yield 46% (443.9 mg, 1.44 mmol). ^{1}H NMR (600 MHz, $CDCl_3$) δ 8.61-8.60 (m, 1H), 8.48-8.47 (m, 1H), 8.03 (d, *J* = 7.98, 1H), 7.67-7.64 (m, 1H), 7.56 (m, 1H), 7.17-7.13 (m, 2H), 7.07-7.05 (m, 1H), 7.03 (s, 1H), 6.19 (s, 1H), 4.28 (q, *J* = 7.14, 2H), 4.22 (q, *J* = 7.14, 1H), 1.35 (t, *J* = 7.14, 3H), 1.22 (t, *J* = 7.14, 2H), 0.98 (s, 6H), 0.94 (s, 9H), 0.26 (s, 4H), 0.17 (s, 6H). ^{13}C NMR (150 MHz, $CDCl_3$) δ 165.64, 165.20, 153.96, 153.85, 149.52, 148.97,

146.51, 142.96, 135.83, 135.68, 125.11, 122.93, 122.10, 121.27, 118.80, 115.02, 61.58, 61.08, 25.93, 25.81, 25.66, 25.52, 18.68, 18.24, 14.22, 13.85, -3.88, -4.66. HRMS ESI$^+$ $C_{16}H_{25}NO_3Si$ $[M+H]^+$ Expected: 308.1676, Found: 308.1691.

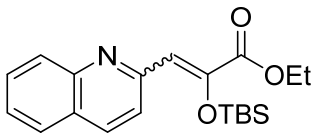

Ethyl 2-((tert-butyldimethylsilyl)oxy)-3-(quinolin-2-yl)acrylate (**2.6**): Procedure 1 was followed using quinoline-2-carbaldehyde (235.76, 1.5 mmol) in THF (5.13 mL). Yield 54% (194.5 mg, 0.54 mmol). ^{1}H NMR (600 MHz, $CDCl_3$) δ 10.25 (s, 1H), 8.34 (d, *J* = 8.34, 1H), 8.27 (d, *J* = 8.46, 1H), 8.17 (d, *J* = 8.58, 1H), 8.13 (d, *J* = 8.58, 1H), 8.06 (t, *J* = 7.44, 1H), 7.93 (d, *J* = 8.22, 1H), 7.85 (t, *J* = 7.65, 1H), 7.80 (d, *J* = 8.04, 1H), 7.71 (t, *J* = 7.59, 1H), 7.53 (t, *J* = 7.41, 1H), 7.27 (s, 1H), 7.21 (s, 1H), 4.32 (q, *J* = 7.08, 2H), 1.38 (t, *J* = 7.08, 3H), 0.97 (s, 9H), 0.18 (s, 6H). ^{13}C NMR (150 MHz, $CDCl_3$) δ 193.80, 165.23, 154.52, 152.63, 148.19, 147.97, 144.04, 137.42, 135.50, 130.52, 130.46, 130.10, 129.58, 129.34, 129.23, 127.89, 127.46, 127.09, 126.56, 122.85, 119.04, 117.39, 61.71, 25.83, 18.72, 14.29, -3.88. HRMS ESI$^+$ $C_{20}H_{27}NO_3Si$ $[M+H]^+$ Expected: 358.1833, Found: 358.1833.

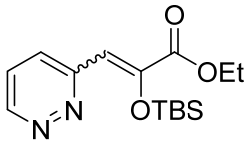

Ethyl 2-((tert-butyldimethylsilyl)oxy)-3-(pyridazin-3-yl)acrylate (**2.7**): Procedure 1 was followed using pyridazine-3-carbaldehyde (251.87, 2.33 mmol) in THF (7.95 mL). Yield 36% (173.3 mg, 0.56 mmol). ^{1}H NMR (600 MHz, $CDCl_3$) δ 8.89 (d, *J* = 4.14, 1H), 7.70-7.67 (m, 1H), 7.64 (d, *J* = 8.82, 1H), 7.58 (d, *J* = 9.72, 1H), 6.62 (s, 1H), 4.67 (q, *J* = 7.08, 2H), 4.62 (q, *J* = 7.08, 1H), 1.72-1.67 (m, 4H), 1.56 (s, 1H), 1.26-1.22 (s, 3H), 0.51 (s, 1H), 0.31 (s, 2H). ^{13}C NMR (150 MHz, $CDCl_3$) δ 164.04, 163.64, 157.40, 145.80, 128.98,

128.23, 127.31, 125.56, 115.18, 94.73, 61.97, 61.93, 25.86, 25.83, 14.21, -3.75, -5.37. HRMS ESI$^+$ $C_{15}H_{24}N_2O_3Si$ $[M+Na]^+$ Expected: 331.1448, Found: 331.1441.

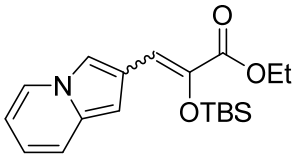

Ethyl 2-((tert-butyldimethylsilyl)oxy)-3-(indolizin-2-yl)acrylate (**2.8**): Procedure 1 was followed using indolizine-2-carbaldehyde (**2.26**, 54.5 mg, 0.375 mmol) in THF (1.28 mL). Yield 45% (38.54 mg, 0.11 mmol). ^{1}H NMR (600 MHz, $CDCl_3$) δ 7.80 (br s, 1H), 7.64 (s, 1H), 7.27 (d, *J* = 9, 1H), 7.24 (d, *J* = 6.72, 1H), 6.97 (s, 1H), 6.62 (s, 1H). 6.60-6.56 (m, 1H), 6.53 (s, 1H), 6.46 (s, 1H), 6.43-6.38 (m, 1H), 4.29-4.24 (m, 2H), 1.35-1.32 (m, 3H), 1.24 (s, 1H), 0.99 (d, *J* = 11.34, 9H), 0.19 (d, *J* = 5.46, 6H). ^{13}C NMR (150 MHz, $CDCl_3$) δ 165.57, 164.92, 139.33, 139.07, 132.59, 132.40, 124.83, 124.77, 122.03, 121.28, 119.16, 118.93, 117.74, 117.13, 117.11, 114.15, 114.09, 113.95, 110.78, 110.65, 101.40, 100.58, 61.03, 60.74, 29.70, 29.37, 26.07, 25.67, 22.70, 18.70, 18.29, 14.36, 14.20, 14.12, -3.40, -4.73. HRMS ESI$^+$ $C_{19}H_{27}NO_3Si$ $[M+Na]^+$ Expected: 368.1652, Found: 368.1650.

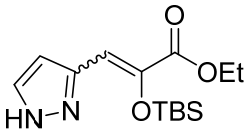

Ethyl 2-((tert-butyldimethylsilyl)oxy)-3-(1H-pyrazol-3-yl)acrylate (**2.9**): Procedure 1 was followed using 1*H*-pyrazole-3-carbaldehyde (144.14 mg, 1.5 mmol) in THF (5.13 mL). Yield 42% (125.3 mg, 0.42 mmol). ^{1}H NMR (600 MHz, $CDCl_3$) δ 12.66 (br s, 1H), 7.56 (s, 1H), 6.37 (s, 1H), 6.30 (s, 1H), 4.33 (q, *J* = 6.96, 2H), 1.60 (br s, 2H), 1.37 (t, *J* = 6.96, 3H), 0.98 (s, 9H), 0.19 (s, 6H). ^{13}C NMR (150 MHz, $CDCl_3$) δ 165.77, 139.87, 139.61,

112.56, 109.31, 61.92, 25.55, 18.24, 14.08, -4.75. HRMS ESI$^+$ $C_{14}H_{24}N_2O_3Si$ $[M+H]^+$ Expected: 297.1629, Found: 297.1621.

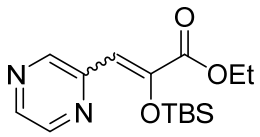

Ethyl 2-((tert-butyldimethylsilyl)oxy)-3-(pyrazin-2-yl)acrylate (**2.10**): Procedure 1 was followed using pyrazine-2-carbaldehyde (162.15 mg, 1.5 mmol) in THF (5.13 mL). Yield 25% (76.6 mg, 0.25 mmol). ^{1}H NMR (600 MHz, $CDCl_3$) δ 9.23 (s, 1H), 8.56 (s, 1H), 8.39 (s, 1H), 6.95 (s, 1H), 4.31 (q, *J* = 7.08, 2H), 1.64-1.58 (m, 2H), 1.37 (t, *J* = 7.08, 3H), 0.96 (s, 9H), 0.20 (s, 6H). ^{13}C NMR (150 MHz, $CDCl_3$) δ 164.61, 150.14, 146.32, 144.46, 144.25, 142.28, 115.42, 61.88, 25.76, 18.72, 14.21, -3.84. HRMS ESI$^+$ $C_{15}H_{24}N_2O_3Si$ $[M+H]^+$ Expected: 309.1629, Found: 309.1620.

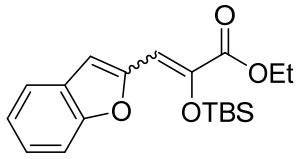

Ethyl 3-(benzofuran-2-yl)-2-((tert-butyldimethylsilyl)oxy)acrylate (**2.11**): Procedure 1 was followed using 2-benzofurancarboxaldehyde (219.23 mg, 1.5 mmol) in THF (5.13 mL). Yield 57% (197.3 mg, 0.57 mmol). ^{1}H NMR (600 MHz, $CDCl_3$) δ 7.56 (d, *J* = 7.74, 1H), 7.45 (d, *J* = 8.22, 1H), 7.30-7.27 (m, 1H), 7.22 (t, *J* = 7.41, 1H), 7.05 (s, 1H), 6.90 (s, 1H), 4.29 (q, *J* = 7.14, 2H), 1.37 (t, *J* = 7.14, 3H), 1.05 (s, 9H), 0.27 (s, 6H). ^{13}C NMR (150 MHz, $CDCl_3$) δ 164.70, 154.65, 151.96, 141.21, 128.73, 124.90, 122.93, 121.09, 111.06, 108.43, 107.80, 61.55, 25.89, 25.52, 18.82, 14.28, -3.62, -4.72. HRMS ESI$^+$ $C_{19}H_{26}O_4Si$ $[M+Na]^+$ Expected: 369.1493, Found: 369.1478.

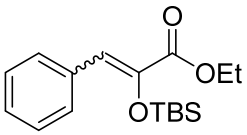

Ethyl 2-((tert-butyldimethylsilyl)oxy)-3-phenylacrylate (**2.12**): Procedure 1 was followed using benzaldehyde (0.38 mL, 3.75 mmol) in THF (12.8 mL). Yield 50% (381.3 mg, 1.24 mmol). ^{1}H NMR (600 MHz, $CDCl_3$) δ 7.28-7.25 (m, 3H), 7.23-7.20 (m, 3H), 6.40 (s, 1H), 4.10 (q, *J* = 7.14, 2H), 1.11 (t, *J* = 7.14, 3H), 0.98 (s, 9H), 0.22 (s, 6H). ^{13}C NMR (150 MHz, $CDCl_3$) δ 165.19, 142.36, 134.85, 129.98, 128.82, 128.25, 128.05, 127.23, 120.37, 61.04, 25.95, 25.75, 18.44, 13.90, -4.60. HRMS ESI$^+$ $C_{17}H_{26}O_3Si$ $[M+Na]^+$ Expected: 329.1543, Found: 329.1534.

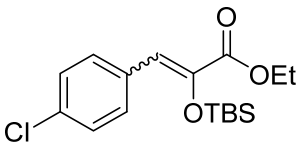

Ethyl 2-((tert-butyldimethylsilyl)oxy)-3-(4-chlorophenyl)acrylate (**2.13**): Procedure 1 was followed using 4-chlorobenzaldehyde (327.53 mg, 2.33 mmol) in THF (7.95 mL). Yield 29% (154 mg, 0.45 mmol). ^{1}H NMR (600 MHz, $CDCl_3$) δ 7.63 (d, *J* = 7.8, 2H), 7.30 (d, *J* = 7.74, 2H), 7.26 (d, *J* = 8.76, 2H), 7.18 (d, *J* = 7.8, 1H), 6.80 (s, 1H), 4.28 (q, *J* = 7.02, 2H), 4.13 (q, *J* = 7.02, 1H), 1.55 (s, 2H), 1.36 (t, *J* = 7.02, 3H), 1.17 (t, *J* = 7.02, 1H), 0.99 (s, 4H), 0.94 (s, 9H), 0.23 (s, 2H), 0.14 (s, 6H). ^{13}C NMR (150 MHz, $CDCl_3$) δ 165.42, 142.72, 141.22, 133.70, 132.84, 131.15, 130.21, 128.49, 128.21, 119.31, 117.58, 61.58, 61.19, 25.94, 25.71, 18.72, 18.43, 14.44, 13.97, -3.72, -4.61. HRMS ESI$^+$ $C_{17}H_{25}ClO_3Si$ $[M+Na]^+$ Expected: 363.1154, Found: 363.1145.

General Procedure 2: In an oven-dried, 50-mL round-bottom flask, the corresponding silyl enol ether (**2.3**-**2.13**, 1 eq) was dissolved in a 4:1 mixture of ethanol and chloroform

(0.098 M) under nitrogen at room temperature. Triethylamine trihydrofluoride (1.7 eq) was added dropwise and the reaction was stirred. After 30 minutes, hydroxylamine hydrochloride (1.7 eq) was added as a solid in two portions and the reaction was stirred for an additional 19 h at room temperature. The solvent was then evaporated and the reaction mixture was dissolved in dichloromethane, which was then washed with water (2x) and saturated aqueous sodium bicarbonate. The organic phase was dried with sodium sulfate and filtered. The filtrate was concentrated *in vacuo* and purified by an automated CombiFlash MPLC system (silica gel, ethyl acetate/hexanes or methanol/dichloromethane depending on polarity), followed by pumping down overnight on high-vac to yield the pure product.

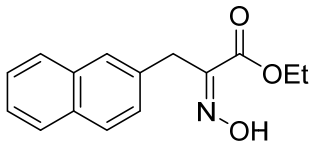

Ethyl 2-(hydroxyimino)-3-(naphthalen-2-yl)propanoate (**2.14**): Procedure 2 was followed using ethyl 2-((tert-butyldimethylsilyl)oxy)-3-(naphthalen-2-yl)acrylate (**2.3**, 202.6 mg, 0.57 mmol) in 4:1 ethanol/chloroform (5.82 mL). Yield 71% (103.7 mg, 0.40 mmol). ^{1}H NMR (600 MHz, $CDCl_3$) δ 9.51 (br s, 1H), 7.79-7.75 (m, 4H), 7.46-7.42 (m, 3H), 4.26 (q, *J* = 7.08, 2H), 4.15 (s, 2H), 1.32 (t, *J* = 7.08, 3H). ^{13}C NMR (150 MHz, $CDCl_3$) δ 163.10, 150.99, 133.37, 132.99, 132.15, 128.00, 127.55, 127.48, 127.44, 127.38, 125.87, 125.44, 61.84, 30.50, 13.90. HRMS ESI$^+$ $C_{15}H_{15}NO_3$ $[M+Na]^+$ Expected: 280.0944, Found: 280.0933.

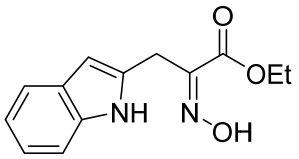

Ethyl 2-(hydroxyimino)-3-(1H-indol-2-yl)propanoate (**2.15**): Procedure 2 was followed using ethyl 2-((tert-butyldimethylsilyl)oxy)-3-(1H-indol-2-yl)acrylate (**2.4**, 117.6 mg, 0.34 mmol) in 4:1 ethanol/chloroform (3.47 mL). Yield 58% (48.2 mg, 0.20 mmol). ^{1}H NMR (600 MHz, $CDCl_3$) δ 9.04 (br s, 1H), 8.51 (br s, 1H), 7.52 (d, *J* = 7.8, 1H), 7.30 (d, *J* = 8.1, 1H), 7.13 (t, *J* = 7.53, 1H), 7.06 (t, *J* = 7.44, 1H), 6.39 (s, 1H), 4.34 (q, *J* = 7.14, 2H), 4.12 (s, 2H), 1.37 (t, *J* = 7.14, 3H). ^{13}C NMR (150 MHz, $CDCl_3$) δ 163.33, 149.91, 135.92, 131.74, 128.15, 121.54, 119.98, 119.61, 110.48, 101.90, 62.25, 23.73, 13.93. HRMS ESI$^+$ $C_{13}H_{14}N_2O_3$ $[M+Na]^+$ Expected: 269.0897, Found: 269.0886.

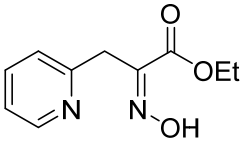

Ethyl 2-(hydroxyimino)-3-(pyridin-2-yl)propanoate (**2.16**): Procedure 2 was followed using ethyl 2-((tert-butyldimethylsilyl)oxy)-3-(pyridin-2-yl)acrylate (**2.5**, 443.9 mg, 1.44 mmol) 4:1 ethanol/chloroform (14.7 mL). Yield 48% (142.8 mg, 0.69 mmol). ^{1}H NMR (600 MHz, $CDCl_3$) δ 8.52-8.51 (m, 1H), 7.64 (t, *J* = 7.02, 1H), 7.28-7.26 (m, 3H), 7.16 (t, *J* = 6.00, 1H), 4.29 (q, *J* = 7.14, 2H), 4.21 (s, 2H), 1.31 (t, *J* = 7.14, 3H). ^{13}C NMR (150 MHz, $CDCl_3$) δ 163.58, 156.50, 150.60, 149.07, 137.06, 123.37, 121.81, 61.92, 33.38, 29.70, 14.08. HRMS ESI$^+$ $C_{10}H_{12}N_2O_3$ $[M+H]^+$ Expected: 209.0921, Found: 209.0903.

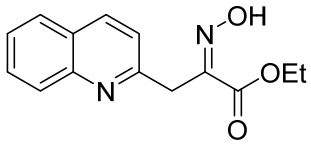

Ethyl 2-(hydroxyimino)-3-(quinolin-2-yl)propanoate (**2.17**): Procedure 2 was followed using ethyl 2-((tert-butyldimethylsilyl)oxy)-3-(quinolin-2-yl)acrylate (**2.6**, 134.9 mg, 0.38 mmol) in 4:1 ethanol/chloroform (3.87 mL). Yield 52% (51 mg, 0.20 mmol). ^{1}H NMR (600 MHz, $CDCl_3$) δ 8.10 (d, *J* = 8.25, 1H), 8.03 (d, *J* = 8.34, 1H), 7.89 (d, *J* = 8.88, 2H), 7.77 (d, *J* = 7.92, 1H), 7.66-7.62 (m, 5H), 7.57 (d, *J* = 8.22, 2H), 7.50 (m, 1H), 7.41-7.36 (m, 3H), 7.02 (d, *J* = 8.94, 2H), 6.37 (s, 2H), 4.40 (s, 2H), 4.35 (q, *J* = 6.96, 4H), 4.28 (q, *J* = 7.08, 2H), 1.62 (br s, 2H), 1.40 (t, *J* = 6.96, 6H), 1.28 (t, *J* = 7.02, 3H). ^{13}C NMR (150 MHz, $CDCl_3$) δ 170.44, 164.48, 163.71, 157.08, 155.19, 147.42, 137.88, 137.10, 131.63, 129.73, 128.70, 127.85, 127.48, 126.90, 126.28, 125.27, 124.34, 121.89, 121.26, 119.56, 93.65, 61.91, 61.67, 34.17, 14.22, 14.11. HRMS ESI$^+$ $C_{14}H_{14}N_2O_3$ $[M+H]^+$ Expected: 259.1077, Found: 259.1068.

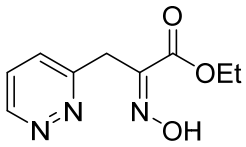

Ethyl 2-(hydroxyimino)-3-(pyridazin-3-yl)propanoate (**2.18**): Procedure 2 was followed using ethyl 2-((tert-butyldimethylsilyl)oxy)-3-(pyridazin-3-yl)acrylate (**2.7**, 173.3 mg, 0.56 mmol) in 4:1 ethanol/chloroform (5.7 mL). Yield 83% (97.3 mg, 0.47 mmol). ^{1}H NMR (600 MHz, $CDCl_3$) δ 12.48 (s, 1H), 9.06 (d, *J* = 4.08, 1H), 7.62-7.59 (m, 1H), 7.53 (d, *J* = 8.34, 1H), 4.18-4.15 (m, 4H), 3.32 (s, 1H), 1.18 (t, *J* = 6.78, 4H). ^{13}C NMR (150 MHz, $CDCl_3$) δ 163.52, 159.42, 150.08, 148.02, 127.09, 126.65, 60.93, 45.75, 30.93, 13.95. HRMS ESI$^+$ $C_9H_{11}N_3O_3$ $[M+H]^+$ Expected: 232.0693, Found: 232.0687.

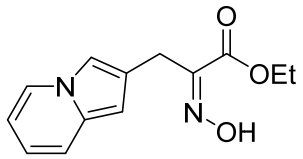

Ethyl 2-(hydroxyimino)-3-(indolizin-2-yl)propanoate (**2.19**): Procedure 2 was followed using ethyl 2-((tert-butyldimethylsilyl)oxy)-3-(indolizin-2-yl)acrylate (**2.8**, 33.6 mg, 0.097 mmol) in 4:1 ethanol/chloroform (1 mL). Yield 70% (16.8 mg, 0.07 mmol). ^{1}H NMR (600 MHz, $CDCl_3$) δ 7.78 (d, *J* = 6.84, 1H), 7.25-7.21 (m, 2H), 6.58 (t, *J* = 7.65, 1H), 6.38 (t, *J* = 6.6, 1H), 6.34 (s, 1H), 4.29 (q, *J* = 6.92, 2H), 4.02 (s, 2H), 1.34-1.32 (m, 4H). ^{13}C NMR (150 MHz, $CDCl_3$) δ 163.33, 151.50, 132.60, 124.73, 122.52, 118.56, 116.77, 111.57, 109.85, 99.55, 61.76, 30.13, 22.64, 14.01. HRMS ESI$^+$ $C_{13}H_{14}N_2O_3$ $[M+Na]^+$ Expected: 269.0897, Found: 269.0886.

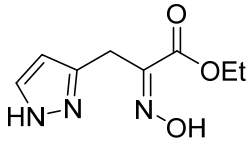

Ethyl 2-(hydroxyimino)-3-(1H-pyrazol-3-yl)propanoate (**2.20**): Procedure 2 was followed using ethyl 2-((tert-butyldimethylsilyl)oxy)-3-(1H-pyrazol-3-yl)acrylate (**2.9**, 125.3 mg, 0.42 mmol) in 4:1 ethanol/chloroform (4.29 mL). ^{1}H NMR (600 MHz, $CDCl_3$) δ 7.61 (s, 1H), 6.23 (s, 1H), 4.29 (q, *J* = 7.12, 2H), 3.99 (s, 2H), 3.21-3.17 (m, 16H), 1.27 (t, *J* = 7.29, 28H). ^{13}C NMR (150 MHz, $CDCl_3$) δ 163.57, 145.92, 128.73, 103.23, 60.74, 54.89, 45.28, 23.29, 13.95, 13.92, 8.37. HRMS ESI$^+$ $C_8H_{11}N_3O_3$ $[M+Na]^+$ Expected: 220.0693, Found: 220.0688.

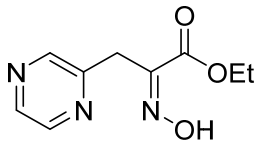

Ethyl 2-(hydroxyimino)-3-(pyrazin-2-yl)propanoate (**2.21**): Procedure 2 was followed using ethyl 2-((tert-butyldimethylsilyl)oxy)-3-(pyrazin-2-yl)acrylate (**2.10**, 76.6 mg, 0.25 mmol) in 4:1 ethanol/chloroform (2.55 mL). Yield 78% (40.8 mg, 0.20 mmol). ^{1}H NMR (600 MHz, $CDCl_3$) δ 12.47 (s, 1H), 8.57 (s, 1H), 8.49 (s, 1H), 8.47 (s, 1H), 4.18-4.16 (m, 2H), 4.06 (s, 2H), 1.19-1.18 (m, 3H). ^{13}C NMR (150 MHz, $CDCl_3$) δ 163.45, 153.14, 147.95, 144.56, 143.85, 142.37, 60.90, 30.19, 13.93. HRMS ESI$^+$ $C_9H_{11}N_3O_3$ $[M+Na]^+$ Expected: 232.0693, Found: 232.0693.

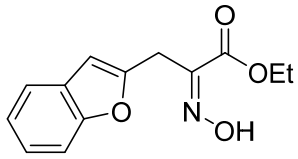

Ethyl 3-(benzofuran-2-yl)-2-(hydroxyimino)propanoate (**2.22**): Procedure 2 was followed using ethyl 3-(benzofuran-2-yl)-2-((tert-butyldimethylsilyl)oxy)acrylate (**2.11**, 197.3 mg, 0.57 mmol) in 4:1 ethanol/chloroform (5.85 mL). Yield 62% (87.2 mg, 0.35 mmol). ^{1}H NMR (600 MHz, $CDCl_3$) δ 9.13 (br s, 1H), 7.46 (d, *J* = 7.62, 1H), 7.41 (d, *J* = 8.10, 1H), 7.22-7.19 (m, 1H), 7.16 (t, *J* = 7.11, 1H), 6.48 (s, 1H), 4.32 (q, *J* = 7.14, 2H), 4.17 (s, 2H), 1.33 (t, *J* = 7.14, 3H). ^{13}C NMR (150 MHz, $CDCl_3$) δ 162.77, 154.71, 151.84, 148.24, 128.60, 123.66, 122.64, 120.49, 111.02, 103.99, 62.21, 24.12, 14.05. HRMS ESI$^+$ $C_{13}H_{13}NO_4$ $[M+Na]^+$ Expected: 270.0737, Found: 270.0724.

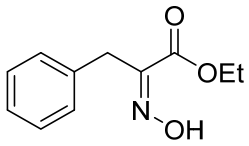

Ethyl 2-(hydroxyimino)-3-phenylpropanoate (**2.23**): Procedure 2 was followed using ethyl 2-((tert-butyldimethylsilyl)oxy)-3-phenylacrylate (**2.12**, 381.3 mg, 1.24 mmol). Yield 77% (198.9 mg, 0.96 mmol) in 4:1 ethanol/chloroform (12.6 mL). ^{1}H NMR (600 MHz, $CDCl_3$) δ 8.78 (br s, 1H), 7.31-7.30 (m, 2H), 7.28-7.25 (m, 4H), 7.21-7.19 (m, 1H), 4.27 (q, *J* = 7.14, 2H), 3.97 (s, 2H), 1.60 (s, 1H) 1.31 (t, *J* = 7.14, 3H). ^{13}C NMR (150 MHz, $CDCl_3$) δ 163.28, 151.67, 135.70, 129.17, 128.04, 128.53, 126.66, 61.95, 30.53, 14.05, 13.76. HRMS ESI$^+$ $C_{11}H_{13}NO_3$ $[M+Na]^+$ Expected: 230.0788, Found: 230.0779.

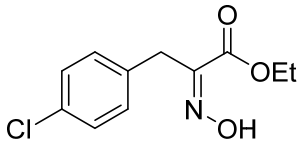

Ethyl 3-(4-chlorophenyl)-2-(hydroxyimino)propanoate (**2.24**): Procedure 2 was followed using ethyl 2-((tert-butyldimethylsilyl)oxy)-3-(4-chlorophenyl)acrylate (**2.13**, 154 mg, 0.45 mmol). Yield 71% (77.2 mg, 0.32 mmol) in 4:1 ethanol/chloroform (4.58 mL). ^{1}H NMR (600 MHz, $CDCl_3$) δ 8.86 (s, 1H), 7.25 (d, *J* = 7.8, 5H), 4.29 (q, *J* = 7.02, 2H), 3.94 (s, 2H), 1.62 (s, 1H), 1.33 (t, *J* = 7.02, 3H). ^{13}C NMR (150 MHz, $CDCl_3$) δ163.11, 151.16, 134.12, 132.56, 130.58, 128.65, 62.08, 29.89, 14.05. HRMS ESI$^+$ $C_{11}H_{12}ClNO_3$ $[M+Na]^+$ Expected: 264.0398, Found: 264.0390.

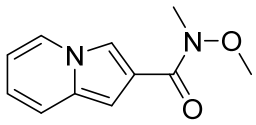

N-methoxy-N-methylindolizine-2-carboxamide (**2.25**): In an oven-dried, 50-mL round bottom flask, indolizine-2-carboxylic acid (161.16 mg, 1 mmol, 1 eq) was dissolved in *N,N*-

dimethylformamide (2.5 mL, 0.4M) at 28°C. *N*-methoxymethanamine (146.33 mg, 1.5 mmol, 1.5 eq), 1-[Bis(dimethylamino)methylene]-1H-1,2,3-triazolo[4,5-b]pyridinium 3-oxide hexafluorophosphate (468.29 mg, 1.2 mmol, 1.2 eq), and triethylamine (0.28 mL, 2 mmol, 2 eq) were added sequentially. The reaction mixture was degassed and purged with nitrogen gas 3 times, then stirred for 12 h at 28°C. Then the reaction mixture was partitioned between water (5 mL) and ethyl acetate (5 mL). The organic phase was separated and washed with water (2 x 5 mL), and brine (2 x 5 mL). The organic phase was dried with sodium sulfate, filtered and concentrated *in vacuo*. The filtrate was then purified using an automated CombiFlash MPLC system (silica gel, 5% methanol/dichloromethane), followed by pumping down overnight to yield the product as a dark brown oil (80.1 mg, 39% yield). ^{1}H NMR (600 MHz, $CDCl_3$) δ 7.86 (br s, 2H), 7.36 (d, *J* = 9.06, 1H), 6.92 (s, 1H), 6.66 (t, *J* = 7.71, 1H), 6.51 (t, *J* = 6.69, 1H), 3.74 (s, 3H), 3.40 (s, 3H). ^{13}C NMR (150 MHz, $CDCl_3$) δ 165.20, 132.18, 125.27, 120.75, 120.18, 117.77, 116.60, 111.90, 101.35, 61.16, 33.21. HRMS ESI$^+$ $C_{11}H_{12}N_2O_2$ $[M+Na]^+$ Expected: 227.0791, Found: 227.0781.

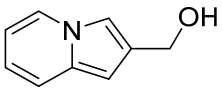

Indolizin-2-ylmethanol (**2.27**): In an oven-dried, 50-mL round-bottom flask under nitrogen atmosphere, indolizine-2-carboxylic acid (500 mg, 3.1 mmol, 1 eq) was dissolved in tetrahydrofuran (10.32 mL, 0.3M) and cooled to 0°C. Lithium aluminum hydride (470.58 mg, 12.4 mmol, 4 eq) was added as a solid in three portions. After gas evolution ceased, the reaction was heated to 63°C and refluxed overnight. After cooling to 0°C, water (0.93 mL) was added dropwise, followed by 10% aqueous sodium hydroxide (0.93 mL), and water (2.79 mL), The quenched reaction mixture was then warmed to room temperature

and stirred for 10 minutes, followed by filtering over celite and washing with THF. The filtrate was then concentrated *in vacuo* and purified using an automated CombiFlash MPLC system (silica gel, 5% methanol/dichloromethane), followed by pumping down overnight to yield product as a brown solid (342 mg, 75% yield). ^{1}H NMR (600 MHz, $CDCl_3$) δ 7.84 (d, *J* = 6.84, 1H), 7.30 (d, *J* = 7.08, 2H), 6.63 (t, *J* = 7.71, 1H), 6.43 (t, *J* = 6.63, 1H), 6.39 (s, 1H), 4.77 (d, *J* = 4.14, 2H), 1.56-1.53 (m, 1H). ^{13}C NMR (150 MHz, $CDCl_3$) δ 133.15, 129.20, 125.14, 119.05, 117.28, 110.74, 110.35, 97.90, 59.24. HRMS ESI$^+$ C_9H_9NO $[M+H]^+$ Expected: 148.0757, Found: 148.0754.

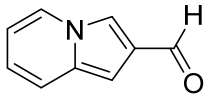

Indolizine-2-carbaldehyde (**2.26**): In an oven-dried, 100-mL round-bottom flask under nitrogen atmosphere, indolizine-2-ylmethanol (**2.27**, 315 mg, 2.14 mmol, 1 eq) was dissolved in tetrahydrofuran (17.8 mL, 0.12M) at room temperature. Manganese (IV) oxide (2.04 g, 23.54 mmol, 11 eq) was added as a solid and the reaction was allowed to stir for 16h. The reaction mixture was then filtered over celite and washed with THF. The filtrate was then concentrated *in vacuo* and purified using an automated CombiFlash MPLC system (silica gel, 30% ethyl acetate/hexanes), followed by pumping down overnight on high-vac to yield the product as a dark red solid (54.5 mg, 17% yield).^{1}H NMR (600 MHz, $CDCl_3$) δ 10.05 (s, 1H), 7.88 (d, *J* = 7.02, 1H), 7.78 (s, 1H), 7.38 (d, *J* = 9.12, 1H), 6.82 (s, 1H), 6.71 (t, *J* = 7.77, 1H), 6.56 (t, *J* = 6.66, 1H), 1.55 (s, 1H). ^{13}C NMR (150 MHz, $CDCl_3$) δ 187.61, 133.88, 128.68, 125.86, 121.04, 119.11, 117.40, 113.19, 99.13. HRMS ESI$^+$ C_9H_7NO $[M+Na]^+$ Expected: 168.0420, Found: 168.0412.

General Procedure 3: In an oven-dried, 16-mL vial, the corresponding hydroxyimino-ester (**2.14**-**2.22**, 1 eq) was dissolved in ethanol (0.5 M) under nitrogen at room temperature. Sodium hydroxide (1 M, 3 eq) was added and the reaction was stirred at room temperature overnight. The reaction mixture was then concentrated by removal of EtOH *in vacuo*, diluted with DI water, and acidified with 1M hydrochloric acid. The product was then extracted with ethyl acetate (3x). The organic phase was then dried with $MgSO_4$, filtered and concentrated *in vacuo* to yield the crude product.

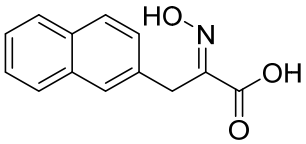

2-(Hydroxyimino)-3-(naphthalen-2-yl)propanoic acid (**2.31**): Procedure 3 was followed using ethyl 2-(hydroxyimino)-3-(naphthalen-2-yl)propanoate (**2.14**, 50 mg, 0.19 mmol) in ethanol (0.38 mL). Yield 97% (42.3 mg, 0.18 mmol). ^{1}H NMR (600 MHz, $CDCl_3$) δ 12.83 (br s, 1H), 12.34 (s, 1H), 7.85-7.81 (m, 3H), 7.64 (s, 1H), 7.48-7.43 (m, 2H), 7.37-7.35 (m, 1H), 3.97 (s, 2H). ^{13}C NMR (150 MHz, $CDCl_3$) δ 165.22,150.05, 134.40, 133.03, 131.65, 127.87, 127.45, 127.34, 127.28, 126.58, 126.13, 125.50, 30.08. HRMS ESI$^+$ $C_{13}H_{11}NO_3$ [M-H]$^-$ Expected: 228.0666, Found: 228.0671.

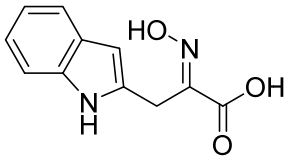

2-(Hydroxyimino)-3-(1H-indol-2-yl)propanoic acid (**2.32**): Procedure 3 was followed using ethyl 2-(hydroxyimino)-3-(1H-indol-2-yl)propanoate (**2.15**, 48.2 mg, 0.196 mmol) in ethanol (0.39 mL). Yield 86% (36.7 mg, 0.17 mmol). ^{1}H NMR (600 MHz, $CDCl_3$) δ 12.83 (br s, 1H), 12.35 (s, 1H), 10.82 (s, 1H), 7.37 (d, *J* = 7.8, 1H), 7.29 (d, *J* = 8.1, 1H), 6.97 (t,

J = 7.53, 1H), 6.90 (t, *J* = 7.41, 1H), 6.00 (s, 1H), 3.93 (s, 2H). ^{13}C NMR (150 MHz, $CDCl_3$) δ 165.07, 148.62, 135.78, 134.00, 128.11, 120.22, 119.09, 118.67, 110.87, 98.85, 23.21. HRMS ESI$^+$ $C_{11}H_{10}N_2O_3$ [M-H]$^-$ Expected: 217.0619, Found: 217.0623.

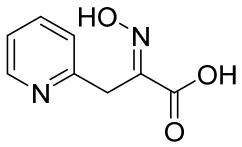

2-(Hydroxyimino)-3-(pyridin-2-yl)propanoic acid (**2.33**): Procedure 3 was followed using ethyl 2-(hydroxyimino)-3-(pyridin-2-yl)propanoate (**2.16**, 19.3 mg, 0.093 mmol) in ethanol (0.19 mL). ^{1}H NMR (600 MHz, $CDCl_3$) δ 12.61 (d, *J* = 33.12, 1H), 10.32 (d, *J* = 25.92, 1H), 8.66 (d, *J* = 12.96, 1H), 8.17 (d, *J* = 27.9, 1H), 7.63 (d, *J* = 25.5, 1H), 7.49 (s, 1H), 4.16 (d, *J* = 15.84, 2H). ^{13}C NMR (150 MHz, $CDCl_3$) δ 164.68, 152.85, 146.28, 145.12, 142.03, 125.73, 124.61, 29.20. HRMS ESI$^+$ $C_8H_8N_2O_3$ [M-H]$^-$ Expected: 179.0462, Found: 179.0458.

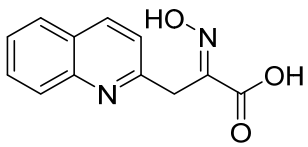

2-(Hydroxyimino)-3-(quinolin-2-yl)propanoic acid (**2.34**): Procedure 3 was followed using ethyl 2-(hydroxyimino)-3-(quinolin-2-yl)propanoate (**2.17**, 13.4 mg, 0.052 mmol) in ethanol (0.11 mL). ^{1}H NMR (600 MHz, $CDCl_3$) δ 8.93 (d, *J* = 8.64, 1H), 8.19 (d, *J* = 8.16, 1H), 8.14 (d, *J* = 8.58, 1H), 8.08 (t, *J* = 7.71, 1H), 7.88 (t, *J* = 7.59, 1H), 7.81 (d, *J* = 8.64, 1H), 4.55 (s, 2H), 3.21 (q, *J* = 7.32, 2H), 1.29 (t, *J* = 7.32, 3H). ^{13}C NMR (150 MHz, $CDCl_3$) δ 165.60, 154.29, 147.21, 137.40, 135.04, 129.68, 128.94, 127.47, 124.03, 121.95, 119.59, 46.69, 8.28. HRMS ESI$^+$ $C_{12}H_{10}N_2O_3$ [M-H]$^-$ Expected: 229.0619, Found: 229.0618.

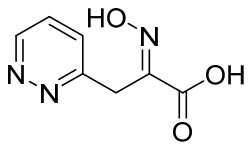

2-(Hydroxyimino)-3-(pyridazin-3-yl)propanoic acid (**2.35**): Procedure 3 was followed using ethyl 2-(hydroxyimino)-3-(pyridazin-3-yl)propanoate (**2.18**, 32.7 mg, 0.156 mmol) in ethanol (0.31 mL). ^{1}H NMR (600 MHz, $CDCl_3$) δ 12.42 (s, 1H), 10.33 (s, 1H), 9.14 (d, *J* = 4.86, 1H), 7.75-7.73 (m, 1H), 7.65 (d, *J* = 8.34), 4.16 (s, 2H). ^{13}C NMR (150 MHz, $CDCl_3$) δ 164.91, 160.39, 149.25, 147.76, 130.12, 129.72, 30.59. HRMS ESI$^+$ $C_7H_7N_3O_3$ $[M-H]^-$ Expected: 180.0415, Found: 180.0410.

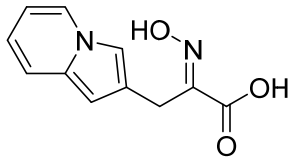

2-(Hydroxyimino)-3-(indolizin-2-yl)propanoic acid (**2.36**): Procedure 3 was followed using ethyl 2-(hydroxyimino)-3-(indolizin-2-yl)propanoate (**2.19**, 30.5 mg, 0.124 mmol) in ethanol (0.25 mL). ^{1}H NMR (600 MHz, $CDCl_3$) δ 12.21 (br s, 1H), 10.42 (s, 4H), 8.22 (d, *J* = 6.72, 1H), 8.15 (d, *J* = 6.9, 1H), 7.84 (s, 1H), 7.33-7.26 (m, 3H), 6.64-6.59 (m, 3H), 6.50-6.42 (m, 3H), 3.79 (s, 2H). ^{13}C NMR (150 MHz, $CDCl_3$) δ 165.84, 157.07, 152.61, 148.56, 144.92, 144.35, 140.52, 122.20, 121.76, 121.16, 120.99, 22.20. HRMS ESI$^+$ $C_{11}H_{10}N_2O_3$ $[M-H]^-$ Expected: 217.0619, Found: 217.0608.

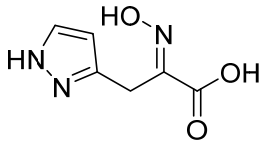

2-(Hydroxyimino)-3-(1H-pyrazol-3-yl)propanoic acid (**2.37**): Procedure 3 was followed using ethyl 2-(hydroxyimino)-3-(1H-pyrazol-3-yl)propanoate (**2.20**, 238.3 mg, 1.21 mmol) in ethanol (2.4 mL). ^{1}H NMR (600 MHz, $CDCl_3$) δ 12.40 (s, 1H), 10.69 (br s, 1H), 7.71 (s,

1H), 6.07 (s, 1H), 3.82 (s, 2H), 3.04-3.00 (m, 2H), 1.18 (t, *J* = 7.26, 4H). ^{13}C NMR (150 MHz, $CDCl_3$) δ 164.94, 148.24, 143.32, 132.68, 104.15, 45.21, 21.98, 8.38. HRMS ESI$^+$ $C_6H_7N_3O_3$ [M-H]$^-$ Expected: 168.0415, Found: 168.0415.

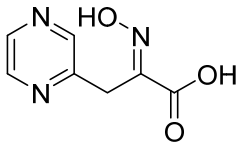

2-(Hydroxyimino)-3-(pyrazin-2-yl)propanoic acid (**2.38**): Procedure 3 was followed using ethyl 2-(hydroxyimino)-3-(pyrazin-2-yl)propanoate (**2.21**, 40.8 mg, 0.195 mmol) in ethanol (0.39 mL). ^{1}H NMR (600 MHz, $CDCl_3$) δ 12.33 (s, 1H), 10.31 (br s, 1H), 8.53 (s, 1H), 8.53 (s, 1H), 8.48 (s, 1H), 8.44 (s, 1H), 4.02 (s, 2H). ^{13}C NMR (150 MHz, $CDCl_3$) δ 165.04, 153.39, 148.44, 144.50, 143.88, 142.28, 30.14. HRMS ESI$^+$ $C_7H_7N_3O_3$ [M-H]$^-$ Expected: 180.0415, Found: 180.0409.

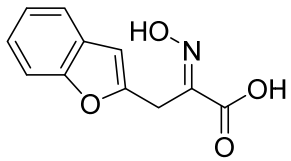

3-(Benzofuran-2-yl)-2-(hydroxyimino)propanoic acid (**2.39**): Procedure 3 was followed using ethyl 3-(benzofuran-2-yl)-2-(hydroxyimino)propanoate (**2.22**, 28.9 mg, 0.117 mmol). Yield 57% (14.5 mg, 0.07 mmol) in ethanol (0.23 mL). ^{1}H NMR (600 MHz, $CDCl_3$) δ 12.97 (br s, 1H), 12.50 (s, 1H), 7.52 (d, *J* = 7.5, 1H), 7.48 (d, *J* = 7.98, 1H), 7.21 (t, *J* = 7.62, 1H), 7.18 (t, *J* = 7.35, 1H), 6.50 (s, 1H), 4.00 (s, 2H). ^{13}C NMR (150 MHz, $CDCl_3$) δ 164.74, 153.85, 153.39, 146.87, 128.37, 123.53, 122.73, 120.49, 110.71, 103.06, 23.71. HRMS ESI$^+$ $C_{11}H_9NO_4$ [M-H]$^-$ Expected: 218.0459, Found: 218.0456.

General Procedure 4: In an oven-dried, 100-mL round bottom flask, sodium hydroxide (3 eq) was dissolved in water (1.22 M) under argon gas at room temperature. The corresponding pyruvic acid (1 eq) and hydroxylamine hydrochloride (2 eq) were added sequentially as solids, and the reaction was stirred at room temperature overnight. The reaction mixture was then acidified with 1M hydrochloric acid, filtered, and the precipitate was collected to yield the final product.

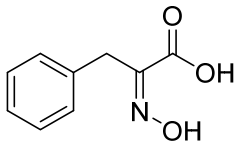

2-(Hydroxyimino)-3-phenylpropanoic acid (**2.40**): Procedure 4 was followed using phenylpyruvic acid (2 g, 12.2 mmol) in water (30 mL). Yield 76% (1.67 g, 9.3 mmol). ^{1}H NMR (600 MHz, $CDCl_3$) δ 12.27 (br s, 1H), 7.26 (t, *J* = 7.26, 2H), 7.17 (t, *J* = 7.26, 3H), 3.79 (s, 2H). ^{13}C NMR (150 MHz, $CDCl_3$) δ 165.18, 150.10, 136.68, 128.53, 128.43, 128.32, 126.14, 29.85. HRMS ESI$^+$ $C_9H_9NO_3$ [M-H]$^-$ Expected: 178.0510, Found: 178.0516.

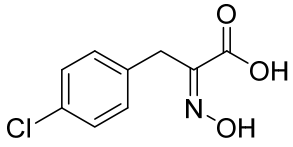

3-(4-Chlorophenyl)-2-(hydroxyimino)propanoic acid (**2.41**): Procedure 4 was followed using 4-chlorophenylpyruvic acid (1 g, 5 mmol) in water (15 mL). ^{1}H NMR (600 MHz, $CDCl_3$) δ 12.86 (br s, 1H), 12.35 (s, 1H), 7.32 (d, *J* = 8.4, 2H), 7.19 (d, *J* = 8.28, 2H), 3.78 (s, 2H). ^{13}C NMR (150 MHz, $CDCl_3$) δ 165.09, 149.76, 135.79, 130.82, 130.43, 128.32, 29.31. HRMS ESI$^+$ $C_9H_8ClNO_3$ [M-H]$^-$ Expected: 212.0120, Found: 212.0130.

2.4: Conclusions and Future Directions

In order to develop an inhibitor of CtBP for the treatment of cancer that is more potent in cell and animal models, we began a modeling study to prioritize synthesis of heteroaromatic HIPP analogues. A library of 36 heteroaromatic HIPP analogues were designed and modeled in docking studies against CtBP1. We hypothesized that modulating the amount and nature of electron density in the aromatic ring system would strengthen inhibitor binding to CtBP. The modeling was performed utilizing two different docking software packages, and the docking results were scored with three scoring functions. From these docking studies it was decided to synthesize nine (9) new compounds that replaced the phenyl ring on HIPP with a heteroaromatic ring. We then tested these compounds in cells for inhibition of cell viability and colony formation, and also tested them against CtBP2 in isothermal titration calorimetry experiments to determine their binding affinities.

In our ITC experiments, we identified that 4-Cl HIPP (**2.41**) had the best binding affinity for CtBP2. We also identified two compounds that had better binding affinity for CtBP2 than HIPP. These compounds replaced the phenyl ring with either a naphthyl ring (**2.31**) or a benzofuranyl ring (**2.39**). We determined that heteroaromatic rings that contain nitrogen have less affinity for CtBP2, and bicyclic compounds have higher affinity than monocyclic compounds. When we compare the measured dissociation constants with the docking studies, we cannot make a definitive conclusion about which modeling software was the most accurate. The GOLD docking studies appear to be slightly more accurate than those from AutoDock Vina, but we should re-score the rest of the GOLD docking

experiments with HINT before deciding between the CHEM-PLP scoring function and the HINT scoring function.

In our cellular assays, we learned that replacing the carboxylic acid in 4-Cl HIPP with an ethyl ester increases its potency 50-fold, and the same substitution on HIPP increases its potency 15-fold. We tested all of the compounds as ethyl esters in an MTT cell viability assay in A2780 cells, and found that the 4-Cl HIPP ester (**2.24**) was the most potent. The naphthyl (**2.14**) and benzofuranyl (**2.22**) compounds were also more potent in A2780 cells than the HIPP ester (**2.23**) but less potent than **2.24**. **2.14** also exhibited improved potency compared to 4-Cl HIPP in the HEY and HCT116 cell lines. In breast cancer cells **2.14** was 8-fold more potent in MDA-MB-231 cells than in MCF-7 cells, which suggests that triple negative breast cancer is more dependent on CtBP than hormone-dependent breast cancer. We also found that replacing HIPP's phenyl ring with a bicyclic heteroaromatic ring resulted in compounds that were more potent in ovarian and colorectal cancer cells, but it is unclear whether all of these compounds are actually targeting CtBP due to the ITC data we obtained. In our clonogenic assays, **2.14** was the most potent compound in A2780 cells and **2.19** was the most potent in Patu8988T cells.

To get a fuller picture of the activity of these compounds, it is important to test compounds **2.31**-**2.39** *in vitro* to determine their ability to inhibit CtBP's dehydrogenase activity. Our collaborators lab is set up to test this in the NADH disappearance assay detailed in Korwar et al (2016),[68] and the compounds have been synthesized and shipped for testing. This assay will measure CtBP's ability to convert NADH to NAD^+ at different concentrations of the inhibitor compounds to calculate a functional IC_{50}. We also intend to undergo crystallography studies with these inhibitors to determine their binding modes.

This will also help answer our hypothesis about Trp318, and whether its orientation can be affected by an inhibitor.

One of the future directions of this project involves treating cells with CtBP inhibitors in conjunction with GMX-1778, an inhibitor of NAD^+ biosynthesis.[96] As cancer cells have a high rate of NAD^+ turnover due to the Warburg effect, modulation of NAD^+ is an attractive approach to cancer chemotherapy. As mentioned in section *1.2.2*, CtBP1/2 are overexpressed in cancer cells, in part due to the Warburg effect. When 4-Cl HIPP and GMX-1778 are combined in Panc1 or Patu8988T pancreatic cancer cells, this leads to a lower EC_{50} compared to treatment with either drug alone. Compounds **2.14**-**2.16** were also tested in A2780 cells with GMX-1778, and all three compounds were more active in A2780 cells than when A2780 cells were treated with the HIPP analogue alone.

Compounds **2.24** and **2.14** are both also in the process of being tested in mice. The compounds have been synthesized in 1g quantity, and there is an animal protocol in place for testing of the maximum tolerable dose (MTD). This protocol involves human xenografts of pancreatic cancer cells, and will be tested in 12-24 mice, where groups of 3 mice will be administered increasing doses of either compound. However, while preparing for these mouse studies, we ran into an issue with the solubility of these compounds. It appears the ethyl ester, while increasing cell permeability, is not soluble in water and may crash out of solution after treatment. We intend to continue these MTD studies by dissolving the compounds in corn oil and delivering the compounds to mice orally. We also intend to synthesize novel analogues of these compounds with different ester moieties to increase solubility for future *in vivo* studies.

Our laboratory also hopes to continue structure activity relationships studies of compounds **2.31** and **2.36**. A small library of compounds will be docked in GOLD by another graduate student in our lab. This project focuses on the addition of substituents to the aromatic rings of these compounds. Specifically, electronically and sterically diverse substituents will be appended to different positions on the ring system. With this project, we plan to prioritize synthesis of fourth generation CtBP inhibitors based on the docking results.

Chapter 3: PROteolysis TArgeting Chimeras

3.1: Ubiquitination and Endogenous Protein Degradation

3.1.1: Ubiquitin Background

Ubiquitin (Ub) is a regulatory protein made up of 76 amino acids and has a molecular weight of 8.5 kDa.[97,98] It is highly conserved across eukaryotes and plays an important role in cellular processes including regulation of the cell cycle, modulation of immune system processes, and control of signal transduction.[99] Originally called chromosomal protein A24, Ub was discovered and isolated in 1975 by Gideon Goldstein and colleagues.[100] It is a branched protein that has two amino termini and one carboxyl terminus.[101]

A common post-translational modification of proteins is ubiquitination, or attachment of Ub to lysine side chains via an isopeptide bond.[102,103] Importantly, Ub has seven lysine residues that can be ubiquitinated, allowing it to form poly-Ub chains.[103] Poly-Ub chains that are linked at the residue Lys48 are known to tag the substrate protein for degradation by recruitment of the proteasome.[104] Endogenous protein degradation is controlled by the ubiquitin/proteasome system (UPS).

3.1.2: The Ubiquitin/Proteasome System

Ubiquitination, also called ubiquitylation, involves a cascade of three enzymes: an E1 Ub activating enzyme, an E2 Ub conjugating enzyme, and an E3 Ub protein ligase, also known as an E3 ligase (**Figure 3.1**).[103,105,106] The cascade begins with the adenylation of Ub, and the Ub-adenylate intermediate reacts with a cysteine residue on the E1 activating enzyme, forming an E1-Ub thioester.[107] The Ub is then transferred from the E1 cysteine residue to a cysteine residue on the E2 conjugating enzyme via trans-

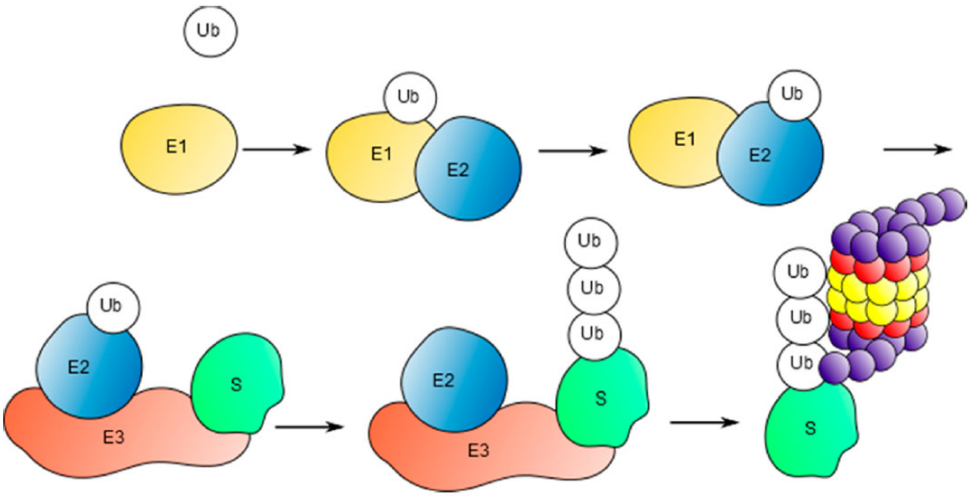

Figure 3.1: Overview of the ubiquitin/proteasome system. *Adapted from reference 103.*

thioesterification.[103,107] Finally, an E3 ligase associates with both the E2 thioester and a protein that is to be degraded, and catalyzes the transfer of Ub from the E2 thioester to a lysine residue on the bound substrate protein. This results in poly-ubiquitination of the substrate protein.[103]

This process has two discrete steps: polyubiquitination of the protein to be degraded, and subsequent degradation by the 26S proteasome.[108] The 26S proteasome consists of a 20S core complex (shown in red and yellow in **Figure 3.1**) and two 19S cap complexes (shown in purple in **Figure 3.1**). The core complex is made up of two 7-

membered rings of β subunits (yellow) surrounded by two 7-membered rings of α subunits (red), and possesses a narrow channel down the center. The 19S cap is responsible for substrate recognition, and deubiquitinates and unfolds the substrate protein to enter the pore of the 20S subunit. The β subunits then proteolyze the substrate into smaller peptides.[109–111] The substrate protein that is degraded by the proteasome is determined by the E3 ligase that binds to it.

3.1.3: E3 Ligases

There are three main types of E3 ligases: those that catalyze ubiquitin transfer from the E2 enzyme to a lysine residue on the substrate protein via an aminolysis reaction, known as RING (really interesting new gene) E3 ligases, and those that transfer the ubiquitin to a cysteine residue on the E3 ligase via a transthioesterification reaction, known as HECT (homologous to E6-AP carboxy terminus) and RBR (RING-Between-RING) E3 ligases.[112,113] Each type of E3 ligase can be further divided into families of proteins. The human genome codes for more than 700 E3 ligases.[114]

RING E3 ligases transfer the ubiquitin molecule directly from the E2 active site to the substrate. The amino group on the substrate lysine performs a nucleophilic attack on the thioester bond between the E2 enzyme and the ubiquitin molecule, causing hydrolysis of the thioester and subsequent formation of an isopeptide bond with the substrate.[113] These enzymes contain a RING domain, which optimizes the position of the E2-Ub complex in preparation for Ub transfer to the substrate.[112] In this way, the RING functions as a scaffold protein that orients the E2-Ub complex in relation to the substrate.

HECT E3 ligases transfer ubiquitin to the substrate by catalyzing two distinct reactions: a transthioesterification reaction that transfers Ub from the E2 enzyme onto a

cysteine residue on the E3 ligase, and a subsequent nucleophillic attack on that Hect-Ub thioester bond by a lysine residue on the substrate.[113] These enzymes possess a C-terminal HECT domain, which consists of an N-terminal lobe containing the binding site for the E2 enzyme, and a smaller C-terminal lobe containing the conserved catalytic cysteine residue.[112]

RBR E3 ligases are fairly new, and share similarities with both HECT and RING E3 ligases. RBRs have two ring domains, known as RING1 and RING2, which are separated by the in-between-ring (IBR) domain.[113] The RING1 domain acts similarly to RING E3 ligases in that it engages with the E2-Ub complex, while the RING2 domain contains a catalytic cysteine and mediates ubiquitination of the substrate in a HECT-like mechanism.[112,113]

3.1.4: Dimeric RING E3 Ligases

Many RING-type E3 ligases tend to form homo- or heterodimers. Typically, each monomeric unit of the dimer is able to bind to an E2 enzyme and bring about ubiquitination of its substrate. RING-type dimers are formed either through interaction of sequences outside of the RING domain, or through direct interaction of the RING domains. In both instances, the E2 binding surfaces of each monomer face away from each other.[115]

One example of a homodimeric RING E3 includes the family of Inhibitors of Apoptosis Proteins (IAPs). Five IAPs specifically possess a RING domain with E3 ligase activity: XIAP, cIAP1, cIAP2, ILP2, and ML-IAP.[116] In the case of cIAP1, the RING interface is sequestered in a "closed," inactive form until activation by an IAP antagonist, such as SMAC (second mitochondrial activator of caspases) or DIABLO (direct IAP-binding protein with low isoelectric point). The IAP antagonist stabilizes the "open," active

conformation, which allows RING dimerization and subsequent E2 binding and ubiquitin transfer.[115] The endogenous substrate for IAPs is the Rho GTPase Rac1.[116]

Another well studied E3 ligase that is able to form dimers is coded for by the murine double minute gene 2 (MDM2). MDM2 is able to form homodimers, as well as heterodimers with MDM4 (also called MDMX in some of the literature).[115] MDM2 acts as an E3 ligase for the tumor suppressor p53.[117] MDM4, on the other hand, does not have any intrinsic E3 ligase activity, though it does have some role in regulation of p53 in conjunction with MDM2.[118] A class of imidazoline derivatives, called nutlins, have demonstrated the ability to inhibit binding between MDM2 and p53 with IC_{50} values in the nanomolar to micromolar range.[119]

3.1.5: Cullin-RING E3 Ligases

The majority of E3 ligases are RING-type E3 ligases.[115,120] These can be further divided into subfamilies, one of which comprises the cullin-based E3 superfamily.[115] There are seven subfamilies of cullin-based E3 ligases, also known as cullin-Ring E3 ligases (CRLs).[114,120,121] CRLs are multi-subunit enzymes, and each subfamily is contains a cullin protein (Cul1, 2, 3, 4a, 4b, 5, 7, or 9), a small RING protein (Rbx1 or Rbx2), and a substrate recognition subunit (SRS), also referred to as a substrate receptor protein.[114,115,122]

The cullin acts as a scaffold protein that brings together the E2 enzyme and the substrate. The C-terminus of the cullin associates with the RING protein, which is required for interaction with the E2 enzyme. The N-terminus of the cullin binds to an adaptor protein, which links the cullin to the variable substrate recruitment subunit.[114] Cullins are activated by covalent conjugation (or neddylation) with Nedd8, a ubiquitin-like protein.[122] A well-studied example is the Skp1-Cul1-F-box protein (SCF) family (**Figure 3.2**), where Skp1 is an adaptor subunit that binds to the variable F-box protein that recognizes the substrate. In humans, there are about 69 interchangeable F-box proteins that can recognize different substrates.[114,115]

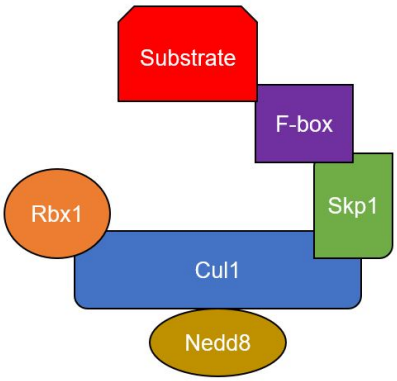

Figure 3.2: A simplified SCF complex

CRLs make up the largest known class of E3 ligases. CRLs can be differentiated based on the cullin subunit, i.e. a CRL that uses Cul2 can be referred to as a CRL2, a CRL that uses Cul4 can be referred to as a CRL4, etc. Each cullin associates with a different family of SRSs; there are as many as 400 distinct CRLs.[122,123] The SRS determines what substrates can bind to the CRL. CRL2s have a similar structure to the SCF complex, where the adaptor proteins are Skp1-related proteins called Elongin B and Elongin C, and the SRS is a von-Hippel-Lindau (VHL)-box protein.[122] CRL4 complexes

are more complicated in that there are two closely related Cul4 proteins that are coded for by two different genes: *Cul4a* and *Cul4b*.

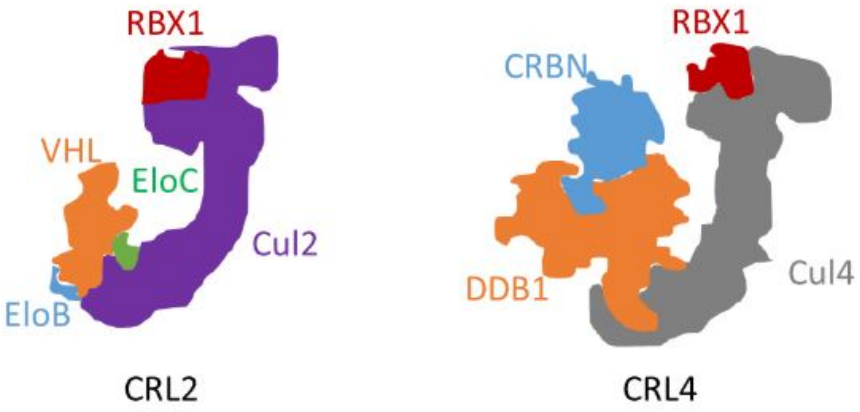

Figure 3.3: Depictions of $CRL2^{VHL}$ and $CRL4^{CRBN}$. *Adapted from https://njbio.com/targeted-protein-degraders/*

CRL4s typically associate with the adaptor (or linker) protein DDB1 (damaged DNA binding protein 1), and several different SRSs.[123,124] One specific SRS that is found in both Cul4a and Cul4b complexes is known as cereblon (CRBN).[124] The CRL2 and CRL4 complexes are shown in **Figure 3.3**.

3.1.6: VHL and CRBN

The *VHL* gene was discovered in 1993, and is named for von Hippel-Lindau disease, a familial cancer syndrome.[125] The VHL gene codes for two splice variants of the VHL protein: VHL_{30}, which has 213 amino acids and a molecular weight of 30 kDa, and VHL_{19}, which as 160 amino acids and a molecular weight of 19 kDa.[126–129] As mentioned previously, VHL acts as an substrate receptor for CRL2s. A small molecule inhibitor of VHL has been developed, known as VH032 (**Figure 3.4**), which has a dissociation constant of 185 nM.[130,131]

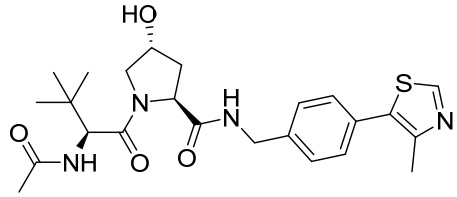

Figure 3.4: VHL Inhibitor VH032

The *CRBN* gene was discovered in 2004.[132,133] The gene encodes for the CRBN protein, which is made up of 442 amino acids and has a molecular weight of 51 kDa.[134] It encompasses an ATP-dependent Lon proteas domain in the N-terminal region, a seven α helical bundle domain that is involved in binding to DDB1, and a substrate binding domain in the N-terminus.[135] As mentioned previously, CRBN acts as a substrate receptor for CRL4s and is involved in endogenous protein degradation. In 2010, it was discovered that CRBN is responsible for thalidomide's teratogenic effects. Thalidomide (**Figure 3.5**) binds to CRBN and inhibits its activity as a ubiquitin E3 ligase.[136] This lead to the investigation of thalidomide as a drug for treating multiple myeloma. The mechanism of action is that thalidomide binds to CRBN and acts as a molecular glue between CRBN and the transcription factors IKZF1 and IKZF3, which are important for the survival of multiple myeloma. This catalyzes the ubiquitination and degradation of these transcription factors.[137] Thalidomide exists as two enantiomers; racemic thalidomide binds to CRBN with a dissociation constant of 18.1 μM. (S)-thalidomide has slightly higher affinity for CRBN (K_d = 3.5 μM) compared to (R)-thalidomide (K_d = 20 μM).[138]

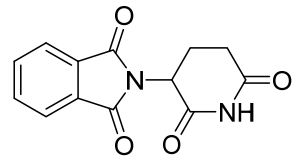

Figure 3.5: Thalidomide structure

VHL and CRBN are the most commonly targeted E3 ligases in PROteolysis TArgeting Chimeras (PROTAC) research. The known inhibitors of both CRBN and VHL have been exploited to target the endogenous UPS in order to catalyze the ubiquitination and degradation of a protein of interest (POI).[139]

3.2: PROTACs

3.2.1: PROTAC Background

Most inhibitory drugs function on two main principles: high equilibrium target occupancy, and maintaining exposure in the diseased tissue.[140] This utilizes what is termed "occupancy-driven pharmacology," in which an inhibitor binds to the target protein (typically in the active site) and blocks the function of the protein. The more of the protein that is blocked by the inhibitor, the more effective the drug, typically in a stoichiometric fashion. Selectivity of the inhibitor is determined by the binding affinity to the target protein. This model is in contrast to what is known as "event-driven pharmacology," in which protein function is controlled by decreasing the concentration of the target protein in the cell, i.e., controlling protein abundance. In event-driven pharmacology, restoration of protein function requires resynthesis of the protein. This is the principle that PROTACs are based on – that one can control the abundance of the target protein through pharmacologically-induced catalysis of ubiquitination and degradation.[141,142]

A PROTAC is a bivalent chemical probe (**Figure 3.6**) that binds to a POI as well as an E3 ligase, and catalyzes the ubiquitination and degradation of the POI by the

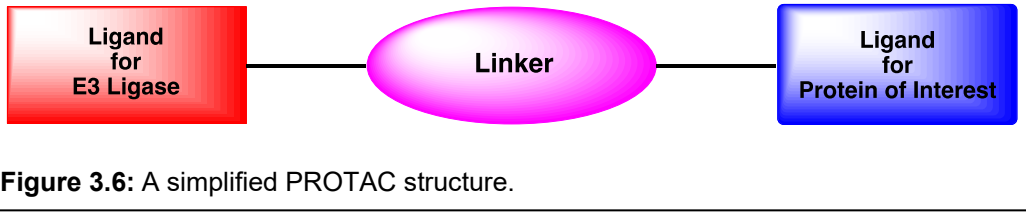

Figure 3.6: A simplified PROTAC structure.

proteasome.[143] Essentially, a PROTAC molecule "highjacks" the UPS to bring about degradation of a POI as a form of disease therapy. The first PROTAC was reported in 2001 by Craig Crews and colleagues. A proof of concept, the first PROTAC (named Protac-1) sought to recruit an unrelated protein, methionine aminopeptidase-2 (MetAP2)

to $SCF^{\beta\text{-}TRCP}$ and catalyze the ubiquitination and degradation of MetAP2. Indeed, Protac-1 was shown to specifically bind to MetAP2, recruit MetAP2 to SCF, mediate the ubiquitination of MetAP2, and degrade MetAP2 in *Xenopus* egg extracts. Protac-1 consisted of a peptide moiety that binds to SCF and a small molecule moiety that binds to MetAP2, and demonstrated the ternary complex that is formed between the E3 ligase, the PROTAC, and the protein of interest.[144]

Functional inhibitors target proteins with druggable active or allosteric sites, which only accesses approximately 20% of the human proteome. PROTACs introduce the idea of targeting the undruggable proteome, as a PROTAC does not need to functionally inhibit its target protein. The PROTAC's sole purpose is to bring the protein of interest in close contact with an E3 ligase. Further, PROTACs can be used in sub-stoichiometric concentrations, because once the target protein has been degraded by the proteasome, the PROTAC is free to bind to another protein molecule.[145,146] A schematic for how a PROTAC works in theory is shown in **Figure 3.7**.

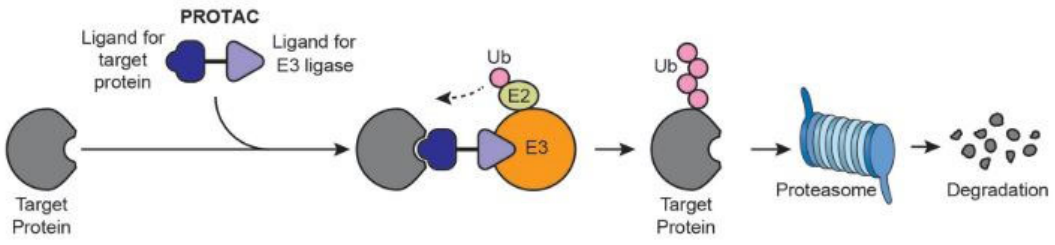

Figure 3.7: A schematic of the PROTAC mechanism. *Adapted from reference 146.*

3.2.2: Peptide-based PROTACs

Protac-1 was a hybrid molecule in that it utilized a small molecule to bind to the protein of interest and a peptide to bind to an E3 ligase. The small molecule ovalicin covalently binds to MetAP2, and is linked to the IκB-α phosphopeptide, which is recognized by the F-box SRS of the $SCF^{\beta\text{-}TRCP}$ complex (**Figure 3.8**).[144,147]

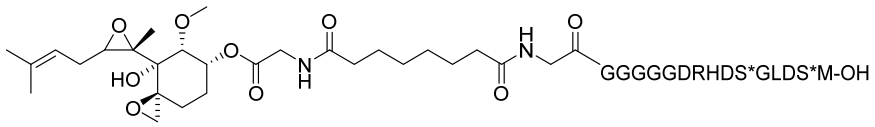

Figure 3.8: The structure of Protac-1. Asterisks indicate phosphorylated residues.

After the initial success of the first PROTAC in 2001, in 2003 the Crews group developed peptide-based PROTACs targeting the estrogen receptor (ER) and the androgen receptor (AR). They synthesized a 10-aa IκB-α peptide and linked it to either 17β-estradiol (E2) or dihydroxytestosterone (DHT). These PROTACs are known as Protac-2 and Protac-3, respectively. It was observed that Protac-2 catalyzed Cul1-dependent ubiquitination of ER at 10 μM concentration. Further, Protac-3 was observed to promote degradation of GFP-AR in HEK-293 cells.[148]

Though the early peptide-based PROTACs were successful at targeting the UPS and catalyzing degradation of a POI, cell permeability remained an issue. In 2004, Crews introduced Protac-4 as a cell permeable PROTAC.[108] This PROTAC contained the small molecule AP21998 to bind to the F36V mutant of FK506 binding protein (FKBP12). Rather than targeting the SCF, this PROTAC was the first to target the E3 ligase VHL. This was done by using the 7-aa sequence ALAPYIP to mimic the minimum recognition domain of hypoxia inducible factor 1α (HIF1α) by VHL. Appended to the end of this peptide was a poly-D-arginine cell-permeating peptide (CPP) to increase cell permeability of the PROTAC. Protac-4 was evidenced to mediate EGFP-FKBP12 degradation in HeLa cells

in a VHL-dependent manner.[108] This group then went on to create Protac-5, which linked the same HIF1α-polyarginine peptide sequence to DHT to induce degradation of GFP-AR in HEK-293 cells.[108]

Following in Crews' footsteps, Zhang et al developed a cell permeable PROTAC that degraded ER in MCF-7 cells in a VHL-dependent manner.[149] A combination of Protacs-2 and -5, Zhang's PROTAC was comprised of the octapeptide MLAPYIPM to exploit the HIF1α-VHL interaction and E2 to involve the ER. Other PROTACs were then designed utilizing HIF1α to target VHL. These include PROTACs targeting ER for the treatment of breast cancer,[150,151] AR for the treatment of prostate cancer,[151] and the aryl hydrocarbon receptor (AHR) for the treatment of liver cancer.[152,153]

Montrose and colleagues then designed a peptide-based PROTAC targeting the cancer-forming X-protein from the hepatitis B virus (HBV).[154] Unlike its predecessors, both ligands of this PROTAC were peptides. Specifically, this PROTAC was comprised of the N-terminal dimerization domain of the X-protein fused to its C-terminal degron domain, which acted as a novel E3 ligase recognition signal. Each peptide was attached at the N-terminus to a poly-arginine CPP. This PROTAC was shown to bind to and degrade both full-length and truncated X-protein in HEPG2 cells.[154] Other homo-peptide PROTACs were created, including those targeting Tau for the treatment of Alzheimer's disease.[155,156]

Though a good proof-of-concept and introduction to PROTAC technology, peptide-based PROTACs typically demonstrated activity in only the micromolar range. This is thought to be in part due to poor cell permeability, though this problem was aided by the addition of CPPs. However, due to their large size, it is also possible that peptide-based

PROTACs are recognized by the immune system and neutralized by antibodies, dampening their clinical applications.[147] Fortunately, the attempts to improve peptide-based PROTACs promoted the development of small molecule-based PROTACs.

3.2.3: Small molecule-based PROTACs

Small molecule-based PROTACs offer several advantages over peptide-based PROTACs. As mentioned previously, small molecule-based PROTACs have a lower molecular weight, which aids in cell penetration. Further, small molecules are more drug-like than peptides and are easier for the human body to absorb. Four main E3 ligases are targeted by small molecule-based PROTACs: VHL, CRBN, MDM2, and IAP.[147]

The first all-small-molecule PROTAC capable of inducing proteasomal degradation was reported in 2008.[157] Like many of the peptide-based PROTACs, this targets the androgen receptor (AR). This is in part because of the previous success of peptide-based PROTACs in degrading AR.[108] However, AR has also been shown to promote growth in prostate tumor cells, and inhibition of AR has demonstrated repression of cell growth in prostate tumors.[158] Rather than DHT, the ligand chosen to bind to AR was a selective androgen receptor modulator (SARM) that inhibits AR with a K_I of 4 nM.[159] The E3 ligase recruited by this PROTAC is the RING E3 ligase MDM2. A nutlin derivative, known as nutlin-3, was synthesized to be the MDM2-binding ligand. The two ligands were connected by a PEG3 linker. The structure of the SARM-nutlin PROTAC is shown in

Figure 3.9. This PROTAC was able to degrade AR in HeLa cells at a concentration of 10 μM.[157]

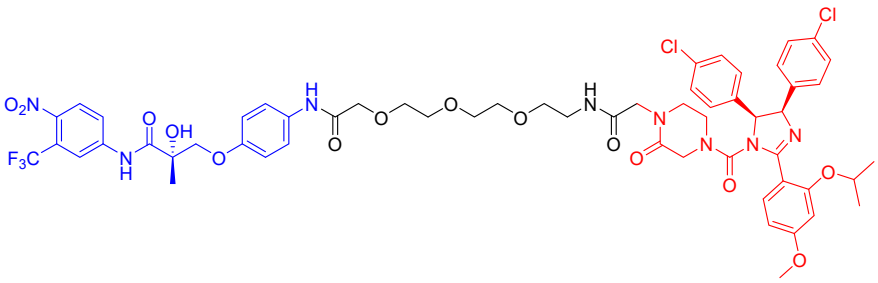

Figure 3.9: Structure of the first all-small-molecule PROTAC, linking together a SARM (blue) to target AR and nutlin-3 (red) to target MDM2.

In 2010, the Hashimoto group designed their own type of small molecule PROTAC known as Specific and Nongenetic IAPs-dependent Protein ERasers (SNIPERs).[160] They chose to target the E3 ligase cellular inhibitor of apoptosis protein 1 (cIAP1), which is an IAP and is overexpressed in some tumor cells. The group chose methyl bestatin (MeBS) to target cIAP1, which is from a class of bestatin ester analogues that bind to the BIR3 domain of cIAP1 and promote autoubiquitination and degradation of cIAP1.[161,162] The first SNIPER molecule was a proof-of-concept, so the researchers selected cellular retinoic acid binding proteins (CRABP-I and -II) as the target proteins to be degraded. ATRA (all-trans retinoic acid), is a specific small molecule ligand for CRABP-I and –II. The two ligands were separated by PEG linkers of varying lengths. These PROTACs were able to degrade CRABP-I in MOLT-4 cells and CRABP-II in HT1080 cells at a concentration of 1 μM.[160] This showed that the SNIPER approach to PROTACs was a viable option; cIAP1 can be targeted by a PROTAC to induce ubiquitination and degradation of a POI.

In 2011, the Hashimoto group expanded their SNIPER approach to target nuclear receptors (NRs), specifically ER, AR, and retinoic acid receptor (RAR).[163] To target binding to cIAP1, they used either MeBS or a related molecule known as BE04 (**Figure 3.10**). A compound known as Ch55 was chosen to target RAR due to its known selectivity for RAR over CRABP-II.[164,165] DHT was chosen as the binding ligand for AR, and estrone was chosen as the binding ligand for ER. It was confirmed via Western Blot that these RAR, AR, and ER SNIPERs effectively reduce the levels of the target protein.[163] However, it was later determined that bestatin is not highly selective for cIAP1 and can also recruit the anaphase-promoting complex/cyclosome (APC/C).[166]

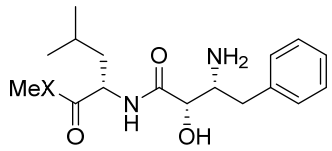

Figure 3.10: Bestatin ester analogues MeBS (X = O), and BE04 (X = NH).

Since 2015, VHL and CRBN have become the main E3 ligase targets for small molecule-based PROTACs.[167] This is due to the discovery of small-molecule ligands for VHL to replace the HIF1α peptide,[168,169] and immunomodulatory drugs (IMiDs) thalidomide, pomalidomide, and lenalidomide that bind to CRBN.[170] VHL-based small molecule PROTACs have been designed, synthesized and shown to degrade many proteins including GFP-HaloTag fusions,[171] ERRα,[172] RIPK2,[172] BCR-ABL,[173] BRD4,[174–176] TBK1,[177] several receptor tyrosine kinases (RTKs),[178] and TRIM24.[179] CRBN-based small molecule PROTACs have also been developed to target many proteins, including BRD2/3/4,[180–182] FKBP12,[180] BCR-ABL,[173] BRD9,[183] Sirt2,[184] CDK9,[185,186] FLT3,[187] BTK,[187,188] and ALK.[189]

An attractive PROTAC target is the class of proteins known as Bromodomain and Extra-Terminal (BET) proteins, specifically the BRomoDomain containing proteins 2, 3, and 4 (BRD2/3/4).[190] This is because BRD2/3/4 are epigenetic readers that bind to AR directly, which has implications in castration-resistant prostate cancer (CRPC). Further, when BRD2/3/4 are inhibited, this abrogates AR-mediated transcription.[191] BRD4 is also known to form a fusion gene with NUclear protein in Testes (NUT) to cause a rare, aggressive form of cancer called NUT midline carcinoma (NMC).[192] The compound (+)-JQ1 inhibits BRD4 with an IC_{50} of 77 nM, and binds to BRD4 with a K_d of 50 nM.[193] Due to this high affinity and potency, (+)-JQ1 has been used in several VHL- and CRBN-based BRD4 degraders.[190] A BET degrader known as ARV-771 (**Figure 3.11**) utilizes a glycol linker to connect (+)-JQ1 and VH032 to catalyze VHL-dependent ubiquitination and degradation of BRD2/3/4. ARV-771 is more potent than (+)-JQ1 alone, with an IC_{50} less than 1 nM and a K_d of 9.6 nM. ARV-771 is also able to degrade BRD4 with a DC_{50} (drug concentration that results in 50% protein degradation) less than 5 nM in 22Rv1, VCaP, and LnCaP95 cells.[174]

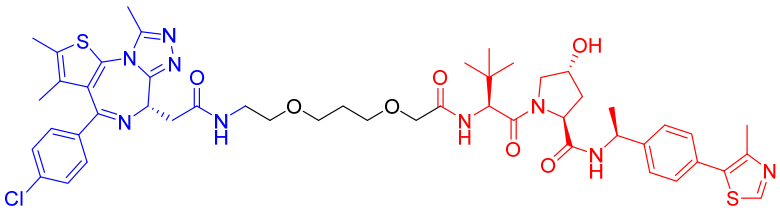

Figure 3. 11: The structure of the BET degrader ARV-771, which combines the BRD4 inhibitor (+)-JQ1 (blue) with the VHL inhibitor VH032 (red).

Zhou et al then optimized (+)-JQ1 through traditional SAR and identified the compound HJB97 as a more potent inhibitor of BRD4 with an IC_{50} of 7 nM and a K_I of 0.5 nM.[194] HJB97 was then utilized as the BET-binding ligand in a series of PROTACs with

varying linker lengths and types. In these PROTACs, thalidomide or its analogue lenalidomide were used to bind CRBN. This study resulted in an even more potent BET degrader known as BETd-260 (**Figure 3.12**), which links together lenalidomide and HJB97 with a 5-carbon aliphatic chain. BETd-260 effectively degrades BRD4 in RS4;11 cells at concentrations as low as 30 pM, and inhibits cell growth with an IC_{50} of 51 pM.[182] Both ARV-771 and BETd-260 show that small molecule-based PROTACs can effectively degrade BRD4 at very low concentrations when compared to treatment with small molecule inhibitors alone.

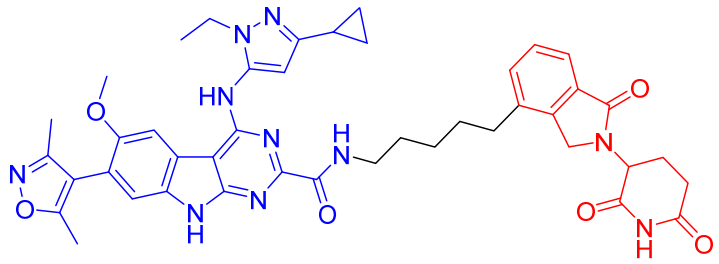

Figure 3.12: The structure of the BET degrader BETd-260, which combines the BRD4 inhibitor HJB97 (blue) with the CRBN inhibitor lenalidomide (red)

3.2.4: Linker Composition

As mentioned above, a PROTAC is a heterobifunctional molecule that consists of two “warheads” that target a POI and an E3 ligase, separated by a linker. While most PROTAC research has focused on development of new POI targets and potent E3-binding ligands, an important part of PROTAC research is determining the proper linker length and composition for effective ternary complex formation, and subsequent POI ubiquitination and degradation. To date, it is believed that linker length, composition, and attachment point must be optimized for each E3/POI pair.[195] For example, in 2011 Cyrus et al showed that in VHL/ER PROTACs, increasing the linker length from 9 atoms to 16 atoms increased potency in cell viability assays 5-fold in MCF-7 cells.[196]

The most popular linker compositions to date include PEG and alkyl chains, with some researchers opting for glycol chains that introduce extra methylene groups to PEG

linkers to extend the chain length.[195] In 2018, the Crews lab published structures of VHL/TBK1 PROTACs with PEG or glycol linkers ranging in length from 7-29 atoms. In this study, PROTACs with linker lengths less than 12 atoms did not degrade TBK1, and the optimal linker length was determined to be 21 atoms (DC_{50} = 3 nM).[177] More diverse linkers have been reported in the literature as well, including those that introduce rigidity such as alkynes, piperazine, and piperidine moieties.[197–199] Triazole-containing linkers have also become more attractive in the field due to their compatibility with click chemistry.[200]

3.2.5: PROTACs in the Clinic

Since the first PROTAC was pioneered in 2001, the field of targeted protein degradation has grown immensely. In 2019, Arvinas Therapeutics inaugurated the first PROTAC to enter into human clinical trials: an AR degrader known as ARV-110.[201,202] Today, 13 PROTAC molecules have entered into human trials (**Figure 3.13**), with diverse targets including AR, ER, BCL-X_L, IRAK4, STAT3, BTK, TRK, and BRD9. All but one of these degraders are for cancer treatment. This field continues to grow: to date there are more than 1600 published PROTAC molecules, acting on more than 100 different molecular targets.[201]

Drug	Sponsor	Properties	Lead indication	Status
Heterobifunctional degraders (PROTACs, BiDACs, etc.)				
ARV-110	Arvinas	Androgen receptor degrader	Prostate cancer	Phase II
ARV-471	Arvinas	Oestrogen receptor degrader	Breast cancer	Phase II
ARV-766	Arvinas	Androgen receptor degrader	Prostate cancer	Phase I in 2021
AR-LDD	Bristol Myers Squibb	Androgen receptor degrader	Prostate cancer	Phase I
DT2216	Dialectic	BCL-XL degrader	Liquid and solid cancers	Phase I
KT-474	Kymera/Sanofi	IRAK4 degrader	Autoimmune including AD, HS and RA	Phase I
KT-413	Kymera	IRAK4 degrader with IMiD activity	MYD88-mutant DLBCL	Phase I in 2H2021
KT-333	Kymera	STAT3 degrader	Liquid and solid tumours	Phase I in 2H2021
NX-2127	Nurix	BTK degrader with IMiD activity	B cell malignancies	Phase I
NX-5948	Nurix	BTK degrader	B cell malignancies and autoimmune	Phase I in 2H2021
CG001419	Cullgen	TRK degrader	Cancer and other diseases	IND in 2021
CFT8634	C4 Therapeutics	BRD9 degrader	Synovial sarcoma	IND in 2H2021
FHD-609	Foghorn	BRD9 degrader	Synovial sarcoma	IND in 1H2021

Figure 3.13: A summary of PROTAC molecules in human clinical trials in 2021. *Adapted from reference 201.*

Chapter 4: Development of CtBP PROTACs

4.1: Design of CtBP PROTACs

4.1.1: Ligand for E3 Ligase

Pomalidomide (**Figure 4.1**), a thalidomide analogue, was chosen as the ligand for the E3 ligase. Pomalidomide binds to the E3 ligase CRBN with a dissociation constant of 3 μM.[203] We decided to target CRBN as the E3 ligase because it is ubiquitously expressed.[139] The aniline nitrogen was chosen as the point of attachment to the ligand because this can be expanded with amide bond coupling chemistry. A glycine residue was attached at this point by reductive amination.

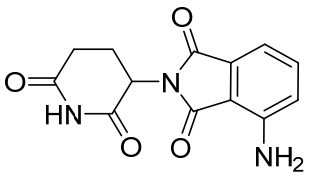

Figure 4.1: Pomalidomide Structure

4.1.2: Ligand for CtBP

HIPP was chosen as the CtBP-binding ligand. It has a dissociation constant for CtBP1 of 370 nM at biological pH.[87] To determine the point of attachment to the linker of the PROTAC, the HIPP-CtBP1 co-crystal structure was observed in PyMOL v2.4.1 as a

space-filling surface model (**Figure 4.2**). The 4-position of the phenyl ring (para to the HIA moiety) was selected as the optimal point of attachment for HIPP-based CtBP

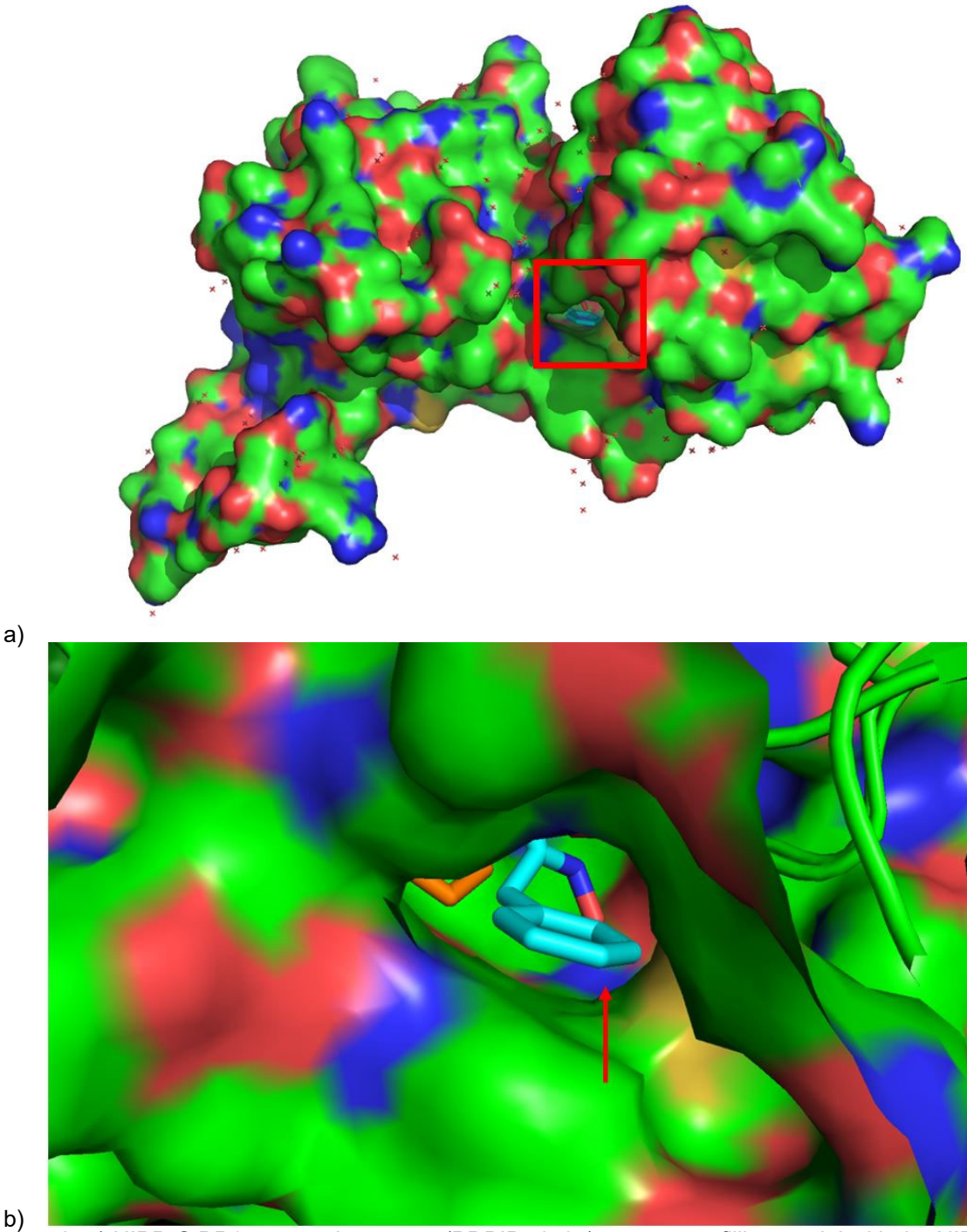

Figure 4.2: a) HIPP-CtBP1 cocrystal structure (PDBID: 4u6q) as a space filling model with the HIPP ligand boxed in red. b) A close-up view of HIPP in the CtBP1 binding pocket with an arrow pointing at the 4-position on the phenyl ring to indicate the optimal point of attachment for HIPP-based PROTACs.

PROTACs due to its position in the binding pocket of CtBP1. With this in mind, we appended an aminomethyl moiety at the 4-position of the phenyl ring for coupling to the linker.

4.1.3: Linker Composition

Aliphatic Fmoc amino acids are commercially available (n = 1-6, **Figure 4.3**) and can be connected to ligands using amide coupling chemistry. In most PROTAC molecules, the linker length is between 10-14 atoms. For the first PROTAC molecule synthesized, Fmoc-amino-heptanoic acid (Fmoc-7-AHP-OH, n = 6) was selected for use as the linker because it is inexpensive and could be used as a proof-of-concept when optimizing synthesis of the PROTACs.

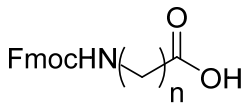

Figure 4.3: Aliphatic Fmoc amino acids.

Once the chemistry was optimized, we opted to use Fmoc-protected PEG linkers (PEG2 and PEG3, **Figure 4.4**) as these are more commonly seen in PROTAC molecules in the literature and are more soluble than fully aliphatic linkers.

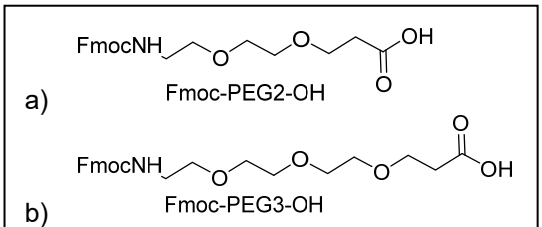

Figure 4.4: PEG2 (a) and PEG3 (b) Fmoc-protected linker molecules.

4.1.4: *Design of 3 HIPP-based CtBP PROTACs*

In total, we designed and synthesized three HIPP-based CtBP PROTACs, which utilized pomalidomide to bind CRBN. These PROTACs (**Figure 4.5**) differ only in linker length and composition. Once assembled, we predicted that these PROTACs would bind to both CtBP and CRBN, which would result in the ubiquitination of CtBP and subsequent degradation by the proteasome. As CtBP degradation is catalytic, the PROTAC is a catalyst that would then be reused to degrade more CtBP (**Figure 4.6**).

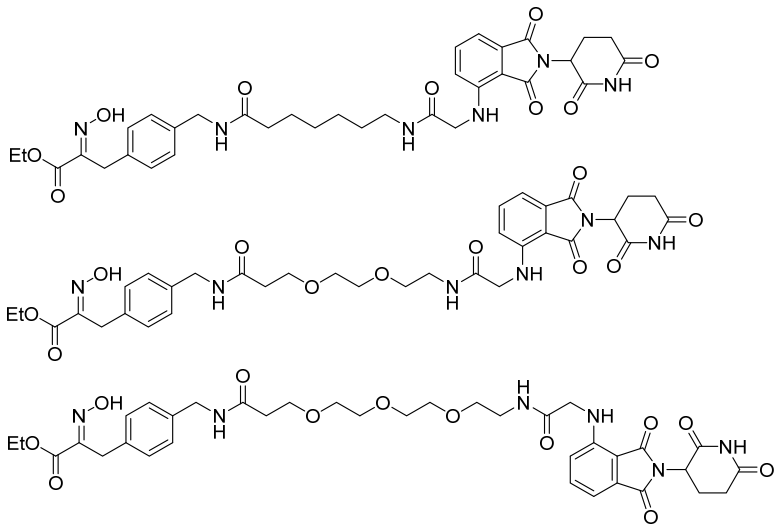

Figure 4.5: Structures of the 3 HIPP-based CtBP PROTACs.

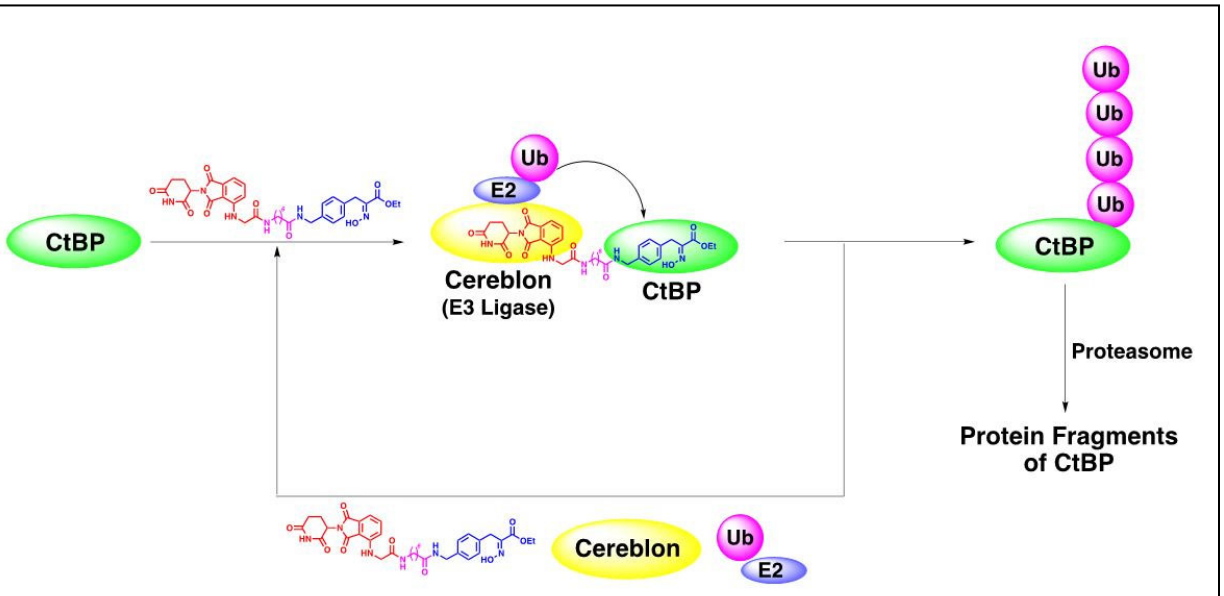

Figure 4.6: The predicted mechanism of HIPP-based CtBP PROTACs.

4.2: Experimental

4.2.1: Synthesis of HIPP-based CtBP PROTACs

We started with synthesis of the CRBN binding partner, POM-Gly-OH based on previously published work by another lab in the VCU Medicinal Chemistry department (**Scheme 4.1**).[204] First, 3-nitrophthalic anhydride (1.5 eq) and 3-aminopiperidine-2,6-dione hydrochloride (1 eq) were heated to reflux in glacial acetic acid with sodium acetate (1.2 eq). This nucleophilic ring opening and closing reaction afforded nitro-pomalidomide (**4.1**). We then performed a one-pot reduction-reductive amination series of reactions to append a glycine linker on pomalidomide. Nitro-pomalidomide was reacted with 5% palladium on carbon (10 wt%) and 50 psi H_2 gas to reduce the nitro functional group to the primary amine. This was followed by addition of glyoxylic acid monohydrate (5 eq) and sodium sulfate (1 g/mmol) in a reductive amination to give Pom-Gly-OH (**4.2**).[205] With this compound in hand, we began pilot reactions to couple the pomalidomide fragment to the linker fragment.

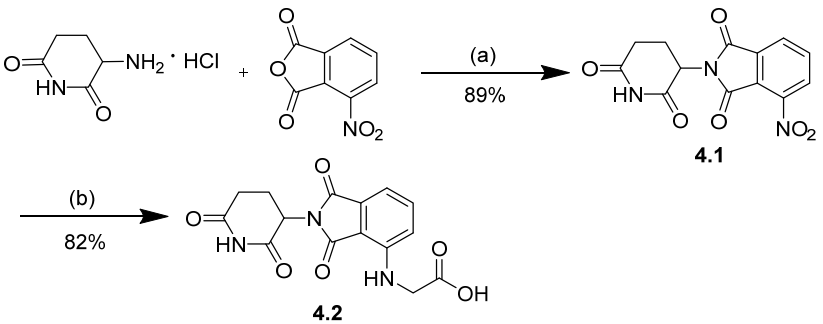

Scheme 4.1: Synthesis of compounds **4.1** and **4.2**. Reagents and conditions: (a) NaOAc, AcOH, 110°C, 5 h. (b) 5% Pd/C, H_2 (50 psi), Na_2SO_4, glyoxylic acid monohydrate, dioxane, rt, 16 h.

First we protected the carboxylic acid of Fmoc-7-AHP-OH as a benzyl ester (**4.3**, **Scheme 4.2**) by addition of thionyl chloride (10 eq) in benzyl alcohol (14 eq) at 0°C, and refluxing for 24 h.[206] The Fmoc group was then deprotected using piperidine (11 eq) to

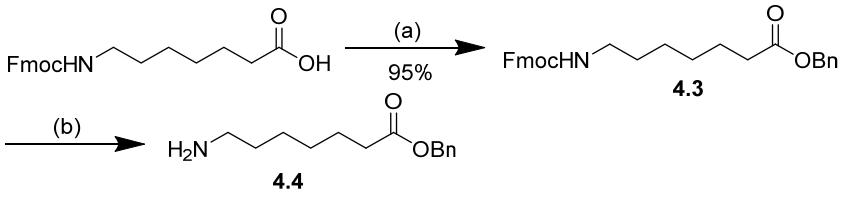

Scheme 4.2: Synthesis of compounds **4.3** and **4.4**. Reagents and conditions: (a) $SOCl_3$, BnOH, 0→100°C, 24 h. (b) Piperidine, DCM, rt, 24 h.

afford the fragment NH_2-7-AHP-OBn (**4.4**).[207] NH_2-7-AHP-OBn (1.2 eq) was then coupled using amide coupling chemistry[182] to the Pom-Gly-OH fragment (1 eq) with HATU (1.2 eq) and DIPEA (3 eq) to yield Pom-Gly-7-AHP-OBn (**4.5**, **Scheme 4.3**). Unfortunately, in our hands we were unable to effectively purify this molecule in either normal or reversed phase column chromatography.

Given these results, we chose to reorder the synthetic steps and instead attach

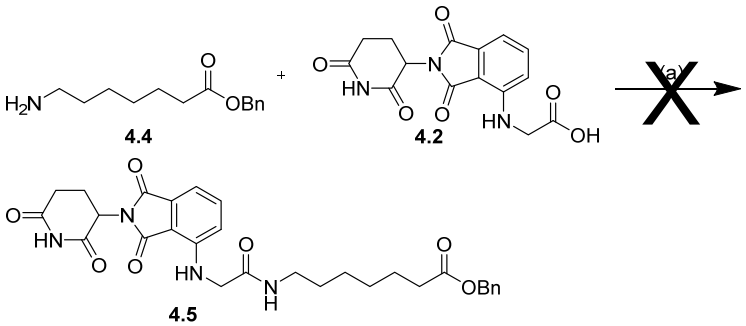

Scheme 4.3: Synthesis of compound **4.5**. Reagents and conditions: (a) HATU, DIPEA, DMF, rt, 2 h.

the linker fragment to the CtBP-binding ligand HIPP prior to attachment to Pom-Gly-OH, as the Fmoc-7-AHP-HIPP intermediate can be purified with normal phase automated MPLC.

Synthesis of the HIPP fragment began with 4-(aminomethyl)benzoic acid (1 eq), which was reduced by LAH (4 eq) to yield (4-(aminomethyl)phenyl)methanol (**4.6**, **Scheme 4.4**). Next, the free amino group needed to be protected in

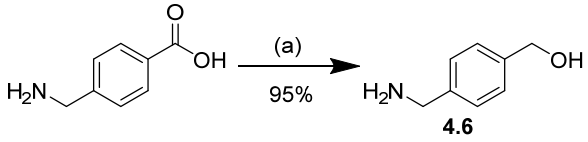

Scheme 4.4: Synthesis of compound **4.6**. Reagents and conditions: (a) LAH, THF, 0→ 63°C, 16 h.

order for us to perform further chemistry on the alcohol moiety. Our lab had previously tried to use a carboxybenzyl (Cbz) protecting group at this position, but we were unable to remove the Cbz group cleanly. Next we attempted a strategy with an allyloxycarbonyl (Alloc) protecting group.

As seen in **Scheme 4.5**, amine **4.6** (1 eq) was reacted with allyl oxycarbonyl chloride (1.1 eq) to afford allyl (4-(hydroxymethyl)benzyl)carbamate (**4.7**). The alcohol of **4.7** was then oxidized with MnO_2 (11 eq) to produce allyl (4-formylbenzyl)carbamate (**4.8**). With the aldehyde **4.8** (1.5 eq) in hand, we performed a HWE reaction with compound **2.2** (1 eq, from **Scheme 2.1**) in the presence of LiHMDS (1.1 eq) to yield ethyl 3-(4-((((allyloxy)carbonyl)amino)methyl)phenyl)-2-((tert-butyldimethylsilyl)oxy)acrylate (**4.9**) as a mixture of E and Z isomers. Similar to the reactions performed in *Section 2.2.4*, this product then underwent a two-step, one-pot reaction to convert the silyl enol ether **4.9** to an oxime. **4.9** was reacted first with triethylamine trihydrofluoride (1.7 eq), followed by hydroxylamine hydrochloride (1.7 eq) to create ethyl 3-(4-((((allyloxy)carbonyl)amino)methyl)phenyl)-2-(hydroxyimino)propanoate (**4.10**).

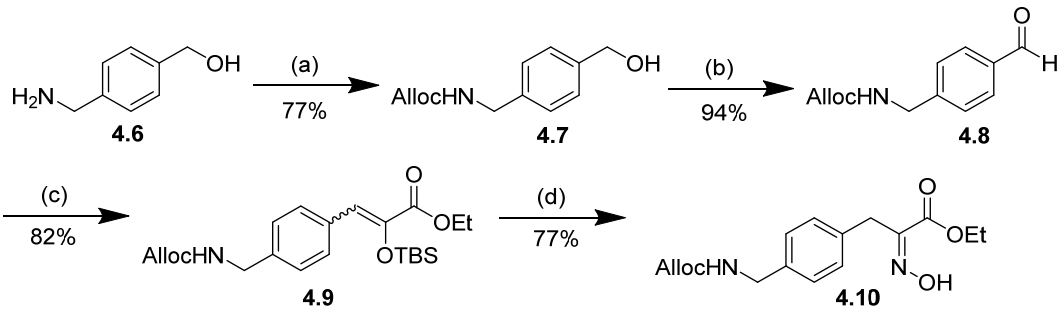

Scheme 4.5: Synthesis of compounds **4.7**-**4.10**. Reagents and conditions: (a) allyl oxycarbonyl chloride, dioxane/1N NaOH (2:1), 0°C → rt, 16 h. (b) MnO_2, THF, rt, 16 h. (c) **2.2**, LiHMDS, THF, -78°C → rt, 15 h. () $3HF \cdot NEt_3$, $H_2NOH \cdot HCl$, EtOH/$CHCl_3$ (4:1), rt, 19 h.

For attachment to Fmoc-7-AHP-OH, we first had to remove the Alloc protecting group and produce ethyl 3-(4-(aminomethyl)phenyl)-2-(hydroxyimino)propanoate (**4.11**,

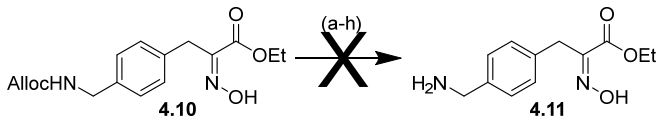

Scheme 4.6: Synthesis of compound **4.11**. Reagents and conditions: (a) $Pd(PPh_3)_4$, K_2CO_3, MeOH, rt, 12 h. (b) $Pd(PPh_3)_4$, DMBA, K_2CO_3, MeOH, rt, 12 h. (c) $Pd(PPh_3)_4$, DMBA, K^+ $^-$OtBu, THF, rt, 12 h. (d) $Pd(PPh_3)_4$, DMBA, K^+ $^-$OtBu, DCM, rt, 12 h. (e) $Pd(PPh_3)_4$, DMBA, NaOH, THF, rt, 12 h. (f) $Pd(PPh_3)_4$, DMBA, NaOH, DCM, rt, 12 h. (g) $Pd(PPh_3)_4$, DMBA, THF, rt, 12 h. (h) $Pd(PPh_3)_4$, DMBA, DCM, rt, 12 h.

Scheme 4.6). We attempted this with several different sets of conditions, all involving the palladium catalyst known as tetrakis ($Pd(PPh_3)_4$, 0.1 eq).[208] These reactions were attempted in MeOH, THF, and DCM. We tried to several bases (3 eq) including K_2CO_3, NaOH, and K^+ $^-$OtBu. We also experimented with addition of 1,3-dimethylbarbituric acid (DMBA, 1.5 eq) to act as a scavenger for Pd. None of these reactions were successful, unfortunately. We were able to determine by ^{13}C NMR that the oxime was not stable to these Alloc deprotection conditions.

Looking in the literature,[209] we chose to attempt a reaction with **4.10**, tetrakis (0.15 eq), and *N,N,*1,1,1-pentamethylsilanamine (1 eq) to yield ethyl (2-(hydroxyimino)-3-(4-(((((trimethylsilyl)oxy)carbonyl)amino)methyl)phenyl)propanoate (**4.12**) in hopes that the trimethylsilyl carbamate would be easier to remove, but this reaction was not successful (**Scheme 4.7**). As a final attempt to remove the Alloc protecting group, we TBS protected the oxime oxygen by reacting **4.10** with imidazole (3 eq), DMAP (0.15 eq), and TBS chloride (2 eq) to afford ethyl 3-(4-((((allyloxy)carbonyl)amino)methyl)phenyl)-2-(((tert-butyldimethylsilyl)oxy)imino)propanoate (**4.13**), which we then carried into a reaction with tetrakis (0.15 eq) and potassium carbonate (3 eq) to remove the Alloc group and yield ethyl (Z)-3-(4-(aminomethyl)phenyl)-2-(((tert-butyldimethylsilyl)oxy)imino)propanoate

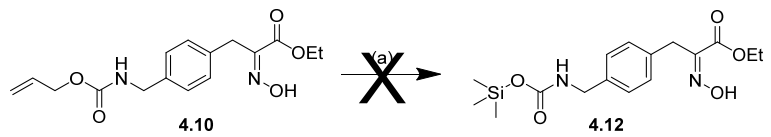

Scheme 4.7: Synthesis of compound **4.12**. Reagents and conditions: (a) $Pd(PPh_3)_4$, $(Me)_2NTMS$, DCM, rt, 2 h.

(**4.14**), but the oxime was unstable to these conditions as well (**Scheme 4.8**). This led us to turn to a different protecting group strategy.

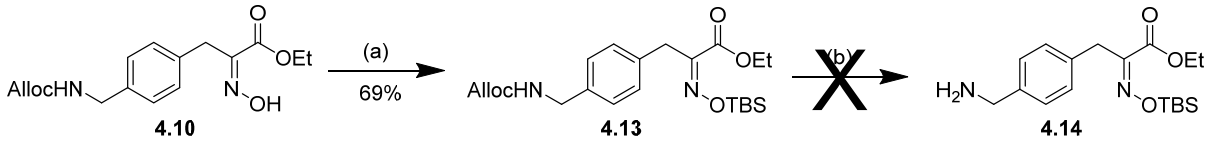

4.10 4.13 4.14

Scheme 4.8: Synthesis of compounds **4.13** and **4.14**. Reagents and conditions: (a) Imidazole, DMAP, TBS chloride, DCM, rt, 18h. (b) Tetrakis, K_2CO_3, MeOH, rt, 3 h.

With amine **4.6** in hand, we next decided to synthesize the HIPP fragment utilizing a Boc protecting group strategy (**Scheme 4.9**). In our initial synthesis, we combined **4.6** with Boc anhydride (1.2 eq) and sodium bicarbonate (3 eq) to Boc protect the free amine and afford *tert*-butyl (4-hydroxymethyl)benzyl)carbamate (**4.15**). This then underwent an oxidation reaction with MnO_2 (11 eq) to yield *tert*-butyl (4-formylbenzyl)carbamate (**4.16**). This aldehyde (1.5 eq) was then combined with **2.2** (1 eq) in a HWE reaction, in the presence of LDA, to produce ethyl 3-(4-(((*tert*-butoxycarbonyl)amino)methyl)phenyl)-2-((*tert*-butyldimethylsilyl)oxy)acrylate as a mixture of E/Z isomers (**4.17**).[92] The TBS group was removed from the silyl enol ether with triethylamine trihydroflouride (1.7 eq) and the enol was converted to an oxime with hydroxylamine hydrochloride (1.7 eq) to afford the Boc-protected HIPP fragment (**4.18**). Finally, we were able to remove the Boc protecting

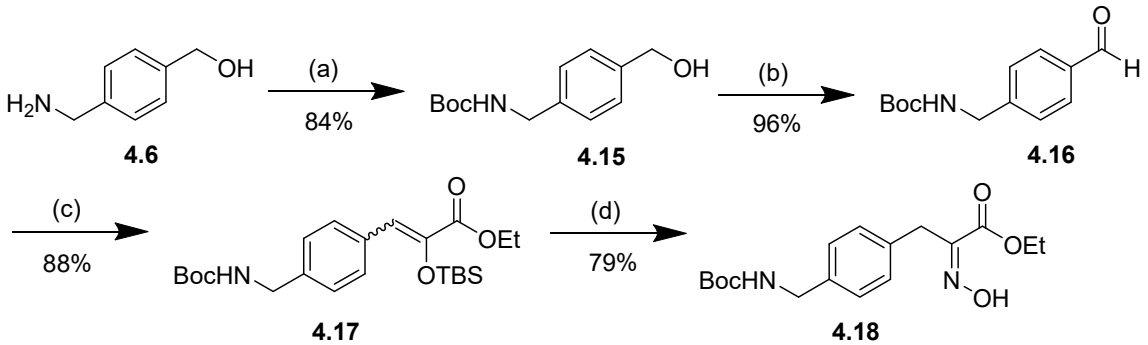

4.6 4.15 4.16

4.17 4.18

Scheme 4.9: Synthesis of compounds **4.15-4.18**. Reagents and conditions: (a) Boc_2O, $NaHCO_3$, H_2O/dioxane (1:1), 0°C → rt, 16 h. (b) MnO_2, THF, rt, 16 h. (c) **2.2**, LDA, THF, -78°C → rt, 15 h. (d) $3HF \cdot NEt_3$, $H_2NOH \cdot HCl$, EtOH/$CHCl_3$ (4:1), rt, 19 h.

group cleanly with hydrochloric acid (4 eq) to generate compound **4.11** as an HCl salt (**Scheme 4.10**).[210]

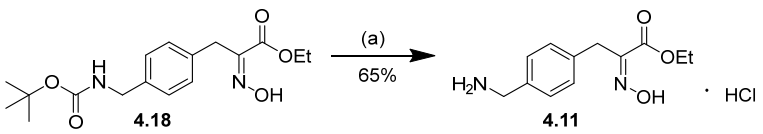

Scheme 4.10: Synthesis of compound **4.11**. Reagents and conditions: (a) 4N HCl, dioxane, rt, 30 min.

As a proof of concept (**Scheme 4.11**), we coupled **4.11** (1.2 eq) to Fmoc-7-AHP-OH (1 eq) with HATU (1.2 eq) and DIPEA (3 eq) to yield ethyl 3-(4-((7-((((9H-fluoren-9-yl)methoxy)carbonyl)amino)heptanamido)methyl)phenyl)-2-(hydroxyimino)propanoate (**4.19**).[211] The Fmoc protecting group was removed with piperidine (11 eq) to afford ethyl 3-(4-((7-aminoheptanamido)methyl)phenyl)-2-(hydroxyimino)propanoate (**4.20**).[207] The HIPP-linker fragment (1.2 eq) was then coupled to Pom-Gly-OH (1 eq) with HATU (1.2 eq) and DIPEA (3 eq) to produce the fully synthesized aliphatic CtBP PROTAC, ethyl 3-(4-((7-(2-((2-(2,6-dioxopiperidin-3-yl)-1,3-dioxoisoindolin-4-yl)amino)acetamido)heptanamido)methyl)phenyl)-2-(hydroxyimino)propanoate (**4.21**), which we purified by preparative HPLC. However, through this method we were only able to obtain 5 mg of final product and the yield was quite poor (6%). We next optimized select reactions of this total synthetic scheme.

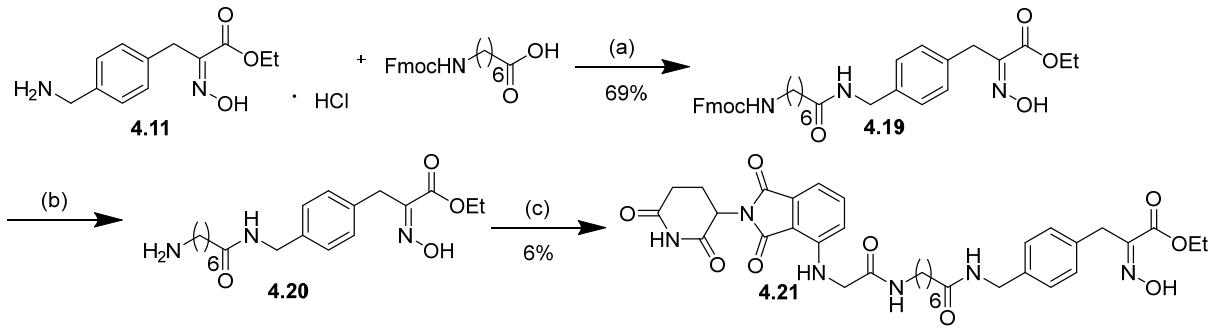

Scheme 4.11: Synthesis of compounds **4.19**-**4.21**. Reagents and conditions: (a) HATU, DIPEA, DMF, rt, 16 h. (b) Piperidine, DCM, rt, 24 h. () **4.2**, HATU, DIPEA, DMF, rt, 16 h.

We chose to optimize the Boc protection step (**Scheme 4.12**), because when the reaction was scaled up from 3.6 mmol (494 mg) to 13.23 mmol (1.81 g), the yield decreased from 84% to 31%. We identified several Boc protection methods in the literature. First we attempted reacting amine **4.6** with Boc anhydride (1.16 eq) in MeOH at rt for 12 h,[212] but this only resulted in 24% yield. Next we reacted **4.6** (1 eq) with TEA (1.03 eq) and Boc anhydride (1.06 eq) in THF at rt overnight,[213] and while we were able to obtain 66% yield we did not get a pure product. Next we mixed **4.6** (1 eq) with TEA (1 eq) for 10 min at rt in THF, followed by addition of Boc anhydride (1 eq) and further stirring at rt for 90 min,[214] but this reaction afforded a 41% yield. Finally, we found optimized conditions in which **4.6** (1 eq) is dissolved in tert-butanol/1M NaOH (2:1), followed by addition of Boc anhydride and stirred for 2 hours.[215] We chose to carry this reaction into the MnO_2 oxidation without purification, and obtained a 64% yield over two steps.

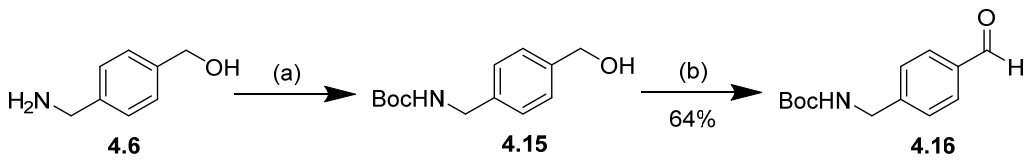

4.6 **4.15** **4.16**

Scheme 4.12: Optimized synthesis of compounds **4.15** and **4.16**. Reagents and conditions: (a) Boc_2O, tBuOH/1M NaOH (2:1), 0°C → rt, 2 h. (b) MnO_2, THF, rt, 16 h.

Next, we optimized the Boc deprotection step of the synthetic scheme (**Scheme 4.13**), because in our previous conditions we recovered 65% yield while the yield reported in the literature was much higher. We continued to react **4.18** with 4N HCl, but optimized the time of the reaction and the work-up. We determined the reaction goes to completion after 19 h through careful monitoring of the reaction by TLC and LC-MS. We also opted to use gentler work-up conditions, where rather than using the rotovap to

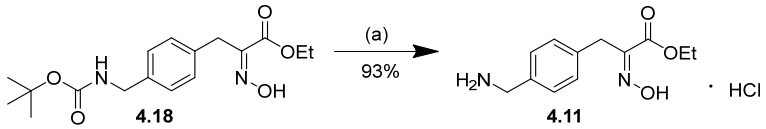

4.18 **4.11**

Scheme 4.13: Optimized synthesis of compound **4.11**. Reagents and conditions: (a) 4N HCl, dioxane, rt, 19 h.

evaporate dioxane, we blew nitrogen gas into the reaction flask overnight for a slower evaporation of solvent. This afforded us a 93% yield on this step.

Once we optimized synthesis of the CtBP-binding ligand of the PROTAC, we moved into optimization of the amide bond coupling steps. In our original coupling conditions to append **4.11** to Fmoc-7-AHP-OH (**Scheme 4.14**), we were unable to purify the reaction product effectively on larger scales. However, we felt it was important to bring pure product into the following steps. We opted to continue utilizing HATU (1.2 eq) as the coupling reagent, but chose to use Fmoc-7-AHP-OH in excess (1.05 eq). To aid in purification, we added an aqueous wash step to the work-up followed by extraction with ethyl acetate. We then were able to purify the reaction product by automated MPLC (CombiflashRf) in DCM/MeOH, where each solvent was treated with 0.1% TEA.

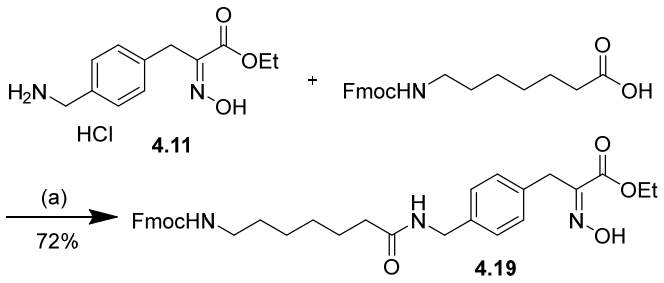

Scheme 4.14: Optimized synthesis of compound **4.19**. Reagents and conditions: (a) HATU, DIPEA, DMF, rt, 16

We next optimized the Fmoc deprotection of the HIPP-linker fragment **4.19** because through LC-MS analysis we were able to determine that piperidine was not an efficient reagent for this reaction. This is because the piperidine cannot be separated from the reaction product, and is carried over into the final coupling to Pom-Gly-OH. The piperidine then forms an unintended side product with **4.2** (**Figure 4.7**) that inhibits this coupling reaction from going to completion. We first attempted an Fmoc deprotection with 1,8-

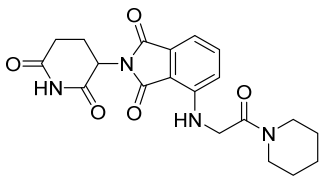

Figure 4.7: Structure of the product of the side reaction between **4.2** and piperidine.

Diazabicyclo[5.4.0]undec-7-ene (DBU, 3 eq)[216] but the reaction product was unstable. We also attempted to deprotect with a catalytic amount of DBU (0.1 eq) using dodecanethiol (10 eq) as a scavenger for the dibenzofulvene side product,[217] but this resulted in degradation of the product. We found a clean, efficient deprotection reagent in polymer-bound piperazine (**Scheme 4.15**).[218] We reacted **4.19** with polymer-bound piperazine (10 eq) to afford compound **4.20**. We were able to filter off the solid-supported piperazine and carry **4.20** into the final coupling reaction without further purification.

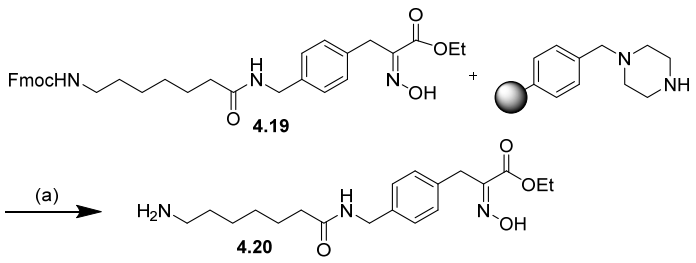

Scheme 4.15: Optimized synthesis of compound **4.20**. Reagents and conditions: (a) DMF, rt, 24 h.

For the final coupling reaction (**Scheme 4.16**), we chose to optimize the coupling reagent utilized, as well as the purification step. We tested reaction conditions utilizing 1-ethyl-3-(3-dimethylaminopropyl)carbodiimide (EDCI) with hydroxybenzotriazole (HOBt), or benzotriazol-1-yloxytripyrrolidinophosphonium hexafluorophosphate (PyBOP). The optimal conditions for this reaction involved mixing **4.2** with PyBOP (1.2 eq) in DMF for 1

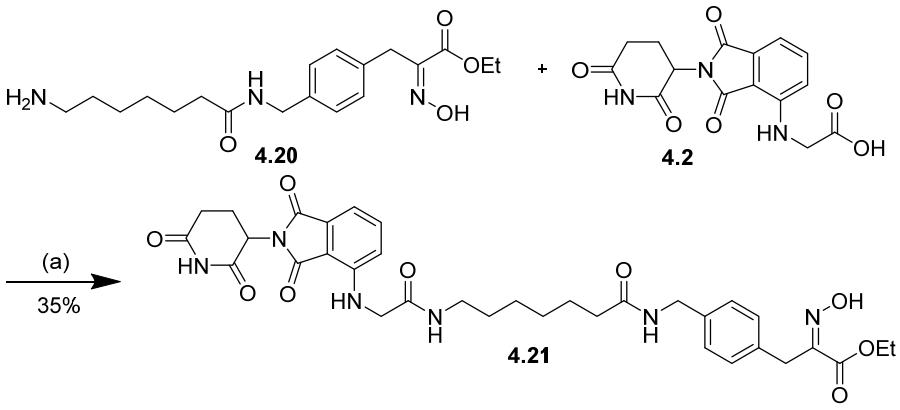

Scheme 4.16: Optimized synthesis of compound **4.21**. Reagents and conditions: (a) PyBOP, DIPEA, DMF, rt, 16 h.

hour, followed by addition of **4.20** and DIPEA sequentially, which was then stirred overnight at rt. For purification, we dried the reaction product on C18 and purified by reversed phase automated MPLC (CombiflashRf), to yield ~100 mg of pure aliphatic PROTAC product (**4.21**).

Once we successfully synthesized and purified the aliphatic PROTAC, we were ready to synthesize the PROTACs with the PEG linkers (**Scheme 4.17**). We coupled HIPP fragment **4.11** (1 eq) to either 1-(9H-fluoren-9-yl)-3-oxo-2,7,10-trioxa-4-azatridecan-13-oic acid (Fmoc-PEG2-OH) or 1-(9H-fluoren-9-yl)-3-oxo-2,7,10,13-tetraoxa-4-azahexadecan-16-oic acid (Fmoc-PEG3-OH) with HATU (1.2 eq) and DIPEA (3 eq) to afford ethyl 3-(4-(1-(9H-fluoren-9-yl)-3,13-dioxo-2,7,10-trioxa-4,14-diazapentadecan-15-yl)phenyl)-2-(hydroxyimino)propanoate (**4.22**) and ethyl 3-(4-(1-(9H-fluoren-9-yl)-3,16-dioxo-2,7,10,13-tetraoxa-4,17-diazaoctadecan-18-yl)phenyl)-2-(hydroxyimino)propanoate (**4.23**). The HIPP-linker fragments **4.22** and **4.23** were then Fmoc-deprotected using polymer-bound piperazine (10 eq) to yield ethyl 3-(4-((3-(2-(2-aminoethoxy)ethoxy)propanamido)methyl)phenyl)-2-(hydroxyimino)propanoate (**4.24**) and ethyl 3-(4-(14-amino-3-oxo-6,9,12-trioxa-2-azatetradecyl)phenyl)-2-

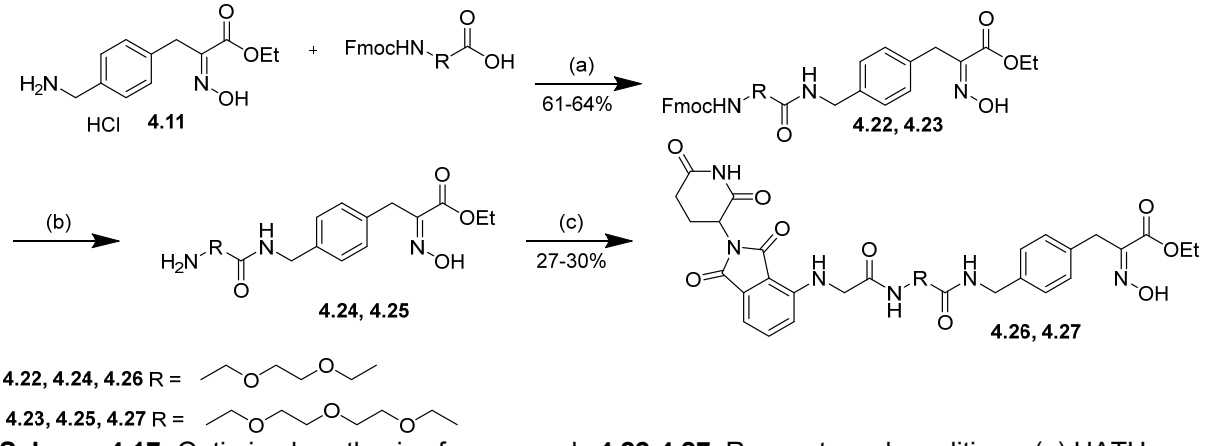

Scheme 4.17: Optimized synthesis of compounds **4.22-4.27**. Reagents and conditions: (a) HATU, DIPEA, DMF, rt, 16 h. (b) Polymer-bound piperazine, DMF, rt, 24 h. (c) **4.2**, PyBOP, DIPEA, DMF, rt, 16h.

(hydroxyimino)propanoate (**4.25**) respectively. Finally, **4.24** and **4.25** were coupled to **4.2** utilizing PyBOP (1.2 eq) and DIPEA (3 eq) to afford the final PROTAC products: ethyl 3-(4-(14-((2-(2,6-dioxopiperidin-3-yl)-1,3-dioxoisoindolin-4-yl)amino)-3,13-dioxo-6,9-dioxa-2,12-diazatetradecyl)phenyl)-2-(hydroxyimino)propanoate (**4.26**) and ethyl 3-(4-(17-((2-(2,6-dioxopiperidin-3-yl)-1,3-dioxoisoindolin-4-yl)amino)-3,16-dioxo-6,9,12-trioxa-2,15-diazaheptadecyl)phenyl)-2-(hydroxyimino)propanoate (**4.27**). For purification, we dried the reaction products on C18 and purified by reversed phase automated MPLC (CombiflashRf), to yield ~100 mg of pure PROTAC product (**4.26** and **4.27**).

4.2.2: Biological evaluation of CtBP PROTACs

A2780 cells were cultured according to standard protocol. CtBP PROTACs **4.21**, **4.26**, and **4.27** were dissolved in DMSO and mixed into the full medium for an overnight period. The original cell medium was then replaced with drug medium. Cells were incubated for 48 h, then lysed by RIPA buffer and supplemented with protease and phosphatase inhibitors. The cell lysates were separated by 4-12% SDS-PAGE (sodium dodecyl-sulfate polyacrylamide gel electrophoresis) gels and blotted into PVDF (polyvinyl diflouride) membranes. The transblotted membranes were blocked with TBST containing 5% milk for 1 h, and probed with CtBP1 or CtBP2 antibody for an overnight period at 4°C. The membranes were then washed with TBST and incubated with conjugated secondary antibody in blocking buffer at room temperature for 1 h. ImageJ was used to quantify the relative intensity of each band. The net protein bands and loading controls are calculated by deducting the background from the inverted band value. The final relative quantification values are the ratio of the net band to the net loading control. Percent band intensity data were normalized to the no inhibitor control well, converted to a percentage,

and plotted against the log of the concentrations of PROTAC. Curve fitting and the determination of the DC_{50} were performed in Prism (Graphpad, Version 9) using non-linear regression to the log(inhibitor) vs normalized response equation. DC_{50} values represent the drug concentration that results in 50% band intensity of the control. Cellular assays and western blots were performed by Dr. Boxiao Ding and Dr. Martin M. Dcona from the University of Southern California.

4.3: Results and Discussion

4.3.1: Results from the biological evaluation of CtBP PROTACs

Initially, our three PROTAC molecules (**4.21**, **4.26** and **4.27**) were tested for their ability to degrade CtBP1/2 in A2780 cells at concentrations ranging from 0.1-10 μM (**Figure 4.8**) in both short- and long-term exposures. In our initial experiments, PROTAC **4.26** was able to degrade approximately 25% of CtBP1 and CtBP2 at 10 μM (**Figure 4.9**). PROTAC **4.27** showed no degradation of CtBP1 or CtBP2 and was not tested further.

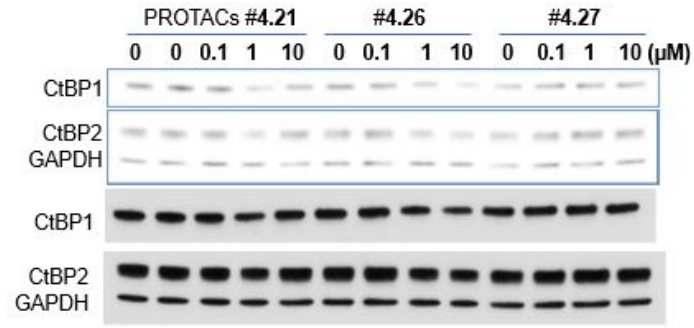

Figure 4.8: Initial Western Blots of PROTACs **4.21**, **4.26**, and **4.27**.

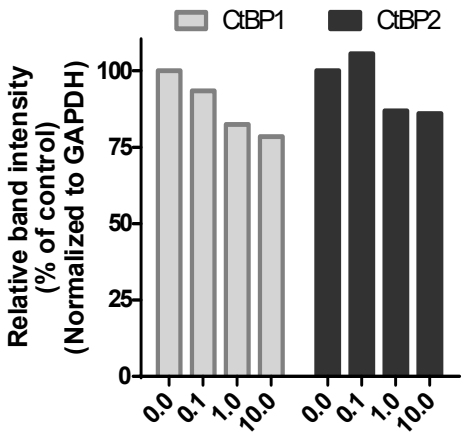

Figure 4.9: Degradation of CtBP1/2 by **4.26**.

We next measured degradation of CtBP with higher concentrations of PROTACs **4.21** and **4.26** (0.1-100 μM). The western blots are shown in **Figure 4.10**. Compound **4.21** showed degradation of CtBP2 but not CtBP1 at concentrations of 1 and 10 μM. We performed a nonlinear regression in Prism to fit the curve, and **4.21** exhibited a DC_{50} of 3.20 μM for CtBP2 (**Figure 4.11**). Compound **4.21** also showed some degradation of CtBP1 at 100 μM concentrations. We calculated the DC_{50} of **4.21** to be 16.43 μM for CtBP1 (**Figure 4.12**).

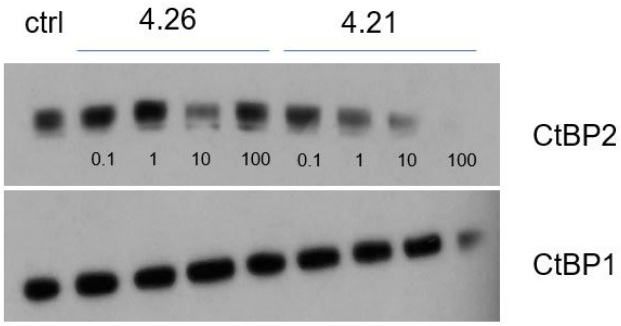

Figure 4.12: Western Blots of PROTACs **4.21** and **4.26**.

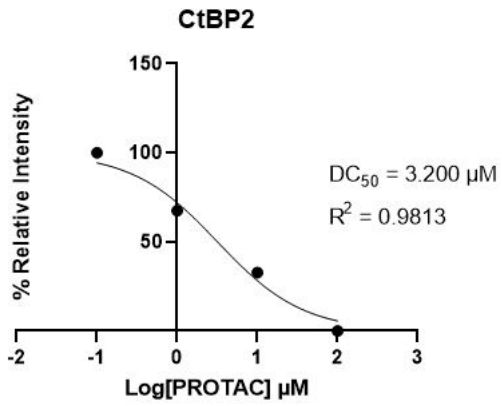

Figure 4.10: Degradation of CtBP2 by **4.21**.

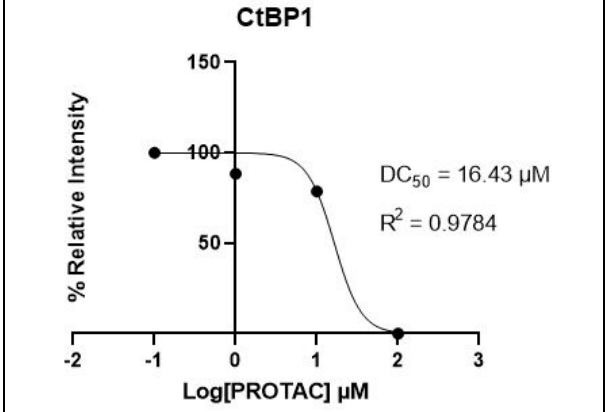

Figure 4.11: Degradation of CtBP1 by **4.21**.

We were unable to calculate DC_{50} values for PROTAC **4.26** because we did not obtain any bands that displayed a relative intensity of 50% or less. However, **4.26** exhibited degradation of CtBP2 at 10 μM concentration, but at 100 μM, the concentration of CtBP increases. This could be due to the hook effect, where rather than forming a ternary complex between the PROTAC, CRBN and CtBP, PROTAC molecules form

binary complexes with either CRBN or CtBP. PROTAC **4.26** degraded approximately 35% of CtBP2 at 10 μM in this experiment (**Figure 4.13**). The DC_{50} is likely greater than 10 μM but less than 100 μM. PROTAC **4.26** did not display degradation of CtBP1 at these concentrations.

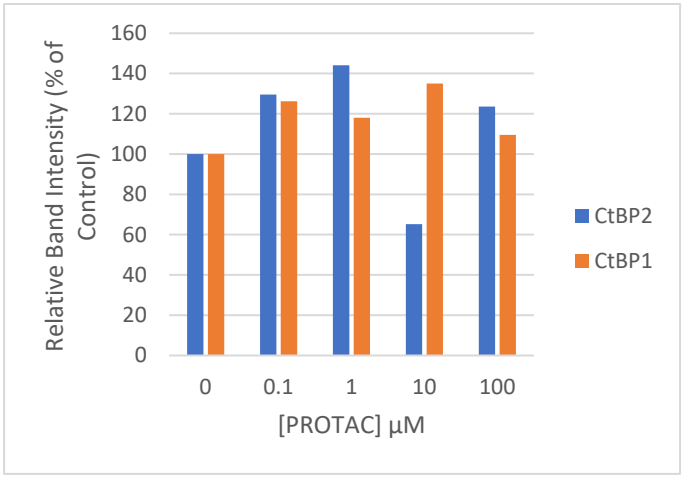

Figure 4.13: Degradation of CtBP1/2 by **4.26**.

4.3.2: Discussion

Previous attempts to design an inhibitor of CtBP for use as a cancer therapeutic have focused on substrate-competitive functional inhibitors. Our lab had previously designed, synthesized, and evaluated two lead inhibitors – HIPP and 4-Cl HIPP. While these two compounds are potent inhibitors of CtBP *in vitro* with IC_{50} values of 240 nM and 180 nM respectively, this potency did not translate when these compounds were tested in cells. HIPP exhibited a cellular IC_{50} of 4.12 mM and 4-Cl HIPP exhibited a cellular IC_{50} of 1.74 mM.[68] The literature was consulted and we hypothesized that degradation of CtBP with a PROTAC would have a strong anti-oncogenic effect in cells.

We designed three PROTAC molecules that utilized HIPP to bind to CtBP and pomalidomide to bind to the E3 ligase CRBN, with linkers of varying length and composition. The point of attachment of the linker to HIPP was chosen based on analysis of the HIPP-CtBP1 co-crystal structure (PDBID: 4U6Q). A modular synthetic route to make these PROTACs was designed using an HWE reaction and amide coupling

reactions as key steps, along with standard protection, deprotection, reduction and oxidation reactions and then executed in the laboratory. After determining the optimal protecting group strategy and optimization of selected synthetic steps, each PROTAC was synthesized in 9 sequential steps in 100 mg quantities. Each compound was synthesized as described in *Section 4.2.1.* Each compound was confirmed by HRMS, and purity was confirmed by analytical, reversed-phase HPLC.

From our western blotting experiments, we found that HIPP-based CtBP PROTACs are able to degrade CtBP1/2 in cells. **4.21** degrades CtBP2 with a DC_{50} of 3.2 μM, and degrades CtBP1 with a DC_{50} of 16.43 μM. **4.26** degrades CtBP2 with a DC_{50} that is greater than 10 μM but is less than 100 μM. **4.27** did not degrade CtBP1 or CtBP2. It is interesting that we see more degradation of CtBP2 than CtBP1 from our two biologically active PROTAC molecules. This is likely because degradation is dependent on the subcellular localization of CRBN.[219] CRBN is mainly expressed in the nucleus, though it is expressed some in the cytoplasm as well.[136] While CtBP2 contains an NLS sequence and is expressed in the nucleus, CtBP1 is only localized to the nucleus when part of a heterodimer with CtBP2. If the PROTAC molecules are able to keep CtBP1/2 from forming dimers, i.e. inhibit dimerization, then it would make sense that there would be less degradation of CtBP1 because there is less CRBN in the cytoplasm. The PROTACs' ability to inhibit dimerization can be measured experimentally using analytical ultracentrifugation to test this hypothesis.

The PROTAC with the fully aliphatic linker (**4.21**) was more potent in A2780 cells than either PROTAC that contained PEG linkers (**4.26** and **4.27**). **4.21** had a linker length of 12 atoms between the aniline of pomalidomide and the phenyl ring of HIPP. **4.26** had

a linker length of 14 atoms and degraded less CtBP1/2 than **4.21**. **4.27** had a linker length of 17 atoms and failed to degrade either CtBP1 or CtBP2. From this data we can conclude that the optimal linker length is around 12 atoms, and the optimal linker composition is an aliphatic carbon chain. However, further research should be performed with HIPP-based PROTACs with more diverse linker lengths and compositions to make a definitive conclusion.

One limitation of this project is that we were unable to measure the binding affinity of the three PROTAC molecules to CtBP due to time constraints. We had intended to measure the dissociation constants of these PROTACs with isothermal titration calorimetry. The CtBP-binding ligand is HIPP, so it is presumed that the PROTACs have similar binding affinities as HIPP. However, this will need to be determined experimentally as it is unknown what affect the rest of the PROTAC molecule would have on HIPP's ability to bind to CtBP.

It is important to note that the CtBP-binding ligand HIPP in our PROTAC molecules is an ethyl ester, as opposed to a carboxylic acid. We showed in Chapter 2 that replacement of the carboxylic acid of HIPP to an ethyl ester increases its potency in the MTT cell viability assay in HCT116 cells 15-fold. We believe this is due to the ethyl ester being more cell permeable than the carboxylic acid, because the acid would be deprotonated and therefore charged at physiological pH. It is also our assumption that the ester will be hydrolyzed to the acid prior to delivery to the target protein. To test these hypotheses, **4.21** should by hydrolyzed and tested in cells again to see if there is a difference in degradation of CtBP1/2. We may also want to consider utilizing a different ester, as the ethyl ester may limit solubility *in vivo*.

While we were able to conclude that CtBP can be effectively degraded in cells by treatment with a PROTAC, we do not know that this degradation will lead to restoration of expression of TSGs or induce apoptosis. **4.21** should be tested in an MTT cell viability assay to determine whether this compound is effective at inducing apoptosis. This will also allow us to compare the efficacy of **4.21** with the potent CtBP inhibitors we designed and synthesized in Chapter 2. We also propose to test the PROTAC molecules in a luciferase assay that will measure the restoration of Bik transcription.[68]

4.3.3: Chemistry Experimental Data

General Chemical Methods

Reagents/chemicals, catalysts, solvents were purchased from Sigma-Aldrich, Fisher, Oakwood, AstaTech Inc., Alfa-Aesar and Enamine. Analytical Thin Layer Chromatography (TLC) was performed using silica gel GHLF plates (Analtech Inc.). Automated MPLC was performed on TELEDYNE ISCO CombiFlash® Rf instrument using RediSep Rf Normal-phase Flash Columns (4-gm, 12-gm, 24-gm, or 40-gm) with gradients of either Hexanes/Ethyl Acetate or Dichloromethane/Methanol, or RediSep Rf Reversed-phase C18 Columns (4.3-gm, 13-gm, 26-gm, or 43-gm) with a gradient of water/acetonitrile. ^{1}H NMR and ^{13}C NMR experiments were recorded on BRUKER 600MHz NMR instrument in deuterated solvents – chloroform ($CDCl_3$), dimethyl sulfoxide ($(CD_3)_2SO$) or deuterium oxide (D_2O). All chemical shifts are reported in parts per million (ppm) with reference to chloroform, DMSO, and H_2O residual peaks at 7.26, 2.50 and 4.80 respectively (^{1}H NMR spectra); 77.16 and 39.52 respectively (^{13}C NMR spectra). The data is reported as: chemical shifts (ppm), multiplicity (s = singlet, d = doublet, t = triplet, q = quartet, m = multiplet), coupling constant(s) (Hz) and integral values.

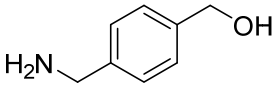

(4-(Aminomethyl)phenyl)methanol (**4.6**): In an oven-dried, 100 mL round-bottom flask 4-(aminomethyl)benzoic acid (2.0 g, 13.23 mmol, 1 eq) was dissolved in anhydrous tetrahydrofuran (40 mL, 0.3 M) under nitrogen and cooled to 0°C. Lithium aluminum hydride (1 g, 52.92 mmol, 4 eq) was added as a solid in three equal portions at 0 °C. After gas evolution ceased, the reaction was heated to 63 °C and refluxed for 16 h. After cooling to 0 °C, water (4 mL) was added dropwise, followed by 10% aqueous sodium hydroxide (4 mL) and water (12 mL). The quenched reaction mixture was then warmed to room temperature and stirred for 10 minutes, followed by filtering over celite and washing with THF. The filtrate was then concentrated *in vacuo* followed by pumping down overnight on high-vac to yield the product as a white solid (1.72 g, 95% yield). ^{1}H NMR (600 MHz, $CDCl_3$) δ 7.33 (d, *J* = 8.04 Hz, 2H), 7.30 (d, *J* = 8.04 Hz, 2H), 4.67 (s, 2H), 3.85 (s, 2H). ^{13}C NMR (150 MHz, $CDCl_3$) δ 142.61, 139.61, 127.30, 127.27, 65.01, 46.19. HRMS ESI^{+} $C_8H_{12}NO$ $[M+H]^{+}$ Expected: 138.0913, Found: 138.0907.

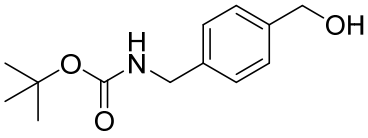

Tert-butyl (4-hydroxymethyl)benzyl)carbamate (**4.15**): In an oven-dried, 100 mL round-bottom flask, 4-(aminomethyl)phenyl)methanol (**4.6**, 1 g, 7.3 mmol, 1 eq) was dissolved in a 2:1 mixture of *tert*-butanol and 1M aqueous sodium hydroxide at 0 °C. Di-*tert*-butyl dicarbonate (3.98 g, 18.25 mmol, 2.5 eq) was added as a solid at 0 °C. The reaction was warmed to room temperature and allowed to stir for 2 h. The reaction was then washed with sodium bicarbonate (2 x 50 mL) and the product was extracted with ethyl acetate (3

x 50 mL). The combined ethyl acetate layers were washed with brine, dried with sodium sulfate, and filtered. The filtrate was then concentrated *in vacuo* followed by pumping down overnight on high-vac to yield the product as a mixture with excess di-*tert*-butyl dicarbonate that was carried over into the next step. ^{1}H NMR (600 MHz, $CDCl_3$) δ 7.33 (d, *J* = 7.32, 2H), 7.27 (d, *J* = 7.5, 2H), 4.68 (d, *J* = 5.7, 2H), 4.30 (s, 2H), 1.46 (s, 9H). ^{13}C NMR (150 MHz, $CDCl_3$) δ 155.75, 139.88, 1378.25, 127.54, 127.15, 79.42, 64.91, 44.27, 28.27. HRMS ESI$^+$ $C_{13}H_{19}NO_3$ $[M+Na]^+$ Expected: 260.1263, Found: 260.1258.

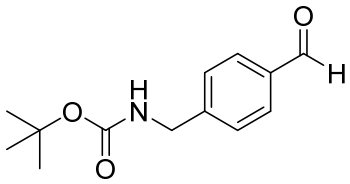

Tert-butyl (4-formylbenzyl)carbamate (**4.16**): In an oven-dried, 250 mL round-bottom flask, *tert*-butyl (4-hydroxymethyl)benzyl)carbamate (**4.15**, 1.73 g, 7.3 mmol, 1 eq), was dissolved in anhydrous tetrahydrofuran (58.75 mL, 0.12 M) under nitrogen at room temperature. Manganese (IV) oxide (6.98 g, 80.3 mmol, 11 eq) was added as a solid and the reaction was allowed to stir over 16 h. The reaction mixture was then filtered over celite and washed with THF. The filtrate was then concentrated *in vacuo* and purified using an automated CombiFlash MPLC system (silica gel, 30% ethyl acetate/hexanes), followed by pumping down overnight on high-vac to yield the product as a white solid (1.10 g, 64% yield). ^{1}H NMR (600 MHz, $CDCl_3$) δ 10.00 (s, 1H), 7.85 (d, *J* = 8.04, 2H), 7.45 (d, *J* = 7.92, 2H), 4.40 (d, *J* = 5.76, 2H), 1.47 (s, 9H). ^{13}C NMR (150 MHz, $CDCl_3$) δ 191.89, 155.91, 146.12, 135.55, 130.10, 127.72, 79.92, 44.37, 28.38. HRMS ESI$^+$ $C_{13}H_{17}NO_3$ $[M+Na]^+$ Expected: 258.1101, Found: 258.1101.

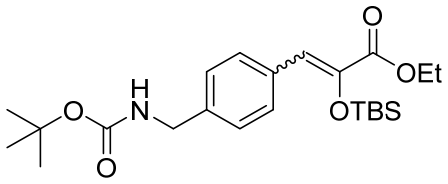

Ethyl 3-(4-(((tert-butoxycarbonyl)amino)methyl)phenyl)-2-((tert-butyldimethylsilyl)oxy)acrylate (**4.17**): In an oven-dried, 50 mL round-bottom flask, ethyl 2-((*tert*-butyldimethylsilyl)oxy)-2-(dimethoxyphosphoryl)acetate (**2.2**, 923.71 mg, 2.83 mmol, 1 eq) was dissolved in tetrahydrofuran (7.22 mL, 0.4 M) and added dropwise to a stirring solution of lithium diisopropylamide in tetrahydrofuran (3.12 mL, 1 M, 1.1 eq) at -78 °C. After stirring for 30 minutes, *tert*-butyl (4-formylbenzyl)carbamate (**4.16**, 1 g, 4.25 mmol, 1.5 eq) was dissolved in tetrahydrofuran (7.22 mL, 0.6 M) and added dropwise to the reaction mixture. The reaction was then stirred at -78 °C and warmed to room temperature over 15 h. The reaction mixture was then quenched with ammonium chloride (24 mL) and diluted with ethyl acetate (120 mL). This was washed with ammonium chloride (3 x 24 mL), water (3 x 24 mL), and saturated sodium chloride (3 x 24 mL). The organic phase was then dried with sodium sulfate and filtered. The filtrate was then concentrated *in vacuo* and purified using an automated CombiFlash MPLC system (silica gel, 20% ethyl acetate/hexanes), followed by pumping down overnight on high vac to yield the product as a yellow oil (1.08 g, 88% yield). ^{1}H NMR (600 MHz, $CDCl_3$) δ 7.22-7.19 (m, 4H), 6.38 (s, 1H), 4.29 (d, *J* = 5.52, 2H), 4.13 (q, *J* = 7.14, 2H), 1.46 (s, 9H), 1.16 (t, *J* = 7.14, 3 H), 0.98 (s, 9H), 0.22 (s. 6H). ^{13}C NMR (150 MHz, $CDCl_3$) δ 164.94, 155.86, 142.15, 137.81, 133.72, 128.98, 127.09, 120.07, 79.50, 60.95, 44.45, 28.42, 25.84, 25.60, 18.29, 14.21, 13.85, -3.85, -4.74. HRMS ESI$^+$ $C_{23}H_{37}NO_5Si$ $[M+Na]^+$ Expected: 458.2333, Found: 458.2312.

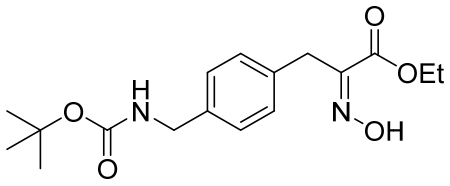

Ethyl 3-(4-(((tert-butoxycarbonyl)amino)methyl)phenyl)-2-(hydroxyimino)propanoate (**4.18**): In an oven-dried, 100 mL round-bottom flask ethyl 3-(4-(((*tert*-butoxycarbonyl)amino)methyl)phenyl)-2-((*tert*-butyldimethylsilyl)oxy)acrylate (**4.17**, 1.08 g, 2.48 mmol, 1 eq) was dissolved in a 4:1 mixture of ethanol and chloroform (25 mL, 0.1M) under nitrogen at room temperature. Triethylamine trihydrofluoride (0.69 mL, 4.22 mmol, 1.7 eq) was added dropwise and the reaction was stirred. After 30 minutes, hydroxylamine hydrochloride (293.25 mg, 4.22 mmol, 1.7 eq) was added as a solid in two portions and the reaction was stirred for an additional 19 h at room temperature. The solvent was then evaporated and the reaction mixture was dissolved in dichloromethane (32 mL). This was washed with water (2 x 64 mL) and saturated aqueous sodium bicarbonate (97 mL). The organic phase was dried with sodium sulfate and filtered. The filtrate was concentrated *in vacuo* and purified by an automated CombiFlash MPLC system (silica gel, 50% ethyl acetate/hexanes), followed by pumping down overnight on high-vac to yield the product as a white solid (658.44 mg, 79% yield). ^{1}H NMR (600 MHz, $CDCl_3$) δ 7.27 (d, *J* = 7.14, 2H), 7.19 (d, *J* = 7.44, 2H), 4.27-4.25 (m, 4H), 3.96 (s, 2H), 1.45 (s, 9H), 1.30 (t, *J* = 7.02, 3H). ^{13}C NMR (150 MHz, $CDCl_3$) δ 163.27, 155.92, 151.06, 137.24, 134.85, 129.41, 127.71, 79.56, 61.89, 44.36, 30.13, 28.40, 14.05. HRMS ESI$^+$ $C_{17}H_{24}N_2O_5$ $[M+Na]^+$ Expected: 359.1577, Found: 359.1564.

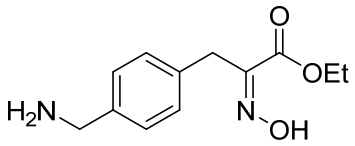

Ethyl 3-(4-(aminomethyl)phenyl)-2-(hydroxyimino)propanoate hydrochloride (**4.11**): In an oven-dried, 8-mL vial ethyl 3-(4-(((tert-butoxycarbonyl)amino)methyl)phenyl)-2-(hydroxyimino)propanoate (**4.18**, 90.72 mg, 0.27 mmol, 1 eq) was dissolved in 1,4-dioxane under nitrogen at room temperature, cooled to 0°C, and 4 M hydrochloric acid in 1,4-dioxane solution (0.51 mL, 1.08 mmol, 4 eq) was added. The reaction was stirred at room temperature for 19 h. The solvent was then allowed to evaporate by blowing nitrogen into the reaction vial overnight followed by pumping down overnight on high-vac to yield the product as an HCl salt (68.52 mg, 93% yield). ^{1}H NMR (600 MHz, $CDCl_3$) δ 12.51 (s, 1H), 8.15 (br s, 2 H), 7.36 (d, *J* = 7.98, 2H), 7.23 (d, *J* = 7.5, 2H), 4.16 (q, *J* = 7.08, 2H), 3.97 (d, *J* = 5.52, 2H), 3.84 (s, 2H), 1.21 (t, *J* = 7.08, 3H). ^{13}C NMR (150 MHz, $CDCl_3$) δ 163.60, 149.25, 136.85, 132.07, 129.11, 128.70, 60.95, 41.84, 28.23, 13.98. HRMS ESI$^+$ $C_{12}H_{16}N_2O_3$ $[M+H]^+$ Expected: 237.1234, Found: 237.1226.

Synthesis of HIPP-based CtBP PROTAC Intermediates

General Procedure 1: In an oven-dried vial, the corresponding Fmoc-protected linker carboxylic acid (1.05 eq) was dissolved in *N,N*-dimethylformamide under nitrogen at room temperature. Ethyl 3-(4-(aminomethyl)phenyl)-2-(hydroxyimino)propanoate hydrochloride (**4.11**, 1 eq), HATU (1.2 eq), and DIPEA (3 eq) were added sequentially. The reaction was stirred at room temperature for 16 h. The reaction mixture was then washed with deionized water and the product was extracted with ethyl acetate (3x). The combined ethyl acetate layers were then washed with brine, dried with sodium sulfate,

and filtered. The filtrate was then concentrated *in vacuo* followed by pumping down overnight on high-vac to yield the crude product. The crude product was then purified using an automated CombiFlash MPLC system (silica gel, methanol/dichloromethane, 0.1% TEA), followed by pumping down overnight on high-vac to yield the pure product.

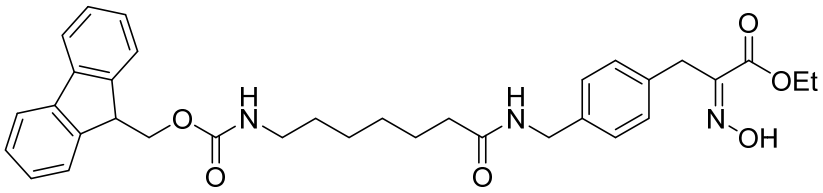

Ethyl 3-(4-((7-((((9H-fluoren-9-yl)methoxy)carbonyl)amino)heptanamido)methyl)phenyl)-2-(hydroxyimino)propanoate (**4.19**): Procedure 1 was followed using 7-((((9H-fluoren-9-yl)methoxy)carbonyl)amino)heptanoic acid (84.88 mg, 0.231 mmol) in DMF (1.15 mL). Yield 72% (92.2 mg, 0.16 mmol). ^{1}H NMR (600 MHz, $CDCl_3$) δ 12.43 (br s, 1H), 8.23 (t, *J* = 5.79, 1H), 7.89 (d, *J* = 7.44, 2H), 7.68 (d, *J* = 7.32, 2H), 7.41 (t, *J* = 7.32, 2H), 7.32 (t, *J* = 7.32, 2H), 7.25 (d, *J* = 5.46, 1H), 7.13 (s, 3H), 5.76 (s, 1H), 4.29 (d, *J* = 6.72, 2H), 4.21-4.18 (m, 2H), 4.15 (q, *J* = 6.48, 2H), 3.79 (s, 2H), 2.96-2.93 (m, 2H), 2.69 (s, 6H), 2.10 (t, *J* = 7.5, 2H), 1.51-1.49 (m, 3H), 1.38-1.37 (m, 2H), 1.23 (m, 6H), 1.19 (t, *J* = 6.81, 3H), 1.01 (m, 9H). ^{13}C NMR (150 MHz, $CDCl_3$) δ 172.01, 163.61, 157.01, 149.57, 142.56, 139.41, 137.72, 137.42, 134.83, 128.91, 128.47, 127.33, 127.28, 127.01, 124.19, 121.37, 120.02, 109.74, 60.89, 60.34, 45.69, 41.69, 38.23, 35.29, 29.66, 29.49, 28.43, 26.03, 25.27, 13.95, 11.43. HRMS ESI$^+$ $C_{34}H_{39}N_3O_6$ $[M+Na]^+$ Expected: 608.2731, Found: 608.2720.

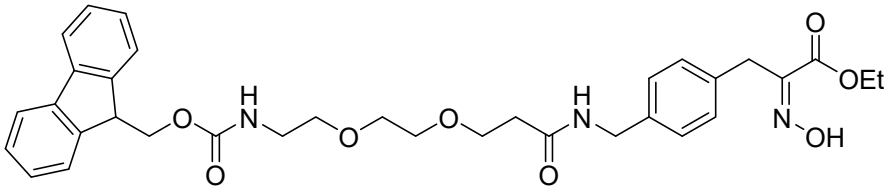

Ethyl 3-(4-(1-(9H-fluoren-9-yl)-3,13-dioxo-2,7,10-trioxa-4,14-diazapentadecan-15-yl)phenyl)-2-(hydroxyimino)propanoate (**4.22**): Procedure 1 was followed using 1-(9H-fluoren-9-yl)-3-oxo-2,7,10-trioxa-4-azatridecan-13-oic acid (276.81 mg, 0.693 mmol) in DMF (3.47 mL). Yield 61% (248.2 mg, 0.40 mmol). ^{1}H NMR (600 MHz, $CDCl_3$) δ 8.32 (br s, 2H), 7.89 (d, *J* = 7.38, 2H), 7.85 (d, *J* = 7.38, 2H), 7.42 (t, *J* = 7.02, 2H), 7.35 (t, *J* = 7.32, 2H), 7.14 (m, 7H), 6.28 (s, 2H), 4.21 (d, *J* = 4.86, 4H), 4.16 (q, *J* = 6.96, 4H), 3.80 (s, 4H), 3.64-3.62 (m, 4H), 3.51 (s, 5H), 3.48 (s, 3H), 3.45 (m, 3H), 2.46-2.43 (m, 13H), 2.36 (m, 4H), 1.21 (t, *J* = 6.96, 6H). ^{13}C NMR (150 MHz, $CDCl_3$) δ 170.07, 170.02, 163.61, 139.40, 137.41, 128.91, 128.45, 127.29, 121.37, 120.02, 109.75, 69.56, 69.41, 66.82, 60.89, 45.70, 41.71, 36.08, 29.66, 13.96, 11.58. HRMS ESI^{+} $C_{34}H_{39}N_3O_8$ $[M+Na]^{+}$ Expected: 640.2629, Found: 640.2599.

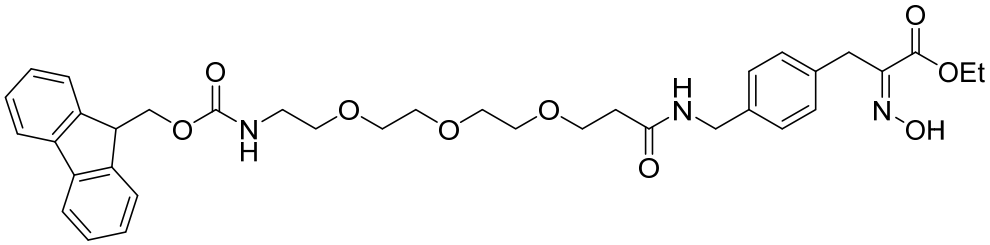

Ethyl 3-(4-(1-(9H-fluoren-9-yl)-3,16-dioxo-2,7,10,13-tetraoxa-4,17-diazaoctadecan-18-yl)phenyl)-2-(hydroxyimino)propanoate (**4.23**): Procedure 1 was followed using 1-(9H-fluoren-9-yl)-3-oxo-2,7,10,13-tetraoxa-4-azahexadecan-16-oic acid (307.35 mg, 0.693 mmol) in DMF (3.47 mL). Yield 64% (278.8 mg, 0.42 mmol). ^{1}H NMR (600 MHz, $CDCl_3$) δ 8.37 (br s, 1H), 7.89 (d, *J* = 7.56, 2H), 7.84 (d, *J* = 7.5, 2H), 7.41 (t, *J* = 7.38, 2H), 7.34 (t, *J* = 7.38, 2H), 7.15-7.12 (m, 8H), 6.28 (s, 2H), 4.21 (d, *J* = 5.64, 4H), 4.16 (q, *J* = 7.02,

4H), 3.80 (s, 4H), 3.63-3.61 (m, 4H), 3.59 (m, 4H), 3.54 (s, 6H), 3.50 (m, 10H), 2.94-2.94 (t, *J* = 4.71, 4H), 2.37 (t, *J* = 6.24, 4H), 1.20 (t, *J* = 7.02, 6H). ^{13}C NMR (150 MHz, $CDCl_3$) δ 170.07, 163.62, 149.51, 142.55, 139.40, 137.46, 137.41, 134.86, 128.91, 128.44, 127.29, 127.28, 121.37, 120.02, 109.75, 69.68, 69.64, 69.49, 66.88, 66.83, 60.88, 45.49, 41.69, 38.63, 36.07, 29.65, 13.96, 9.64. HRMS ESI$^+$ $C_{36}H_{43}N_3O_9$ $[M+Na]^+$ Expected: 684.2892, Found: 684.2879.

General Procedure 2: In an oven-dried, 40-mL vial, polymer-bound piperazine (10 eq) was swollen by addition of 5-10 mL of DMF, which was allowed to stir for several minutes, followed by decantation of excess solvent. This was repeated 2-3 times, then the corresponding Fmoc-protected HIPP-linker fragment (**4.19**, **4.22**, or **4.23**) was dissolved in DMF (1.9 mL, 0.1M) and added at room temperature. The reaction was stirred at room temperature for 24 h. The piperazine was then filtered off using a solid-phase extraction cartridge under vacuum, and washed with DCM. The product was concentrated *in vacuo* and added to the following reaction without further purification.

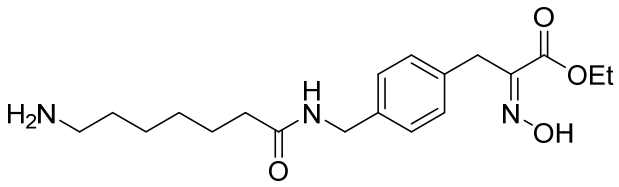

Ethyl 3-(4-((7-aminoheptanamido)methyl)phenyl)-2-(hydroxyimino)propanoate (**4.20**): Procedure 2 was followed using ethyl 3-(4-((7-((((9H-fluoren-9-yl)methoxy)carbonyl)amino)heptanamido)methyl)phenyl)-2-(hydroxyimino)propanoate (**4.19**, 110.1 mg, 0.19 mmol) in DMF (1.9 mL).

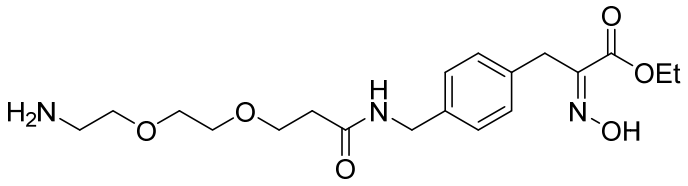

Ethyl 3-(4-((3-(2-(2-aminoethoxy)ethoxy)propanamido)methyl)phenyl)-2-(hydroxyimino)propanoate (**4.24**): Procedure 2 was followed using ethyl 3-(4-(1-(9H-fluoren-9-yl)-3,13-dioxo-2,7,10-trioxa-4,14-diazapentadecan-15-yl)phenyl)-2-(hydroxyimino)propanoate (**4.22**, 313.3 mg, 0.51 mmol) in DMF (5.1 mL).

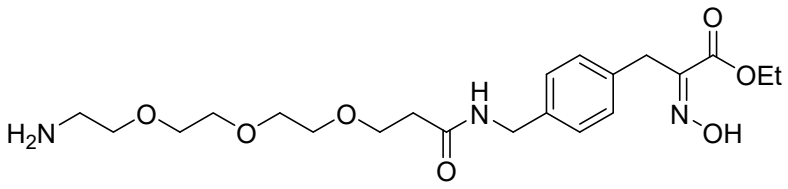

Ethyl 3-(4-(14-amino-3-oxo-6,9,12-trioxa-2-azatetradecyl)phenyl)-2-(hydroxyimino)propanoate (**4.25**): Procedure 2 was followed using ethyl 3-(4-(1-(9H-fluoren-9-yl)-3,16-dioxo-2,7,10,13-tetraoxa-4,17-diazaoctadecan-18-yl)phenyl)-2-(hydroxyimino)propanoate (**4.23**, 329.9 mg, 0.5 mmol) in DMF (5 mL).

General Procedure 3: In an oven-dried, 100-mL round-bottom flask, (2-(2,6-dioxopiperidin-3-yl)-1,3-dioxoisoindolin-4-yl)glycine (**4.2**, 1.2 eq) was dissolved in DMF (0.1M) under nitrogen at room temperature. PyBOP (1.2 eq) was added as a solid, and the reaction was stirred at room temperature for 1 h. After 1 h, the corresponding HIPP-linker fragment (**4.20**, **4.24**, or **4.25**, 1 eq) and DIPEA (3 eq) were added sequentially and the reaction was stirred at room temperature for 16 h. The reaction mixture was then dry-loaded onto C18 silica gel, and purified using an automated CombiFlash MPLC system

(C18, acetonitrile/water), followed by pumping down overnight on high-vac to yield the pure product.

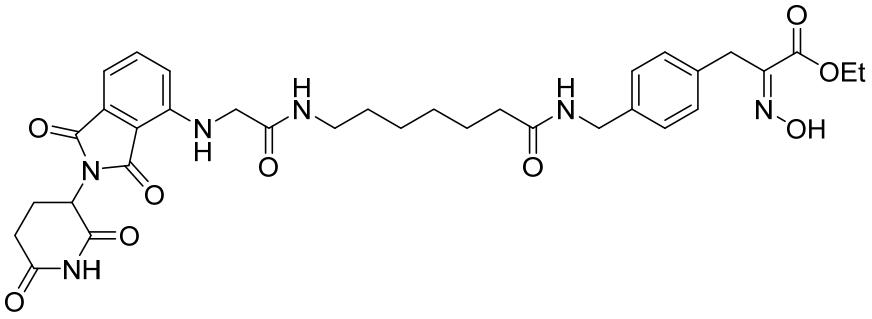

Ethyl 3-(4-((7-(2-((2-(2,6-dioxopiperidin-3-yl)-1,3-dioxoisoindolin-4-yl)amino)acetamido)heptanamido)methyl)phenyl)-2-(hydroxyimino)propanoate (**4.21**): Procedure 3 was followed using ethyl 3-(4-((7-aminoheptanamido)methyl)phenyl)-2-(hydroxyimino)propanoate (**4.20**, 69.09 mg, 0.19 mmol) in DMF (1.9 mL). Yield 35% (45.1 mg, 0.07 mmol). ^{1}H NMR (600 MHz, $CDCl_3$) δ 12.44 (br s, 1H), 11.10 (br s, 1H), 8.22 (br s, 1H), 8.17 (s, 2H), 8.07 (br s, 1H), 7.58 (t, *J* = 7.8, 1H), 7.12 (s, 4H), 7.06 (d, *J* = 6.9, 1H), 6.94 (br s, 1H), 6.85 (d, *J* = 8.4, 1H) 5.08-5.05 (m, 1H), 4.19-4.13 (m, 5H), 3.91 (d, *J* = 5.16, 2H), 3.78 (s, 2H), 3.07-3.06 (m, 3H), 3.02-3.00 (m, 9H), 2.88 (m, 2H), 2.60-2.54 (m, 2H), 2.10-2.01 (m, 8H), 1.86 (br s, 1H), 1.72 (s, 8H), 1.48 (m, 3H), 1.38 (m, 3H), 1.23-1.18 (m, 12H). ^{13}C NMR (150 MHz, $CDCl_3$) δ 172.83, 172.06, 170.06, 168.71, 168.24, 167.34, 163.63, 163.37, 149.59, 145.85, 137.73, 136.20, 134.86, 132.07, 128.49, 127.34, 118.09, 117.45, 110.95, 109.86, 79.78, 60.92, 48.58, 45.88, 45.85, 45.18, 41.71, 38.56, 35.30, 30.99, 29.67, 28.93, 28.40, 26.11, 25.94, 25.89, 25.25, 22.17, 13.97, 1.16. HRMS ESI$^+$ $C_{34}H_{40}N_6O_9$ $[M+Na]^+$ Expected: 699.2749, Found: 699.2729.

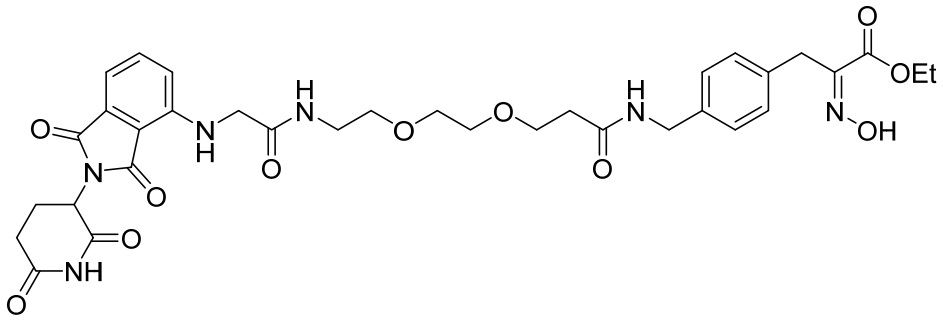

Ethyl 3-(4-(14-((2-(2,6-dioxopiperidin-3-yl)-1,3-dioxoisoindolin-4-yl)amino)-3,13-dioxo-6,9-dioxa-2,12-diazatetradecyl)phenyl)-2-(hydroxyimino)propanoate (**4.26**): Procedure 3 was followed using ethyl 3-(4-((3-(2-(2-aminoethoxy)ethoxy)propanamido)methyl)phenyl)-2-(hydroxyimino)propanoate (**4.24**, 201.68 mg, 0.51 mmol) in DMF (5.1 mL). Yield 27% (97.1 mg, 0.14 mmol). ^{1}H NMR (600 MHz, $CDCl_3$) δ 12.44 (s, 1H), 11.11 (s, 1H), 8.31 (m, 1H), 8.15 (s, 4H), 7.58 (t, *J* = 7.74, 1H), 7.15-7.12 (m, 4H), 7.07 (d, *J* = 6.84, 1H), 6.95 (m, 1H), 6.86 (d, *J* = 8.46, 1H), 5.09-5.06 (m, 1H), 4.21 (d, *J* = 5.46, 2H), 4.15 (q, *J* = 7.02, 2H), 3.94 (d, *J* = 5.28, 2H), 3.79 (s, 2H), 3.62 (t, *J* = 6.24, 2H), 3.48 (s, 5H), 3.42 (t, *J* = 5.46m, 3H), 3.26-3.25 (m, 3H), 3.02-3.01 (m, 19H), 2.92-2.86 (m, 1H), 2.61-2.54 (m, 2H), 2.36 (t, *J* = 6.15, 2H), 2.08 (s, 5H), 1.73 (s, 18H), 1.24-1.19 (m, 6H). ^{13}C NMR (150 MHz, $CDCl_3$) δ 172.77, 170.04, 170.02, 168.67, 168.56, 167.29, 163.58, 149.55, 145.79, 137.44, 136.17, 134.84, 132.03, 128.43, 127.28, 117.43, 110.93, 109.82, 69.50, 69.41, 68.95, 66.82, 60.87, 48.54, 45.84, 45.82, 45.10, 41.70, 40.04, 38.62, 36.09, 30.96, 30.66, 29.64, 25.91, 25.86, 22.13, 13.93, 1.12. HRMS ESI$^+$ $C_{34}H_{40}N_6O_{11}$ $[M+Na]^+$ Expected: 731.2647, Found: 731.2621.

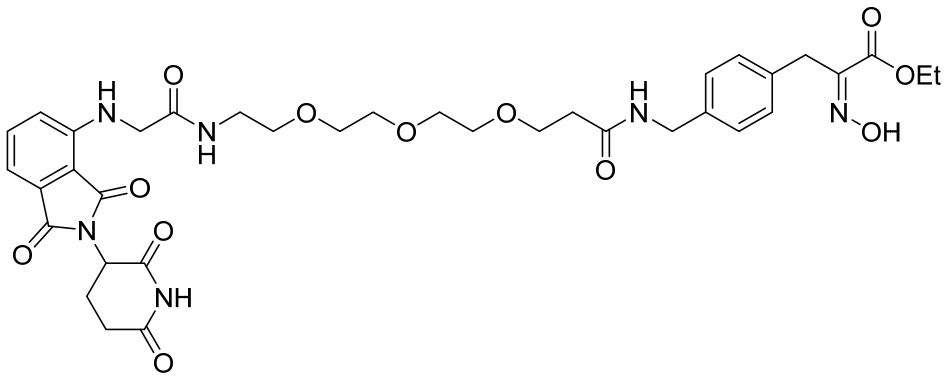

Ethyl 3-(4-(17-((2-(2,6-dioxopiperidin-3-yl)-1,3-dioxoisoindolin-4-yl)amino)-3,16-dioxo-6,9,12-trioxa-2,15-diazaheptadecyl)phenyl)-2-(hydroxyimino)propanoate (**4.27**): Procedure 3 was followed using ethyl 3-(4-(14-amino-3-oxo-6,9,12-trioxa-2-azatetradecyl)phenyl)-2-(hydroxyimino)propanoate (**4.25**, 219.76 mg, 0.5 mmol) in DMF (5 mL). Yield 30% (114.4 mg, 0.15 mmol). ^{1}H NMR (600 MHz, $CDCl_3$) δ 12.44 (br s, 1H), 11.10 (s, 1H), 8.29 (m, 1H), 8.16-8.15 (m, 5H), 7.58 (t, *J* = 7.71, 1H), 7.14-7.11 (m, 4H), 7.07 (d, *J* = 7.02, 1H), 6.94 (br s, 1H), 6.85 (d, *J* = 8.64, 1H), 5.08-5.05 (m, 1H), 4.20 (d, *J* = 5.52, 2H), 4.15 (q, *J* = 7.02, 2H), 3.93 (d, *J* = 5.22, 2H), 3.79 (s, 2H), 3.61 (t, *J* = 6.24, 3H), 3.48 (s, 10H), 3.42-3.40 (m, 4H), 3.26-3.25 (m, 4H), 3.01 (m, 14H), 2.92-2.86 (m, 2H), 2.60-2.24 (m, 2H), 2.35 (t, *J* = 6.09, 2H), 2.07 (s, 6H), 2.03-2.01 (m, 1H), 1.73 (s, 13H), 1.23-1.18 (m, 6H). ^{13}C NMR (150 MHz, $CDCl_3$) δ 172.79, 170.03, 168.69, 168.58, 167.31, 163.61, 163.16, 149.56, 145.81, 137.47, 136.20, 134.84, 132.05, 128.45, 127.29, 118.06, 117.44, 110.96, 109.84, 69.73, 69.70, 69.57, 69.52, 68.95, 66.85, 60.89, 48.53, 45.86, 45.84, 45.14, 41.71, 38.65, 36.11, 30.98, 30.68, 29.66, 25.93, 25.88, 22.16, 13.95, 1.14. HRMS ESI$^+$ $C_{36}H_{44}N_6O_{12}$ $[M+Na]^+$ Expected: 775.2909, Found: 775.2878.

4.4: Conclusions and Future Directions

Three HIPP-based CtBP PROTACs were designed and successfully synthesized and purified in the laboratory. These were then tested in A2780 cells and subjected to western blotting to measure their ability to degrade CtBP. From the western blot data shown in *Section 4.3.1*, we showed that CtBP1/2 can be successfully degraded in cells with HIPP-based PROTACs. The PROTAC with a fully aliphatic linker (**4.21**) showed to be the most potent in cells with a calculated DC_{50} of 3.2 μM for CtBP2 and a DC_{50} of 16.43 μM for CtBP1. We were unable to calculate DC_{50} values for **4.26**, though it is likely higher than 10 μM but less than 100 μM because it is subject to the hook effect. PROTAC **4.27** did not exhibit degradation of CtBP1/2.

This project only used three different linkers – 1 aliphatic linker and 2 PEG linkers. From this data we determined the optimal linker composition to be an aliphatic chain connected by amide bonds, with a linker length of 12 atoms. The PEG2 linker containing 14 atoms was less potent, and the PEG3 linker containing 17 atoms did not result in degradation of CtBP1 or CtBP2. Now that the basic scheme has been identified for HIPP-based PROTACs, new PROTACs should be designed to determine the optimal linker length and composition experimentally for degradation of CtBP. These PROTAC molecules should contain HIPP to bind to CtBP and pomalidomide to bind to CRBN, but with chemically diverse linkers of varying lengths.

The results from the ITC experiments detailed in *Section 2.3.5* reveal that certain heteroaromatic analogues of HIPP are able to bind to CtBP with higher affinity than HIPP. A future direction of this project is synthesis of CtBP PROTACs that have a heteroaromatic HIPP analogue as the CtBP-binding ligand. We believe that by utilizing a

ligand that has more affinity for CtBP, a more potent PROTAC might result. A logical next step would be to synthesize CtBP PROTACs that employ **2.14** or **2.22** (**Figure 4.14**) to bind to CtBP, as opposed to HIPP. Initial PROTACs based on this idea should keep pomalidomide to bind to CRBN, and contain the same 12-atom aliphatic linker, so that we can optimize the CtBP ligand and observe the differences in DC_{50} values.

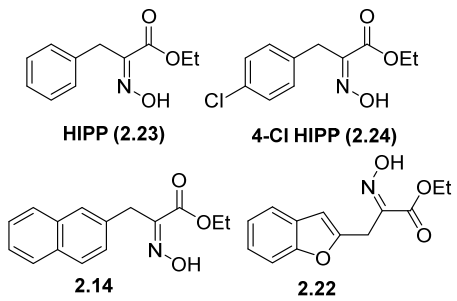

Figure 4.14: Structures of HIPP, 4-Cl HIPP, **2.14**, and **2.22**.

Our PROTAC molecules target the E3 ligase CRBN. Another future direction of this project includes synthesis and biological evaluation of a CtBP PROTAC that targets a different E3 ligase other than CRBN. There are a multitude of PROTACs designed to target and ubiquitinate BET proteins, especially BRD2/3/4. Two such PROTACs are ARV-825 and ARV-771. Both PROTACs employ the small molecule (+)-JQ1 to bind to BRD4, but differ in the E3 ligase recruited for ubiquitination and degradation. ARV-825 has the CRBN ligand thalidomide while ARV-771 has a VHL ligand. ARV-825 has a DC_{50} for BRD4 degradation that is below 1 nM, while ARV-771 induces rapid BRD2/3/4 degradation with DC_{50} less than 5 nM.[190] This shows that the choice of E3 ligase can make a difference in terms of selectivity and potency. Novel PROTAC molecules should be designed and synthesized that use HIPP to target CtBP but contain VH032 or another VHL ligand as opposed to the CRBN ligand pomalidomide.

Finally, our lab also intends to test CtBP degradation utilizing a hydrophobic tag as opposed to a PROTAC molecule. The theory behind this approach, as introduced by the Crews group, is that by introducing a hydrophobic tag (such as adamantane) to the

surface of a protein, it could potentially destabilize the protein fold and result in degradation of that protein. We have designed a CtBP hydrophobic tag molecule that contains HIPP and the 12-atom aliphatic linker from **4.21**, but instead of pomalidomide **4.20** is appended to an adamantane moiety. This would introduce a hydrophobic tag to CtBP upon HIPP binding in the active site.

Literature Cited

(1) Boyd, J. M.; Subramanian, T.; Schaeper, U.; La Regina, M.; Bayley, S.; Chinnadurai, G. A Region in the C-Terminus of Adenovirus 2/5 E1a Protein Is Required for Association with a Cellular Phosphoprotein and Important for the Negative Modulation of T24-Ras Mediated Transformation Tumorigenesis and Metastasis. *EMBO J.* **1993**, *12* (2), 469–478.

(2) Schaeper, U.; Boyd, J. M.; Verma, S.; Uhlmann, E.; Subramanian, T.; Chinnadurai, G. Molecular Cloning and Characterization of a Cellular Phosphoprotein That Interacts with a Conserved C-Terminal Domain of Adenovirus E1A Involved in Negative Modulation of Oncogenic Transformation. *Proc. Natl. Acad. Sci. U. S. A.* **1995**, *92*, 10467–10471.

(3) Katsanis, N.; Fisher, E. M. C. A Novel C-Terminal Binding Protein (CTBP2) Is Closely Related to CTBP1, an Adenovirus E1A-Binding Protein, and Maps to Human Chromosome 21q21.3. *Genomics* **1998**, *47* (2), 294–299.

(4) Verger, A.; Quinlan, K. G. R.; Crofts, L. A.; Spanò, S.; Corda, D.; Kable, E. P. W.; Braet, F.; Crossley, M. Mechanisms Directing the Nuclear Localization of the CtBP Family Proteins. *Mol. Cell. Biol.* **2006**, *26* (13), 4882–4894.

(5) Dcona, M. M.; Morris, B. L.; Ellis, K. C.; Grossman, S. R. CtBP- an Emerging Oncogene and Novel Small Molecule Drug Target: Advances in the Understanding of Its Oncogenic Action and Identification of Therapeutic Inhibitors. *Cancer Biol. Ther.* **2017**, *18* (6), 379–391.

(6) Barnes, C. J.; Vadlamudi, R. K.; Mishra, S. K.; Jacobson, R. H.; Li, F.; Kumar, R. Functional Inactivation of a Transcriptional Corepressor by a Signaling Kinase. *Nat. Struct. Biol.* **2003**, *10* (8), 622–628.

(7) Riefler, G. M.; Firestein, B. L. Binding of Neuronal Nitric-Oxide Synthase (NNOS) to Carboxyl-Terminal-Binding Protein (CtBP) Changes the Localization of Ctbp from the Nucleus to the Cytosol: A Novel Function for Targeting by the PDZ Domain of NNOS. *J. Biol. Chem.* **2001**, *276* (51), 48262–48268.

(8) Weigert, R.; Silletta, M. G.; Spano, S.; Turacchio, G.; Cericola, C.; Colanzi, A.; Senatore, S.; Manciini, R.; Polishchuk, E. V.; Salmona, M.; et al. CtBP/BARS Induces Fission of Golgi Membranes by Acylating Lysophosphatidic Acid. *Nature* **1999**, *402*, 429–433.

(9) Schmitz, F.; Königstorfer, A.; Südhof, T. C. RIBEYE, a Component of Synaptic Ribbons: A Protein's Journey through Evolution Provides Insight into Synaptic Ribbon Function. *Neuron* **2000**, *28* (3), 857–872.

(10) Magupalli, V. G.; Schwarz, K.; Alpadi, K.; Natarajan, S.; Seigel, G. M.; Schmitz, F. Multiple RIBEYE-RIBEYE Interactions Create a Dynamic Scaffold for the Formation of Synaptic Ribbons. *J. Neurosci.* **2008**, *28* (32), 7954–7967.

(11) Tom Dieck, S.; Altrock, W. D.; Kessels, M. M.; Qualmann, B.; Regus, H.; Brauner, D.; Fejtová, A.; Bracko, O.; Gundelfinger, E. D.; Brandstätter, J. H. Molecular Dissection of the Photoreceptor Ribbon Synapse: Physical Interaction of Bassoon and RIBEYE Is Essential for the Assembly of the Ribbon Complex. *J. Cell Biol.* **2005**, *168* (5), 825–836.

(12) Chinnadurai, G. CtBP , an Unconventional Transcriptional Corepressor in Development and Oncogenesis. **2002**, *9*, 213–224.

(13) Kumar, V.; Carlson, J. E.; Ohgi, K. A.; Edwards, T. A.; Rose, D. W.; Escalante, C.

R.; Rosenfeld, M. G.; Aggarwal, A. K. Transcripton Corepressor CtBP Is an NAD+-Regulated Dehydrogenase. *Mol. Cell* **2002**, *10*, 857–869.
(14) Paliwal, S.; Pande, S.; Kovi, R. C.; Sharpless, N. E.; Bardeesy, N.; Grossman, S. R. Targeting of C-Terminal Binding Protein (CtBP) by ARF Results in P53-Independent Apoptosis. *Mol. Cell. Biol.* **2006**, *26* (6), 2360–2372.
(15) Lin, X.; Sun, B.; Liang, M.; Liang, Y. Y.; Gast, A.; Hildebrand, J.; Brunicardi, F. C.; Melchior, F.; Feng, X. H. Opposed Regulation of Corepressor CtBP by SUMOylation and PDZ Binding. *Mol. Cell* **2003**, *11* (5), 1389–1396.
(16) Razeto, A.; Kochhar, S.; Hottinger, H.; Dauter, M.; Wilson, K. S.; Lamzin, V. S. Domain Closure, Substrate Specificity and Catalysis of D-Lactate Dehydrogenase from Lactobacillus Bulgaricus. *J. Mol. Biol.* **2002**, *318* (1), 109–119.
(17) Antonyuk, S. V.; Strange, R. W.; Ellis, M. J.; Bessho, Y.; Kuramitsu, S.; Inoue, Y.; Yokoyama, S.; Hasnain, S. S. Structure of D-Lactate Dehydrogenase from Aquifex Aeolicus Complexed with NAD+ and Lactic Acid (or Pyruvate). *Acta Crystallogr. Sect. F Struct. Biol. Cryst. Commun.* **2009**, *65* (12), 1209–1213.
(18) Dengler, U.; Niefind, K.; Kieß, M.; Schomburg, D. Crystal Structure of a Ternary Complex of D-2-Hydroxy-Isocaproate Dehydrogenase from Lactobacillus Casei, NAD+ and 2-Oxoisocaproate at 1.9 Å Resolution. *J. Mol. Biol.* **1997**, *267* (3), 640–660.
(19) Lamzin, V. S.; Dauter, Z.; Popov, V. O.; Harutyunyan, E. H.; Wilson, K. S. High Resolution Structures of Holo and Apo Formate Dehydrogenase. *Journal of Molecular Biology*. 1994, pp 759–785.
(20) Goldberg, J. D.; Yoshida, T.; Brick, P. Crystal Structure of a NAD-Dependent d-Glycerate Dehydrogenase at 2·4 Å Resolution. *J. Mol. Biol.* **1994**, *236* (4), 1123–1140.
(21) Booth, M. P. S.; Conners, R.; Rumsby, G.; Brady, R. L. Structural Basis of Substrate Specificity in Human Glyoxylate Reductase/Hydroxypyruvate Reductase. *J. Mol. Biol.* **2006**, *360* (1), 178–189.
(22) Erlandsen, H.; Jecrois, A. M.; Nichols, J. C.; Cole, J. L.; Royer, W. E. NADH/NAD+ Binding and Linked Tetrameric Assembly of the Oncogenic Transcription Factors CtBP1 and CtBP2. *FEBS Lett.* **2022**, *596* (4), 479–490.
(23) Madison, D. L.; Wirz, J. A.; Siess, D.; Lundblad, J. R. Nicotinamide Adenine Dinucleotide-Induced Multimerization of the Co-Repressor CtBP1 Relies on a Switching Tryptophan. *J. Biol. Chem.* **2013**, *288* (39), 27836–27848.
(24) Zhang, Q.; Wang, S. Y.; Nottke, A. C.; Rocheleau, J. V.; Piston, D. W.; Goodman, R. H. Redox Sensor CtBP Mediates Hypoxia-Induced Tumor Cell Migration. *Proc. Natl. Acad. Sci. U. S. A.* **2006**, *103* (24), 9029–9033.
(25) Zhang, Q.; Piston, D. W.; Goodman, R. H. Regulation of Corepressor Function by Nuclear NADH. *Science (80-.).* **2002**, *295* (5561), 1895–1897.
(26) Zhao, L. J.; Kuppuswamy, M.; Vijayalingam, S.; Chinnadurai, G. Interaction of ZEB and Histone Deacetylase with the PLDLS-Binding Cleft Region of Monomeric C-Terminal Binding Protein 2. *BMC Mol. Biol.* **2009**, *10* (89).
(27) Michael Dcona, M.; Damle, P. K.; Zarate-Perez, F.; Morris, B. L.; Nawaz, Z.; Dennis, M. J.; Deng, X.; Korwar, S.; Singh, S. J.; Ellis, K. C.; et al. Active-Site Tryptophan, the Target of Antineoplastic C-Terminal Binding Protein Inhibitors, Mediates Inhibitor Disruption of CtBP Oligomerization and Transcription Coregulatory

Activities S. *Mol. Pharmacol.* **2019**, *96* (1), 99108.
(28) Grooteclaes, M. L.; Frisch, S. M. Evidence for a Function of CtBP in Epithelial Gene Regulation and Anoikis. *Oncogene* **2000**, *19* (33), 3823–3828.
(29) Sollerbrant, K.; Chinnadurai, G.; Svensson, C. The CtBP Binding Domain in the Adenovirus E1A Protein Controls CR1-Dependent Transactivation. *Nucleic Acids Res.* **1996**, *24* (13), 2578–2584.
(30) Postigo, A. A.; Dean, D. C. ZEB Represses Transcription through Interaction with the Corepressor CtBP. *Proc. Natl. Acad. Sci. U. S. A.* **1999**, *96* (12), 6683–6688.
(31) Turner, J.; Crossley, M. Cloning and Characterization of MCtBP2, a Co-Repressor That Associates with Basic Kruppel-like Factor and Other Mammalian Transcriptional Regulators. *EMBO J.* **1998**, *17* (17), 5129–5140.
(32) Stankiewicz, T. R.; Gray, J. J.; Winter, A. N.; Linseman, D. A. C-Terminal Binding Proteins: Central Players in Development and Disease. *Biomol. Concepts* **2014**, *5* (6), 489–511.
(33) Zhao, L. J.; Subramanian, T.; Vijayalingam, S.; Chinnadurai, G. CtBP2 Proteome: Role of CtBP in E2F7-Mediated Repression and Cell Proliferation. *Genes and Cancer* **2015**, *5* (1–2), 31–40.
(34) Hilbert, B. J.; Grossman, S. R.; Schiffer, C. A.; Royer, W. E. Crystal Structures of Human CtBP in Complex with Substrate MTOB Reveal Active Site Features Useful for Inhibitor Design. *FEBS Lett.* **2014**, *588* (9), 1743–1748.
(35) Kuppuswamy, M.; Vijayalingam, S.; Zhao, L.-J.; Zhou, Y.; Subramanian, T.; Ryerse, J.; Chinnadurai, G. Role of the PLDLS-Binding Cleft Region of CtBP1 in Recruitment of Core and Auxiliary Components of the Corepressor Complex. *Mol. Cell. Biol.* **2008**, *28* (1), 269–281.
(36) Kagey, M. H.; Melhuish, T. A.; Wotton, D. The Polycomb Protein Pc2 Is a SUMO E3. *Cell* **2003**, *113* (1), 127–137.
(37) Quinlan, K. G. R.; Nardini, M.; Verger, A.; Francescato, P.; Yaswen, P.; Corda, D.; Bolognesi, M.; Crossley, M. Specific Recognition of ZNF217 and Other Zinc Finger Proteins at a Surface Groove of C-Terminal Binding Proteins. *Mol. Cell. Biol.* **2006**, *26* (21), 8159–8172.
(38) Poortinga, G.; Watanabe, M.; Susan, S. M. Drosophila CtBP: A Hairy-Interacting Protein Required for Embryonic Segmentation and Hairy-Mediated Transcriptional Repression. *EMBO J.* **1998**, *17* (7), 2067–2078.
(39) Nibu, Y.; Zhang, H.; Levine, M. Interaction of Short-Range Repressors with Drosophila CtBP in the Embryo. *Science (80-.).* **1998**, *280* (5360), 101–104.
(40) Hoang, C. Q.; Burnett, M. E.; Curtiss, J. Drosophila CtBP Regulates Proliferation and Differentiation of Eye Precursors and Complexes with Eyeless, Dachshund, Dan, and Danr during Eye and Antennal Development. *Dev. Dyn.* **2010**, *239* (9), 2367–2385.
(41) Perrimon, N.; Lanjuin, A.; Arnold, C.; Noll, E. Zygotic Lethal Mutations with Maternal Effect Phenotypes in Drosophila Melanogaster. *Genetics* **1996**, *144* (4), 1681–1692.
(42) Stern, M. D.; Aihara, H.; Roccaro, G. A.; Cheung, L.; Zhang, H.; Negeri, D.; Nibu, Y. CtBP Is Required for Proper Development of Peripheral Nervous System in Drosophila. *Mech. Dev.* **2009**, *126* (1–2), 68–79.
(43) Hildebrand, J. D.; Soriano, P. Overlapping and Unique Roles for C-Terminal

Binding Protein 1 (CtBP1) and CtBP2 during Mouse Development. *Mol. Cell. Biol.* **2002**, *22* (15), 5296–5307.
(44) Sewalt, R. G. A. B.; Gunster, M. J.; van der Vlag, J.; Satijn, D. P. E.; Otte, A. P. C-Terminal Binding Protein Is a Transcriptional Repressor That Interacts with a Specific Class of Vertebrate Polycomb Proteins. *Mol. Cell. Biol.* **1999**, *19* (1), 777–787.
(45) Melhuish, T. A.; Wotton, D. The Interaction of the Carboxyl Terminus-Binding Protein with the Smad Corepressor TGIF Is Disrupted by a Holoprosencephaly Mutation in TGIF. *J. Biol. Chem.* **2000**, *275* (50), 39762–39766.
(46) Siegel, R. L.; Miller, K. D.; Fuchs, H. E.; Jemal, A. Cancer Statistics, 2021. *CA. Cancer J. Clin.* **2021**, *71* (1), 7–33.
(47) Hanahan, D.; Weinberg, R. A. The Hallmarks of Cancer. *Cell* **2000**, *100*, 57–70.
(48) Padma, V. V. An Overview of Targeted Cancer Therapy. *Biomed.* **2015**, *5* (4), 1–6.
(49) Birts, C. N.; Harding, R.; Soosaipillai, G.; Halder, T.; Azim-Araghi, A.; Darley, M.; Cutress, R. I.; Bateman, A. C.; Blaydes, J. P. Expression of CtBP Family Protein Isoforms in Breast Cancer and Their Role in Chemoresistance. *Biol. Cell* **2011**, *103* (1), 1–19.
(50) Byun, J. S.; Gardner, K. C-Terminal Binding Protein: A Molecular Link between Metabolic Imbalance and Epigenetic Regulation in Breast Cancer. *Int. J. Cell Biol.* **2013**, *2013*.
(51) Di, L. J.; Byun, J. S.; Wong, M. M.; Wakano, C.; Taylor, T.; Bilke, S.; Baek, S.; Hunter, K.; Yang, H.; Lee, M.; et al. Genome-Wide Profiles of CtBP Link Metabolism with Genome Stability and Epithelial Reprogramming in Breast Cancer. *Nat. Commun.* **2013**, *4*.
(52) Ding, B.; Yuan, F.; Damle, P. K.; Litovchick, L.; Drapkin, R.; Grossman, S. R. CtBP Determines Ovarian Cancer Cell Fate through Repression of Death Receptors. *Cell Death Dis.* **2020**, *11* (4).
(53) Barroilhet, L.; Yang, J.; Hasselblatt, K.; Paranal, R. M.; Ng, S.; Rauh-hain, J. A.; Welch, W. R.; Bradner, J. E.; Berkowitz, R. S.; Ng, S. C-Terminal Binding Protein-2 Regulates Response of Epithelial Ovarian Cancer Cells to Histone Deacetylase Inhibitors. *Oncogene* **2013**, *32*, 3896–3903.
(54) He, Y.; Zhicheng, H.; Lin, J.; Chen, C.; Chen, Y.; Liu, S. CtBP1/2 Differentially Regulate Genomic Stability and DNA Repair Pathway in High-Grade Serous Ovarian Cancer Cell. *Oncogenesis* **2021**, *10* (49).
(55) Zheng, X.; Song, T.; Dou, C.; Jia, Y.; Liu, Q. CtBP2 Is an Independent Prognostic Marker That Promotes GLI1 Induced Epithelial-Mesenchymal Transition in Hepatocellular Carcinoma. *Oncotarget* **2015**, *6* (6), 3752–3769.
(56) Bizama, C.; Benavente, F.; Salvatierra, E.; Gutiérrez-Moraga, A.; Espinoza, J. A.; Fernández, E. A.; Roa, I.; Mazzolini, G.; Sagredo, E. A.; Gidekel, M.; et al. The Low-Abundance Transcriptome Reveals Novel Biomarkers, Specific Intracellular Pathways and Targetable Genes Associated with Advanced Gastric Cancer. *Int. J. Cancer* **2014**, *134* (4), 755–764.
(57) Moiola, C. P.; Luca, P. De; Zalazar, F.; Cotignola, J.; Rodríguez-Seguí, S. A.; Gardner, K.; Meiss, R.; Vallecorsa, P.; Pignataro, O.; Mazza, O.; et al. Prostate Tumor Growth Is Impaired by CtBP1 Depletion in High-Fat Diet-Fed Mice. *Clin. Cancer Res.* **2014**, *20* (15), 4086–4095.

(58) Wang, R.; Asangani, I. A.; Chakravarthi, B. V. S. K.; Ateeq, B.; Lonigro, R. J.; Cao, Q.; Mani, R. S.; Camacho, D. F.; McGregor, N.; Schumann, T. E. W.; et al. Role of Transcriptional Corepressor CtBP1 in Prostate Cancer Progression. *Neoplasia (United States)* **2012**, *14* (10), 905–914.
(59) Chawla, A. T.; Chougoni, K. K.; Joshi, P. J.; Cororaton, A. D.; Memari, P.; Stans, J. C.; Park, H.; Seth, R.; Szomju, B.; Sima, A. P.; et al. CtBP — a Targetable Dependency for Tumor-Initiating Cell Activity and Metastasis in Pancreatic Adenocarcinoma. **2019**.
(60) Vander, M. G.; Cantley, L. C.; Thompson, C. B. Understanding the Warburg Effect : Cell Proliferation Abu Nant Scarce Ah Proliferative Starvation h Wowth No. **2009**, *324* (5930), 1029–1033.
(61) Koppenol, W. H.; Bounds, P. L.; Dang, C. V. Otto Warburg's Contributions to Current Concepts of Cancer Metabolism. *Nat. Rev. Cancer* **2011**, *11* (5), 325–337.
(62) Yu, Q.; Heikal, A. A. Two-Photon Autofluorescence Dynamics Imaging Reveals Sensitivity of Intracellular NADH Concentration and Conformation to Cell Physiology at the Single-Cell Level. *J. Photochem. Photobiol. B Biol.* **2009**, *95* (1), 46–57.
(63) Uppal, A.; Gupta, P. K. Measurement of NADH Concentration in Normal and Malignant Human Tissues from Breast and Oral Cavity. *Biotechnol. Appl. Biochem.* **2003**, *37* (1), 45.
(64) Schwartz, J.; Passonneau, V.; Johnson, G. S.; Pastan, I. The Effect of Growth Conditions on NAD+ and NADH Concentrations and the NAD+:NADH Ratio in Normal and Transformed Fibroblasts. *J. Biol. Chem.* **1974**, *249* (13), 4138–4143.
(65) Wang, L. H.; Wu, C. F.; Rajasekaran, N.; Shin, Y. K. Loss of Tumor Suppressor Gene Function in Human Cancer: An Overview. *Cell. Physiol. Biochem.* **2019**, *51* (6), 2647–2693.
(66) Shimazu, T.; Degenhardt, K.; Nur-E-Kamal, A.; Zhang, J.; Yoshida, T.; Zhang, Y.; Mathew, R.; White, E.; Inouye, M. NBK/BIK Antagonizes MCL-1 and BCL-XL and Activates BAK-Mediated Apoptosis in Response to Protein Synthesis Inhibition. *Genes Dev.* **2007**, *21* (8), 929–941.
(67) Kovi, R. C.; Paliwal, S.; Pande, S.; Grossman, S. R. An ARF/CtBP2 Complex Regulates BH3-Only Gene Expression and P53-Independent Apoptosis. *Cell Death Differ.* **2010**, *17* (3), 513–521.
(68) Korwar, S.; Morris, B. L.; Parikh, H. I.; Coover, R. A.; Doughty, T. W.; Love, I. M.; Hilbert, B. J.; Royer, W. E.; Kellogg, G. E.; Grossman, S. R.; et al. Design, Synthesis, and Biological Evaluation of Substrate-Competitive Inhibitors of C-Terminal Binding Protein (CtBP). *Bioorganic Med. Chem.* **2016**, *24* (12), 2707–2715.
(69) Simpson, L.; Parsons, R. PTEN: Life as a Tumor Suppressor. *Exp. Cell Res.* **2001**, *264* (1), 29–41.
(70) Sansal, I.; Sellers, W. R. The Biology and Clinical Relevance of the PTEN Tumor Suppressor Pathway. *J. Clin. Oncol.* **2004**, *22* (14), 2954–2963.
(71) Paliwal, S.; Ho, N.; Parker, D.; Grossman, S. R. CtBP2 Promotes Human Cancer Cell Migration by Transcriptional Activation of Tiam1. *Genes and Cancer* **2012**, *3* (7–8), 481–490.
(72) Yamada, K. M.; Araki, M. Tumor Suppressor PTEN: Modulator of Cell Signaling,

Growth, Migration and Apoptosis. *J. Cell Sci.* **2001**, *114* (13), 2375–2382.
(73) Takayama, K. I.; Suzuki, T.; Fujimura, T.; Urano, T.; Takahashi, S.; Homma, Y.; Inoue, S. CtBP2 Modulates the Androgen Receptor to Promote Prostate Cancer Progression. *Cancer Res.* **2014**, *74* (22), 6542–6553.
(74) Paliwal, S.; Kovi, R. C.; Nath, B.; Chen, Y. W.; Lewis, B. C.; Grossman, S. R. The Alternative Reading Frame Tumor Suppressor Antagonizes Hypoxia-Induced Cancer Cell Migration via Interaction with the COOH-Terminal Binding Protein Corepressor. *Cancer Res.* **2007**, *67* (19), 9322–9329.
(75) Van Roy, F.; Berx, G. The Cell-Cell Adhesion Molecule E-Cadherin. *Cell. Mol. Life Sci.* **2008**, *65* (23), 3756–3788.
(76) Zhang, X. L.; Huang, C. X.; Zhang, J.; Inoue, A.; Zeng, S. E.; Xiao, S. J. CtBP1 Is Involved in Epithelial-Mesenchymal Transition and Is a Potential Therapeutic Target for Hepatocellular Carcinoma. *Oncol. Rep.* **2013**, *30* (2), 809–814.
(77) Di, L. J.; Fernandez, A. G.; De Siervi, A.; Longo, D. L.; Gardner, K. Transcriptional Regulation of BRCA1 Expression by a Metabolic Switch. *Nat. Struct. Mol. Biol.* **2010**, *17* (12), 1406–1413.
(78) Venkitaraman, A. R. Cancer Susceptibility and the Functions of BRCA1 and BRCA2. *Cell* **2002**, *108* (2), 171–182.
(79) Deng, Y.; Deng, H.; Liu, J.; Han, G.; Malkoski, S.; Liu, B.; Zhao, R.; Wang, X. J.; Zhang, Q. Transcriptional Down-Regulation of Brca1 and E-Cadherin by CtBP1 in Breast Cancer. *Mol. Carcinog.* **2012**, *51* (6), 500–507.
(80) Minard, M. E.; Kim, L.; Price, J. E.; Gallick, G. E. The Role of the Guanine Nucleotide Exchange Factor Tiam1 in Cellular Migration, Invasion, Adhesion and Tumor Progression Meghan. *Breast Cancer Res. Treat.* **2004**, *84*, 21–32.
(81) Jin, W.; Scotto, K. W.; Hait, W. N.; Yang, J. M. Involvement of CtBP1 in the Transcriptional Activation of the MDR1 Gene in Human Multidrug Resistant Cancer Cells. *Biochem. Pharmacol.* **2007**, *74* (6), 851–859.
(82) Birts, C. N.; Nijjar, S. K.; Mardle, C. A.; Hoakwie, F.; Duriez, P. J.; Blaydes, J. P.; Tavassoli, A. A Cyclic Peptide Inhibitor of C-Terminal Binding Protein Dimerization Links Metabolism with Mitotic Fidelity in Breast Cancer Cells. *Chem. Sci.* **2013**, *4* (8), 3046–3057.
(83) Blevins, M. A.; Kouznetsova, J.; Krueger, A. B.; King, R.; Griner, L. M.; Hu, X.; Southall, N.; Marugan, J. J.; Zhang, Q.; Ferrer, M.; et al. Small Molecule, NSC95397, Inhibits the CTBP1-Protein Partner Interaction and CTBP1-Mediated Transcriptional Repression. *J. Biomol. Screen.* **2015**, *20* (5), 663–672.
(84) Lazo, J. S.; Nemoto, K.; Pestell, K. E.; Cooley, K.; Southwick, E. C.; Mitchell, D. A.; Furey, W.; Gussio, R.; Zaharevitz, D. W.; Joo, B.; et al. Identification of a Potent and Selective Pharmacophore for Cdc25 Dual Specificity Phosphatase Inhibitors. *Mol. Pharmacol.* **2002**, *61* (4), 720–728.
(85) Berg, M. G.; Wan, L.; Younis, I.; Diem, M. D.; Soo, M.; Wang, C.; Dreyfuss, G. A Quantitative High-Throughput In Vitro Splicing Assay Identifies Inhibitors of Spliceosome Catalysis . *Mol. Cell. Biol.* **2012**, *32* (7), 1271–1283.
(86) Straza, M. W.; Paliwal, S.; Kovi, R. C.; Rajeshkumar, B.; Trenh, P.; Parker, D.; Whalen, G. F.; Lyle, S.; Schiffer, C. A.; Grossman, S. R.; et al. Therapeutic Targeting of C-Terminal Binding Protein in Human Cancer. **2010**, *4101*.
(87) Hilbert, B. J.; Morris, B. L.; Ellis, K. C.; Paulsen, J. L.; Schiffer, C. A.; Grossman, S.

R.; Royer, W. E. Structure-Guided Design of a High Affinity Inhibitor to Human CtBP. *ACS Chem. Biol.* **2015**, *10* (4), 1118–1127.
(88) Neese, F. The ORCA Program System. *Wiley Interdiscip. Rev. Comput. Mol. Sci.* **2012**, *2* (1), 73–78.
(89) Neese, F. Software Update: The ORCA Program System, Version 4.0. *Wiley Interdiscip. Rev. Comput. Mol. Sci.* **2018**, *8* (e1327).
(90) Trott, O.; Olson, A. J. AutoDock Vina: Improving the Speed and Accuracy of Docking with a New Scoring Function, Efficient Optimization, and Multithreading. *J. Comput. Chem.* **2010**, *31*, 455–461.
(91) Schiessl, K.; Roller, A.; Hammerschmidt, F. Determination of Absolute Configuration of the Phosphonic Acid Moiety of Fosfazinomycins. *Org. Biomol. Chem.* **2013**, *11* (42), 7420–7426.
(92) He, S.; Lai, Z.; Yang, D. X.; Hong, Q.; Reibarkh, M.; Nargund, R. P.; Hagmann, W. K. Synthesis of SS-Carbolines from Aldehydes and Ketones via the α-Siloxy α,ß-Unsaturated Esters. *Tetrahedron Lett.* **2010**, *51* (33), 4361–4364.
(93) Burnett, Duane A.; Vacca, J. P. Cyclohexyl Derivs. and Related Compounds Used as Inclusion and Stress Granule Modulators and Their Preparation. WO 2018119395, 2018.
(94) Fell, S. C. M.; Pearson, M. J.; Burton, G.; Elder, J. S. Synthesis and Biological Activity of New C-6 and C-7 Substituted Vinyloxyimino-Penicillins and -Cephalosporins. *J. Chem. Soc. Perkin Trans.* **1995**, 1483–1493.
(95) Bergman, L. M.; Birts, C. N.; Darley, M.; Gabrielli, B.; Blaydes, J. P. CtBPs Promote Cell Survival through the Maintenance Of. **2009**, *29* (16), 4539–4551.
(96) Watson, M.; Roulston, A.; Bélec, L.; Billot, X.; Marcellus, R.; Bédard, D.; Bernier, C.; Branchaud, S.; Chan, H.; Dairi, K.; et al. The Small Molecule GMX1778 Is a Potent Inhibitor of NAD + Biosynthesis: Strategy for Enhanced Therapy in Nicotinic Acid Phosphoribosyltransferase 1-Deficient Tumors . *Mol. Cell. Biol.* **2009**, *29* (21), 5872–5888.
(97) Kornitzer, D.; Ciechanover, A. Modes of Regulation of Ubiquitin-Mediated Protein Degradation. *J. Cell. Physiol.* **2000**, *182* (1), 1–11.
(98) Jadhav, T.; Wooten, M. W. Defining an Embedded Code for Protein Ubiquitination. *J. Proteomics Bioinform.* **2009**, *2* (316), 1–7.
(99) Ciechanover, A.; Orian, A.; Schwartz, A. L. Ubiquitin-Mediated Proteolysis: Biological Regulation via Destruction. *BioEssays* **2000**, *22* (5), 442–451.
(100) Goldstein, G.; Scheid, M.; Hammerling, U.; Schlesinger, D. H.; Niall, H. D.; Boyse, E. A. Isolation of a Polypeptide That Has Lymphocyte Differentiating Properties and Is Probably Represented Universally in Living Cells. *Proc. Natl. Acad. Sci. U. S. A.* **1975**, *72* (1), 11–15.
(101) Goldknopf, I. L.; Busch, H. Isopeptide Linkage between Nonhistone and Histone 2A Polypeptides of Chromosomal Conjugate Protein A24. *Proc. Natl. Acad. Sci. U. S. A.* **1977**, *74* (3), 864–868.
(102) Mukhopadhyay, D.; Riezman, H. Proteasome-Independent Functions of Ubiquitin in Endocytosis and Signaling. *Science (80-.).* **2007**, *315* (5809), 201–205.
(103) Burslem, G. M.; Crews, C. M. Small-Molecule Modulation of Protein Homeostasis. *Chemical Reviews*. American Chemical Society September 13, 2017, pp 11269–11301.

(104) Komander, D.; Rape, M. The Ubiquitin Code. *Annu. Rev. Biochem.* **2012**, *81*, 203–229.
(105) Haas, A. L.; Warms, J. V.; Hershko, A.; Rose, I. A. Ubiquitin-Activating Enzyme. Mechanism and Role in Protein-Ubiquitin Conjugation. *J. Biol. Chem.* **1982**, *257* (5), 2543–2548.
(106) Yau, R.; Rape, M. The Increasing Complexity of the Ubiquitin Code. *Nat. Cell Biol.* **2016**, *18* (6), 579–586.
(107) Pickart, C. M.; Eddins, M. J. Ubiquitin: Structures, Functions, Mechanisms. *Biochim. Biophys. Acta - Mol. Cell Res.* **2004**, *1695* (1–3), 55–72.
(108) Schneekloth, J. S.; Fonseca, F. N.; Koldobskiy, M.; Mandal, A.; Deshaies, R.; Sakamoto, K.; Crews, C. M. Chemical Genetic Control of Protein Levels: Selective in Vivo Targeted Degradation. *J. Am. Chem. Soc.* **2004**, *126* (12), 3748–3754.
(109) Saeki, Y. Ubiquitin Recognition by the Proteasome. *J. Biochem.* **2017**, *161* (2), 113–124.
(110) Verma, R.; Aravind, L.; Oania, R.; McDonald, W. H.; Yates, J. R.; Koonin, E. V.; Deshaies, R. J. Role of Rpn11 Metalloprotease in Deubiquitination and Degradation by the 26S Proteasome. *Science (80-.).* **2002**, *298* (5593), 611–615.
(111) Baumeister, W.; Walz, J.; Zühl, F.; Seemüller, E. The Proteasome: Paradigm of a Self-Compartmentalizing Protease. *Cell* **1998**, *92* (3), 367–380.
(112) Spratt, D. E.; Walden, H.; Shaw, G. S. RBR E3 Ubiquitin Ligases: New Structures, New Insights, New Questions. *Biochem. J.* **2014**, *458* (3), 421–437.
(113) Berndsen, C. E.; Wolberger, C. New Insights into Ubiquitin E3 Ligase Mechanism. *Nat. Struct. Mol. Biol.* **2014**, *21* (4), 301–307.
(114) Fouad, S.; Wells, O. S.; Hill, M. A.; D'Angiolella, V. Cullin Ring Ubiquitin Ligases (CRLs) in Cancer: Responses to Ionizing Radiation (IR) Treatment. *Front. Physiol.* **2019**, *10* (October).
(115) Metzger, M. B.; Pruneda, J. N.; Klevit, R. E.; Weissman, A. M. RING-Type E3 Ligases: Master Manipulators of E2 Ubiquitin-Conjugating Enzymes and Ubiquitination. *Biochim. Biophys. Acta - Mol. Cell Res.* **2014**, *1843* (1), 47–60.
(116) Oberoi-Khanuja, T. K.; Rajalingam, K. IAPs as E3 Ligases of Rac1. *Small GTPases* **2012**, *3* (2), 131–136.
(117) Honda, R.; Tanaka, H.; Yasuda, H. Oncoprotein MDM2 Is a Ubiquitin Ligase E3 for Tumor Suppressor P53. *FEBS Lett.* **1997**, *420* (1), 25–27.
(118) Toledo, F.; Wahl, G. M. MDM2 and MDM4: P53 Regulators as Targets in Anticancer Therapy. *Int. J. Biochem. Cell Biol.* **2007**, *39* (7–8), 1476–1482.
(119) Vassilev, L. T.; Vu, B. T.; Graves, B.; Carvajal, D.; Podlaski, F.; Filipovic, Z.; Kong, N.; Kammlott, U.; Lukacs, C.; Klein, C.; et al. In Vivo Activation of the P53 Pathway by Small-Molecule Antagonists of MDM2. *Science (80-.).* **2004**, *303* (5659), 844–848.
(120) Nakayama, K. I.; Nakayama, K. Ubiquitin Ligases: Cell-Cycle Control and Cancer. *Nat. Rev. Cancer* **2006**, *6* (5), 369–381.
(121) Scott, D. C.; Rhee, D. Y.; Duda, D. M.; Kelsall, I. R.; Olszewski, J. L.; Paulo, J. A.; de Jong, A.; Ovaa, H.; Alpi, A. F.; Harper, J. W.; et al. Two Distinct Types of E3 Ligases Work in Unison to Regulate Substrate Ubiquitylation. *Cell* **2016**, *166* (5), 1198-1214.e24.
(122) Bosu, D. R.; Kipreos, E. T. Cullin-RING Ubiquitin Ligases: Global Regulation and

Activation Cycles. *Cell Div.* **2008**, *3*, 1–13.
(123) Jackson, S.; Xiong, Y. CRL4s: The CUL4-RING E3 Ubiquitin Ligases. *Trends Biochem. Sci.* **2009**, *34* (11), 562–570.
(124) Chen, Y. A.; Peng, Y. J.; Hu, M. C.; Huang, J. J.; Chien, Y. C.; Wu, J. T.; Chen, T. Y.; Tang, C. Y. The Cullin 4A/B-DDB1-Cereblon E3 Ubiquitin Ligase Complex Mediates the Degradation of CLC-1 Chloride Channels. *Sci. Rep.* **2015**, *5* (December 2014), 1–13.
(125) Latif, F.; Tory, K.; Gnarra, J.; Yao, M.; Duh, F.; Orcutt, L.; Stackhouse, T.; Kuzmin, I.; Modi, W.; Geil, L.; et al. Identification of the von Hippel-Lindau Disease Tumor Suppressor Gene Published by : American Association for the Advancement of Science Stable URL : Https://Www.Jstor.Org/Stable/2881766 American Association for the Advancement of Science Is Collaborating. **1993**, 31–35.
(126) Schoenfeld, A.; Davidowitz, E. J.; Burk, R. D. A Second Major Native von Hippel-Lindau Gene Product, Initiated from an Internal Translation Start Site, Functions as a Tumor Suppressor. *Proc. Natl. Acad. Sci. U. S. A.* **1998**, *95* (15), 8817–8822.
(127) Blankenship, C.; Naglich, J. G.; Whaley, J. M.; Seizinger, B.; Kley, N. Alternate Choice of Initiation Codon Produces a Biologically Active Product of the von Hippel Lindau Gene with Tumor Suppressor Activity. *Oncogene* **1999**, *18* (8), 1529–1535.
(128) Iliopoulos, O.; Ohh, M.; Kaelin Jr., W. G. PVHL19 Is a Biologically Active Product of the von Hippel-Lindau Gene Arising from Internal Translation Initiation 10215. *Proc.Natl.Acad.Sci.U.S.A* **1998**, *95* (0027–8424), 11661–11666.
(129) Gossage, L.; Eisen, T.; Maher, E. R. VHL, the Story of a Tumour Suppressor Gene. *Nat. Rev. Cancer* **2015**, *15* (1), 55–64.
(130) Frost, J.; Rocha, S.; Ciulli, A. Von Hippel-Lindau (VHL) Small-Molecule Inhibitor Binding Increases Stability and Intracellular Levels of VHL Protein. *J. Biol. Chem.* **2021**, *297* (2), 100910.
(131) Galdeano, C.; Gadd, M. S.; Soares, P.; Scaffidi, S.; Van Molle, I.; Birced, I.; Hewitt, S.; Dias, D. M.; Ciulli, A. Structure-Guided Design and Optimization of Small Molecules Targeting the Protein-Protein Interaction between the von Hippel-Lindau (VHL) E3 Ubiquitin Ligase and the Hypoxia Inducible Factor (HIF) Alpha Subunit with in Vitro Nanomolar Affinities. *J. Med. Chem.* **2014**, *57* (20), 8657–8663.
(132) Higgins, J. J.; Pucilowska, J.; Lombardi, R. Q.; Rooney, J. P. A Mutation in a Novel ATP-Dependent Lon Protease Gene in a Kindred with Mild Mental Retardation. *Neurology* **2004**, *63* (10), 1927–1931.
(133) Ota, T.; Suzuki, Y.; Nishikawa, T.; Otsuki, T.; Sugiyama, T.; Irie, R.; Wakamatsu, A.; Hayashi, K.; Sato, H.; Nagai, K.; et al. Complete Sequencing and Characterization of 21,243 Full-Length Human CDNAs. *Nat. Genet.* **2004**, *36* (1), 40–45.
(134) Kim, H. K.; Ko, T. H.; Nyamaa, B.; Lee, S. R.; Kim, N.; Ko, K. S.; Rhee, B. D.; Park, C. S.; Nilius, B.; Han, J. Cereblon in Health and Disease. *Pflugers Arch. Eur. J. Physiol.* **2016**, *468* (8), 1299–1309.
(135) Fischer, E. S.; Böhm, K.; Lydeard, J. R.; Yang, H.; Stadler, M. B.; Cavadini, S.; Nagel, J.; Serluca, F.; Acker, V.; Lingaraju, G. M.; et al. Structure of the DDB1-CRBN E3 Ubiquitin Ligase in Complex with Thalidomide. *Nature* **2014**, *512* (1), 49–53.
(136) Ito, T.; Ando, H.; Suzuki, T.; Ogura, T.; Hotta, K.; Imamura, Y.; Yamaguchi, Y.;

Handa, H. Identification of a Primary Target of Thalidomide Teratogenicity. *Science (80-.).* **2010**, *327* (5971), 1345–1350.
(137) Asatsuma-Okumura, T.; Ito, T.; Handa, H. Molecular Mechanisms of Cereblon-Based Drugs. *Pharmacol. Ther.* **2019**, *202*, 132–139.
(138) Mori, T.; Ito, T.; Liu, S.; Ando, H.; Sakamoto, S.; Yamaguchi, Y.; Tokunaga, E.; Shibata, N.; Handa, H.; Hakoshima, T. Structural Basis of Thalidomide Enantiomer Binding to Cereblon. *Sci. Rep.* **2018**, *8* (1), 1–14.
(139) Girardini, M.; Maniaci, C.; Hughes, S. J.; Testa, A.; Ciulli, A. Cereblon versus VHL: Hijacking E3 Ligases against Each Other Using PROTACs. *Bioorganic Med. Chem.* **2019**, *27* (12), 2466–2479.
(140) Churcher, I. Protac-Induced Protein Degradation in Drug Discovery: Breaking the Rules or Just Making New Ones? *J. Med. Chem.* **2018**, *61* (2), 444–452.
(141) Lai, A. C.; Crews, C. M. Induced Protein Degradation: An Emerging Drug Discovery Paradigm. *Nature Reviews Drug Discovery*. Nature Publishing Group February 2, 2017, pp 101–114.
(142) Cromm, P. M.; Crews, C. M. Targeted Protein Degradation: From Chemical Biology to Drug Discovery. *Cell Chemical Biology*. Elsevier Ltd September 21, 2017, pp 1181–1190.
(143) Sakamoto, K. M.; Kim, K. B.; Kumagai, A.; Mercurio, F.; Crews, C. M.; Deshaies, R. J. *Protacs: Chimeric Molecules That Target Proteins to the Skp1-Cullin-F Box Complex for Ubiquitination and Degradation*; 2001.
(144) Sakamoto, K. M.; Kim, K. B.; Kumagai, A.; Mercurio, F.; Crews, C. M.; Deshaies, R. J. Protacs: Chimeric Molecules That Target Proteins to the Skp1-Cullin-F Box Complex for Ubiquitination and Degradation. *PNAS* **2001**, *98* (15), 8554–8559.
(145) Ottis, P.; Crews, C. M. Proteolysis-Targeting Chimeras: Induced Protein Degradation as a Therapeutic Strategy. *ACS Chemical Biology*. American Chemical Society April 21, 2017, pp 892–898.
(146) Huang, X.; Dixit, V. M. Drugging the Undruggables: Exploring the Ubiquitin System for Drug Development. *Cell Research*. Nature Publishing Group April 1, 2016, pp 484–498.
(147) Zou, Y.; Ma, D.; Wang, Y. The PROTAC Technology in Drug Development. *Cell Biochem. Funct.* **2019**, *37* (1), 21–30.
(148) Sakamoto, K. M.; Kim, K. B.; Verma, R.; Ransick, A.; Stein, B.; Crews, C. M.; Deshaies, R. J. Development of Protacs to Target Cancer-Promoting Proteins for Ubiquitination and Degradation. *Mol. Cell. Proteomics* **2003**, *2* (12), 1350–1358.
(149) Zhang, D.; Baek, S. H.; Ho, A.; Kim, K. Degradation of Target Protein in Living Cells by Small-Molecule Proteolysis Inducer. *Bioorganic Med. Chem. Lett.* **2004**, *14* (3), 645–648.
(150) Bargagna-Mohan, P.; Baek, S. H.; Lee, H.; Kim, K.; Mohan, R. Use of PROTACS as Molecular Probes of Angiogenesis. *Bioorganic Med. Chem. Lett.* **2005**, *15* (11), 2724–2727.
(151) Rodriguez-Gonzalez, A.; Cyrus, K.; Salcius, M.; Kim, K.; Crews, C. M.; Deshaies, R. J.; Sakamoto, K. M. Targeting Steroid Hormone Receptors for Ubiquitination and Degradation in Breast and Prostate Cancer. *Oncogene* **2008**, *27* (57), 7201–7211.
(152) Lee, H.; Puppala, D.; Choi, E. Y.; Swanson, H.; Kim, K. B. Targeted Degradation of the Aryl Hydrocarbon Receptor by the PROTAC Approach: A Useful Chemical

Genetic Tool. *ChemBioChem* **2007**, *8* (17), 2058–2062.
(153) Puppala, D.; Lee, H.; Kyung, B. K.; Swanson, H. I. Development of an Aryl Hydrocarbon Receptor Antagonist Using the Proteolysis-Targeting Chimeric Molecules Approach: A Potential Tool for Chemoprevention. *Mol. Pharmacol.* **2008**, *73* (4), 1064–1071.
(154) Montrose, K.; Krissansen, G. W. Design of a PROTAC That Antagonizes and Destroys the Cancer-Forming X-Protein of the Hepatitis B Virus. *Biochem. Biophys. Res. Commun.* **2014**, *453* (4), 735–740.
(155) Chu, T. T.; Gao, N.; Li, Q. Q.; Chen, P. G.; Yang, X. F.; Chen, Y. X.; Zhao, Y. F.; Li, Y. M. Specific Knockdown of Endogenous Tau Protein by Peptide-Directed Ubiquitin-Proteasome Degradation. *Cell Chem. Biol.* **2016**, *23* (4), 453–461.
(156) Lu, M.; Liu, T.; Jiao, Q.; Ji, J.; Tao, M.; Liu, Y.; You, Q.; Jiang, Z. Discovery of a Keap1-Dependent Peptide PROTAC to Knockdown Tau by Ubiquitination-Proteasome Degradation Pathway. *Eur. J. Med. Chem.* **2018**, *146*, 251–259.
(157) Schneekloth, A. R.; Pucheault, M.; Tae, H. S.; Crews, C. M. Targeted Intracellular Protein Degradation Induced by a Small Molecule: En Route to Chemical Proteomics. *Bioorganic Med. Chem. Lett.* **2008**, *18* (22), 5904–5908.
(158) Debes, J. D.; Schmidt, L. J.; Huang, H.; Tindall, D. J. P300 Mediates Androgen-Independent Transactivation of the Androgen Receptor By Interleukin 6. *Cancer Res.* **2002**, *62* (20), 5632–5636.
(159) Marhefka, C. A.; Gao, W.; Chung, K.; Kim, J.; He, Y.; Yin, D.; Bohl, C.; Dalton, J. T.; Miller, D. D. Design, Synthesis, and Biological Characterization of Metabolically Stable Selective Androgen Receptor Modulators. *J. Med. Chem.* **2004**, *47* (4), 993–998.
(160) Itoh, Y.; Ishikawa, M.; Naito, M.; Hashimoto, Y. Protein Knockdown Using Methyl Bestatin-Ligand Hybrid Molecules: Design and Synthesis of Inducers of Ubiquitination-Mediated Degradation of Cellular Retinoic Acid-Binding Proteins. *J. Am. Chem. Soc.* **2010**, *132* (16), 5820–5826.
(161) Sato, S.; Aoyama, H.; Miyachi, H.; Naito, M.; Hashimoto, Y. Demonstration of Direct Binding of CIAP1 Degradation-Promoting Bestatin Analogs to BIR3 Domain: Synthesis and Application of Fluorescent Bestatin Ester Analogs. *Bioorganic Med. Chem. Lett.* **2008**, *18* (11), 3354–3358.
(162) Sekine, K.; Takubo, K.; Kikuchi, R.; Nishimoto, M.; Kitagawa, M.; Abe, F.; Nishikawa, K.; Tsuruo, T.; Naito, M. Small Molecules Destabilize CIAP1 by Activating Auto-Ubiquitylation. *J. Biol. Chem.* **2008**, *283* (14), 8961–8968.
(163) Itoh, Y.; Kitaguchi, R.; Ishikawa, M.; Naito, M.; Hashimoto, Y. Design, Synthesis and Biological Evaluation of Nuclear Receptor-Degradation Inducers. *Bioorganic Med. Chem.* **2011**, *19* (22), 6768–6778.
(164) Kagechika, H.; Kawachi, E.; Hashimoto, Y.; Shudo, K. Retinobenzoic Acids. 2. Structure-Activity Relationships of Chalcone-4-Carboxylic Acids and Flavone-4'-Carboxylic Acids. *J. Med. Chem.* **1989**, *321*, 834–840.
(165) Kagechika, H.; Himi, T.; Kawachi, E.; Shudo, K. Retinobenzoic Acids. 4. Conformation of Aromatic Amides with Retinoidal Activity. Importance of Trans-Amide Structure for Activity. *J. Medi* **1989**, *32*, 2292–2296.
(166) Ohoka, N.; Nagai, K.; Hattori, T.; Okuhira, K.; Shibata, N.; Cho, N.; Naito, M. Cancer Cell Death Induced by Novel Small Molecules Degrading the TACC3 Protein via

the Ubiquitin-Proteasome Pathway. *Cell Death Dis.* **2014**, *5* (11), 1–10.
(167) An, S.; Fu, L. Small-Molecule PROTACs: An Emerging and Promising Approach for the Development of Targeted Therapy Drugs. *EBioMedicine* **2018**, *36*, 553–562.
(168) Buckley, D. L.; Van Molle, I.; Gareiss, P. C.; Tae, H. S.; Michel, J.; Noblin, D. J.; Jorgensen, W. L.; Ciulli, A.; Crews, C. M. Targeting the von Hippel-Lindau E3 Ubiquitin Ligase Using Small Molecules to Disrupt the VHL/HIF-1α Interaction. *J. Am. Chem. Soc.* **2012**, *134* (10), 4465–4468.
(169) Buckley, D. L.; Gustafson, J. L.; Van-Molle, I.; Roth, A. G.; Tae, H. S.; Gareiss, P. C.; Jorgensen, W. L.; Ciulli, A.; Crews, C. M. Small-Molecule Inhibitors of the Interaction between the E3 Ligase VHL and HIF1α. *Angew. Chemie - Int. Ed.* **2012**, *51* (46), 11463–11467.
(170) Lopez-Girona, A.; Mendy, D.; Ito, T.; Miller, K.; Gandhi, A. K.; Kang, J.; Karasawa, S.; Carmel, G.; Jackson, P.; Abbasian, M.; et al. Cereblon Is a Direct Protein Target for Immunomodulatory and Antiproliferative Activities of Lenalidomide and Pomalidomide. *Leukemia* **2012**, *26* (11), 2326–2335.
(171) Buckley, D. L.; Raina, K.; Darricarrere, N.; Hines, J.; Gustafson, J. L.; Smith, I. E.; Miah, A. H.; Harling, J. D.; Crews, C. M. HaloPROTACS: Use of Small Molecule PROTACs to Induce Degradation of HaloTag Fusion Proteins. *ACS Chem. Biol.* **2015**, *10* (8), 1831–1837.
(172) Bondeson, D. P.; Mares, A.; Smith, I. E. D.; Ko, E.; Campos, S.; Miah, A. H.; Mulholland, K. E.; Routly, N.; Buckley, D. L.; Gustafson, J. L.; et al. Catalytic in Vivo Protein Knockdown by Small-Molecule PROTACs. *Nat. Chem. Biol.* **2015**, *11* (8), 611–617.
(173) Lai, A. C.; Toure, M.; Hellerschmied, D.; Salami, J.; Jaime-Figueroa, S.; Ko, E.; Hines, J.; Crews, C. M. Modular PROTAC Design for the Degradation of Oncogenic BCR-ABL. *Angew. Chemie - Int. Ed.* **2016**, *55* (2), 807–810.
(174) Raina, K.; Lu, J.; Qian, Y.; Altieri, M.; Gordon, D.; Rossi, A. M. K.; Wang, J.; Chen, X.; Dong, H.; Siu, K.; et al. PROTAC-Induced BET Protein Degradation as a Therapy for Castration-Resistant Prostate Cancer. *Proc. Natl. Acad. Sci. U. S. A.* **2016**, *113* (26), 7124–7129.
(175) Zengerle, M.; Chan, K. H.; Ciulli, A. Selective Small Molecule Induced Degradation of the BET Bromodomain Protein BRD4. *ACS Chem. Biol.* **2015**, *10* (8), 1770–1777.
(176) Gadd, M. S.; Testa, A.; Lucas, X.; Chan, K. H.; Chen, W.; Lamont, D. J.; Zengerle, M.; Ciulli, A. Structural Basis of PROTAC Cooperative Recognition for Selective Protein Degradation. *Nat. Chem. Biol.* **2017**, *13* (5), 514–521.
(177) Crew, A. P.; Raina, K.; Dong, H.; Qian, Y.; Wang, J.; Vigil, D.; Serebrenik, Y. V.; Hamman, B. D.; Morgan, A.; Ferraro, C.; et al. Identification and Characterization of von Hippel-Lindau-Recruiting Proteolysis Targeting Chimeras (PROTACs) of TANK-Binding Kinase 1. *J. Med. Chem.* **2018**, *61* (2), 583–598.
(178) Burslem, G. M.; Smith, B. E.; Lai, A. C.; Jaime-Figueroa, S.; McQuaid, D. C.; Bondeson, D. P.; Toure, M.; Dong, H.; Qian, Y.; Wang, J.; et al. The Advantages of Targeted Protein Degradation Over Inhibition: An RTK Case Study. *Cell Chem. Biol.* **2018**, *25* (1), 67-77.e3.
(179) Gechijian, L. N.; Buckley, D. L.; Lawlor, M. A.; Reyes, J. M.; Paulk, J.; Ott, C. J.; Winter, G. E.; Erb, M. A.; Scott, T. G.; Xu, M.; et al. Functional TRIM24 Degrader

via Conjugation of Ineffectual Bromodomain and VHL Ligands Article. *Nat. Chem. Biol.* **2018**, *14* (4), 405–412.
(180) Winter, G. E.; Buckley, D. L.; Paulk, J.; Roberts, J. M.; Souza, A.; Dhe-Paganon, S.; Bradner, J. E. Phthalimide Conjugation as a Strategy for in Vivo Target Protein Degradation. *Science (80-.).* **2015**, *348* (6241), 1376–1381.
(181) Lu, J.; Qian, Y.; Altieri, M.; Dong, H.; Wang, J.; Raina, K.; Hines, J.; Winkler, J. D.; Crew, A. P.; Coleman, K.; et al. Hijacking the E3 Ubiquitin Ligase Cereblon to Efficiently Target BRD4. *Chem. Biol.* **2015**, *22* (6), 755–763.
(182) Zhou, B.; Hu, J.; Xu, F.; Chen, Z.; Bai, L.; Fernandez-Salas, E.; Lin, M.; Liu, L.; Yang, C. Y.; Zhao, Y.; et al. Discovery of a Small-Molecule Degrader of Bromodomain and Extra-Terminal (BET) Proteins with Picomolar Cellular Potencies and Capable of Achieving Tumor Regression. *J. Med. Chem.* **2018**, *61* (2), 462–481.
(183) Remillard, D.; Buckley, D. L.; Paulk, J.; Brien, G. L.; Sonnett, M.; Seo, H. S.; Dastjerdi, S.; Wühr, M.; Dhe-Paganon, S.; Armstrong, S. A.; et al. Degradation of the BAF Complex Factor BRD9 by Heterobifunctional Ligands. *Angew. Chemie - Int. Ed.* **2017**, *56* (21), 5738–5743.
(184) Schiedel, M.; Herp, D.; Hammelmann, S.; Swyter, S.; Lehotzky, A.; Robaa, D.; Oláh, J.; Ovádi, J.; Sippl, W.; Jung, M. Chemically Induced Degradation of Sirtuin 2 (Sirt2) by a Proteolysis Targeting Chimera (PROTAC) Based on Sirtuin Rearranging Ligands (SirReals). *J. Med. Chem.* **2018**, *61* (2), 482–491.
(185) Robb, C. M.; Contreras, J. I.; Kour, S.; Taylor, M. A.; Abid, M.; Sonawane, Y. A.; Zahid, M.; Murry, D. J.; Natarajan, A.; Rana, S. Chemically Induced Degradation of CDK9 by a Proteolysis Targeting Chimera (PROTAC). *Chem. Commun.* **2017**, *53* (54), 7577–7580.
(186) Olson, C. M.; Jiang, B.; Erb, M. A.; Liang, Y.; Doctor, Z. M.; Zhang, Z.; Zhang, T.; Kwiatkowski, N.; Boukhali, M.; Green, J. L.; et al. Pharmacological Perturbation of CDK9 Using Selective CDK9 Inhibition or Degradation. *Nat. Chem. Biol.* **2018**, *14* (2), 163–170.
(187) Huang, H. T.; Dobrovolsky, D.; Paulk, J.; Yang, G.; Weisberg, E. L.; Doctor, Z. M.; Buckley, D. L.; Cho, J. H.; Ko, E.; Jang, J.; et al. A Chemoproteomic Approach to Query the Degradable Kinome Using a Multi-Kinase Degrader. *Cell Chem. Biol.* **2018**, *25* (1), 88-99.e6.
(188) Buhimschi, A. D.; Armstrong, H. A.; Toure, M.; Jaime-Figueroa, S.; Chen, T. L.; Lehman, A. M.; Woyach, J. A.; Johnson, A. J.; Byrd, J. C.; Crews, C. M. Targeting the C481S Ibrutinib-Resistance Mutation in Bruton's Tyrosine Kinase Using PROTAC-Mediated Degradation. *Biochemistry* **2018**, *57* (26), 3564–3575.
(189) Zhang, C.; Han, X. R.; Yang, X.; Jiang, B.; Liu, J.; Xiong, Y.; Jin, J. Proteolysis Targeting Chimeras (PROTACs) of Anaplastic Lymphoma Kinase (ALK). *Eur. J. Med. Chem.* **2018**, *151*, 304–314.
(190) Yang, C. Y.; Qin, C.; Bai, L.; Wang, S. Small-Molecule PROTAC Degraders of the Bromodomain and Extra Terminal (BET) Proteins — A Review. *Drug Discov. Today Technol.* **2019**, *31*, 43–51.
(191) Asangani, I. A.; Dommeti, V. L.; Wang, X.; Malik, R.; Cieslik, M.; Yang, R.; Escara-Wilke, J.; Wilder-Romans, K.; Dhanireddy, S.; Engelke, C.; et al. Therapeutic Targeting of BET Bromodomain Proteins in Castration-Resistant Prostate Cancer.

Nature **2014**, *510* (7504), 278–282.
(192) French, C. A. NUT Midline Carcinoma. *Cancer Genet. Cytogenet.* **2010**, *203* (1), 16–20.
(193) Filippakopoulos, P.; Qi, J.; Picaud, S.; Shen, Y.; Smith, W. B.; Fedorov, O.; Morse, E. M.; Keates, T.; Hickman, T. T.; Felletar, I.; et al. Selective Inhibition of BET Bromodomains. *Nature* **2010**, *468* (7327), 1067–1073.
(194) Ran, X.; Zhao, Y.; Liu, L.; Bai, L.; Yang, C. Y.; Zhou, B.; Meagher, J. L.; Chinnaswamy, K.; Stuckey, J. A.; Wang, S. Structure-Based Design of γ-Carboline Analogues as Potent and Specific BET Bromodomain Inhibitors. *J. Med. Chem.* **2015**, *58* (12), 4927–4939.
(195) Troup, R. I.; Fallan, C.; Baud, M. G. J. Current Strategies for the Design of PROTAC Linkers: A Critical Review. *Explor. Target. Anti-tumor Ther.* **2020**, *1* (5), 273–312.
(196) Cyrus, K.; Wehenkel, M.; Choi, E. Y.; Han, H. J.; Lee, H.; Swanson, H.; Kim, K. B. Impact of Linker Length on the Activity of PROTACs. *Mol. Biosyst.* **2011**, *7* (2), 359–364.
(197) Han, X.; Zhao, L.; Xiang, W.; Qin, C.; Miao, B.; Xu, T.; Wang, M.; Yang, C. Y.; Chinnaswamy, K.; Stuckey, J.; et al. Discovery of Highly Potent and Efficient PROTAC Degraders of Androgen Receptor (AR) by Employing Weak Binding Affinity VHL E3 Ligase Ligands. *J. Med. Chem.* **2019**, *62* (24), 11218–11231.
(198) Qin, C.; Hu, Y.; Zhou, B.; Fernandez-Salas, E.; Yang, C. Y.; Liu, L.; McEachern, D.; Przybranowski, S.; Wang, M.; Stuckey, J.; et al. Discovery of QCA570 as an Exceptionally Potent and Efficacious Proteolysis Targeting Chimera (PROTAC) Degrader of the Bromodomain and Extra-Terminal (BET) Proteins Capable of Inducing Complete and Durable Tumor Regression. *J. Med. Chem.* **2018**, *61* (15), 6685–6704.
(199) Han, X.; Wang, C.; Qin, C.; Xiang, W.; Fernandez-Salas, E.; Yang, C. Y.; Wang, M.; Zhao, L.; Xu, T.; Chinnaswamy, K.; et al. Discovery of ARD-69 as a Highly Potent Proteolysis Targeting Chimera (PROTAC) Degrader of Androgen Receptor (AR) for the Treatment of Prostate Cancer. *J. Med. Chem.* **2019**, *62* (2), 941–964.
(200) Xia, L. W.; Ba, M. Y.; Liu, W.; Cheng, W.; Hu, C. P.; Zhao, Q.; Yao, Y. F.; Sun, M. R.; Duan, Y. T. Triazol: A Privileged Scaffold for Proteolysis Targeting Chimeras. *Future Med. Chem.* **2019**, *11* (22), 2919–2973.
(201) Mullard, A. Targeted Protein Degraders Crowd into the Clinic. *Nat. Rev. Drug Discov.* **2021**, *20* (4), 247–250.
(202) Mullard, A. First Targeted Protein Degrader Hits the Clinic. *Nat. Rev. Drug Discov.* **2019**, *18* (4), 237–239.
(203) Duan, Y.; Guan, Y.; Qin, W.; Zhai, X.; Yu, B.; Liu, H. Targeting Brd4 for Cancer Therapy: Inhibitors and Degraders. *Medchemcomm* **2018**, *9* (11), 1779–1802.
(204) Liu, K.; Zhang, S. Design and Characterization of 3-Azidothalidomide as a Selective Hydrogen Sulfide Probe. *Tetrahedron Lett.* **2014**, *55* (40), 5566–5569.
(205) Luzi, N. AN ENZYMOLOGY AND INHIBITION STUDY OF A CAMP-DEPENDENT PROTEIN KINASE LINKED TO ACTH-INDEPENDENT CUSHING'S SYNDROME, Virginia Commonwealth University, 2018.
(206) Smith, R. L.; Lee, T. jyh; Gould, N. P.; Cragoe, E. J.; Oien, H. G.; Kuehl, F. A. Prostaglandin Isosteres. 1. (8-Aza-, 8,10-Diaza-, and 8-Aza-11-Thia)-9-Oxoprostanoic Acids and Their Derivatives. *J. Med. Chem.* **1977**, *20* (10), 1292–

1299.
(207) Kutty, S. K.; Lutz, J. A.; Felder, S.; Hahn, P.; Taylor, C. M. Thioether Macrocycles of the Microbisporicins via Reductive Desulfurization. *Tetrahedron* **2018**, *74* (31), 4247–4258.
(208) Vutukuri, D. R.; Bharathi, P.; Yu, Z.; Rajasekaran, K.; Tran, M. H.; Thayumanavan, S. A Mild Deprotection Strategy for Allyl-Protecting Groups and Its Implications in Sequence Specific Dendrimer Synthesis. *J. Org. Chem.* **2003**, *68* (3), 1146–1149.
(209) Speckmeier, E.; Zeitler, K. Desyl and Phenacyl as Versatile, Photocatalytically Cleavable Protecting Groups: A Classic Approach in a Different (Visible) Light. *ACS Catal.* **2017**, *7* (10), 6821–6826.
(210) Han, G.; Tamaki, M.; Hruby, V. J. Fast, Efficient and Selective Deprotection of the Tert-Butoxycarbonyl (Boc) Group Using HCL/Dioxane (4 M). *J. Pept. Res.* **2001**, *58* (4), 338–341.
(211) Zhou, B.; Hu, J.; Xu, F.; Chen, Z.; Bai, L.; Fernandez-Salas, E.; Lin, M.; Liu, L.; Yang, C. Y.; Zhao, Y.; et al. Discovery of a Small-Molecule Degrader of Bromodomain and Extra-Terminal (BET) Proteins with Picomolar Cellular Potencies and Capable of Achieving Tumor Regression. *J. Med. Chem.* **2018**, *61* (2), 462–481.
(212) Grant, J.; Modica, J. A.; Roll, J.; Perkovich, P.; Mrksich, M. An Immobilized Enzyme Reactor for Spatiotemporal Control over Reaction Products. *Small* **2018**, *14* (31), 1–11.
(213) Yang, X.; Dai, C.; Dayan Calderon Molina, A.; Wang, B. Boronic Acid-Modified DNA That Changes Fluorescent Properties upon Carbohydrate Binding. *Chem. Commun.* **2010**, *46* (7), 1073–1075.
(214) Gillespie, R. J.; Bamford, S. J.; Botting, R.; Comer, M.; Denny, S.; Gaur, S.; Griffin, M.; Jordan, A. M.; Knight, A. R.; Lerpiniere, J.; et al. Antagonists of the Human A2A Adenosine Receptor. 4. Design, Synthesis, and Preclinical Evaluation of 7-Aryltriazolo[4,5-d]Pyrimidines. *J. Med. Chem.* **2009**, *52* (1), 33–47.
(215) Bernardes, G. J. L.; Casi, G.; Trüssel, S.; Hartmann, I.; Schwager, K.; Scheuermann, J.; Neri, D. A Traceless Vascular-Targeting Antibody-Drug Conjugate for Cancer Therapy. *Angew. Chemie - Int. Ed.* **2012**, *51* (4), 941–944.
(216) Wu, Y.; Hai, L.; Guan, M.; Zhao, Y.; Yue, Q.; Fu, Q.; Yang, Y. Targeted Magnetic Nanoparticles for Treating Central Nervous System Diseases, 2018.
(217) Sheppeck, J. E.; Kar, H.; Hong, H. A Convenient and Scaleable Procedure for Removing the Fmoc Group in Solution. *Tetrahedron Lett.* **2000**, *41* (28), 5329–5333.
(218) Armstrong, Louis A.; Williams, J. R. Polymeric De-Blocking Agents for the Fluoren-9 -Ylmethoxycarbonyl (FMOC) Amino-Protecting Group. *J. Chem. Soc. Chem. Commun.* **1978**, 450–451.
(219) Tateno, S.; Iida, M.; Fujii, S.; Suwa, T.; Katayama, M.; Tokuyama, H.; Yamamoto, J.; Ito, T.; Sakamoto, S.; Handa, H.; et al. Genome-Wide Screening Reveals a Role for Subcellular Localization of CRBN in the Anti-Myeloma Activity of Pomalidomide. *Sci. Rep.* **2020**, *10* (1), 1–11.

Appendix 1

Docking and scoring against CtBP1 data tables

	AutoDock		**AutoDock**	
	Rigid		**Rigid**	
	AM1BCC		**AM1BCC**	
	HSP315		**HSD315**	
Ranking	**Compound**	**Score**	**Compound**	**Score**
1	Pyridazine-3-(C3HIA)	-8.5	Pyridazine-3-(C3HIA)	-8
2	HIPP	-8.3	Pyridine-2-(C3HIA)	-7.9
3	Pyridine-2-(C3HIA)	-8.2	Indole-2-(C2HIA)	-7.8
4	Pyrrole-2-(C3HIA)	-8.1	HIPP	-7.7
5	Naphthalene-2-(C3HIA)	-8	Furan-2-(C3HIA)	-7.7
6	Quinoline-2-(C3HIA)	-8	Pyrimidine-4-(C3HIA)	-7.6
7	Pyrazole-3-(C3HIA)	-7.9	Isoxazole-5-(C3HIA)	-7.6
8	Pyrimidine-4-(C3HIA)	-7.9	Naphthalene-2-(C2HIA)	-7.6
9	Furan-2-(C3HIA)	-7.8	Benzofuran-2-(C2HIA)	-7.6
10	Triazine-2-(C3HIA)	-7.8	Quinoline-2-(C3HIA)	-7.5
11	Imidazole-4-(C3HIA)	-7.7	Isoquinoline-3-(C2HIA)	-7.5
12	Indole-2-(C3HIA)	-7.7	Pyrrole-2-(C3HIA)	-7.4
13	Isoxazole-5-(C3HIA)	-7.7	Naphthalene-2-(C3HIA)	-7.4
14	Pyrazine-2-(C3HIA)	-7.7	Pyrazine-2-(C3HIA)	-7.4
15	Triazole-4-(C3HIA)	-7.7	Benzimidazole-2-(C2HIA)	-7.4
16	Quinazoline-2-(C3HIA)	-7.6	Triazine-2-(C3HIA)	-7.3
17	Naphthyridine-2-(C3HIA)	-7.4	Triazole-4-(C3HIA)	-7.3
18	Benzofuran-2-(C3HIA)	-7.2	Quinoxaline-2-(C2HIA)	-7.3
19	Quinoxaline-2-(C3HIA)	-7.2	Pyrazole-3-(C3HIA)	-7.2
20	Benzimidazole-2-(C2HIA)	-7.1	Isoindole-1-(C2HIA)	-7.2
21	Isoquinoline-3-(C3HIA)	-7.1	Quinazoline-2-(C2HIA)	-7.2
22	Naphthalene-2-(C2HIA)	-7.1	Oxazole-5-(C3HIA)	-7.2
23	Indole-2-(C2HIA)	-7	Imidazole-4-(C3HIA)	-7.1
24	Isoquinoline-3-(C2HIA)	-7	Quinazoline-2-(C3HIA)	-7
25	Indazole-3-(C3HIA)	-6.9	Indazole-3-(C2HIA)	-7
26	Quinoline-2-(C2HIA)	-6.9	Isoquinoline-3-(C3HIA)	-6.9
27	Isoindole-1-(C3HIA)	-6.8	Indole-2-(C3HIA)	-6.8
28	Benzofuran-2-(C2HIA)	-6.7	Naphthyridine-2-(C3HIA)	-6.8
29	Indolizine-2-(C2HIA)	-6.6	Indolizine-2-(C2HIA)	-6.8
30	Indolizine-2-(C3HIA)	-6.6	Naphthyridine-2-(C2HIA)	-6.8
31	Naphthyridine-2-(C2HIA)	-6.6	Benzofuran-2-(C3HIA)	-6.7
32	Quinoxaline-2-(C2HIA)	-6.6	Quinoxaline-2-(C3HIA)	-6.7
33	Isoindole-1-(C2HIA)	-6.5	Quinoline-2-(C2HIA)	-6.7
34	Quinazoline-2-(C2HIA)	-6.5	Indazole-3-(C3HIA)	-6.6

35	Benzimidazole-2-(C3HIA)	-6.1	Isoindole-1-(C3HIA)	-6.4
36	Indazole-3-(C2HIA)	-6	Benzimidazole-2-(C3HIA)	-6.4
37	MTOB	-6	Indolizine-2-(C3HIA)	-6.3
38	Oxazole-5-(C3HIA)	-5.7	MTOB	-5.9

	AutoDock		**AutoDock**	
	Flexible		**Flexible**	
	AM1BCC		**CHELPG**	
	HSD315		**HSD315**	
Ranking	**Compound**	**Score**	**Compound**	**Score**
1	Quinoline-2-(C3HIA)	-9.2	Naphthalene-2-(C3HIA)	-9.4
2	Naphthalene-2-(C3HIA)	-9.2	Quinoline-2-(C3HIA)	-9.2
3	Naphthyridine-2-(C3HIA)	-9.2	Naphthyridine-2-(C3HIA)	-9.2
4	Isoindole-1-(C3HIA)	-8.8	Isoindole-1-(C3HIA)	-8.8
5	Quinazoline-2-(C3HIA)	-8.7	HIPP	-8.7
6	Pyridine-2-(C3HIA)	-8.6	Quinazoline-2-(C3HIA)	-8.7
7	HIPP	-8.6	Pyridine-2-(C3HIA)	-8.6
8	Isoquinoline-3-(C3HIA)	-8.6	Indole-2-(C3HIA)	-8.6
9	Indole-2-(C3HIA)	-8.6	Isoquinoline-3-(C3HIA)	-8.6
10	Indazole-3-(C3HIA)	-8.6	Indazole-3-(C3HIA)	-8.6
11	Pyridazine-3-(C3HIA)	-8.5	Pyridazine-3-(C3HIA)	-8.5
12	Naphthalene-2-(C2HIA)	-8.5	Naphthalene-2-(C2HIA)	-8.5
13	Isoquinoline-3-(C2HIA)	-8.5	Isoquinoline-3-(C2HIA)	-8.5
14	Benzofuran-2-(C3HIA)	-8.5	Quinoxaline-2-(C3HIA)	-8.5
15	Quinoxaline-2-(C3HIA)	-8.4	Benzofuran-2-(C3HIA)	-8.4
16	Benzimidazole-2-(C3HIA)	-8.4	Benzimidazole-2-(C3HIA)	-8.4
17	Pyrrole-2-(C3HIA)	-8.3	Pyrrole-2-(C3HIA)	-8.3
18	Indole-2-(C2HIA)	-8.1	Indole-2-(C2HIA)	-8.2
19	Furan-2-(C3HIA)	-8.1	Furan-2-(C3HIA)	-8.1
20	Pyrimidine-4-(C3HIA)	-8.1	Pyrimidine-4-(C3HIA)	-8.1
21	Isoxazole-5-(C3HIA)	-8.1	Isoxazole-5-(C3HIA)	-8.1
22	Pyrazole-3-(C3HIA)	-8.1	Pyrazole-3-(C3HIA)	-8.1
23	Indolizine-2-(C3HIA)	-8.1	Indolizine-2-(C3HIA)	-8.1
24	Triazine-2-(C3HIA)	-8	Triazine-2-(C3HIA)	-8
25	Triazole-4-(C3HIA)	-8	Triazole-4-(C3HIA)	-8
26	Benzofuran-2-(C2HIA)	-7.9	Benzofuran-2-(C2HIA)	-8
27	Pyrazine-2-(C3HIA)	-7.9	Pyrazine-2-(C3HIA)	-7.9
28	Quinazoline-2-(C2HIA)	-7.9	Imidazole-4-(C3HIA)	-7.9
29	Imidazole-4-(C3HIA)	-7.9	Quinazoline-2-(C2HIA)	-7.9
30	Quinoline-2-(C2HIA)	-7.9	Quinoline-2-(C2HIA)	-7.9
31	Benzimidazole-2-(C2HIA)	-7.8	Isoindole-1-(C2HIA)	-7.9
32	Quinoxaline-2-(C2HIA)	-7.8	Benzimidazole-2-(C2HIA)	-7.8
33	Isoindole-1-(C2HIA)	-7.8	Quinoxaline-2-(C2HIA)	-7.8

34	Oxazole-5-(C3HIA)	-7.8	Oxazole-5-(C3HIA)	-7.8
35	Naphthyridine-2-(C2HIA)	-7.7	Naphthyridine-2-(C2HIA)	-7.7
36	Indazole-3-(C2HIA)	-7.6	Indolizine-2-(C2HIA)	-7.6
37	Indolizine-2-(C2HIA)	-7.6	Indazole-3-(C2HIA)	-7.6
38	MTOB	-6	MTOB	-6

	Gold		**Gold**	
	Rigid		**Rigid**	
	AM1BCC		**AM1BCC**	
	HSD315		**HSE315**	
Ranking	**Compound**	**Score**	**Compound**	**Score**
1	Indolizine-2-(C3HIA)	79.33	Indolizine-2-(C3HIA)	81.2
2	Naphthalene-2-(C3HIA)	78.75	Naphthalene-2-(C3HIA)	80.93
3	Isoquinoline-3-(C3HIA)	77.32	Isoquinoline-3-(C3HIA)	80.07
4	Quinazoline-2-(C3HIA)	76.73	Quinoline-2-(C3HIA)	79.03
5	Quinoline-2-(C3HIA)	76.34	Quinazoline-2-(C3HIA)	78.77
6	Benzofuran-2-(C3HIA)	75.2	Isoindole-1-(C3HIA)	78.12
7	Isoindole-1-(C3HIA)	75.19	Benzofuran-2-(C3HIA)	77.55
8	Naphthyridine-2-(C3HIA)	74.96	Indole-2-(C3HIA)	77.28
9	Indole-2-(C3HIA)	74.9	Quinoxaline-2-(C3HIA)	75.57
10	Quinoxaline-2-(C3HIA)	73.08	Naphthyridine-2-(C3HIA)	75.56
11	Benzimidazole-2-(C3HIA)	72.07	Benzimidazole-2-(C3HIA)	74.83
12	Indazole-3-(C3HIA)	71.49	Indazole-3-(C3HIA)	71.25
13	Indolizine-2-(C2HIA)	65	Pyridine-2-(C3HIA)	66.59
14	Pyridine-2-(C3HIA)	63.9	Pyrrole-2-(C3HIA)	65.75
15	HIPP	63.45	HIPP	65.62
16	Pyrimidine-4-(C3HIA)	62.78	Furan-2-(C3HIA)	65.19
17	Pyrazine-2-(C3HIA)	61.18	Pyrimidine-4-(C3HIA)	65
18	Pyrrole-2-(C3HIA)	60.56	Indolizine-2-(C2HIA)	64.63
19	Furan-2-(C3HIA)	60.09	Indole-2-(C2HIA)	63.52
20	Pyridazine-3-(C3HIA)	60.07	Pyridazine-3-(C3HIA)	63.31
21	Benzofuran-2-(C2HIA)	59.78	Pyrazine-2-(C3HIA)	63.14
22	Indole-2-(C2HIA)	59.34	Benzofuran-2-(C2HIA)	62.11
23	Quinoline-2-(C2HIA)	59.02	Indazole-3-(C2HIA)	61.07
24	Isoquinoline-3-(C2HIA)	58.78	Imidazole-4-(C3HIA)	60.94
25	Triazine-2-(C3HIA)	58.39	Oxazole-5-(C3HIA)	60.81
26	Naphthalene-2-(C2HIA)	58.33	Triazine-2-(C3HIA)	60.78
27	Isoxazole-5-(C3HIA)	57.96	Benzimidazole-2-(C2HIA)	60.78
28	Quinazoline-2-(C2HIA)	57.62	Pyrazole-3-(C3HIA)	59.98
29	Indazole-3-(C2HIA)	57.6	Isoxazole-5-(C3HIA)	59.77
30	Benzimidazole-2-(C2HIA)	57.33	Isoquinoline-3-(C2HIA)	59.3
31	Oxazole-5-(C3HIA)	57.32	Quinoline-2-(C2HIA)	59.22

32	Naphthyridine-2-(C2HIA)	57.3	Naphthalene-2-(C2HIA)	58.67
33	Imidazole-4-(C3HIA)	57.2	Quinazoline-2-(C2HIA)	57.79
34	Quinoxaline-2-(C2HIA)	55.56	Quinoxaline-2-(C2HIA)	57.05
35	Pyrazole-3-(C3HIA)	54.71	Triazole-4-(C3HIA)	56.26
36	Triazole-4-(C3HIA)	52.35	Naphthyridine-2-(C2HIA)	55.99
37	Isoindole-1-(C2HIA)	51.05	Isoindole-1-(C2HIA)	55.3
38	MTOB	50.63	MTOB	55.06

	Gold		**Gold**	
	Flexible		**Flexible**	
	AM1BCC		**AM1BCC**	
	HSD315		**HSE315**	
Ranking	**Compound**	**Score**	**Compound**	**Score**
1	Naphthalene-2-(C3HIA)	70.08	Indolizine-2-(C3HIA)	73.28
2	Indolizine-2-(C3HIA)	67.99	Naphthalene-2-(C3HIA)	68.91
3	Indole-2-(C3HIA)	67.91	Isoquinoline-3-(C3HIA)	67
4	Isoquinoline-3-(C3HIA)	66.44	Quinoline-2-(C3HIA)	66.74
5	Quinoline-2-(C3HIA)	66.42	Quinazoline-2-(C3HIA)	66.49
6	Benzofuran-2-(C3HIA)	65.27	Naphthalene-2-(C2HIA)	65.57
7	Naphthalene-2-(C2HIA)	64.79	Quinoline-2-(C2HIA)	62.72
8	Isoquinoline-3-(C2HIA)	64.7	Indolizine-2-(C2HIA)	61.73
9	Indolizine-2-(C2HIA)	64.13	Quinoxaline-2-(C3HIA)	61.05
10	Quinoxaline-2-(C3HIA)	61.22	Indole-2-(C3HIA)	58.78
11	Indole-2-(C2HIA)	61.07	Quinazoline-2-(C2HIA)	58.63
12	Benzimidazole-2-(C3HIA)	60.85	Naphthyridine-2-(C3HIA)	57.49
13	Indazole-3-(C3HIA)	59.83	Benzimidazole-2-(C3HIA)	57.38
14	Quinazoline-2-(C3HIA)	59.21	Isoquinoline-3-(C2HIA)	56.99
15	HIPP	59.01	Benzimidazole-2-(C2HIA)	56.97
16	Benzofuran-2-(C2HIA)	56.86	Naphthyridine-2-(C2HIA)	56.73
17	Quinazoline-2-(C2HIA)	56.65	Quinoxaline-2-(C2HIA)	55.91
18	Naphthyridine-2-(C3HIA)	56.05	HIPP	55.39
19	Quinoline-2-(C2HIA)	55.98	Isoindole-1-(C3HIA)	55.07
20	Isoindole-1-(C2HIA)	55.7	Benzofuran-2-(C2HIA)	55.04
21	Isoindole-1-(C3HIA)	55.39	Indazole-3-(C3HIA)	55.02
22	Naphthyridine-2-(C2HIA)	55.15	Indole-2-(C2HIA)	54.46
23	Benzimidazole-2-(C2HIA)	54.58	Pyridine-2-(C3HIA)	54.02
24	Pyridazine-3-(C3HIA)	51.34	Benzofuran-2-(C3HIA)	53.21
25	Quinoxaline-2-(C2HIA)	50.32	Pyrrole-2-(C3HIA)	52.39
26	Imidazole-4-(C3HIA)	50.04	Indazole-3-(C2HIA)	52.02
27	Pyrrole-2-(C3HIA)	48.55	Furan-2-(C3HIA)	49.19

28	Indazole-3-(C2HIA)	47.83	Pyrazine-2-(C3HIA)	48.54
29	Pyrazine-2-(C3HIA)	47.11	Pyridazine-3-(C3HIA)	48.17
30	Triazine-2-(C3HIA)	46.07	Imidazole-4-(C3HIA)	47.61
31	Furan-2-(C3HIA)	45.92	Pyrimidine-4-(C3HIA)	46.77
32	Pyridine-2-(C3HIA)	45.82	Isoxazole-5-(C3HIA)	46
33	Pyrimidine-4-(C3HIA)	45.45	Oxazole-5-(C3HIA)	45.43
34	Isoxazole-5-(C3HIA)	45.42	Isoindole-1-(C2HIA)	44.27
35	Oxazole-5-(C3HIA)	42.22	Triazine-2-(C3HIA)	43.82
36	Pyrazole-3-(C3HIA)	42.07	Pyrazole-3-(C3HIA)	42.61
37	Triazole-4-(C3HIA)	41.97	MTOB	40.54
38	MTOB	36.73	Triazole-4-(C3HIA)	38.22

	HINT		**HINT**	
	Rigid		**Rigid**	
	AM1BCC		**AM1BCC**	
	HSD315		**HSE315**	
Ranking	**Compound**	**Score**	**Compound**	**Score**
1	HIPP	1875.669	HIPP	1972.712
2	Quinoline-2-(C3HIA)	1714.676	Quinoline-2-(C3HIA)	1650.191
3	Naphthalene-2-(C3HIA)	1415.396	Naphthalene-2-(C3HIA)	1541.538
4	Quinoxaline-2-(C3HIA)	1368.304	Quinoxaline-2-(C3HIA)	1540.226
5	Indolizine-2-(C3HIA)	1339.607	Indolizine-2-(C3HIA)	1439.738
6	Quinazoline-2-(C3HIA)	1292.323	Quinazoline-2-(C3HIA)	1398.002
7	Isoquinoline-3-(C3HIA)	1285.102	Isoquinoline-3-(C3HIA)	1348.295
8	Indole-2-(C3HIA)	1245.631	Indole-2-(C3HIA)	1272.356
9	Benzimidazole-2-(C3HIA)	1072.769	Benzimidazole-2-(C3HIA)	1070.315

	HINT		**HINT**	
	Flexible		**Flexible**	
	AM1BCC		**AM1BCC**	
	HSD315		**HSE315**	
Ranking	**Compound**	**Score**	**Compound**	**Score**
1	Quinoline-2-(C3HIA)	1143.933	Indolizine-2-(C3HIA)	1226.436
2	Indole-2-(C3HIA)	1129.534	Quinoline-2-(C3HIA)	1140.78
3	Naphthalene-2-(C3HIA)	1099.549	Indole-2-(C3HIA)	1128.223
4	Quinoxaline-2-(C3HIA)	990.4216	Naphthalene-2-(C3HIA)	1104.693

5	Isoquinoline-3-(C3HIA)	857.0989	HIPP	926.1904
6	Benzimidazole-2-(C3HIA)	743.6815	Quinoxaline-2-(C3HIA)	893.2845
7	HIPP	420.5435	Quinazoline-2-(C3HIA)	852.1588
8	Quinazoline-2-(C3HIA)	40.13692	Benzimidazole-2-(C3HIA)	825.6909
9	Indolizine-2-(C3HIA)	-12.2078	Isoquinoline-3-(C3HIA)	-431.305

2.1

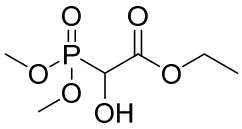

Appendix 2

Proton and Carbon NMR data for all small molecule intermediates characterized.

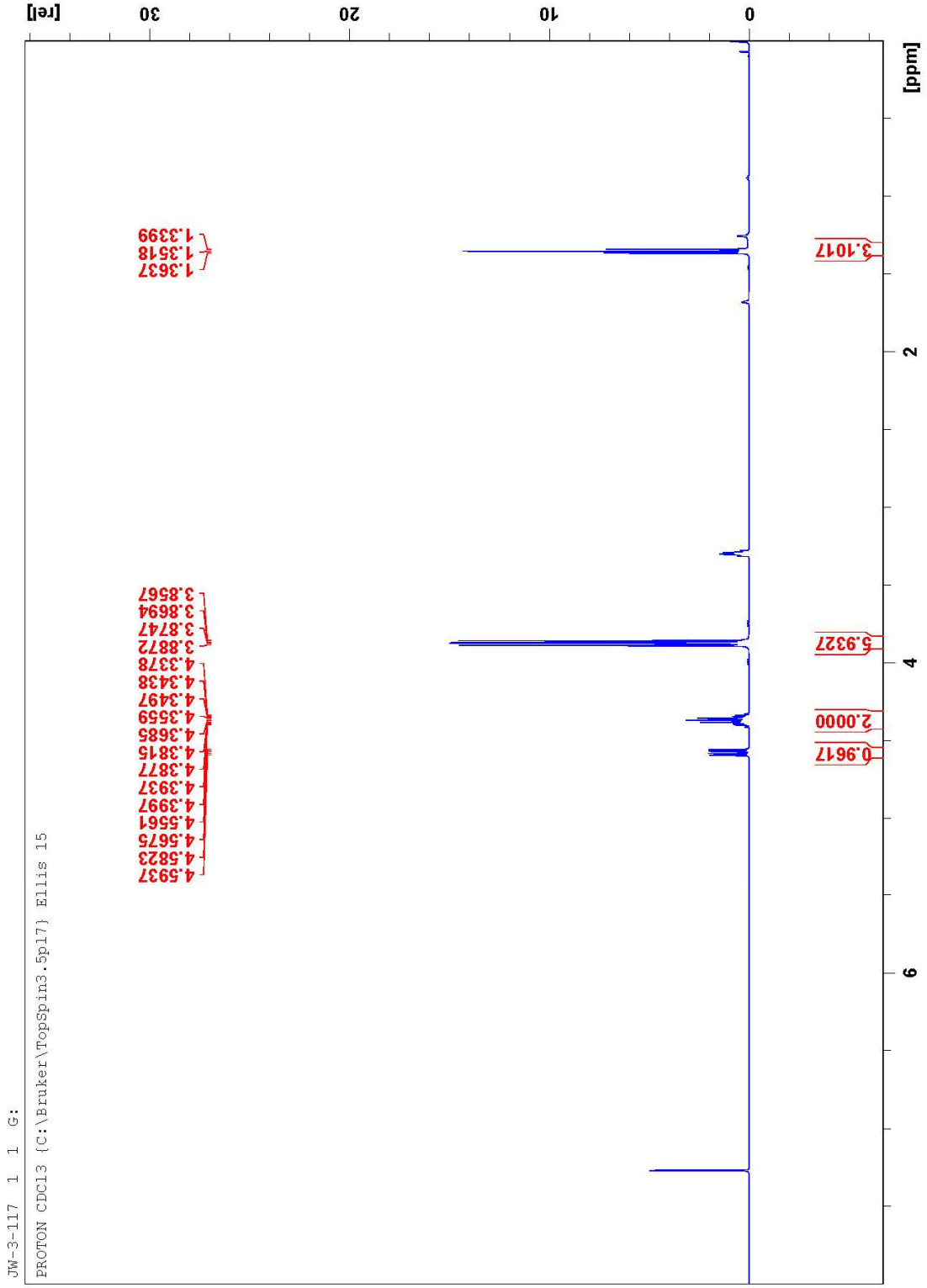

2.1

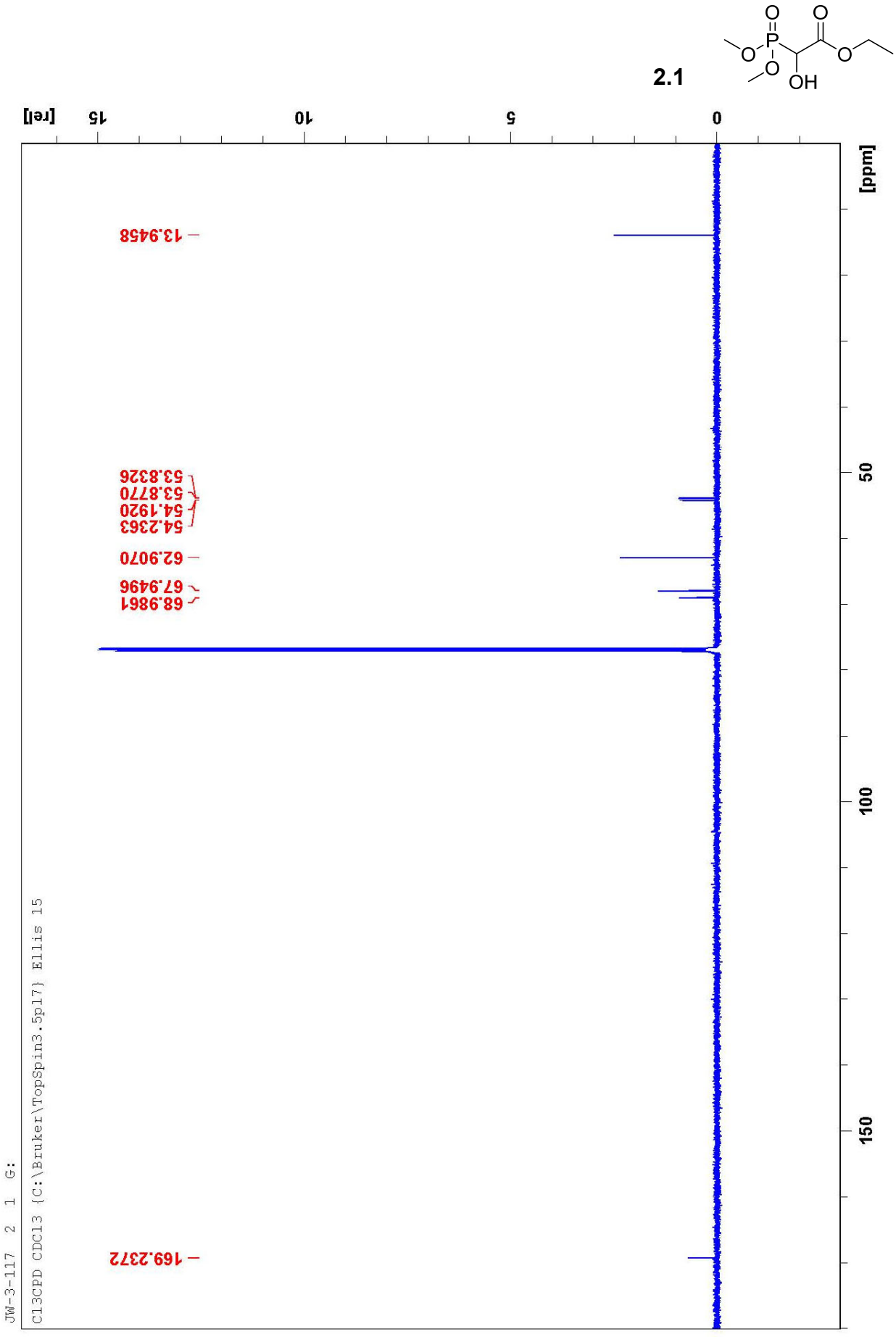
[rel]
15
10
5
0
[ppm]
50
100
150
13.9458
53.8326
53.8770
54.1920
54.2363
62.9070
67.9496
68.9861
169.2372
JW-3-117 2 1 G:
C13CPD CDCl3 {C:\Bruker\TopSpin3.5pl7} Ellis 15

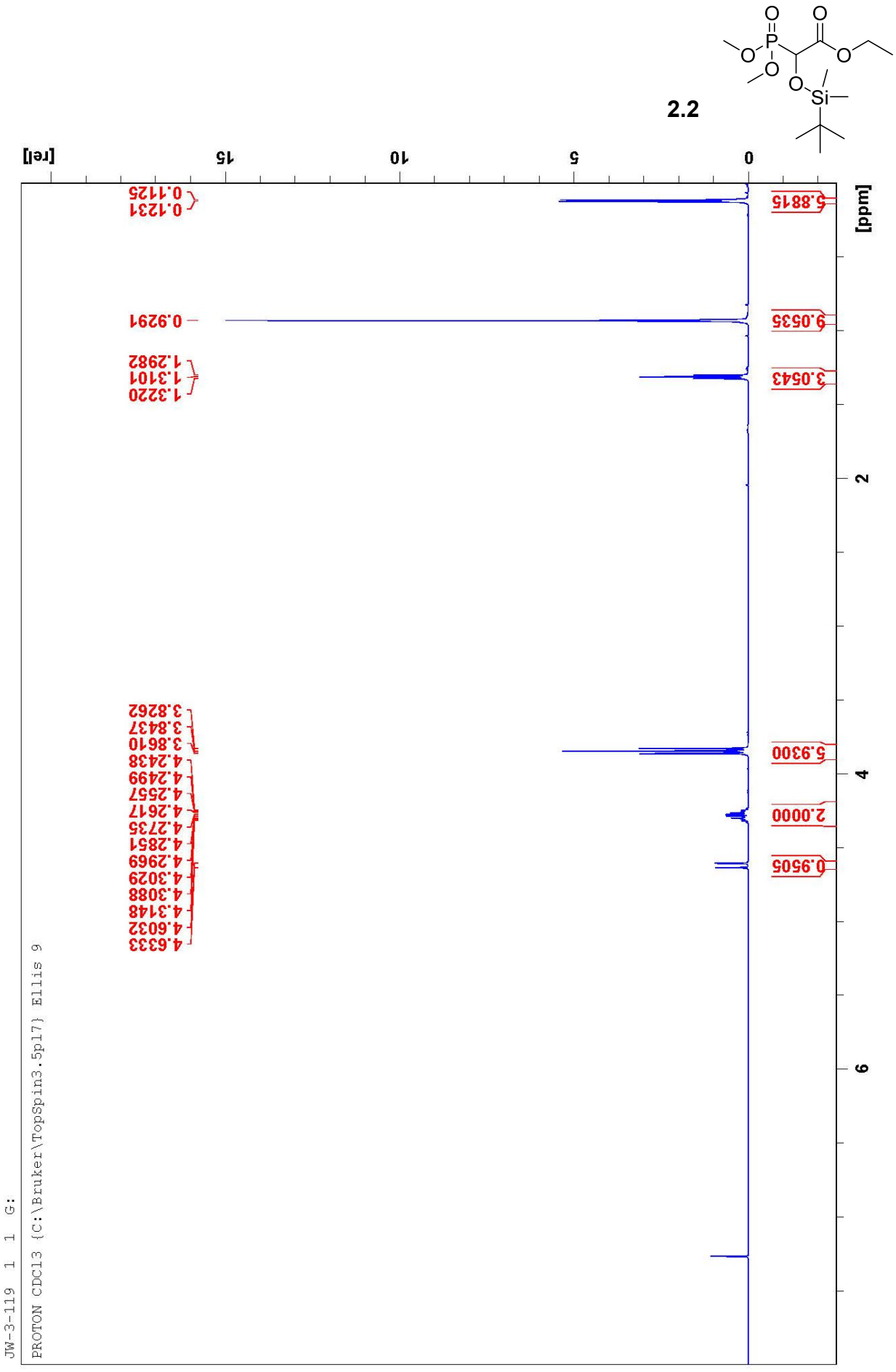
2.2
[rel]
15
10
5
0
[ppm]
6
4
2
5.8815
9.0535
3.0543
5.9300
2.0000
0.9505
4.6333
4.6032
4.3148
4.3088
4.3029
4.2969
4.2851
4.2735
4.2617
4.2557
4.2499
4.2438
3.8610
3.8437
3.8262
1.3220
1.3101
1.2982
0.9291
0.1231
0.1125
JW-3-119 1 1 G:
PROTON CDCl3 {C:\Bruker\TopSpin3.5pl7} Ellis 9

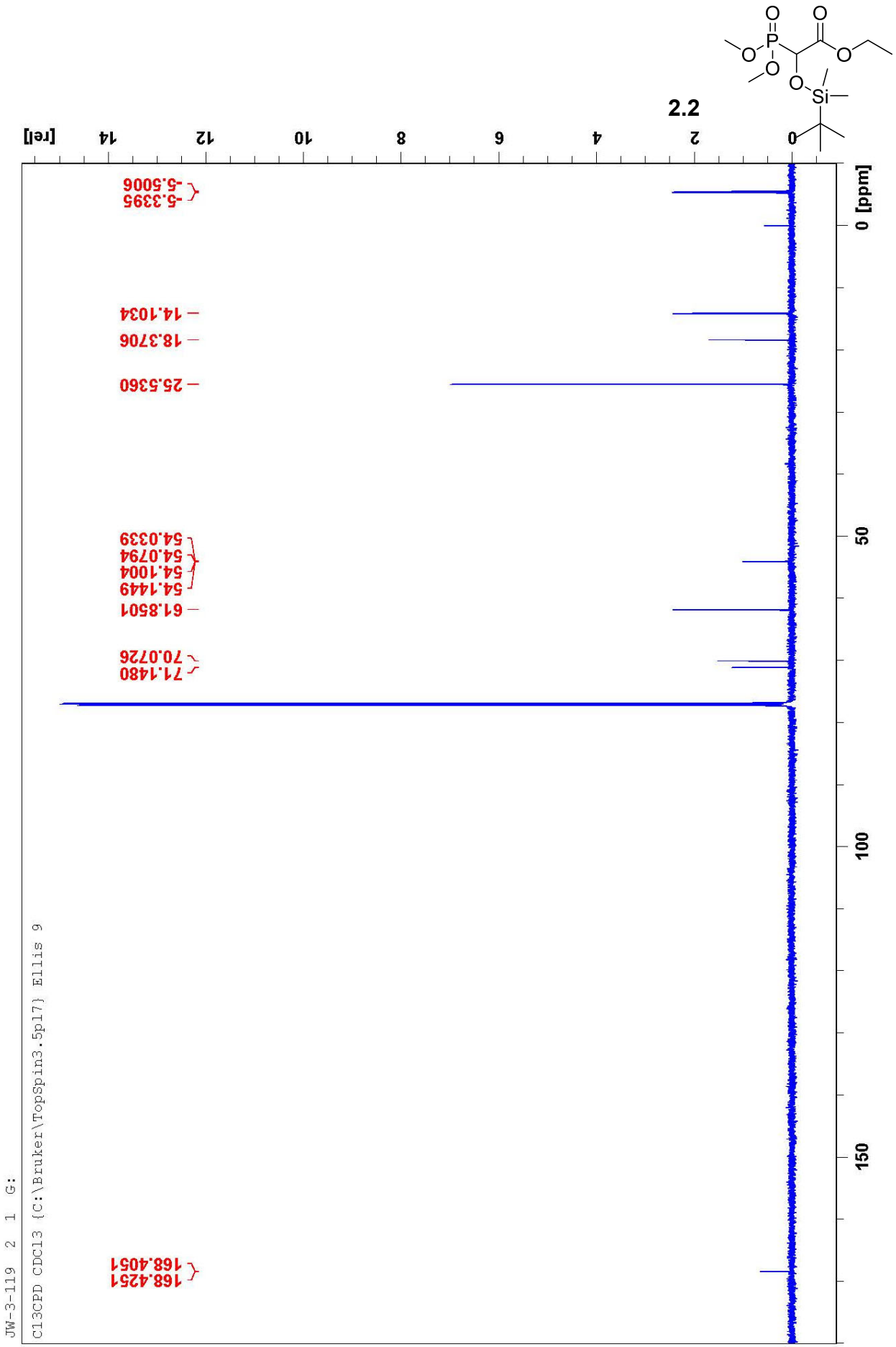
2.2
[rel]
14
12
10
8
6
4
2
0
0 [ppm]
50
100
150
-5.5006
-5.3395
14.1034
18.3706
25.5360
54.0339
54.0794
54.1004
54.1449
61.8501
70.0726
71.1480
168.4051
168.4251
JW-3-119 2 1 G:
C13CPD CDCl3 {C:\Bruker\TopSpin3.5pl7} Ellis 9

2.3

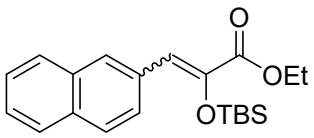
O
OEt
OTBS

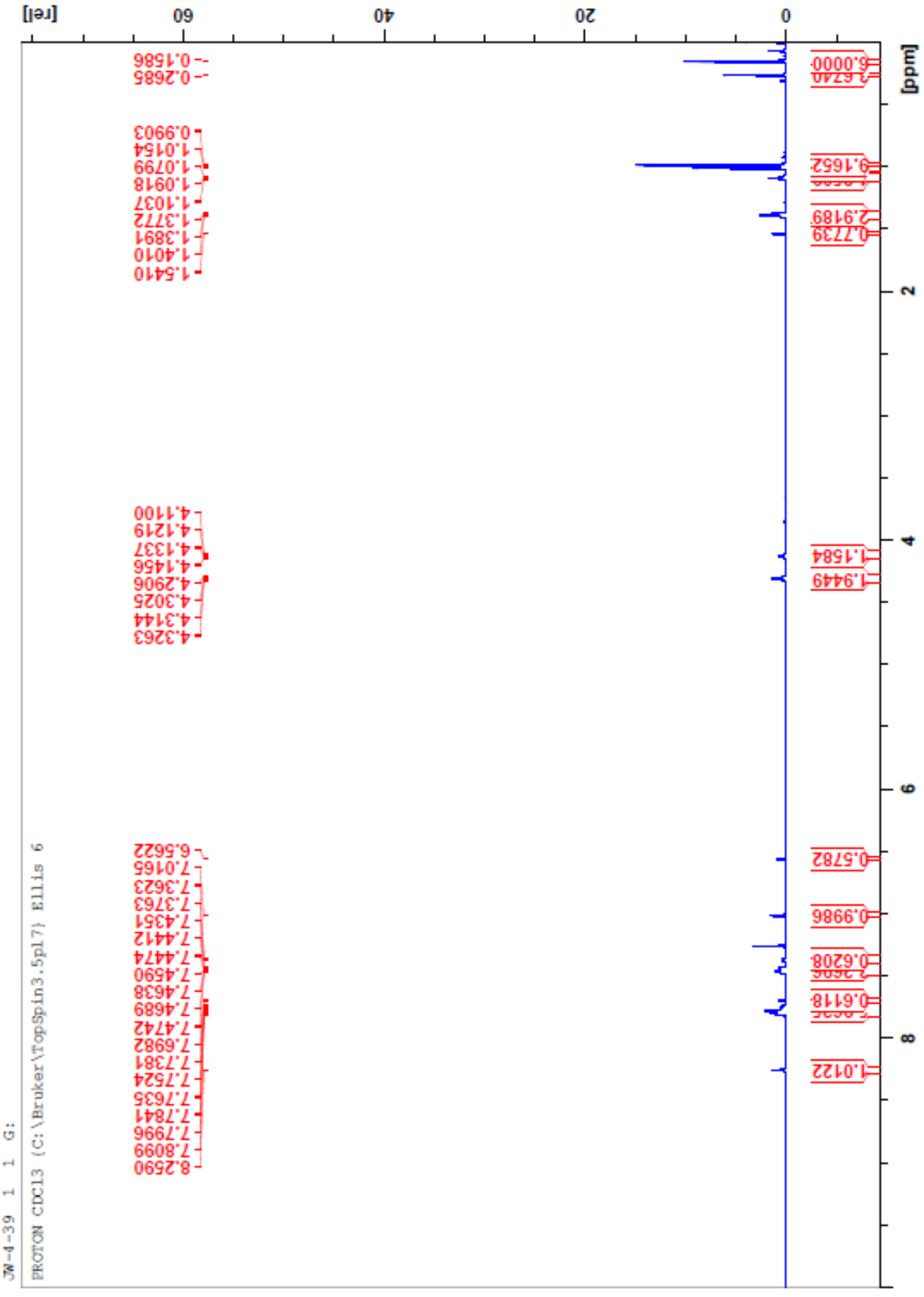
[rel]
60
40
20
0
[ppm]
2
4
6
8
0.1586
0.2685
0.9903
1.0154
1.0799
1.0918
1.1037
1.3772
1.3891
1.4010
1.5410
4.1100
4.1219
4.1337
4.1456
4.2906
4.3025
4.3144
4.3263
6.5622
7.0165
7.3623
7.3763
7.4351
7.4412
7.4474
7.4590
7.4638
7.4689
7.4742
7.6982
7.7381
7.7524
7.7635
7.7841
7.7996
7.8099
8.2590
6.0000
2.9189
0.7739
1.1584
1.9449
0.5782
0.9986
0.6208
0.6118
1.0122
JW-4-39 1 1 G:
PROTON CDCl3 (C:\Bruker\TopSpin3.5pl7) Ellis 6

2.3

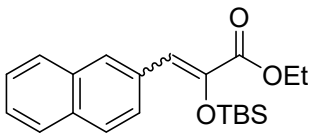
O
OEt
OTBS

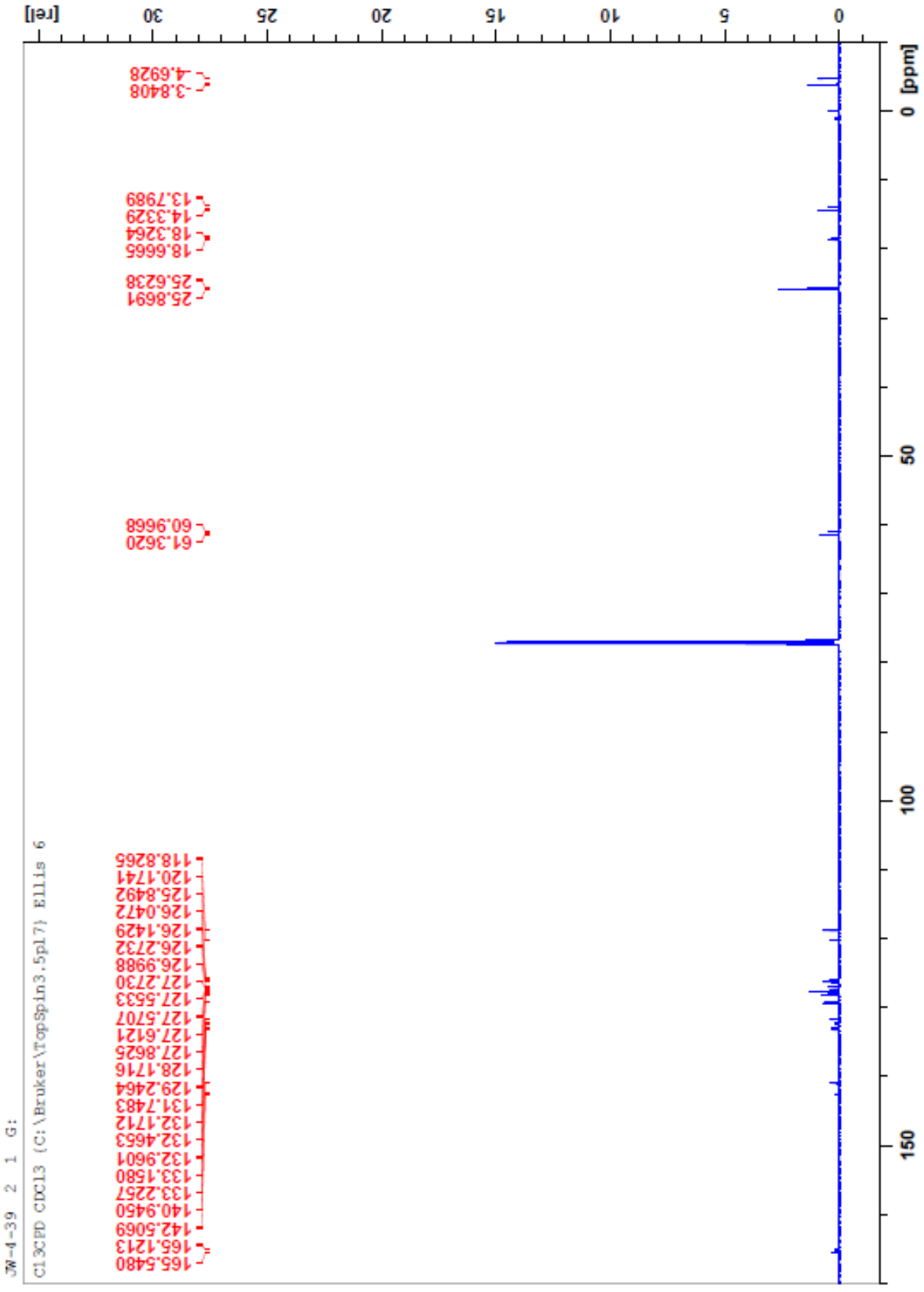
[rel]
30
25
20
15
10
5
0
[ppm]
0
50
100
150
4.6928
3.8408
13.7989
14.3329
18.3264
18.6665
25.6238
25.8691
60.9668
61.3620
118.8265
120.1741
125.8492
126.0472
126.1429
126.2732
126.9988
127.2730
127.5533
127.5707
127.6121
127.8625
128.1716
129.2464
131.7483
132.1712
132.4653
132.9601
133.1580
133.2257
140.9450
142.5069
165.1213
165.5480
C13CPD CDCl3 (C:\Bruker\TopSpin3.5pl7) Ellis 6
JW-4-39 2 1 G:

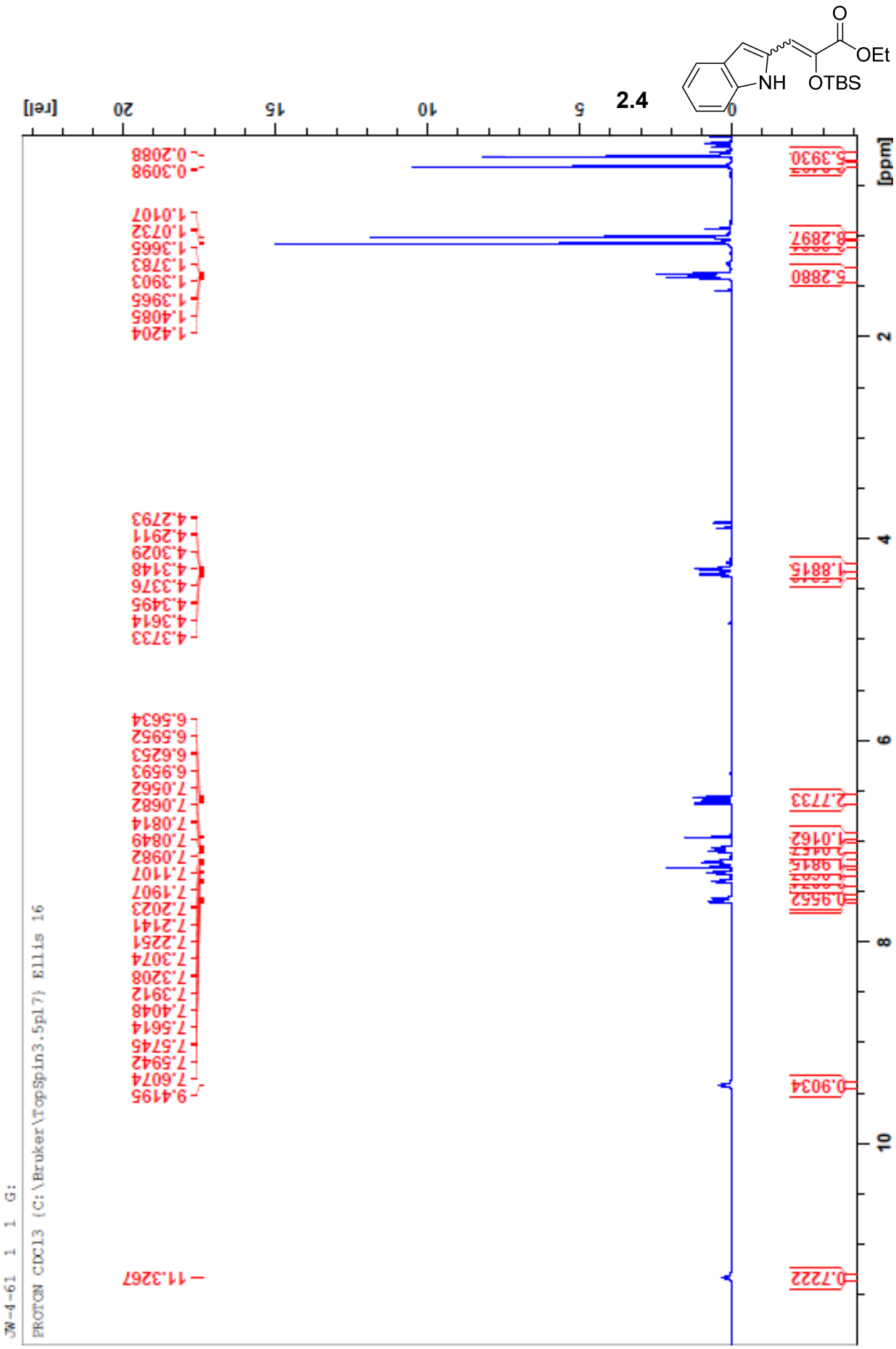
2.4
O
OEt
NH
OTBS
[rel]
20
15
10
5
0
[ppm]
2
4
6
8
10
JW-4-61 1 1 G:
PROTON CDCl3 (C:\Bruker\TopSpin3.5pl7) Ellis 16

2.4

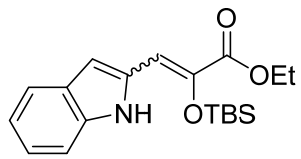
O
OEt
NH
OTBS

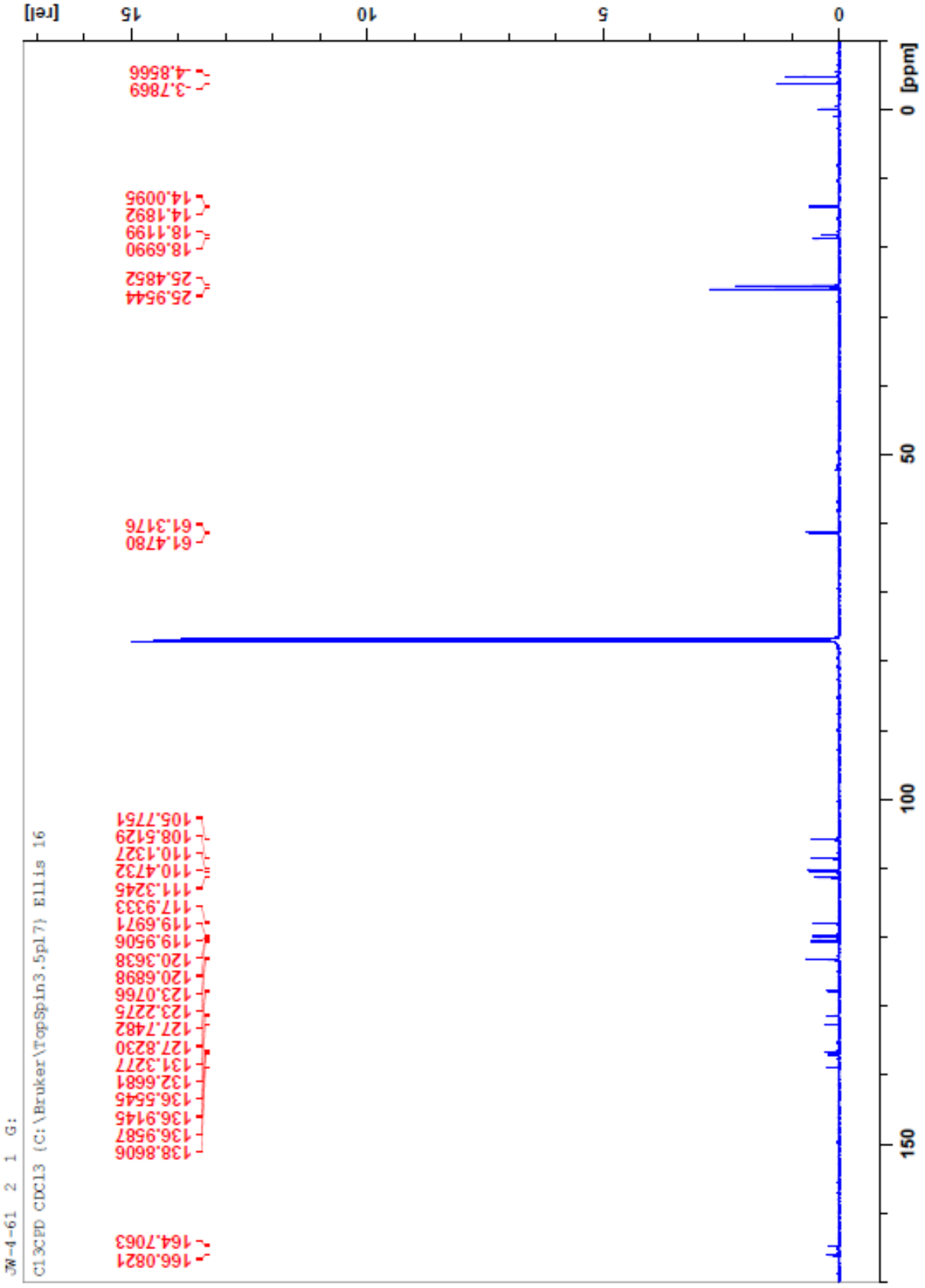
[rel]
15
10
5
0
0 [ppm]
50
100
150
4.8566
3.7869
14.0095
14.1892
18.1199
18.6990
25.4852
25.9544
61.4780
61.3176
105.7751
108.5129
110.1327
110.4732
111.3245
117.9333
119.6971
119.9506
120.3638
120.6898
123.0766
123.2275
127.7482
127.8230
131.3277
132.6681
136.5545
136.9145
136.9587
138.8606
164.7063
166.0821
JW-4-61 2 1 G:
C13CPD CDCl3 (C:\Bruker\TopSpin3.5pl7) Ellis 16

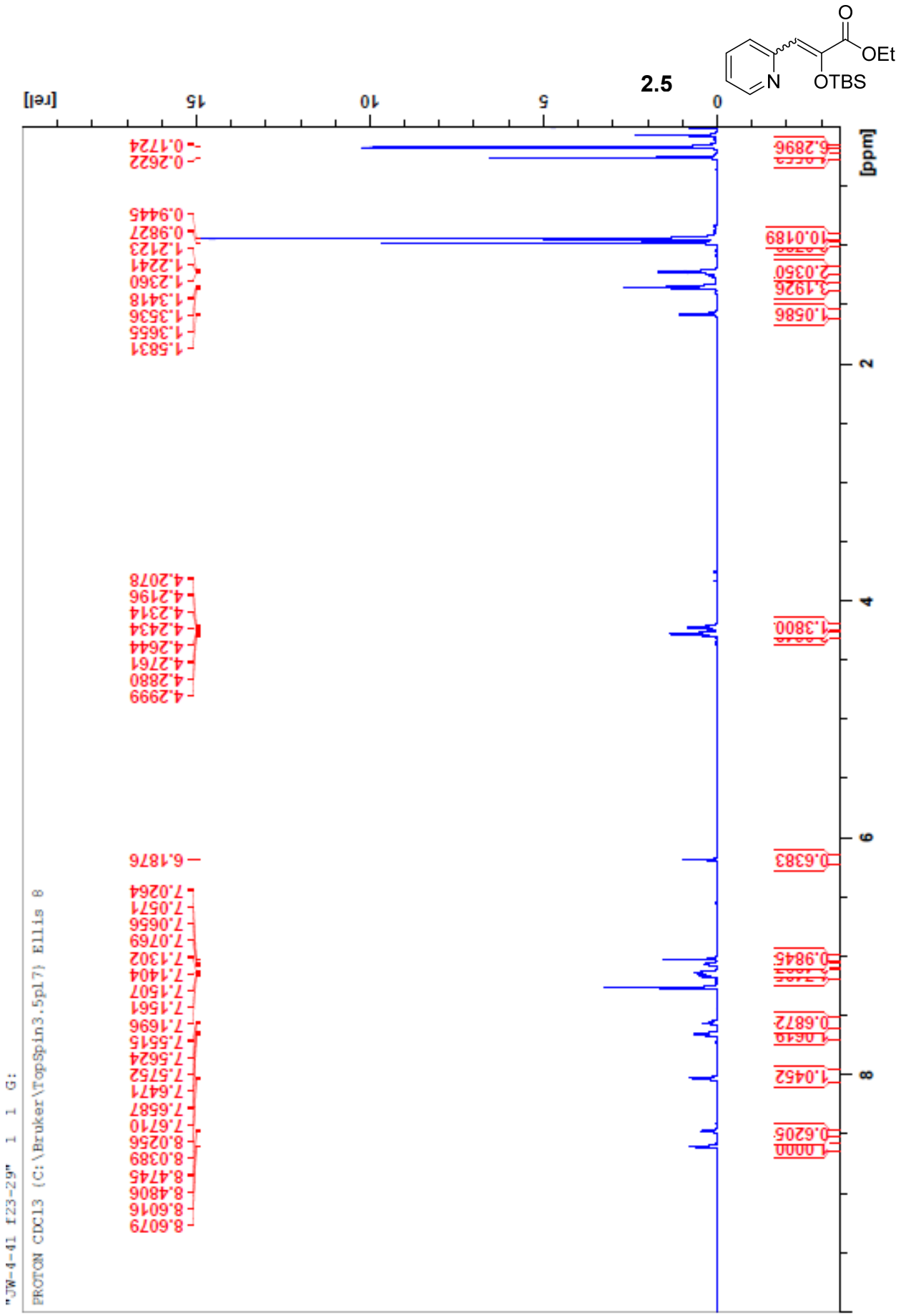
2.5
O
OEt
N
OTBS
[rel]
15
10
5
0
[ppm]
2
4
6
8
0.1724
0.2622
0.9445
0.9827
1.2123
1.2241
1.2360
1.3418
1.3536
1.3655
1.5831
4.2078
4.2196
4.2314
4.2434
4.2644
4.2761
4.2880
4.2999
6.1876
7.0264
7.0571
7.0656
7.0769
7.1302
7.1404
7.1507
7.1561
7.1696
7.5515
7.5624
7.5752
7.6471
7.6587
7.6710
8.0256
8.0389
8.4745
8.4806
8.6016
8.6079
6.2896
10.0189
2.0350
3.1926
1.0586
1.3800
0.6383
0.9845
0.6872
1.0452
0.6205
1.0000
"JW-4-41 F23-29" 1 1 G:
PROTON CDCl3 (C:\Bruker\TopSpin3.5pl7) Ellis 8

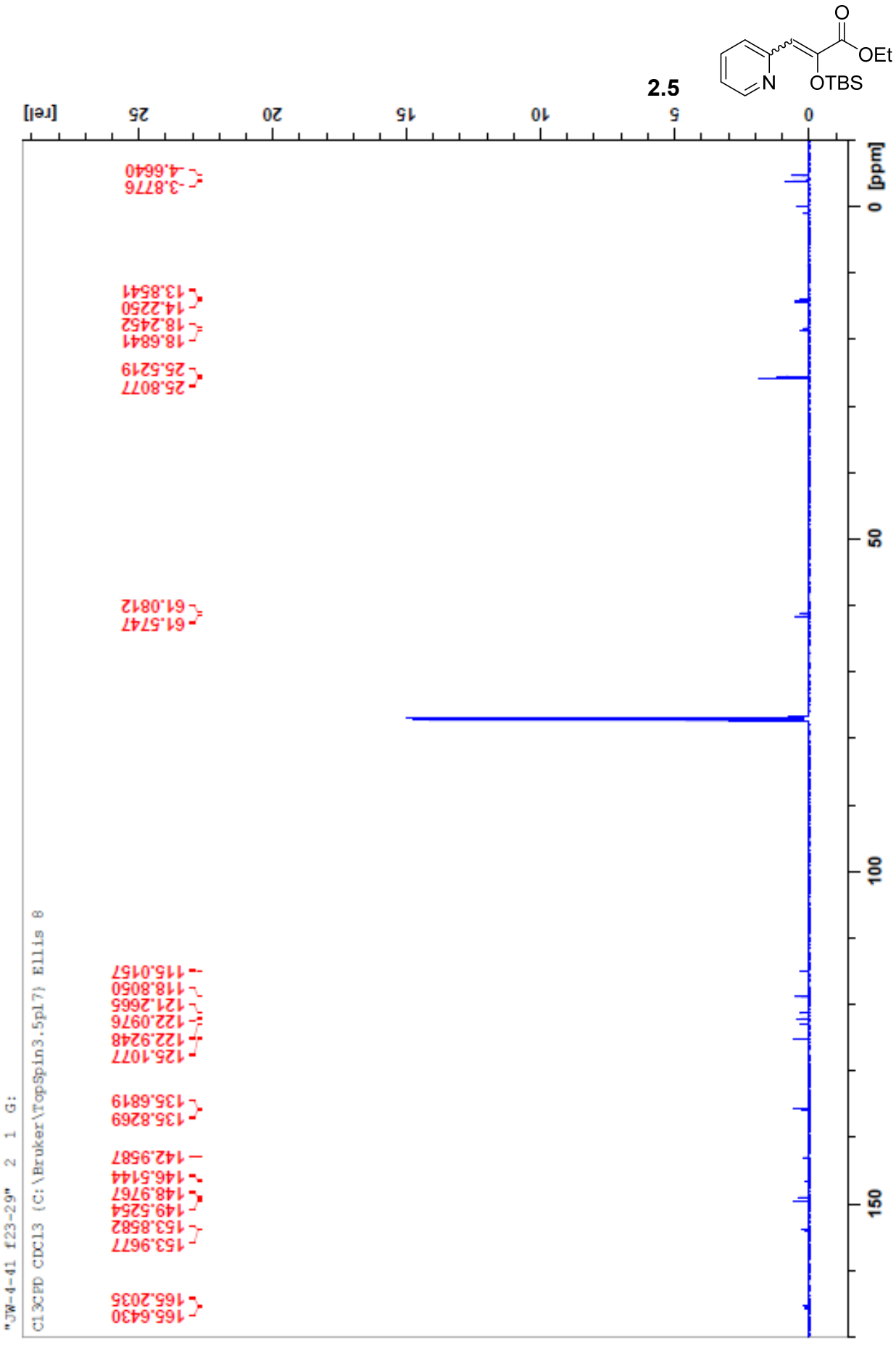
2.5
O
OEt
N
OTBS
[rel]
25
20
15
10
5
0
[ppm]
0
50
100
150
-4.6640
-3.8776
13.8541
14.2250
18.2452
18.6841
25.5219
25.8077
61.5747
61.0812
115.0157
118.8050
121.2665
122.0976
122.9248
125.1077
135.6819
135.8269
142.9587
146.5144
148.9767
149.5254
153.8582
153.9677
165.6430
165.2035
"JW-4-41 f23-29" 2 1 G:
C13CPD CDCl3 (C:\Bruker\TopSpin3.5pl7) Ellis 8

2.6

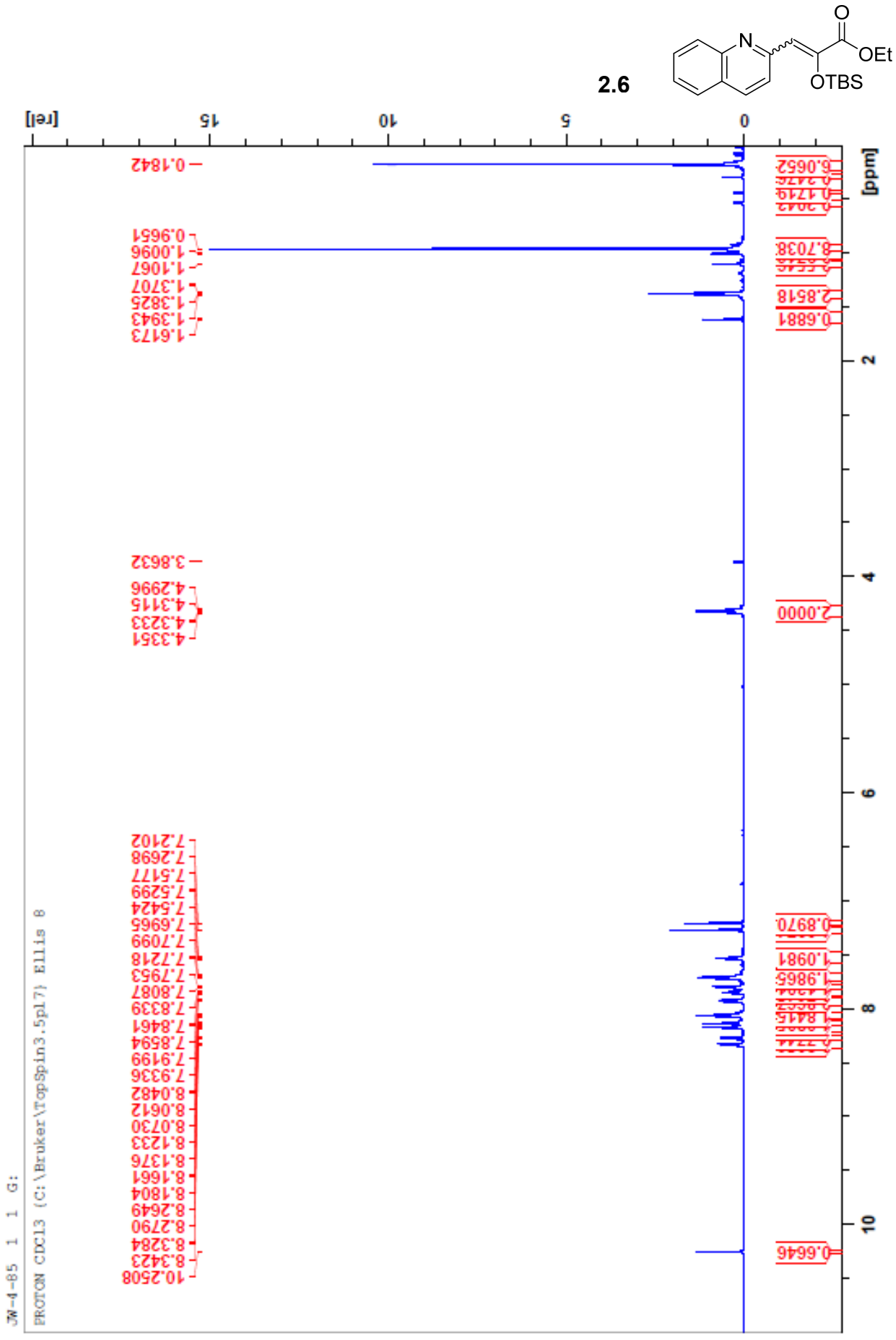
O
N
OEt
OTBS
[rel]
15
10
5
0
[ppm]
2
4
6
8
10
0.1842
0.9651
1.0096
1.1067
1.3707
1.3825
1.3943
1.6173
3.8632
4.2996
4.3115
4.3233
4.3351
7.2102
7.2698
7.5177
7.5299
7.5424
7.6965
7.7099
7.7218
7.7953
7.8087
7.8339
7.8461
7.8594
7.9199
7.9336
8.0482
8.0612
8.0730
8.1233
8.1376
8.1661
8.1804
8.2649
8.2790
8.3284
8.3423
10.2508
0.6646
2.0000
0.8970
1.0981
1.9865
2.8518
0.6881
8.7038
5.0652
JW-4-85 1 1 G:
PROTON CDCl3 (C:\Bruker\TopSpin3.5pl7) Ellis 8

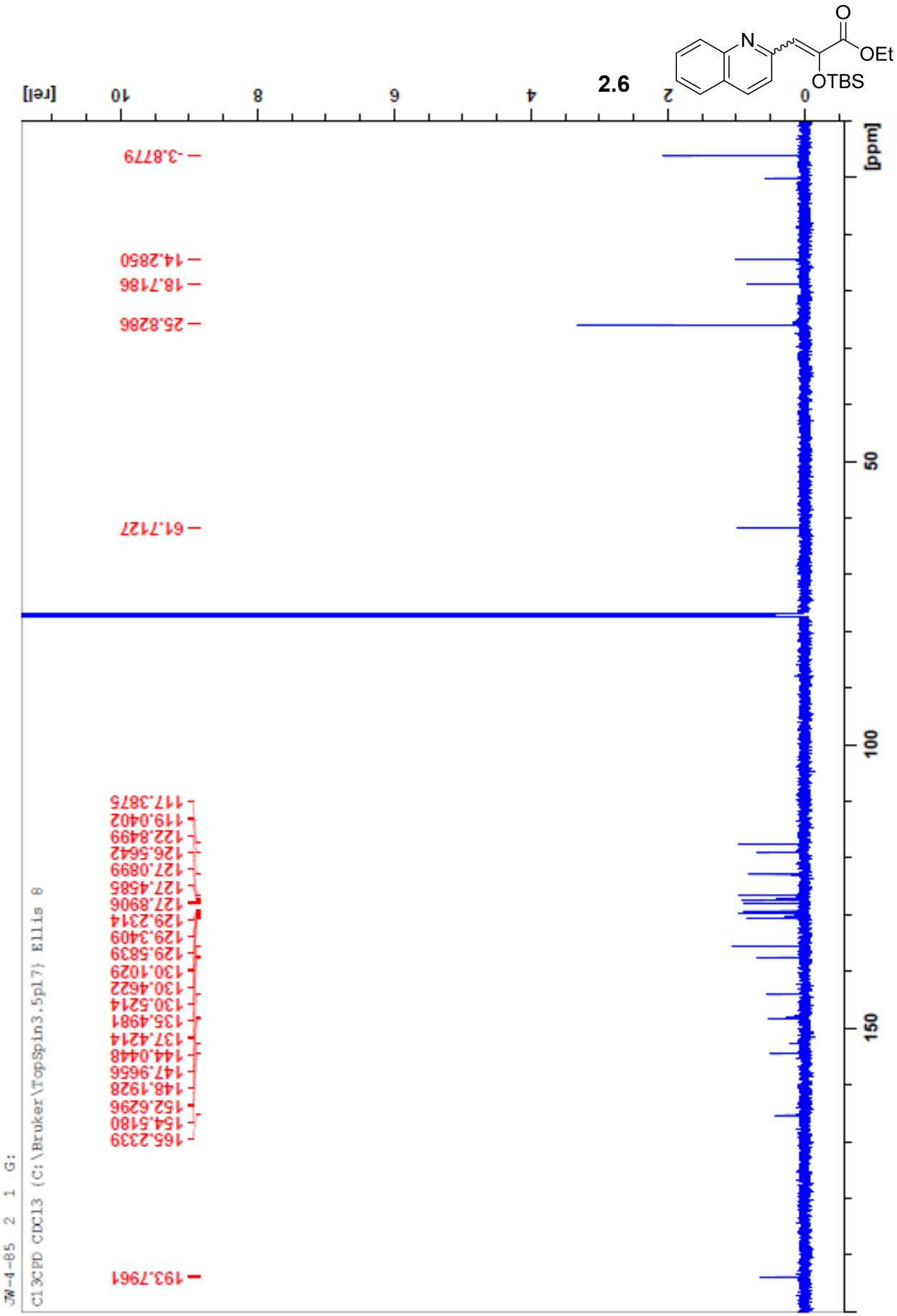
2.6
N
O
OEt
OTBS
[rel]
10
8
6
4
2
0
[ppm]
50
100
150
-3.8779
14.2850
18.7186
25.8286
61.7127
117.3875
119.0402
122.8499
126.5642
127.0899
127.4585
127.8906
129.2314
129.3409
129.5839
130.1029
130.4622
130.5214
135.4981
137.4214
144.0448
147.9656
148.1928
152.6296
154.5180
165.2339
193.7961
JW-4-85 2 1 G:
C13CPD CDCl3 (C:\Bruker\TopSpin3.5pl7) Ellis 8

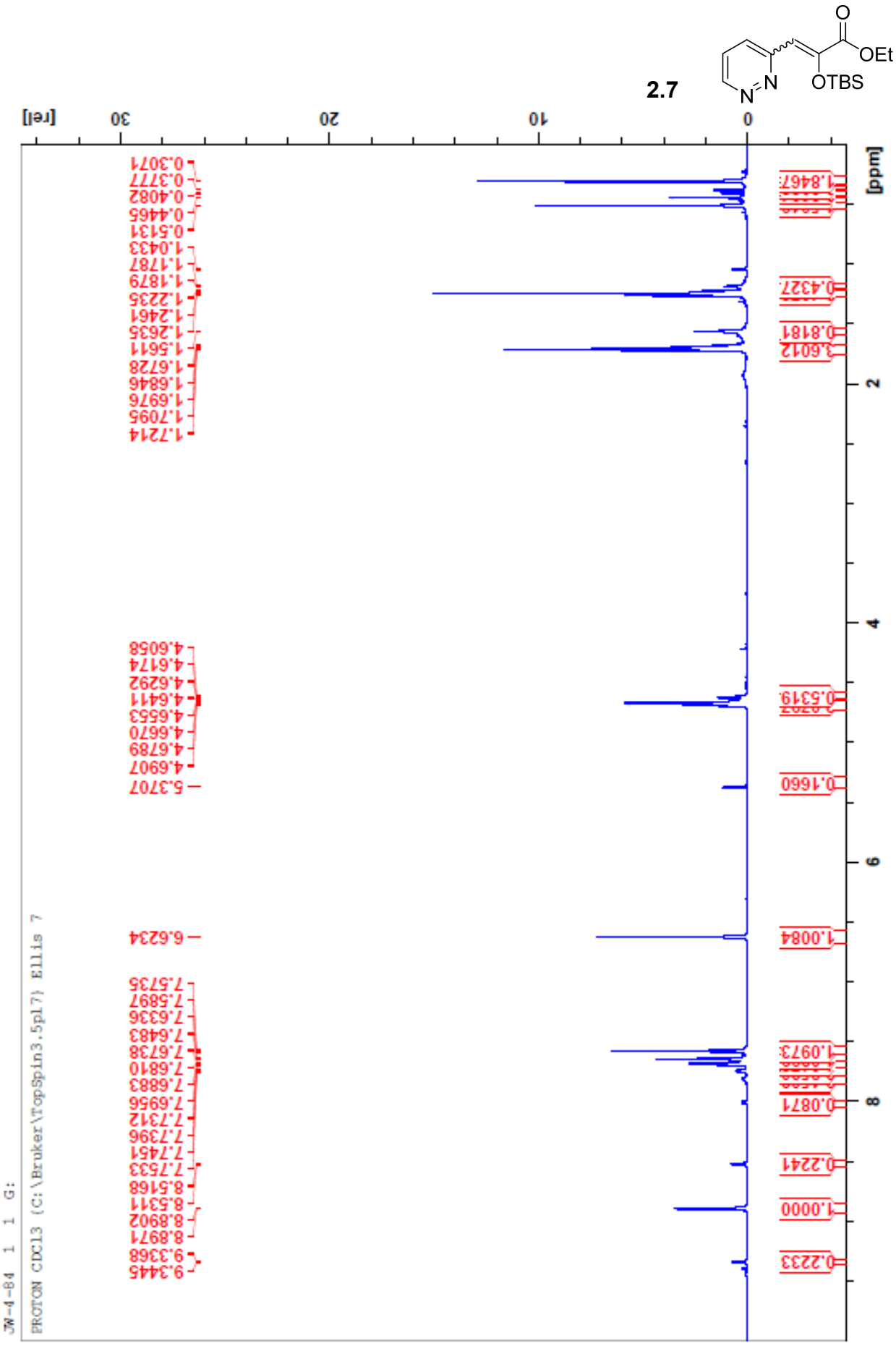
2.7
O
OEt
OTBS
N
N
[rel]
30
20
10
0
[ppm]
2
4
6
8
0.3071
0.3777
0.4082
0.4465
0.5131
1.0433
1.1787
1.1879
1.2235
1.2461
1.2635
1.5611
1.6728
1.6846
1.6976
1.7095
1.7214
4.6058
4.6174
4.6292
4.6411
4.6553
4.6670
4.6789
4.6907
5.3707
6.6234
7.5735
7.5897
7.6336
7.6483
7.6738
7.6810
7.6883
7.6956
7.7312
7.7396
7.7451
7.7533
8.5168
8.5311
8.8902
8.8971
9.3368
9.3445
1.8467
0.4327
0.8181
3.6012
0.5319
0.1660
1.0084
1.0973
0.0871
0.2241
1.0000
0.2233
JW-4-84 1 1 G:
PROTON CDCl3 (C:\Bruker\TopSpin3.5pl7) Ellis 7

2.7

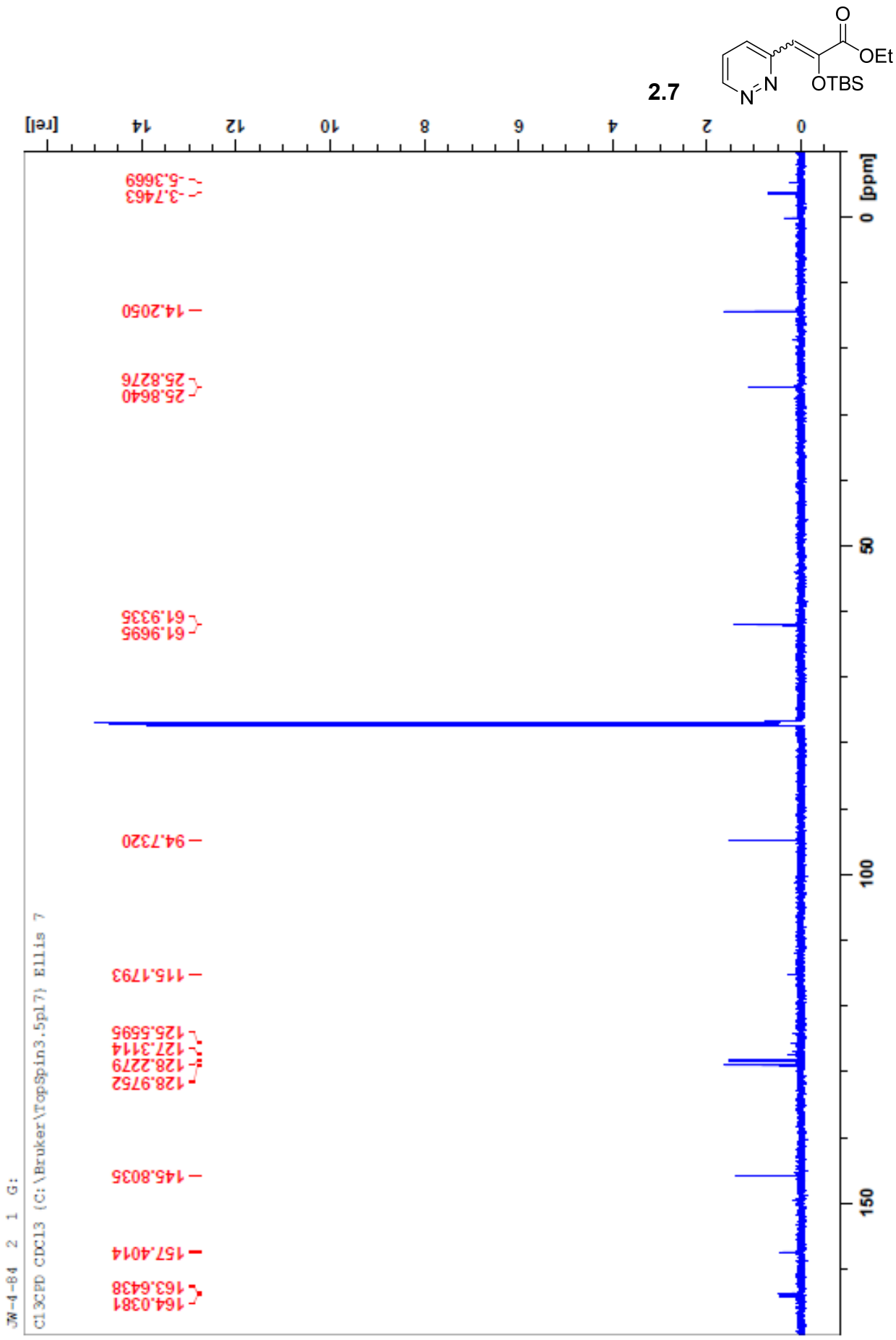
O
OEt
N
N
OTBS
[rel]
0
2
4
6
8
10
12
14
0 [ppm]
50
100
150
-5.3669
-3.7463
14.2050
25.8640
25.8276
61.9335
61.9695
94.7320
115.1793
125.5595
127.3114
128.2279
128.9752
145.8035
157.4014
163.6438
164.0381
JW-4-84 2 1 G:
C13CPD CDCl3 (C:\Bruker\TopSpin3.5pl7) Ellis 7

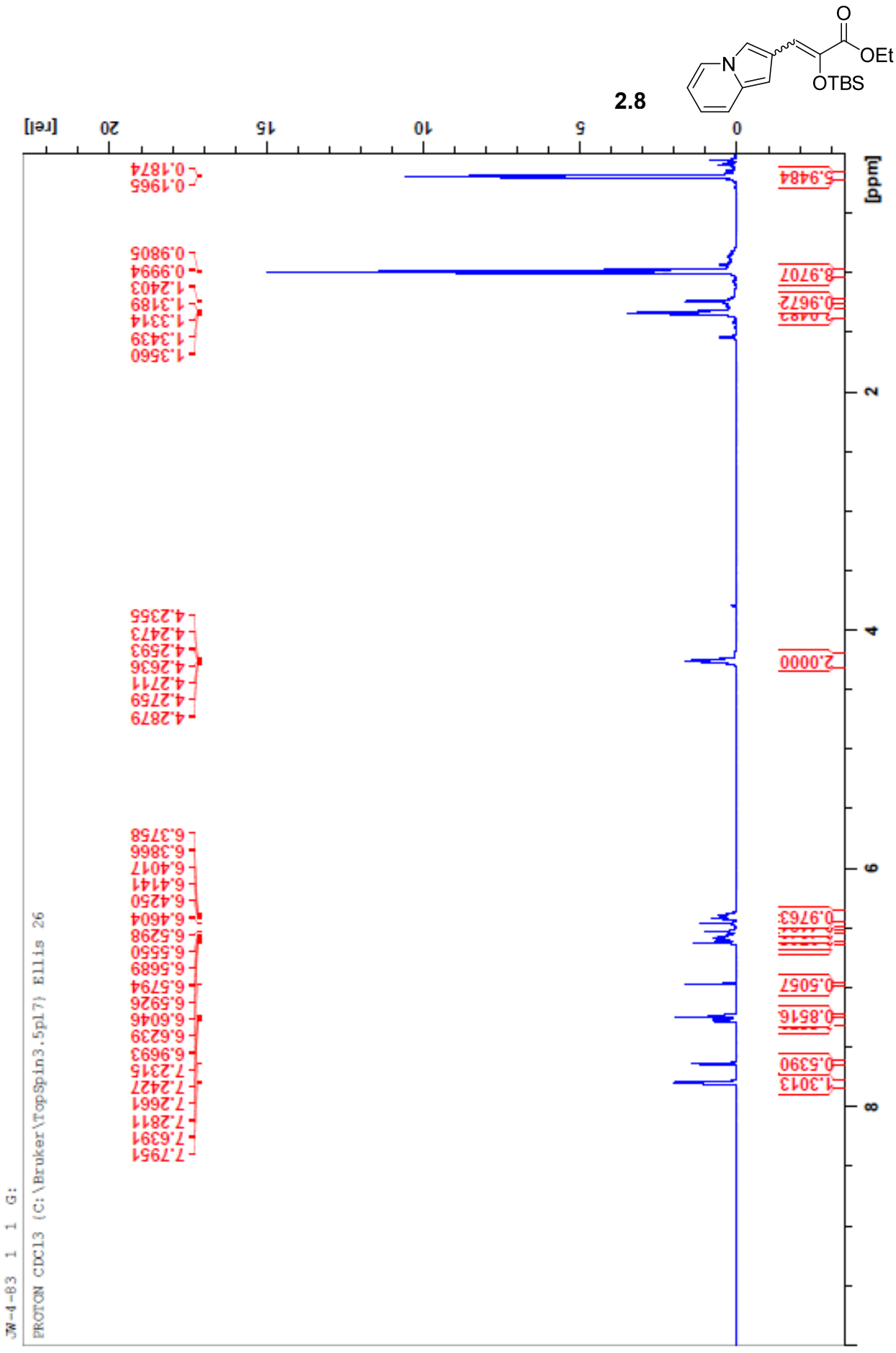
2.8
O
OEt
OTBS
N
[rel]
20
15
10
5
0
[ppm]
2
4
6
8
0.1874
0.1965
0.9805
0.9994
1.2403
1.3189
1.3314
1.3439
1.3560
4.2355
4.2473
4.2593
4.2636
4.2711
4.2759
4.2879
6.3758
6.3866
6.4017
6.4141
6.4250
6.4604
6.5298
6.5550
6.5689
6.5794
6.5926
6.6046
6.6239
6.9693
7.2315
7.2427
7.2661
7.2811
7.6391
7.7951
5.9484
8.9707
0.9672
2.0000
0.9763
0.6057
0.8516
0.5390
1.3013
JW-4-83 1 1 1 G:
PROTON CDCl3 (C:\Bruker\TopSpin3.5pl7) Ellis 26

2.8

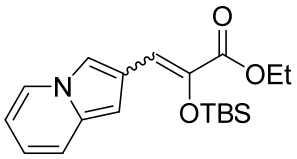
O
OEt
N
OTBS

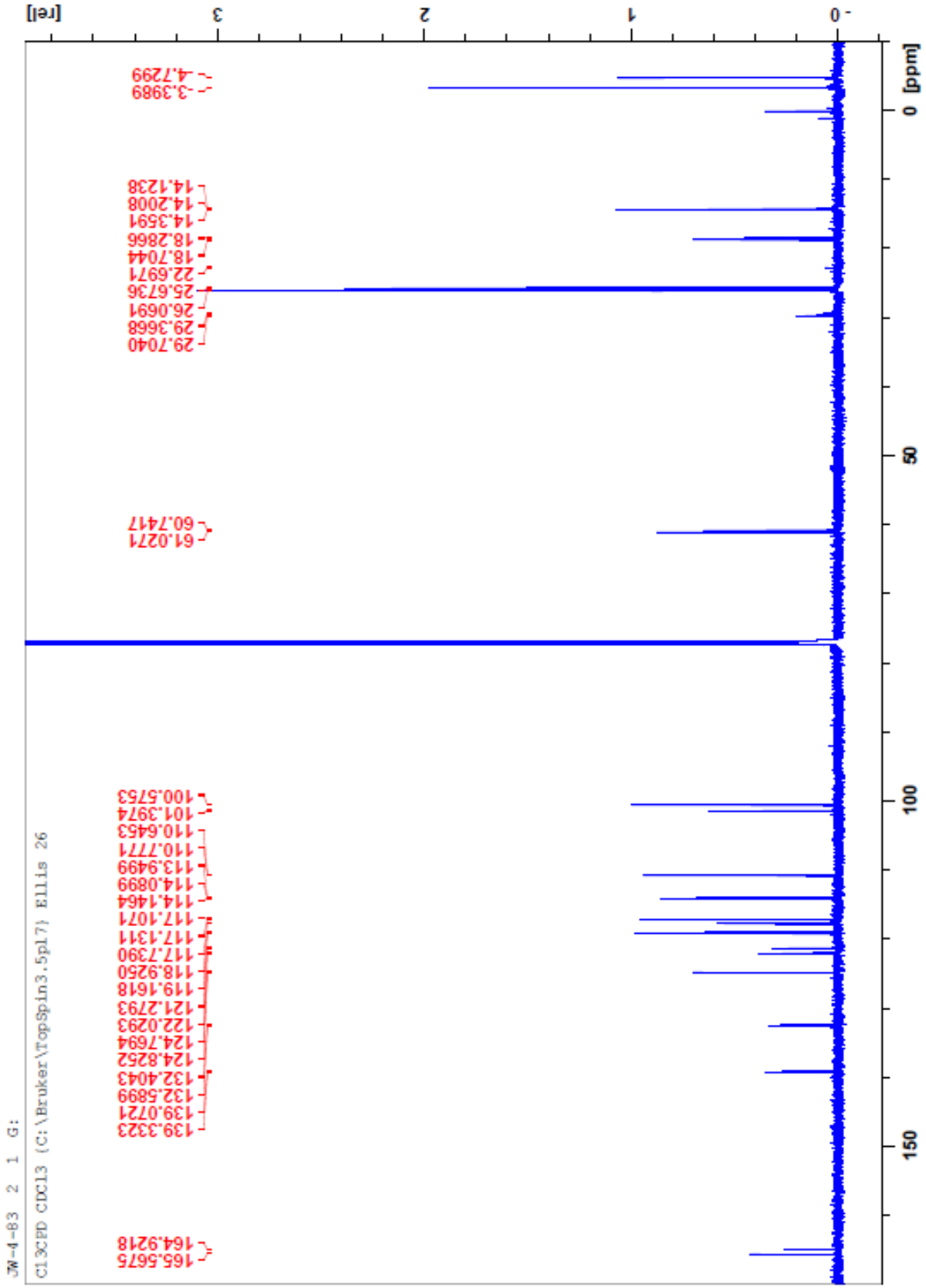
[rel]
3
2
1
0
[ppm]
0
50
100
150
4.7299
3.3989
14.1238
14.2008
14.3591
18.2866
18.7044
22.6971
25.6736
26.0691
29.3668
29.7040
60.7417
61.0271
100.5753
101.3974
110.6453
110.7771
113.9499
114.0899
114.1464
117.1071
117.1311
117.7390
118.9250
119.1618
121.2793
122.0293
124.7694
124.8252
132.4043
132.5899
139.0721
139.3323
164.9218
165.5675
JW-4-83 2 1 G:
C13CPD CDCl3 (C:\Bruker\TopSpin3.5pl7) Ellis 26

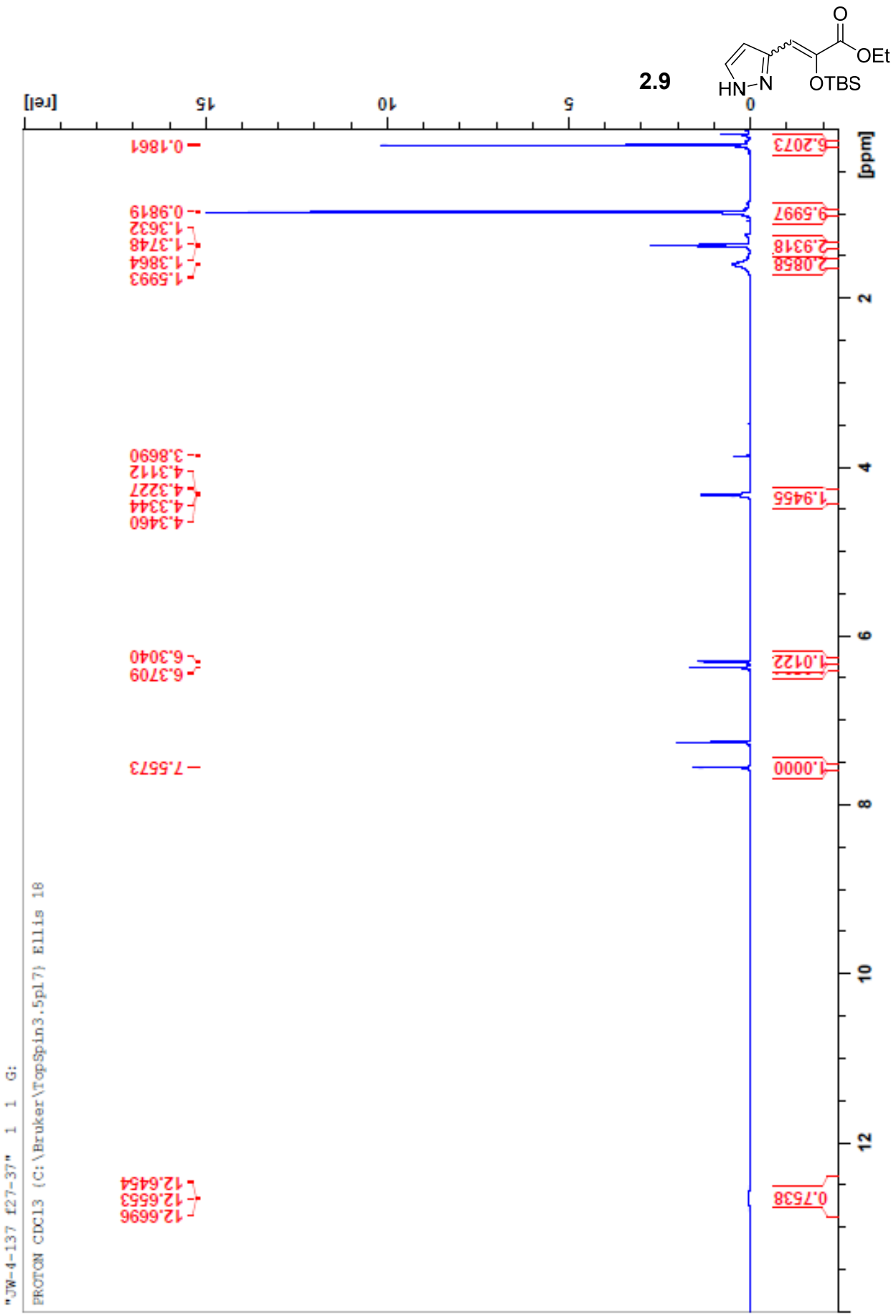
2.9
O
OEt
HN–N
OTBS
"JW-4-137 f27-37" 1 1 G:
PROTON CDCl3 (C:\Bruker\TopSpin3.5pl7) Ellis 18
[rel]
[ppm]
0.1861
0.9819
1.3632
1.3748
1.3864
1.5993
3.8690
4.3112
4.3227
4.3344
4.3460
6.3040
6.3709
7.5573
12.6454
12.6553
12.6696
5.2073
9.5997
2.9318
2.0858
1.9455
1.0122
1.0000
0.7538

2.9

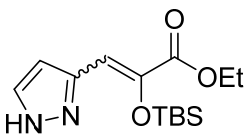
O
OEt
HN–N
OTBS

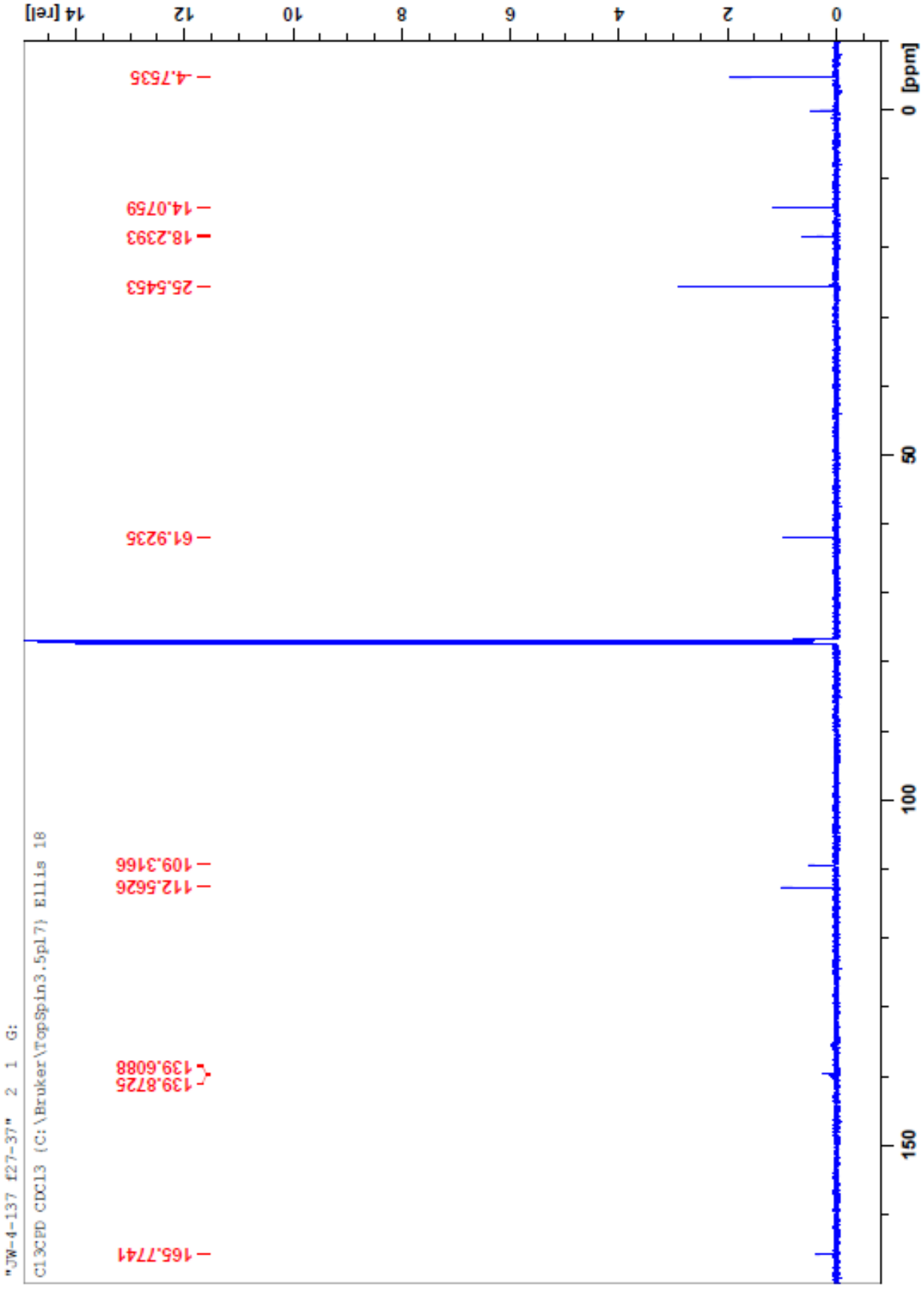
"JW-4-137 f27-37" 2 1 G:
C13CPD CDCl3 (C:\Bruker\TopSpin3.5pl7) Ellis 18
[rel]
[ppm]
4.7535
14.0759
18.2393
25.5453
61.9235
109.3166
112.5626
139.8725
139.6088
165.7741

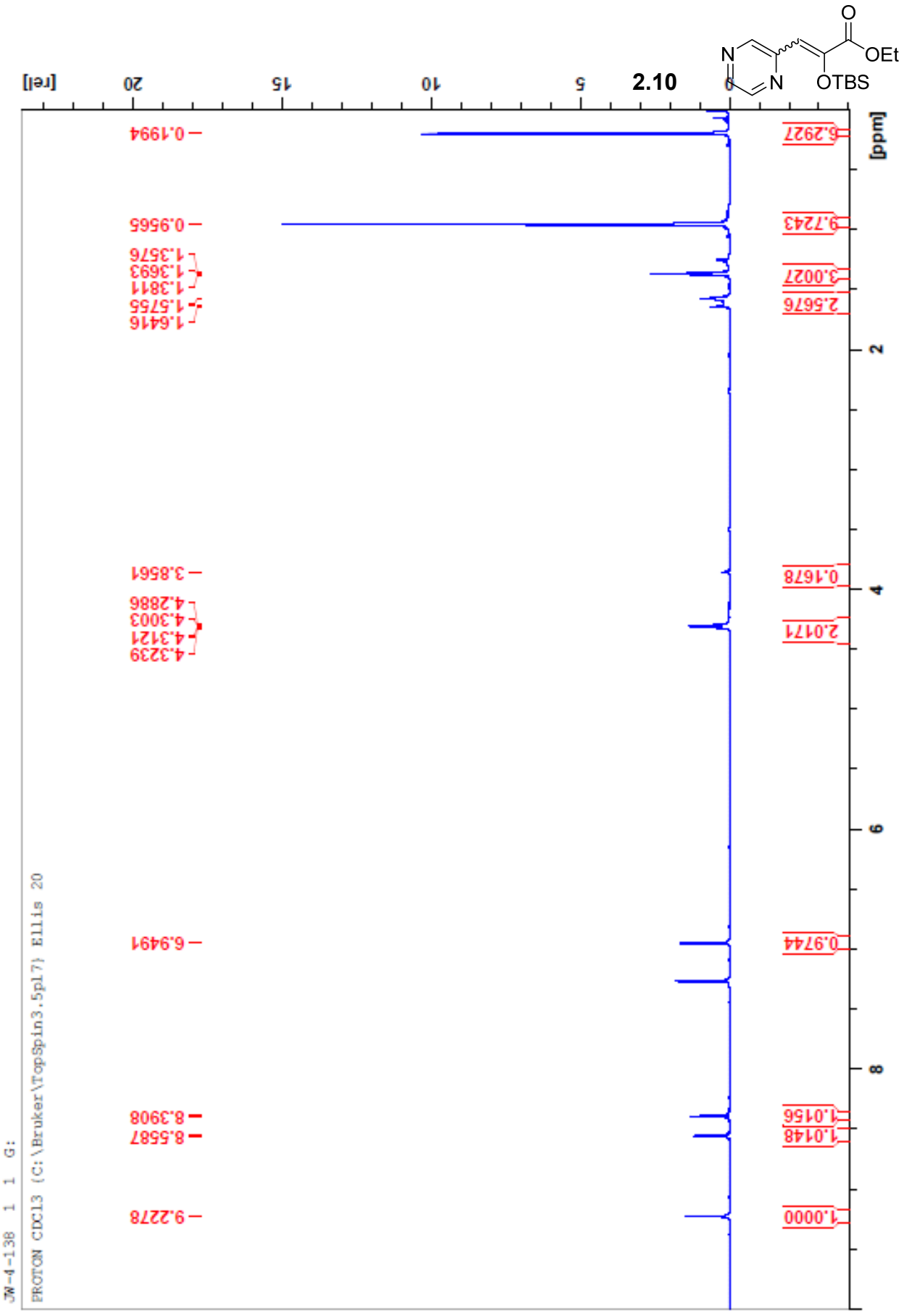
O
OEt
N
N
OTBS
2.10
[rel]
20
15
10
5
0
[ppm]
8
6
4
2
0.1994
0.9565
1.3576
1.3693
1.3811
1.5755
1.6416
3.8561
4.2886
4.3003
4.3121
4.3239
6.9491
8.3908
8.5587
9.2278
6.2927
9.7243
3.0027
2.5676
0.1678
2.0171
0.9744
1.0156
1.0148
1.0000
JW-4-138 1 1 G:
PROTON CDCl3 (C:\Bruker\TopSpin3.5pl7) Ellis 20

2.10

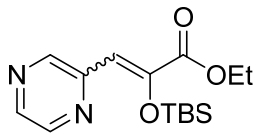
O
OEt
N
N
OTBS

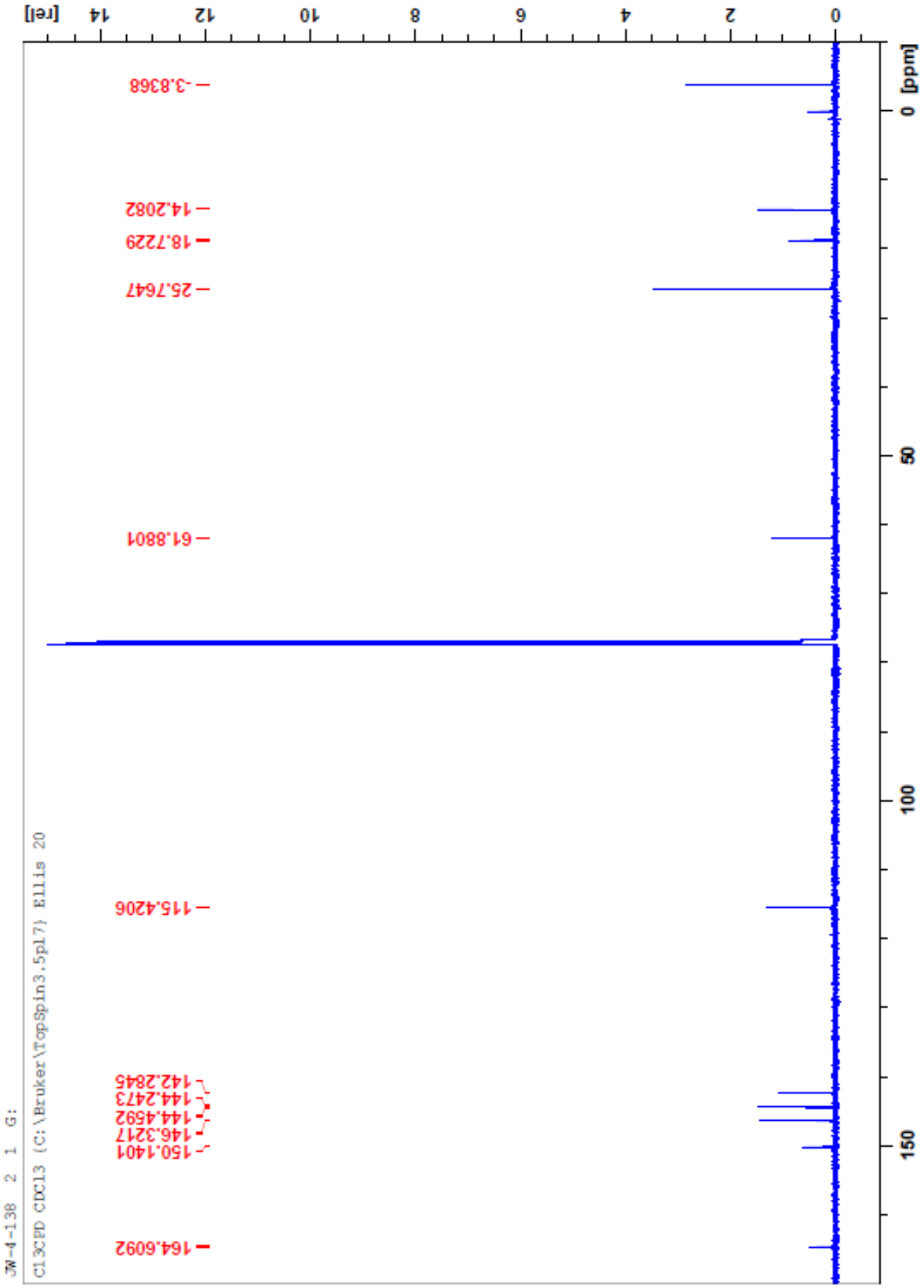
[rel]
14
12
10
8
6
4
2
0
[ppm]
0
50
100
150
-3.8368
14.2082
18.7229
25.7647
61.8801
115.4206
142.2845
144.2473
144.4592
146.3217
150.1401
164.6092
JW-4-138 2 1 G:
C13CPD CDCl3 (C:\Bruker\TopSpin3.5pl7) Ellis 20

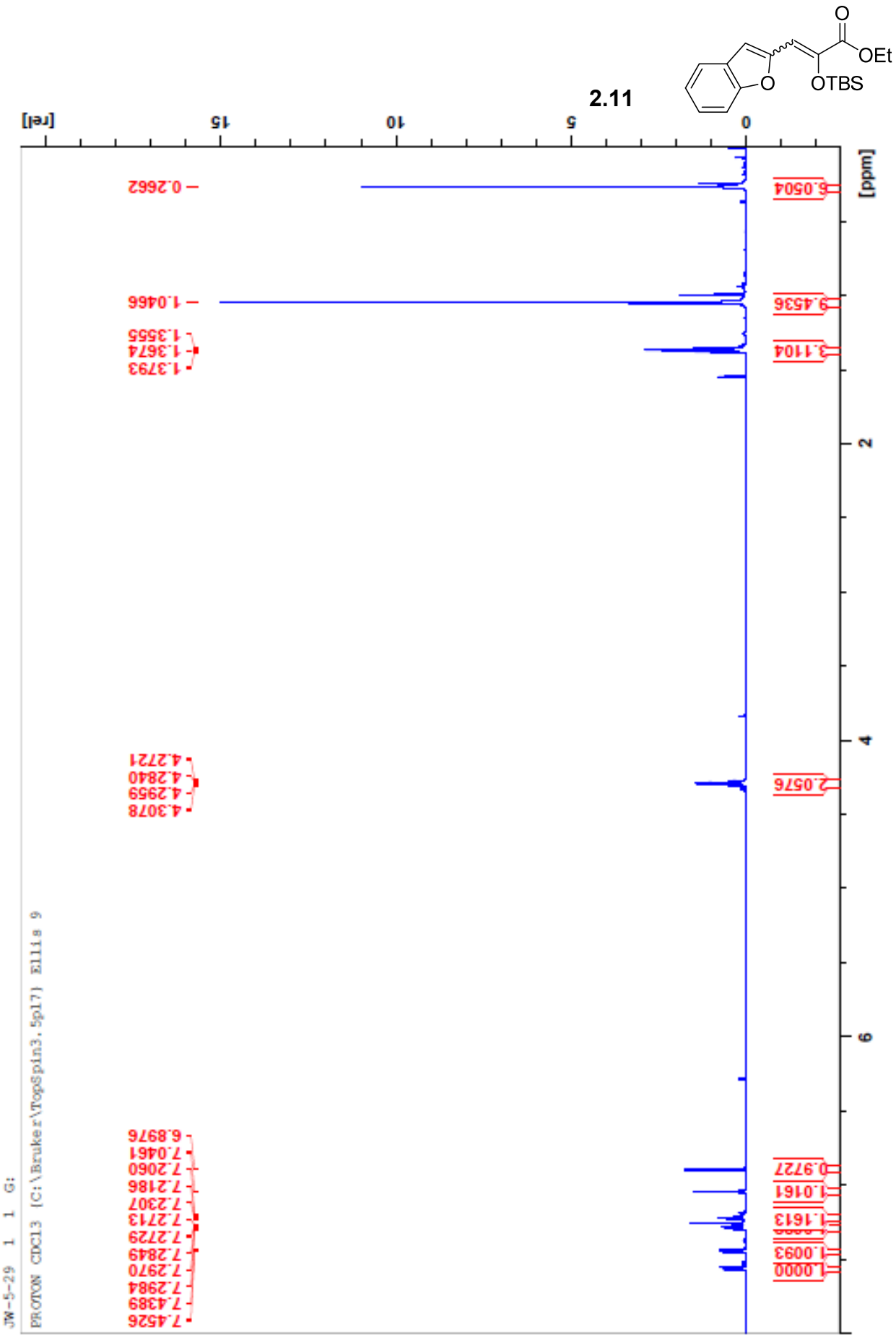
2.11
O
OEt
O
OTBS
[rel]
15
10
5
0
[ppm]
2
4
6
0.2662
1.0466
1.3555
1.3674
1.3793
4.2721
4.2840
4.2959
4.3078
6.8976
7.0461
7.2060
7.2186
7.2307
7.2713
7.2729
7.2849
7.2970
7.2984
7.4389
7.4526
6.0504
9.4536
3.1104
2.0576
0.9727
1.0161
1.1613
1.0093
1.0000
JW-5-29 1 1 G:
PROTON CDCl3 (C:\Bruker\TopSpin3.5pl7) Ellis 9

2.11

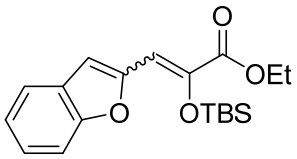
O
OEt
O
OTBS

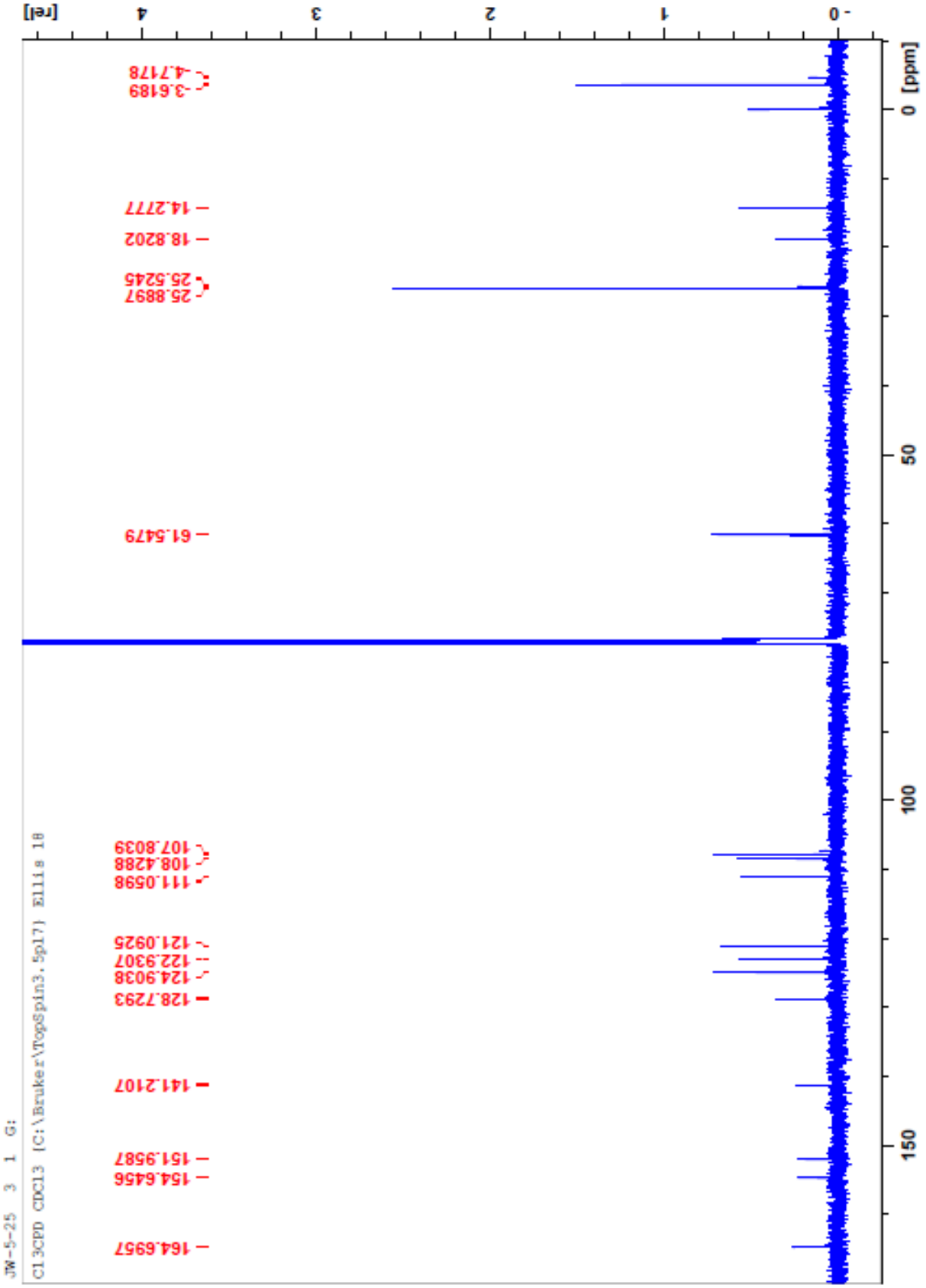
[rel]
4
3
2
1
0
[ppm]
0
50
100
150
4.7178
3.6189
14.2777
18.8202
25.5245
25.8897
61.5479
107.8039
108.4288
111.0598
121.0925
122.9307
124.9038
128.7293
141.2107
151.9587
154.6456
164.6957
JW-5-25 3 1 G:
C13CPD CDCl3 (C:\Bruker\TopSpin3.5pl7) E111 8 18

2.12

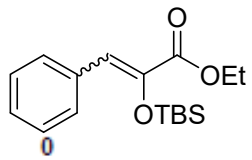
O
OEt
OTBS

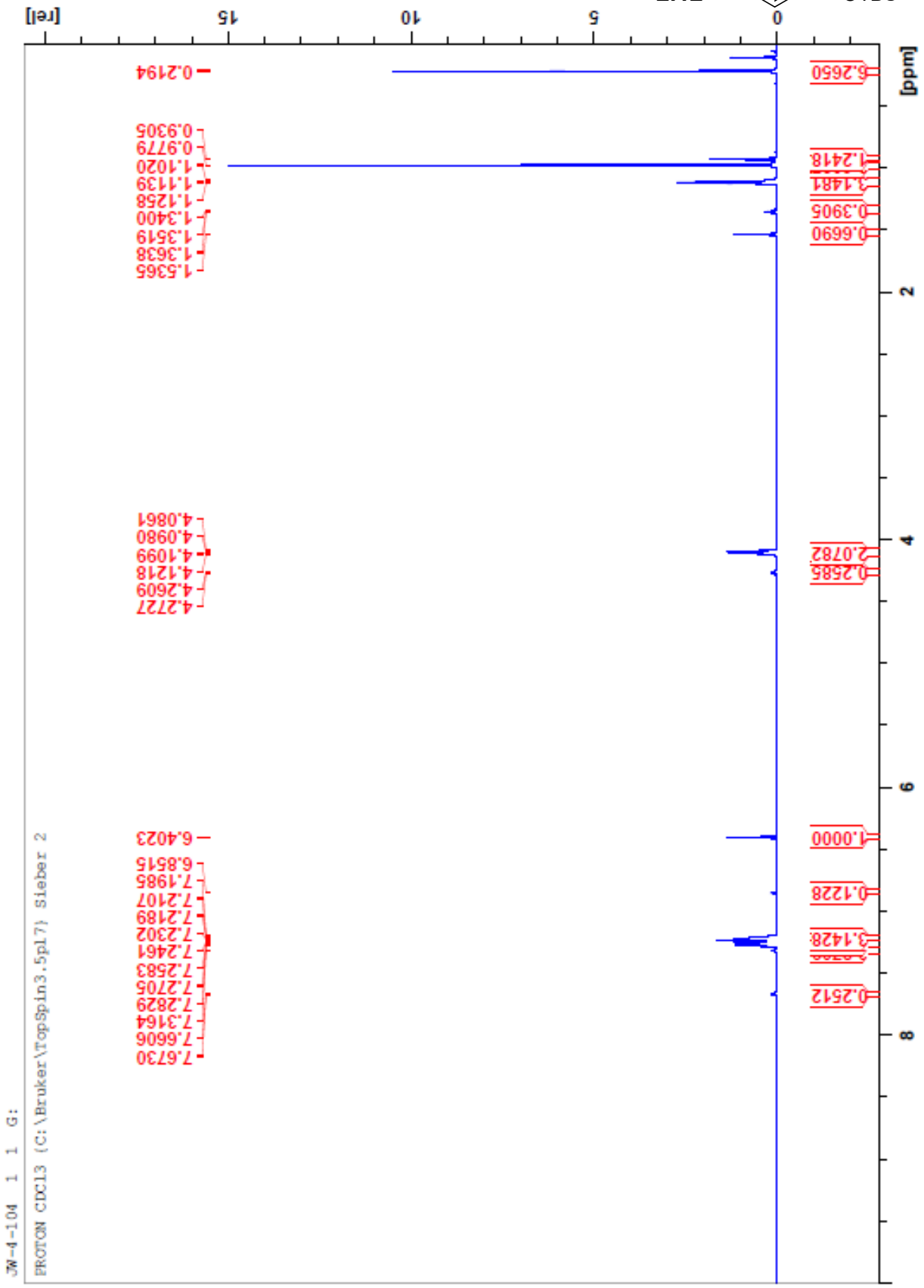
[rel]
15
10
5
0
[ppm]
2
4
6
8
0.2194
0.9305
0.9779
1.1020
1.1139
1.1258
1.3400
1.3519
1.3638
1.5365
4.0861
4.0980
4.1099
4.1218
4.2609
4.2727
6.4023
6.8515
7.1985
7.2107
7.2189
7.2302
7.2461
7.2583
7.2705
7.2829
7.3164
7.6606
7.6730
6.2650
1.2418
3.1481
0.3905
0.6690
2.0782
0.2585
1.0000
0.1228
3.1428
0.2512
JW-4-104 1 1 G:
PROTON CDCl3 (C:\Bruker\TopSpin3.5pl7) Sieber 2

2.12

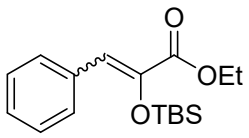
O
OEt
OTBS

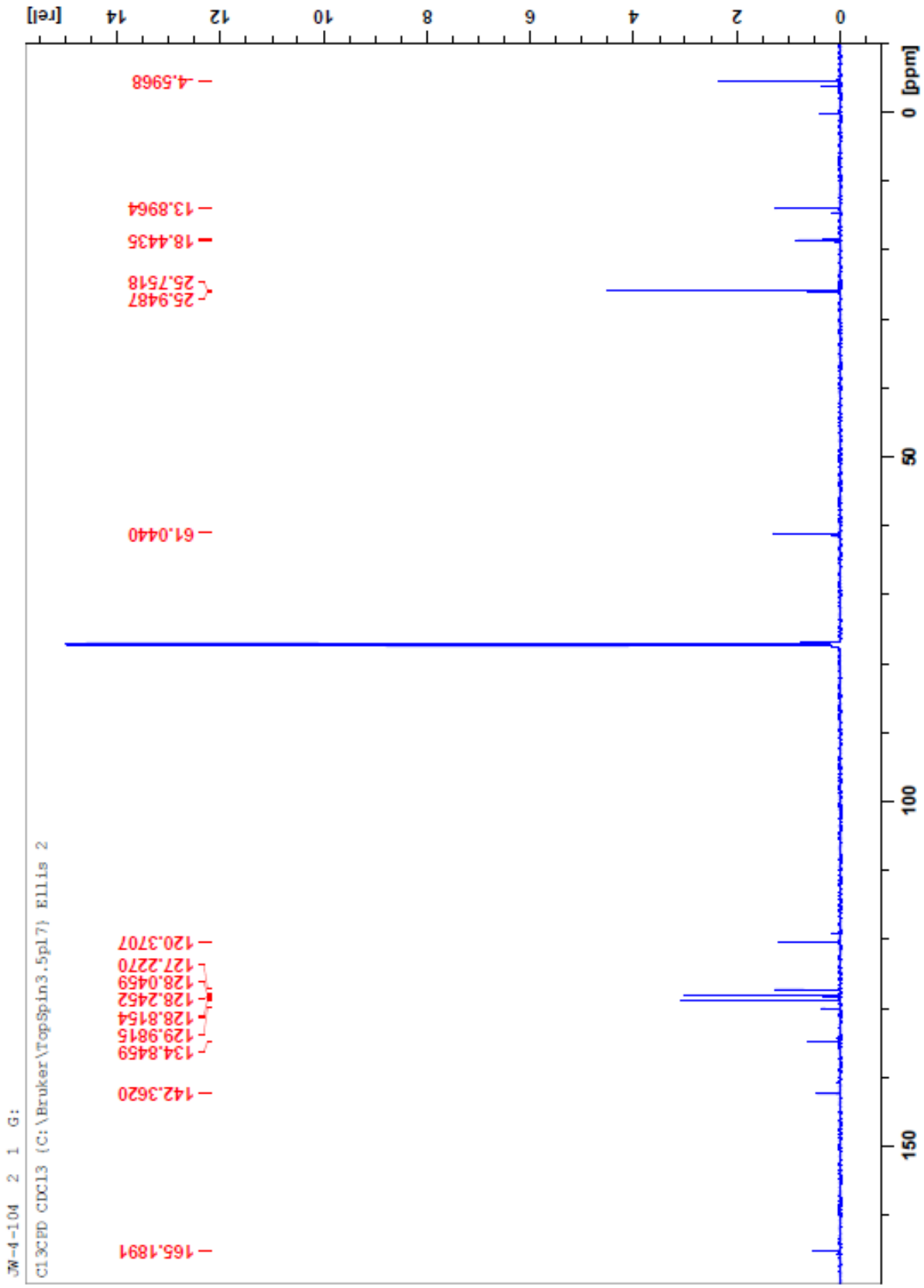
[rel]
14
12
10
8
6
4
2
0
[ppm]
0
50
100
150
4.5968
13.8964
18.4435
25.7518
25.9487
61.0440
120.3707
127.2270
128.0459
128.2452
128.8154
129.9815
134.8459
142.3620
165.1891
JW-4-104 2 1 G:
C13CPD CDCl3 (C:\Bruker\TopSpin3.5pl7) Ellis 2

2.13

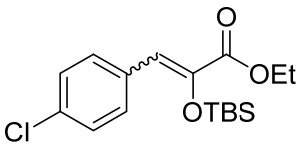
O
OEt
OTBS
Cl

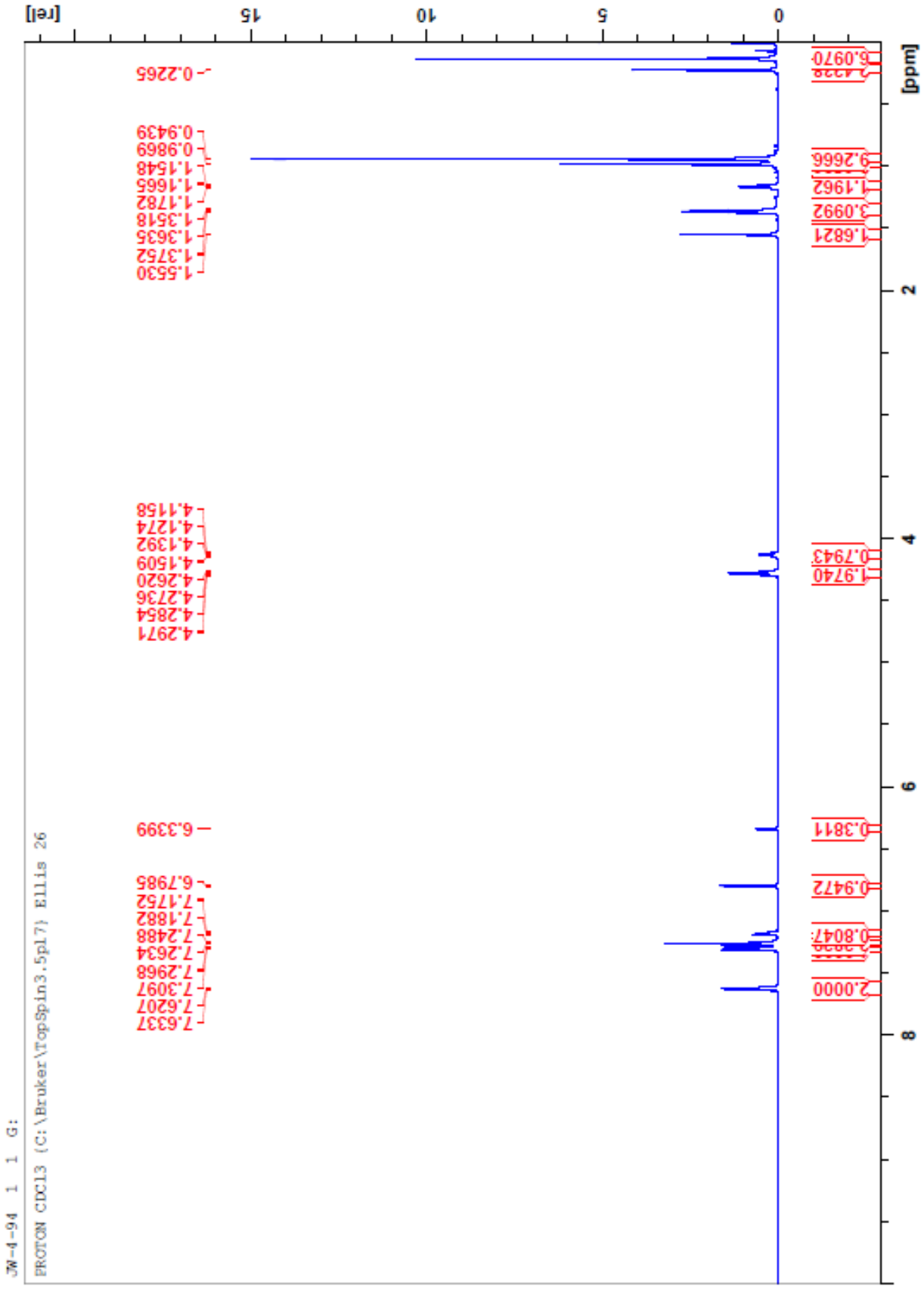
[rel]
15
10
5
0
[ppm]
2
4
6
8
6.0970
4.238
9.2666
1.1962
3.0992
1.6821
0.7943
1.9740
0.3811
0.9472
0.8047
2.0000
0.2265
0.9439
0.9869
1.1548
1.1665
1.1782
1.3518
1.3635
1.3752
1.5530
4.1158
4.1274
4.1392
4.1509
4.2620
4.2736
4.2854
4.2971
6.3399
6.7985
7.1752
7.1882
7.2488
7.2634
7.2968
7.3097
7.6207
7.6337
JW-4-94 1 1 G:
PROTON CDCl3 (C:\Bruker\TopSpin3.5pl7) Ellis 26

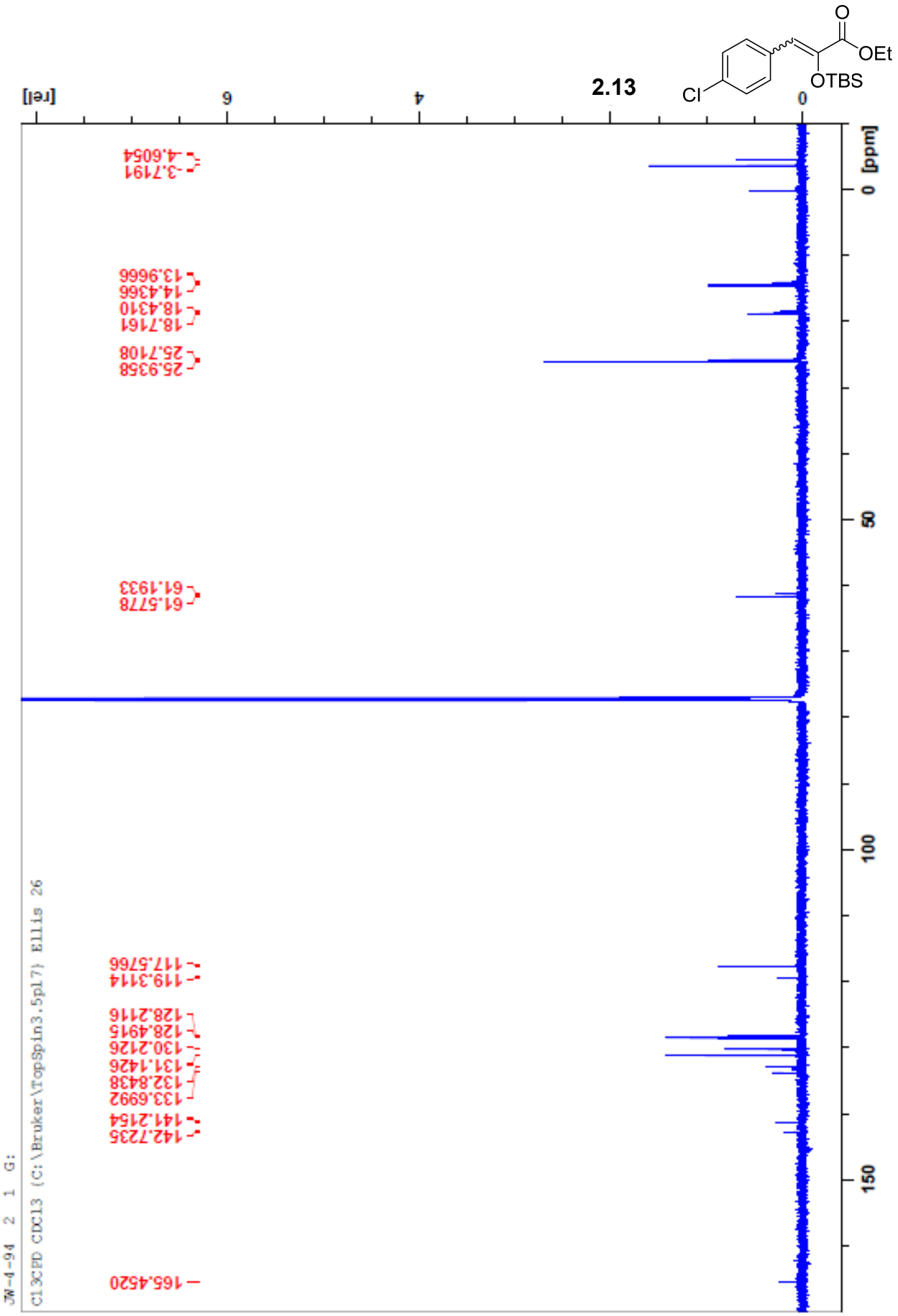
2.13
O
OEt
OTBS
Cl
[rel]
6
4
0
[ppm]
0
50
100
150
4.6054
3.7191
13.9666
14.4366
18.4310
18.7161
25.7108
25.9358
61.1933
61.5778
117.5766
119.3114
128.2116
128.4915
130.2126
131.1426
132.8438
133.6992
141.2154
142.7235
165.4520
JW-4-94 2 1 G:
C13CPD CDCl3 (C:\Bruker\TopSpin3.5pl7) Ellis 26

2.14

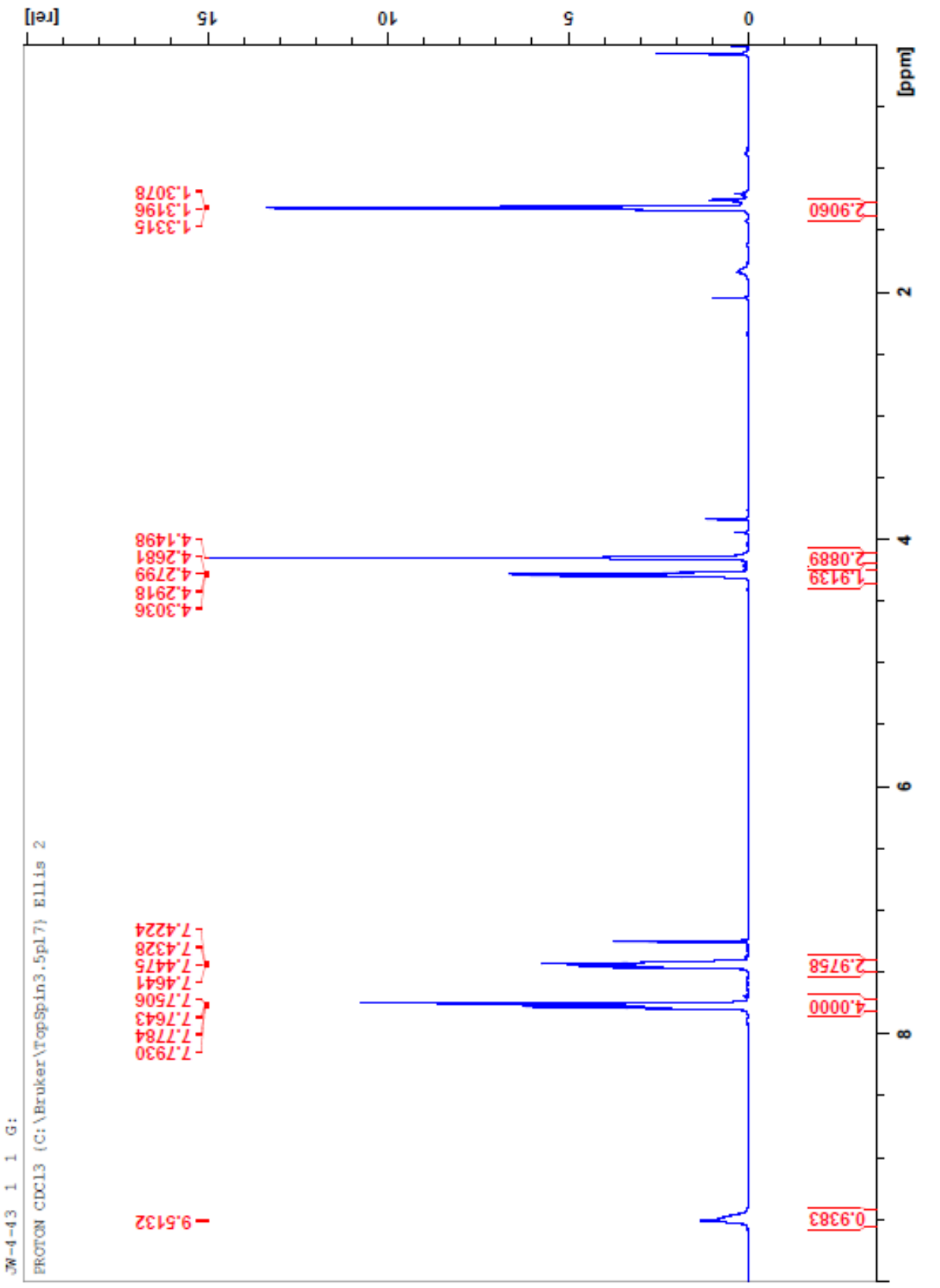
[rel]
15
10
5
0
[ppm]
2
4
6
8
1.3078
1.3196
1.3315
4.1498
4.2681
4.2799
4.2918
4.3036
7.4224
7.4328
7.4475
7.4641
7.7506
7.7643
7.7784
7.7930
9.5132
2.9060
2.0889
1.9139
2.9758
4.0000
0.9383
JW-4-43 1 1 G:
PROTON CDCl3 (C:\Bruker\TopSpin3.5pl7) Ellis 2

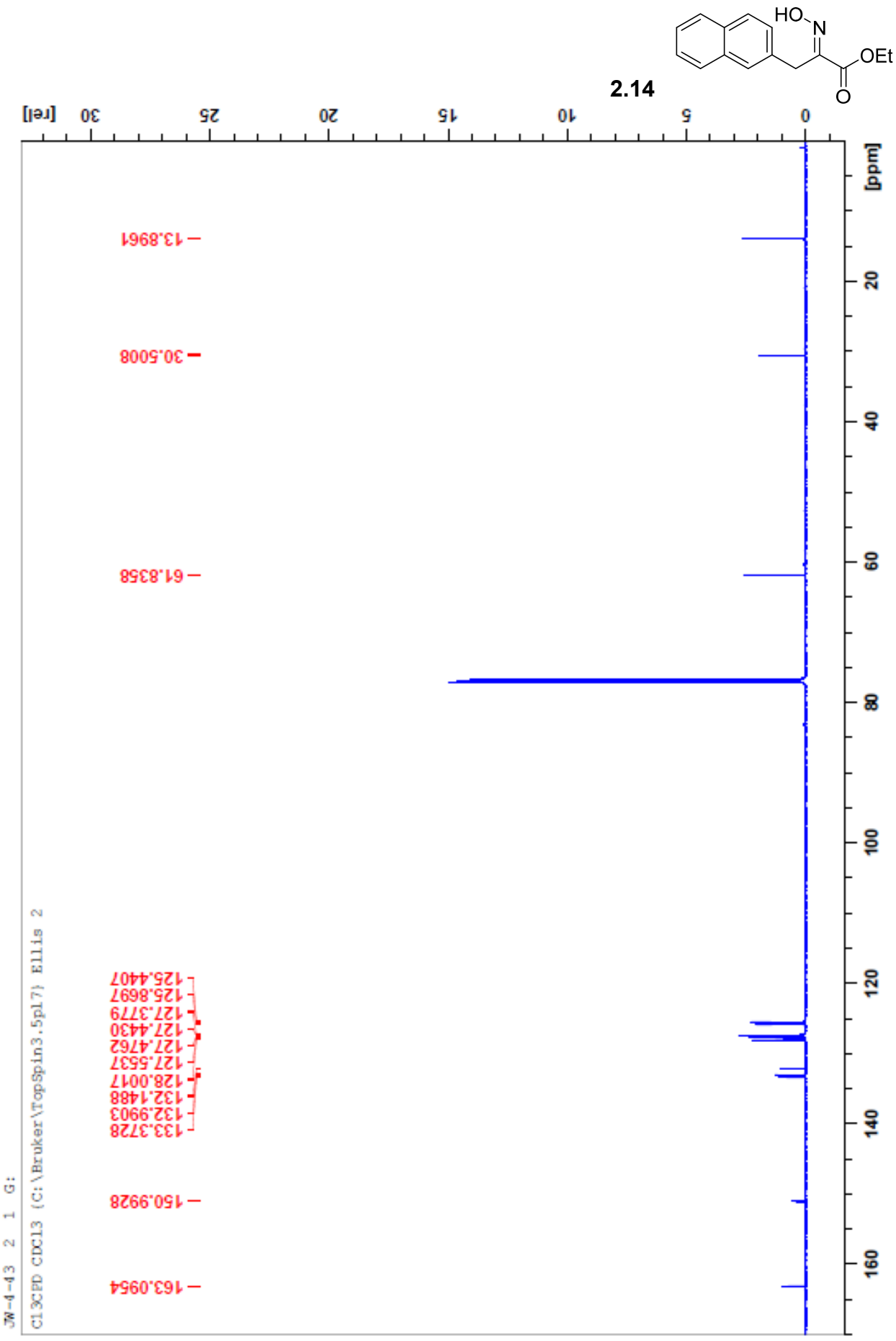
HO
N
OEt
O
2.14
[rel]
30
25
20
15
10
5
0
[ppm]
20
40
60
80
100
120
140
160
13.8961
30.5008
61.8358
125.4407
125.8697
127.3779
127.4430
127.4762
127.5537
128.0017
132.1488
132.9903
133.3728
150.9928
163.0954
JW-4-43 2 1 G:
C13CPD CDCl3 (C:\Bruker\TopSpin3.5pl7) Ellis 2

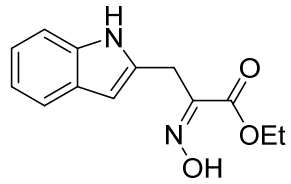
H
N
O
OEt
N
OH

2.15

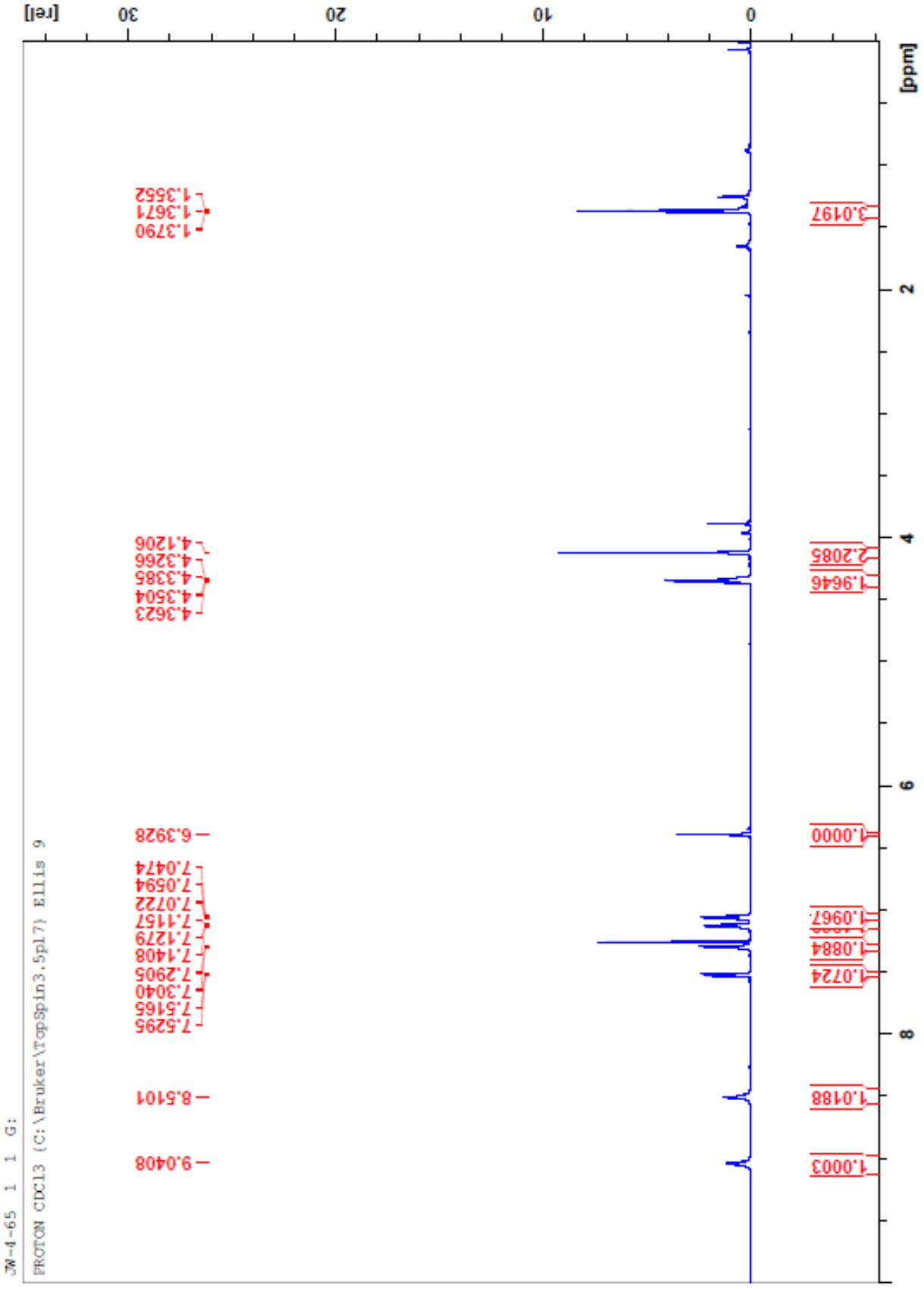
[rel]
30
20
10
0
[ppm]
2
4
6
8
1.3552
1.3671
1.3790
4.1206
4.3266
4.3385
4.3504
4.3623
6.3928
7.0474
7.0594
7.0722
7.1157
7.1279
7.1408
7.2905
7.3040
7.5165
7.5295
8.5101
9.0408
3.0197
2.2085
1.9646
1.0000
1.0967
1.0884
1.0724
1.0188
1.0003
JW-4-65 1 1 G:
PROTON CDCl3 (C:\Bruker\TopSpin3.5pl7) Ellis 9

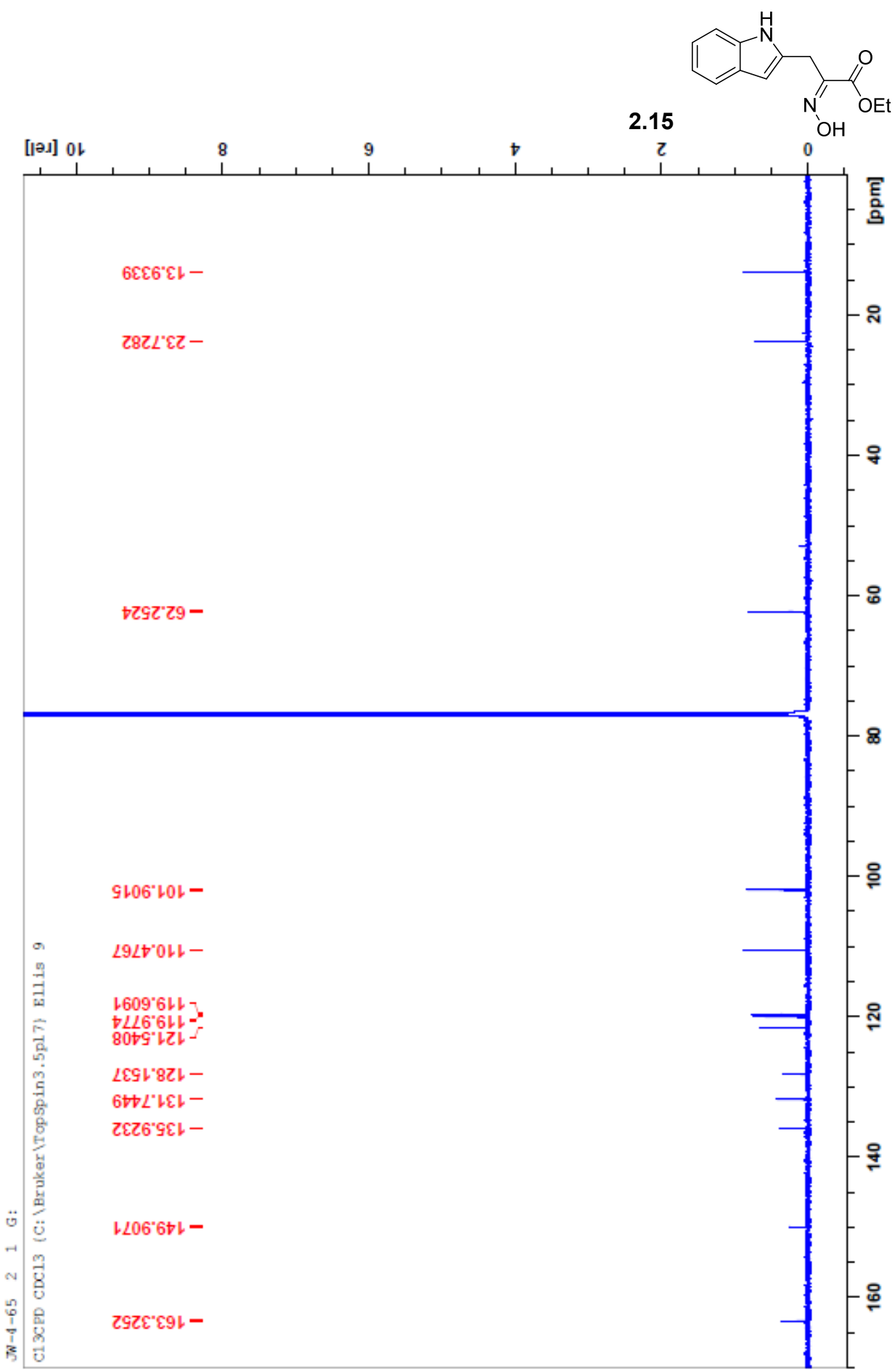
2.15
H
N
O
OEt
N
OH
[rel]
10
8
6
4
2
0
[ppm]
20
40
60
80
100
120
140
160
13.9339
23.7282
62.2524
101.9015
110.4767
119.6091
119.9774
121.5408
128.1537
131.7449
135.9232
149.9071
163.3252
JW-4-65 2 1 G:
C13CPD CDCl3 (C:\Bruker\TopSpin3.5pl7) Ellis 9

2.16

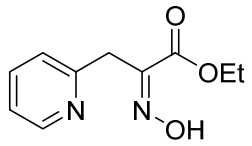
O
OEt
N
N
OH

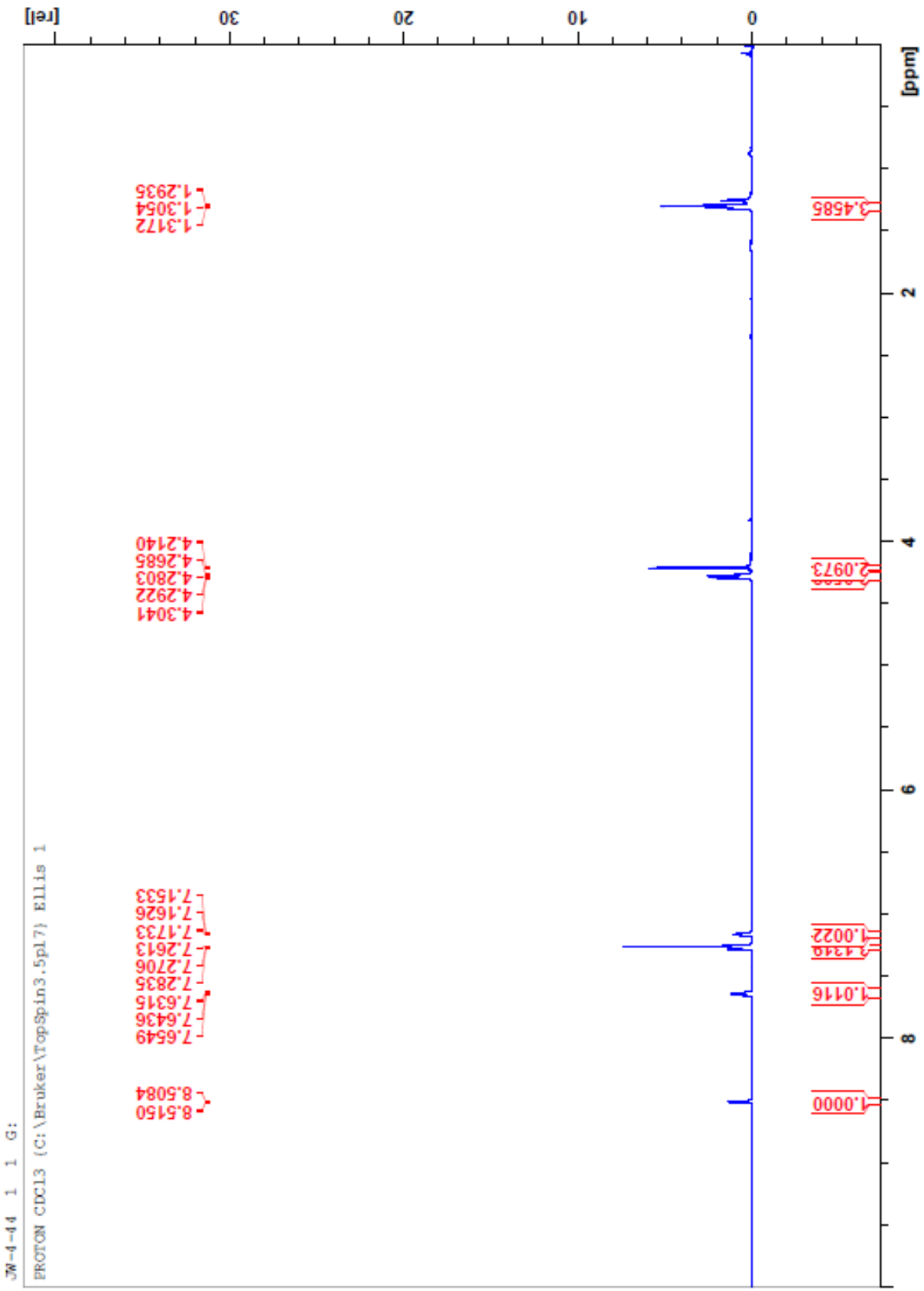
[rel]
30
20
10
0
[ppm]
2
4
6
8
1.2935
1.3054
1.3172
4.2140
4.2685
4.2803
4.2922
4.3041
7.1533
7.1626
7.1733
7.2613
7.2706
7.2835
7.6315
7.6436
7.6549
8.5084
8.5150
3.4585
2.0973
1.0022
1.0116
1.0000
JW-4-44 1 1 G:
PROTON CDCl3 (C:\Bruker\TopSpin3.5pl7) Ellis 1

2.16

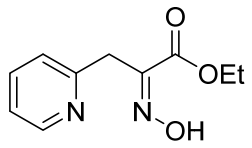
O
OEt
N
N
OH

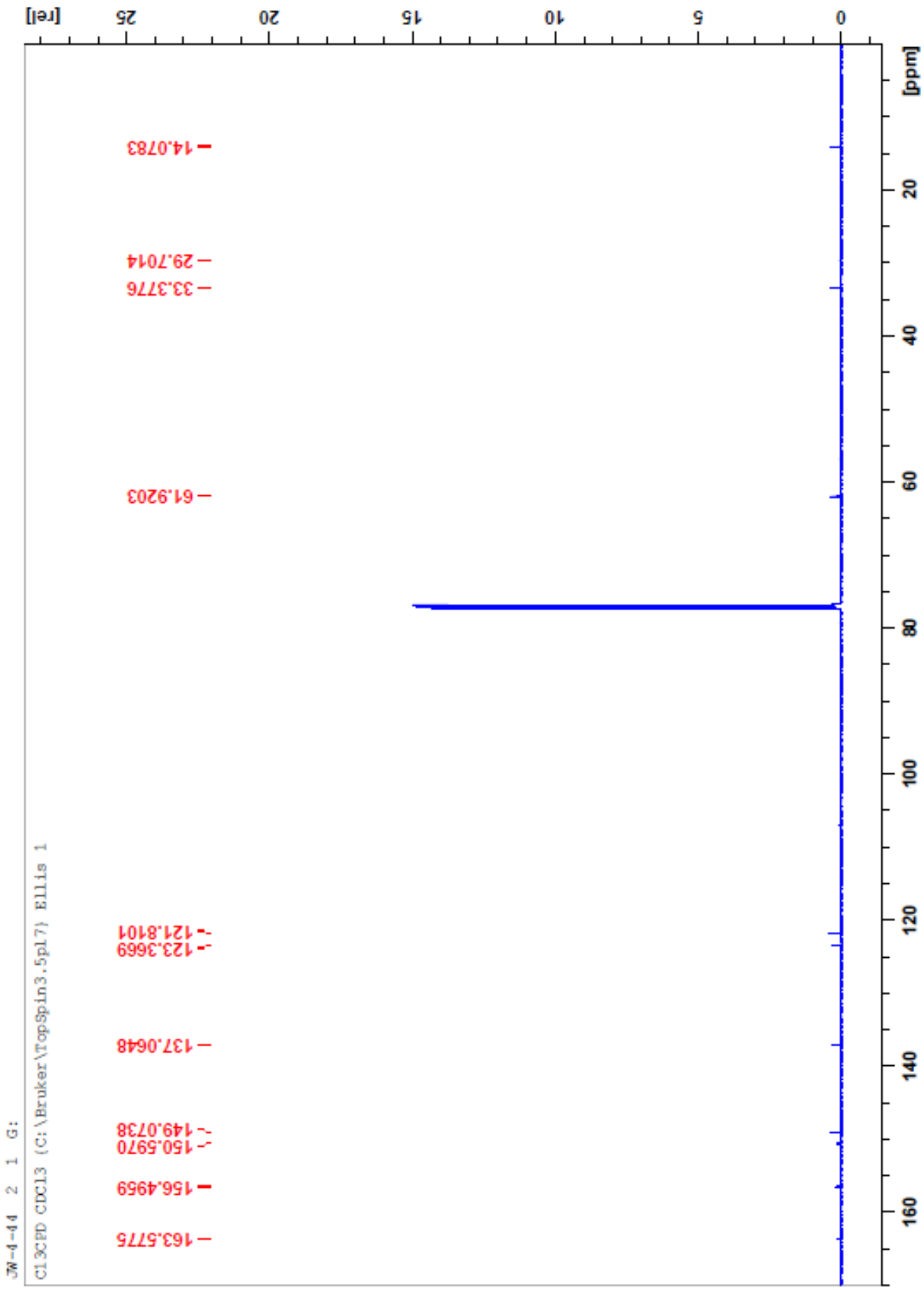
[rel]
25
20
15
10
5
0
[ppm]
20
40
60
80
100
120
140
160
14.0783
29.7014
33.3776
61.9203
121.8101
123.3669
137.0648
149.0738
150.5970
156.4959
163.5775
JW-4-44 2 1 G:
C13CPD CDCl3 (C:\Bruker\TopSpin3.5pl7) Ellis 1

2.17

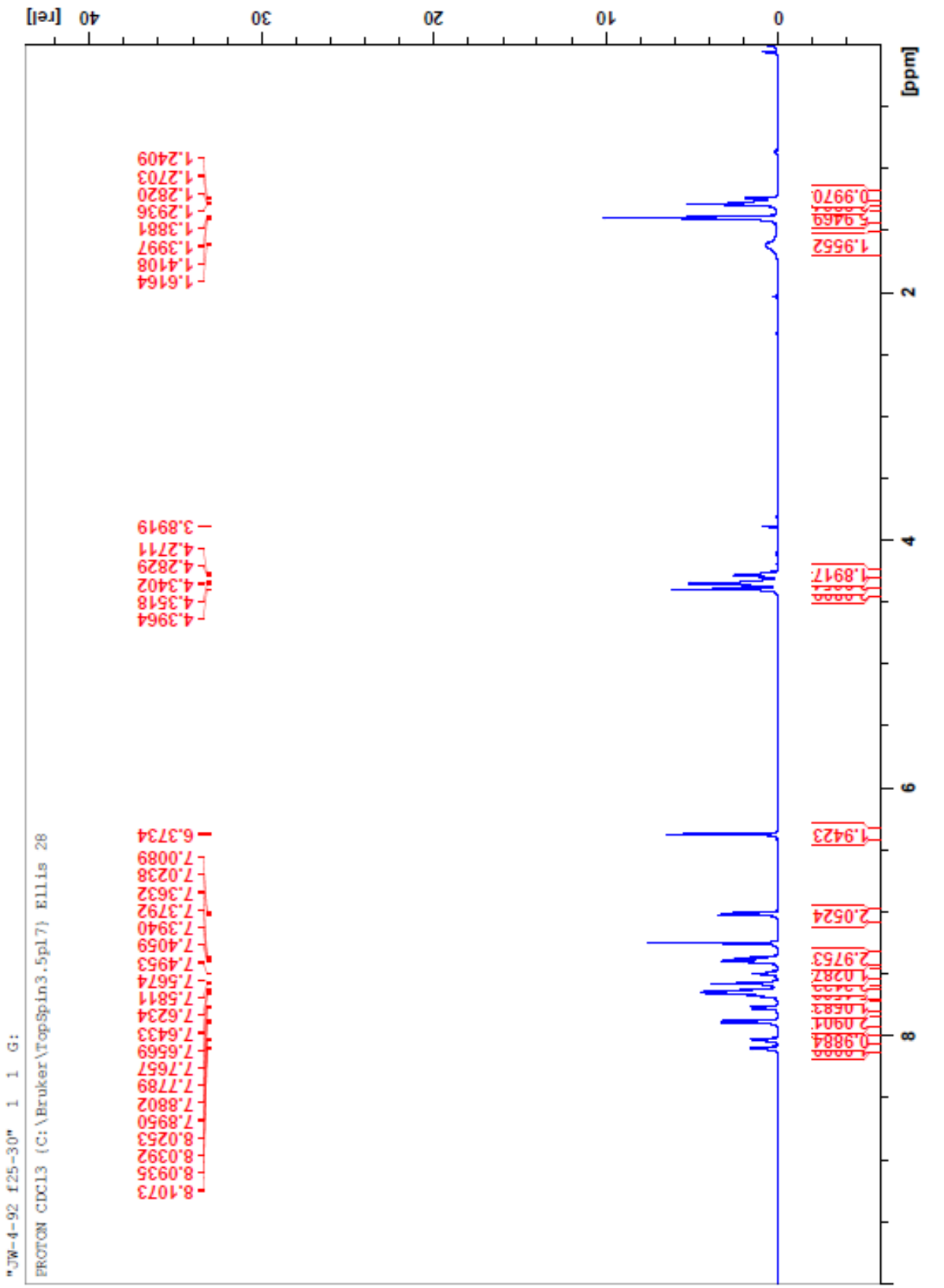
"JW-4-92 f25-30" 1 1 G:
PROTON CDCl3 (C:\Bruker\TopSpin3.5pl7) Ellis 28
[rel]
[ppm]

2.17

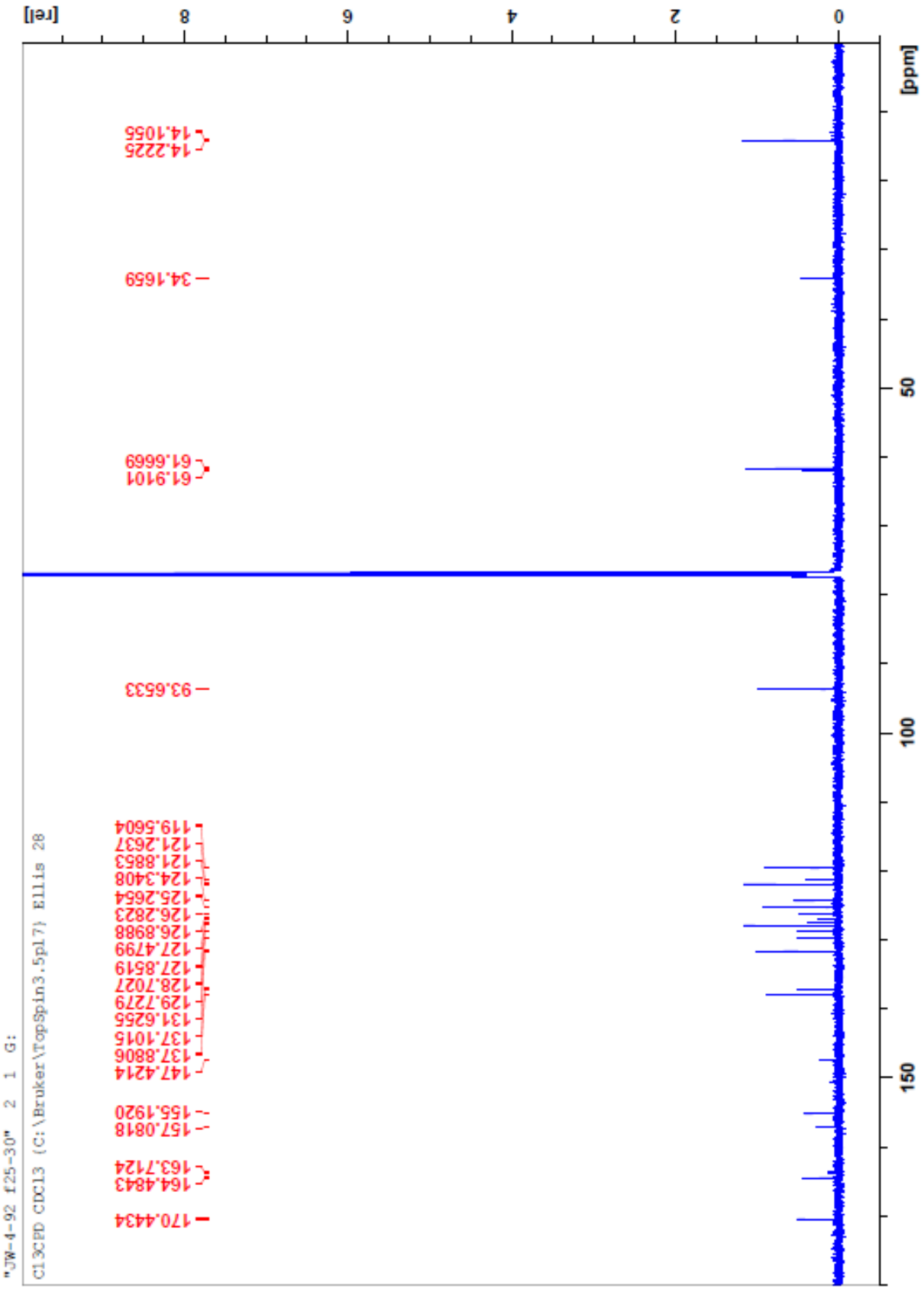
"JW-4-92 f25-30" 2 1 G:
C13CPD CDCl3 (C:\Bruker\TopSpin3.5pl7) Ellis 28
[rel]
[ppm]
14.2225
14.1055
34.1659
61.9101
61.6669
93.6533
119.5604
121.2637
121.8853
124.3408
125.2654
126.2823
126.8988
127.4799
127.8519
128.7027
129.7279
131.6255
137.1015
137.8806
147.4214
155.1920
157.0818
163.7124
164.4843
170.4434

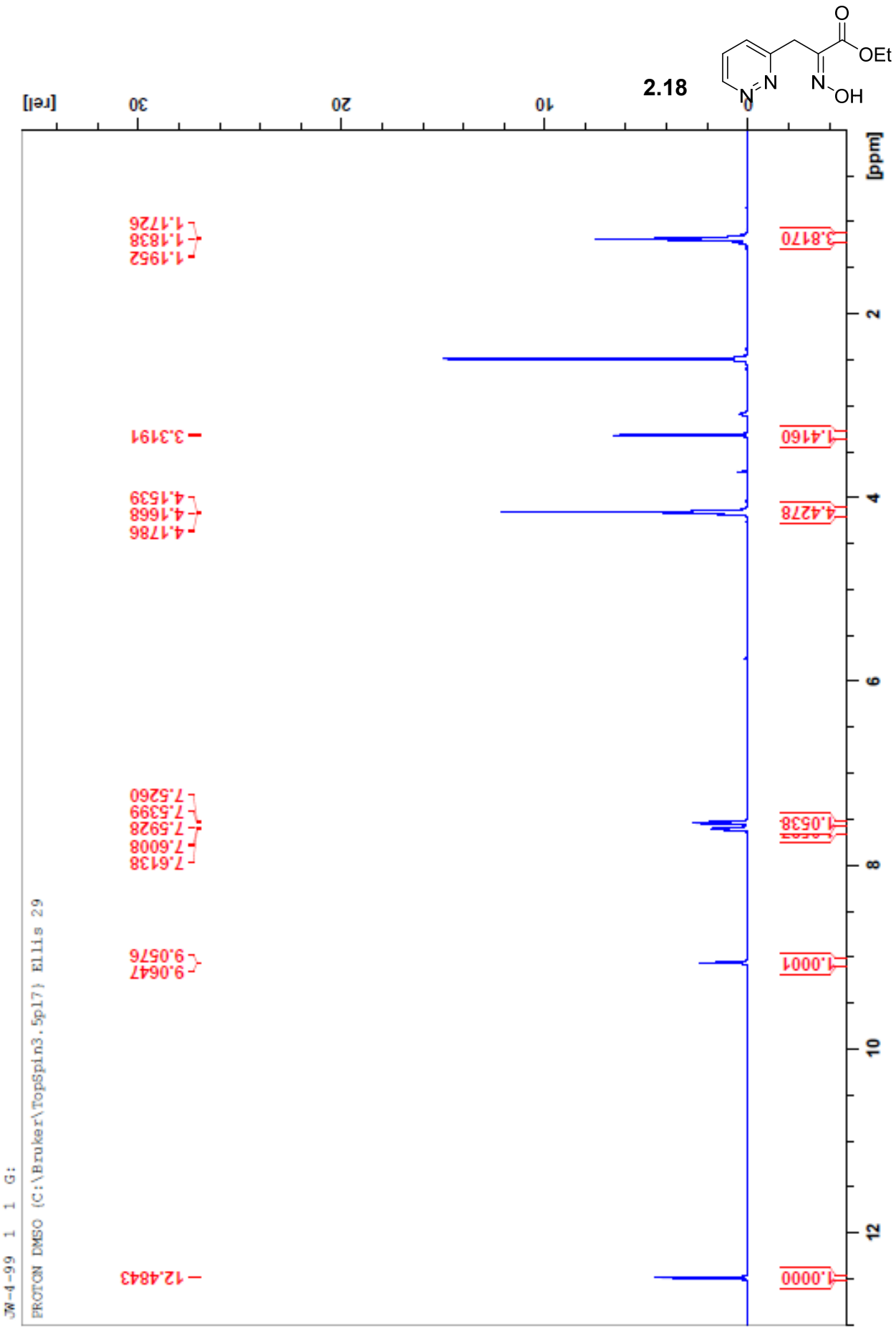
2.18
O
OEt
N
N
N
OH
[rel]
30
20
10
0
[ppm]
2
4
6
8
10
12
1.1726
1.1838
1.1952
3.3191
4.1539
4.1668
4.1786
7.5260
7.5399
7.5928
7.6008
7.6138
9.0576
9.0647
12.4843
3.8170
1.4160
4.4278
1.0538
1.0001
1.0000
JW-4-99 1 1 G:
PROTON DMSO (C:\Bruker\TopSpin3.5pl7) Ellis 29

2.18

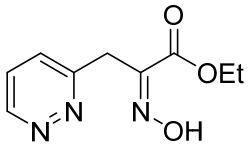
O
OEt
N
N
N
OH

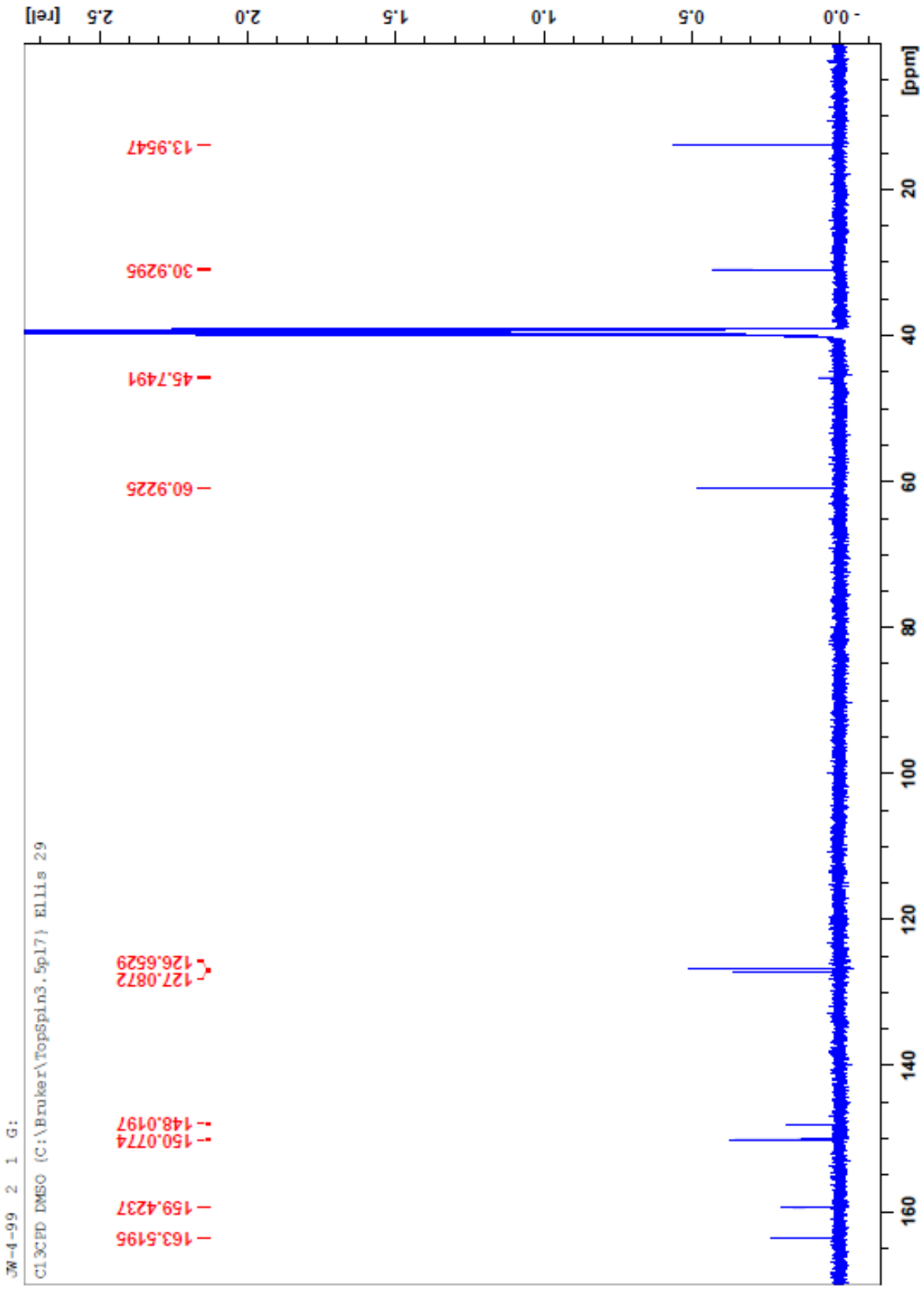
[rel]
2.5
2.0
1.5
1.0
0.5
0.0
[ppm]
20
40
60
80
100
120
140
160
13.9547
30.9295
45.7491
60.9225
126.6529
127.0872
148.0197
150.0774
159.4237
163.5195
JW-4-99 2 1 G:
C13CPD DMSO (C:\Bruker\TopSpin3.5pl7) Ellis 29

2.19

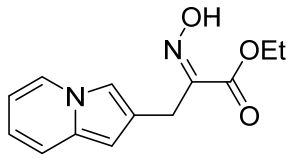
OH
N
OEt
N
O

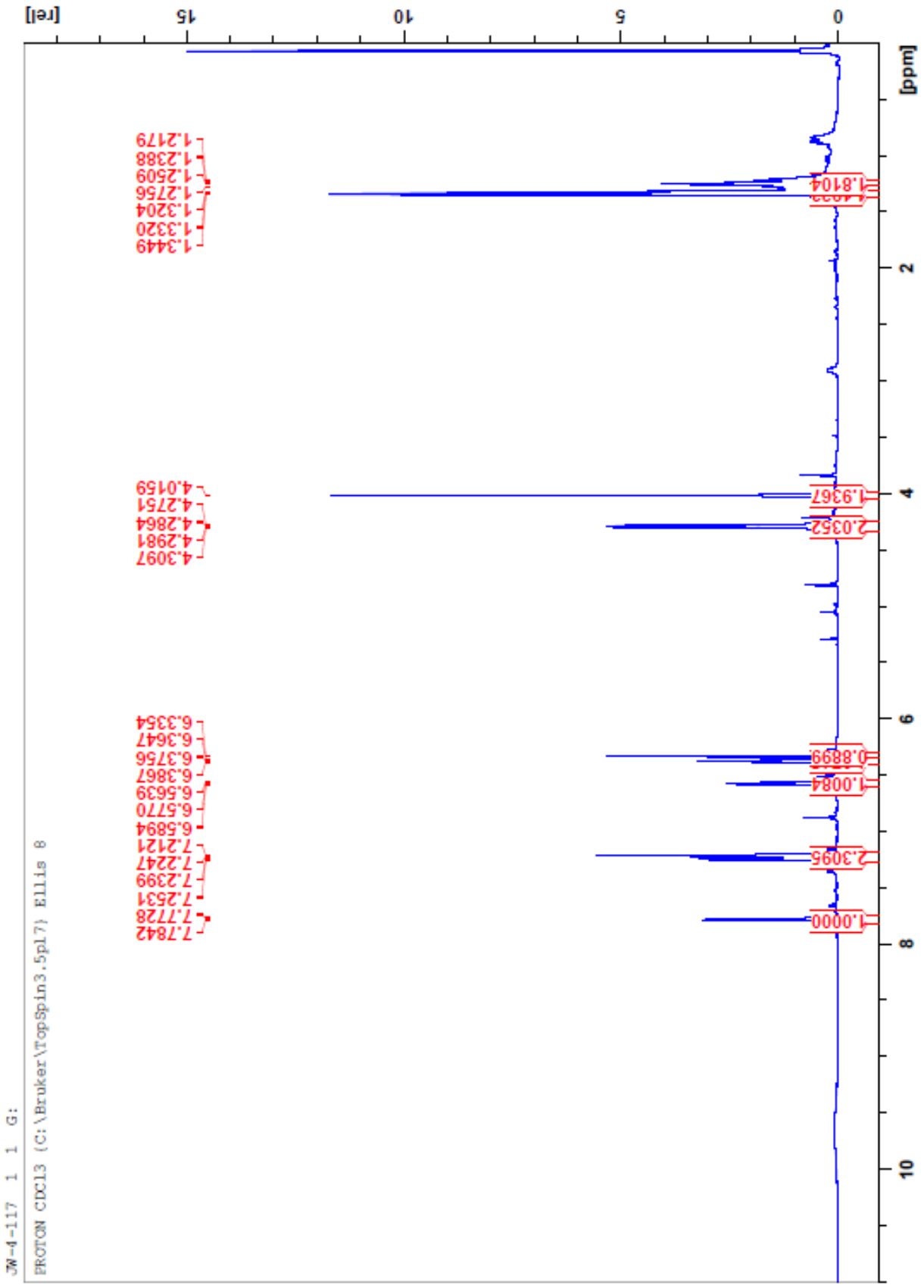
[rel]
15
10
5
0
[ppm]
2
4
6
8
10
1.2179
1.2388
1.2509
1.2756
1.3204
1.3320
1.3449
4.0159
4.2751
4.2864
4.2981
4.3097
6.3354
6.3647
6.3756
6.3867
6.5639
6.5770
6.5894
7.2121
7.2247
7.2399
7.2531
7.7728
7.7842
1.8104
1.9367
2.0362
0.8899
1.0084
2.3095
1.0000
JW-4-117 1 1 G:
PROTON CDCl3 (C:\Bruker\TopSpin3.5pl7) Ellis 8

2.19

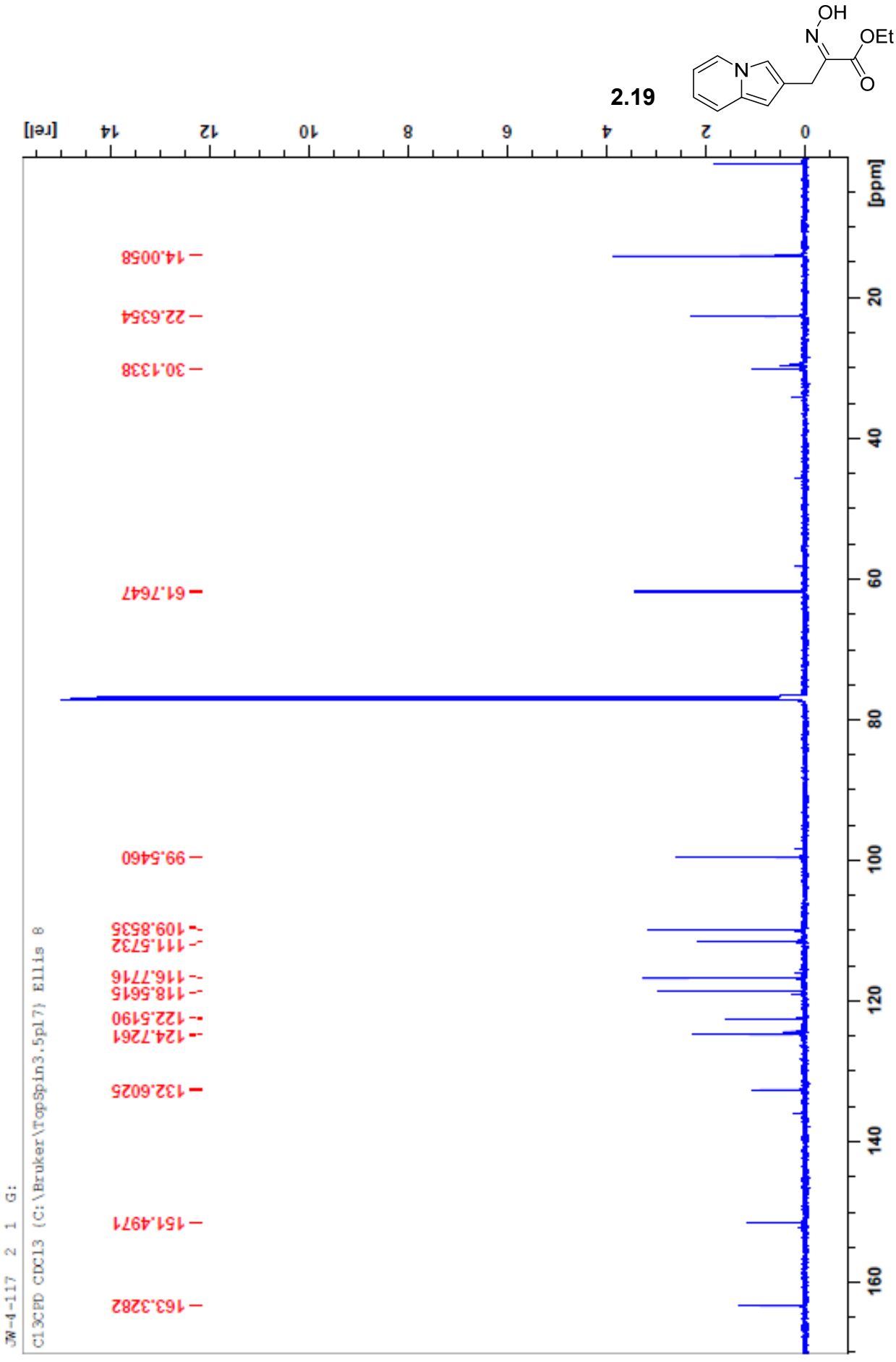
OH
N
OEt
O
N
[rel]
14
12
10
8
6
4
2
0
[ppm]
20
40
60
80
100
120
140
160
14.0058
22.6354
30.1338
61.7647
99.5460
109.8535
111.5732
116.7716
118.5615
122.5190
124.7261
132.6025
151.4971
163.3282
JW-4-117 2 1 G:
C13CPD CDCl3 (C:\Bruker\TopSpin3.5pl7) Ellis 8

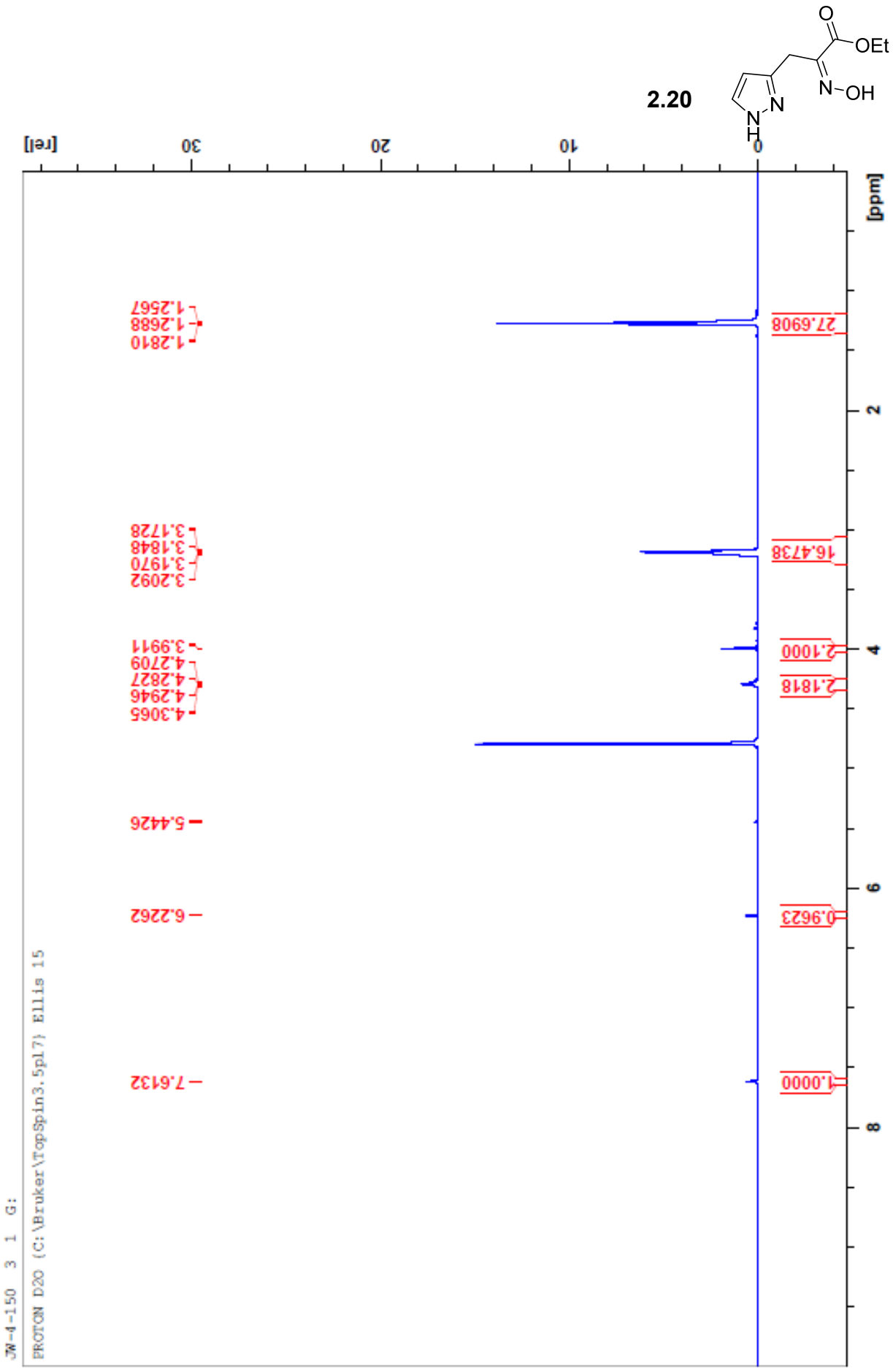
2.20
O
OEt
N-OH
N
N
H
[rel]
0
10
20
30
[ppm]
2
4
6
8
27.6908
16.4738
2.1000
2.1818
0.9623
1.0000
1.2567
1.2688
1.2810
3.1728
3.1848
3.1970
3.2092
3.9911
4.2709
4.2827
4.2946
4.3065
5.4426
6.2262
7.6132
JW-4-150 3 1 G:
PROTON D2O (C:\Bruker\TopSpin3.5pl7) Ellis 15

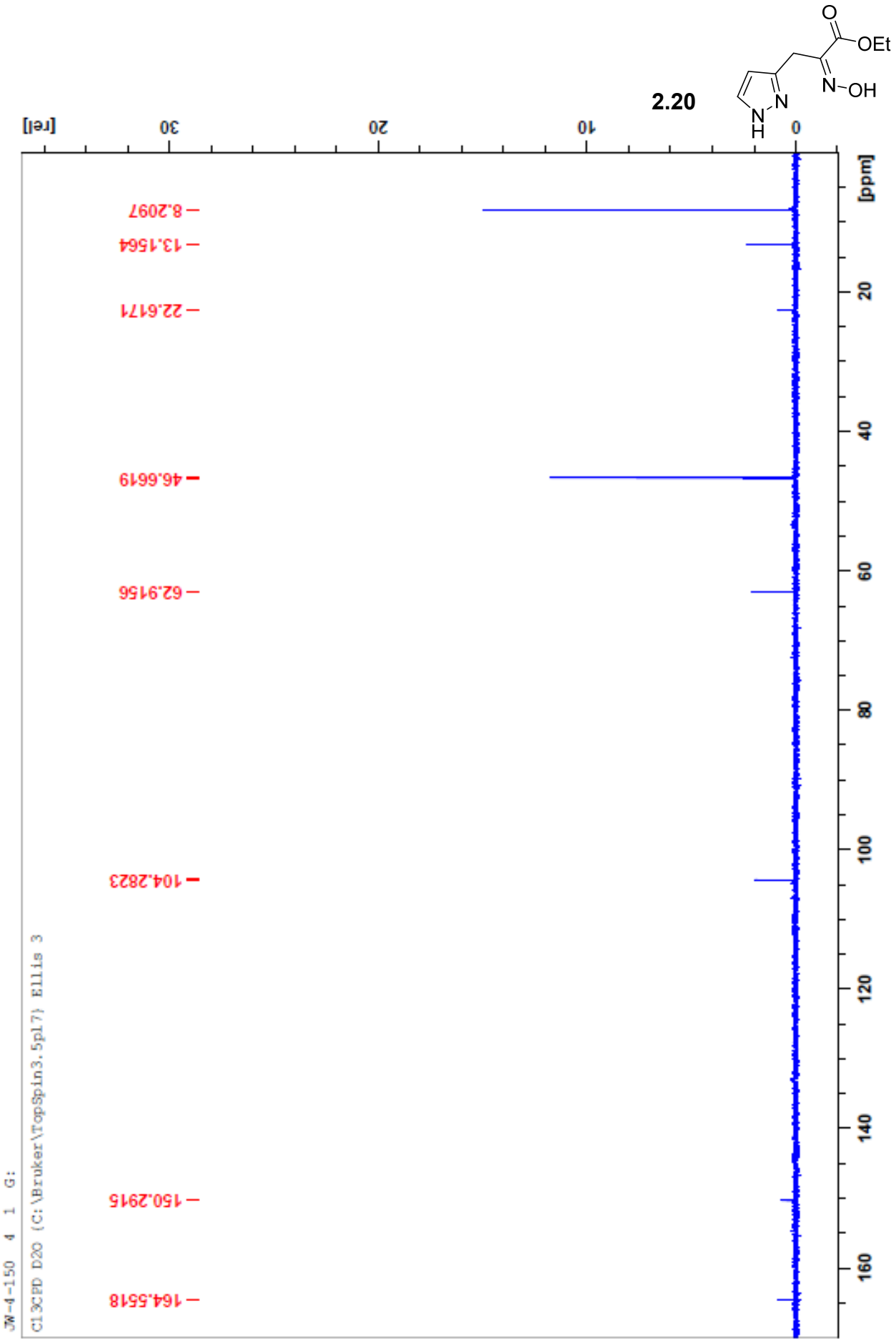
2.20
O
OEt
N-OH
N
N
H
[rel]
30
20
10
0
[ppm]
20
40
60
80
100
120
140
160
8.2097
13.1564
22.6171
46.6619
62.9156
104.2823
150.2915
164.5518
JW-4-150 4 1 G:
C13CPD D2O (C:\Bruker\TopSpin3.5pl7) Ellis 3

2.21

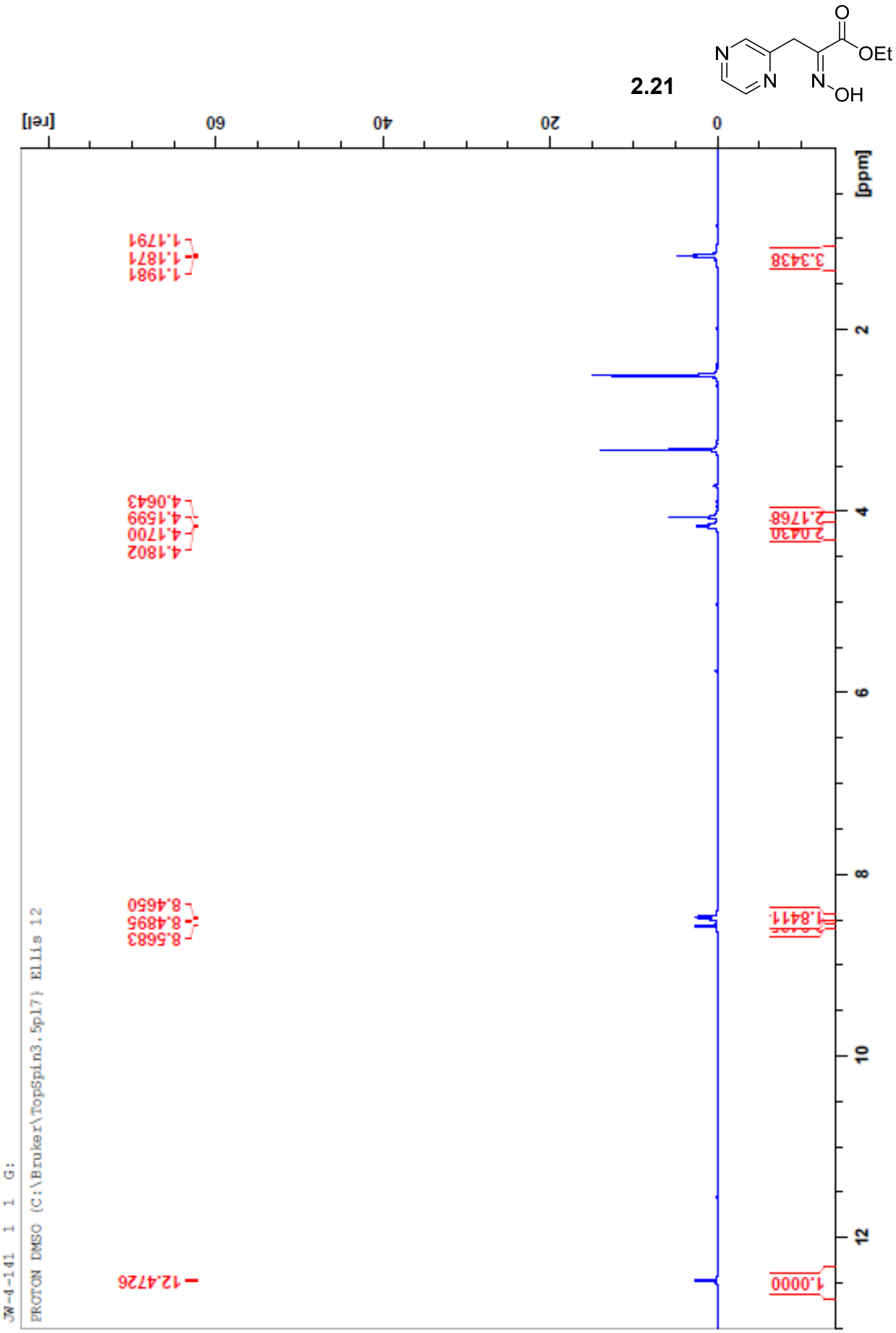
JW-4-141 1 1 G:
PROTON DMSO (C:\Bruker\TopSpin3.5pl7) Ellis 12
12.4726
8.5683
8.4895
8.4650
4.1802
4.1700
4.1599
4.0643
1.1981
1.1871
1.1791
1.8411
2.1768
3.3438
1.0000
[rel]
[ppm]

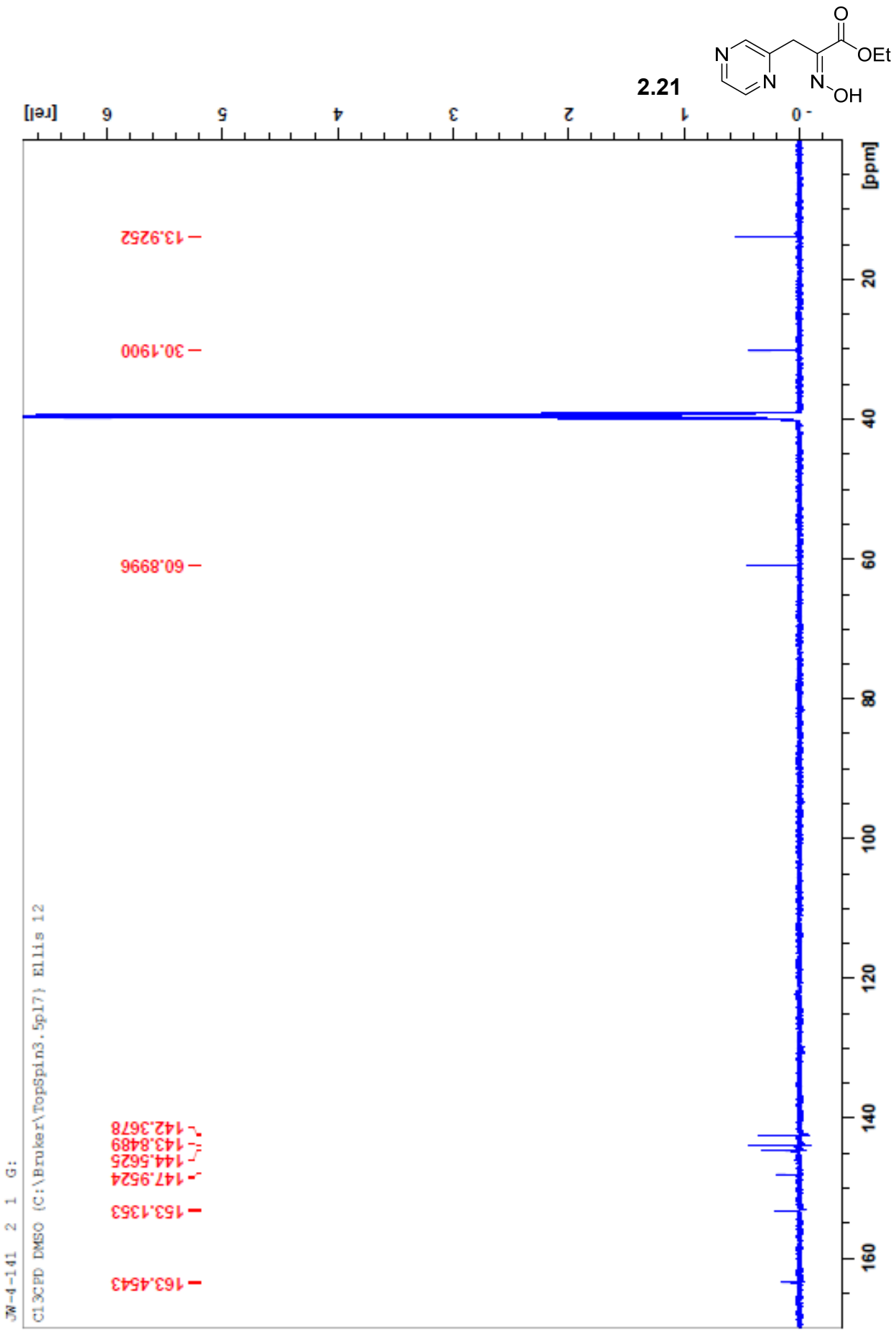
2.21
O
OEt
N
N
N
OH
[rel]
0
1
2
3
4
5
6
[ppm]
20
40
60
80
100
120
140
160
13.9252
30.1900
60.8996
142.3678
143.8489
144.5625
147.9524
153.1353
163.4543
JW-4-141 2 1 G:
C13CPD DMSO (C:\Bruker\TopSpin3.5pl7) Ellis 12

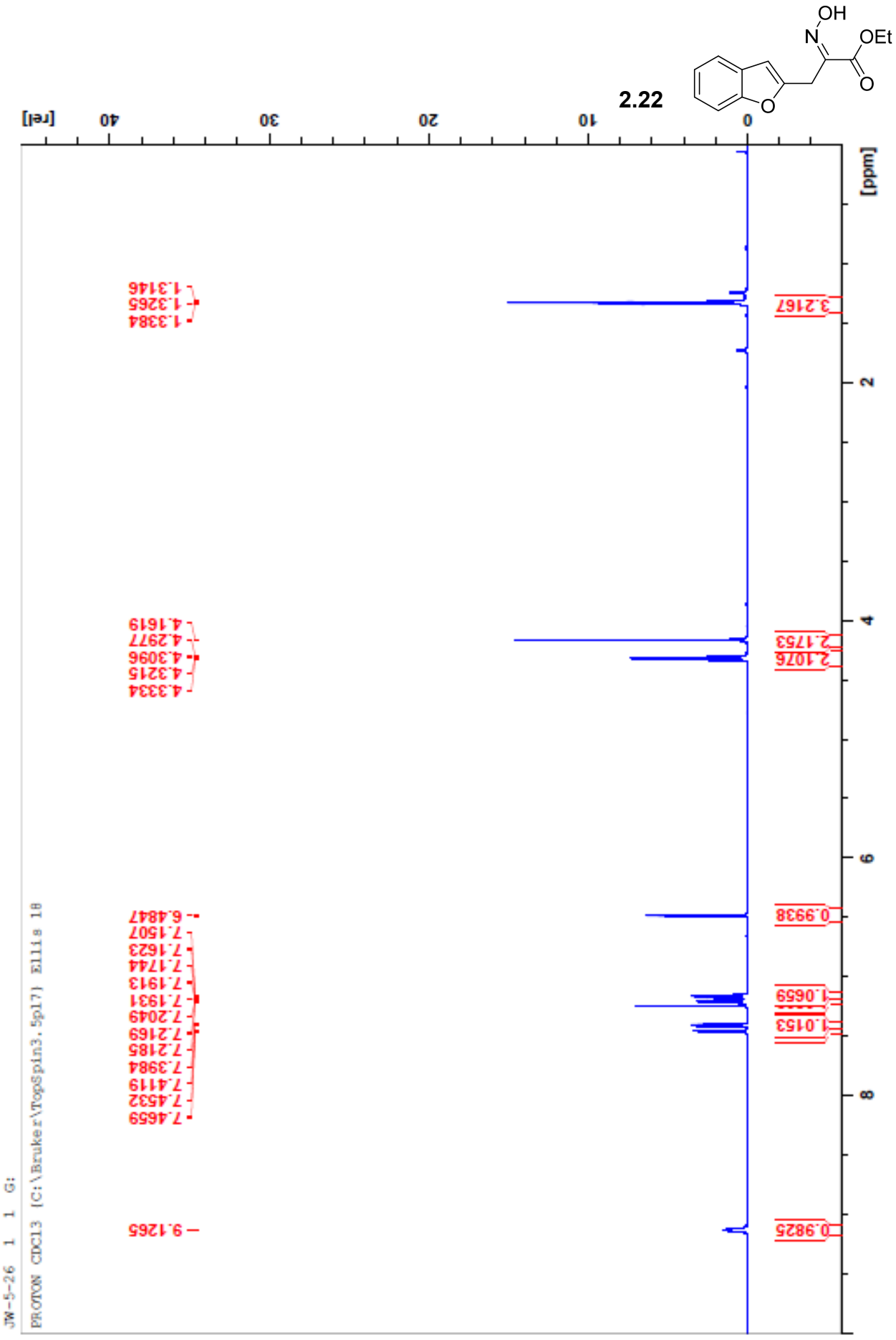
2.22
OH
N
OEt
O
O
[rel]
40
30
20
10
0
[ppm]
2
4
6
8
1.3146
1.3265
1.3384
3.2167
4.1619
4.2977
4.3096
4.3215
4.3334
2.1753
2.1076
6.4847
0.9938
7.1507
7.1623
7.1744
7.1913
7.1931
7.2049
7.2169
7.2185
7.3984
7.4119
7.4532
7.4659
1.0659
1.0153
9.1265
0.9825
JW-5-26 1 1 G:
PROTON CDCl3 [C:\Bruker\TopSpin3.5pl7] E111a 18

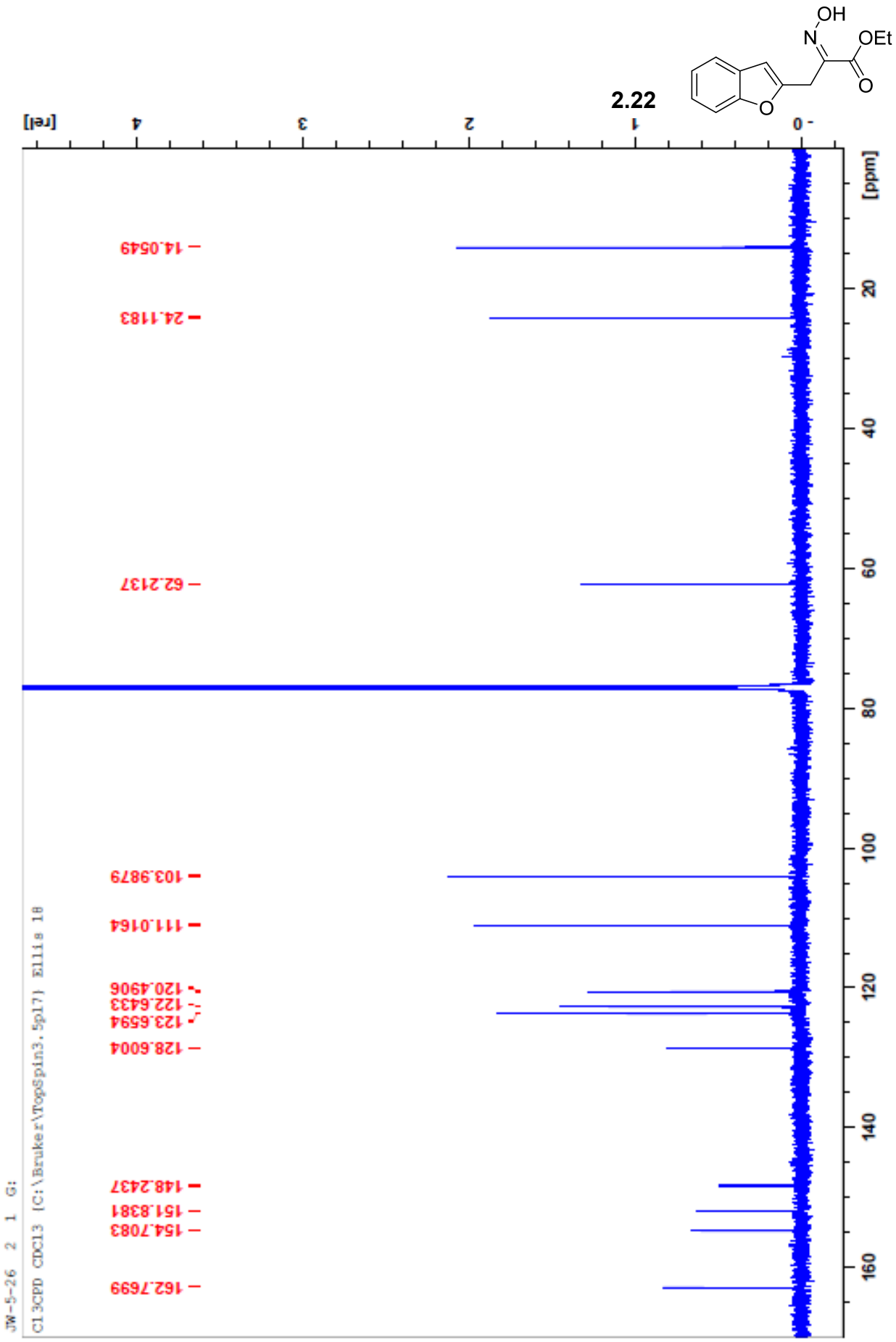
2.22
OH
N
OEt
O
O
[rel]
[ppm]
14.0549
24.1183
62.2137
103.9879
111.0164
120.4906
122.6433
123.6594
128.6004
148.2437
151.8381
154.7083
162.7699
JW-5-26 2 1 G:
C13CPD CDCl3 (C:\Bruker\TopSpin3.5pl7) E111s 18

2.23

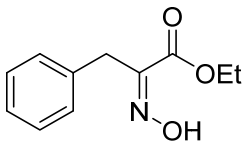
O
OEt
N
OH

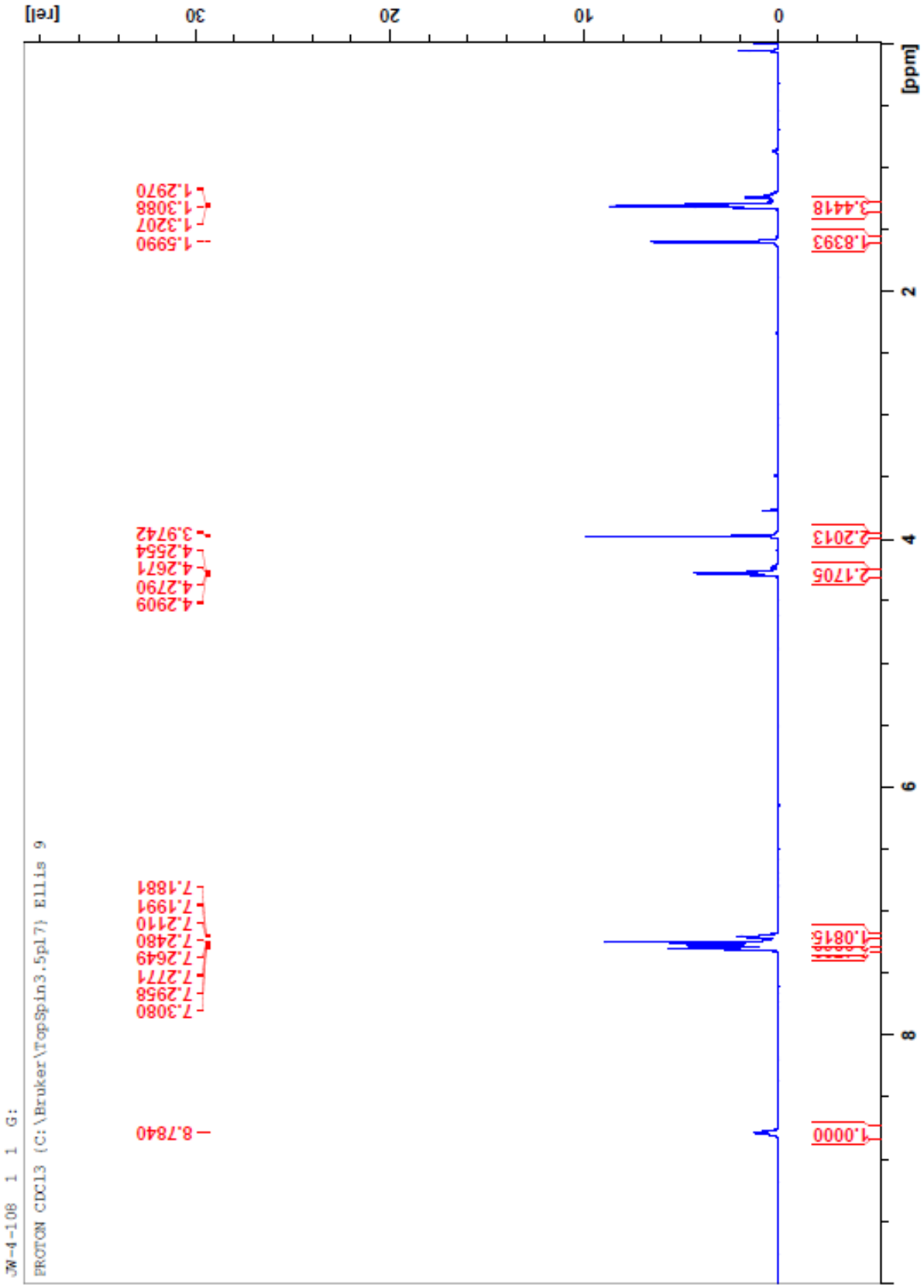
[rel]
30
20
10
0
[ppm]
2
4
6
8
1.0000
1.0815
1.8393
3.4418
2.2013
2.1705
1.5990
1.3207
1.3088
1.2970
8.7840
7.3080
7.2958
7.2771
7.2649
7.2480
7.2110
7.1991
7.1881
4.2909
4.2790
4.2671
4.2554
3.9742
JW-4-108 1 1 G:
PROTON CDCl3 (C:\Bruker\TopSpin3.5pl7) Ellis 9

2.23

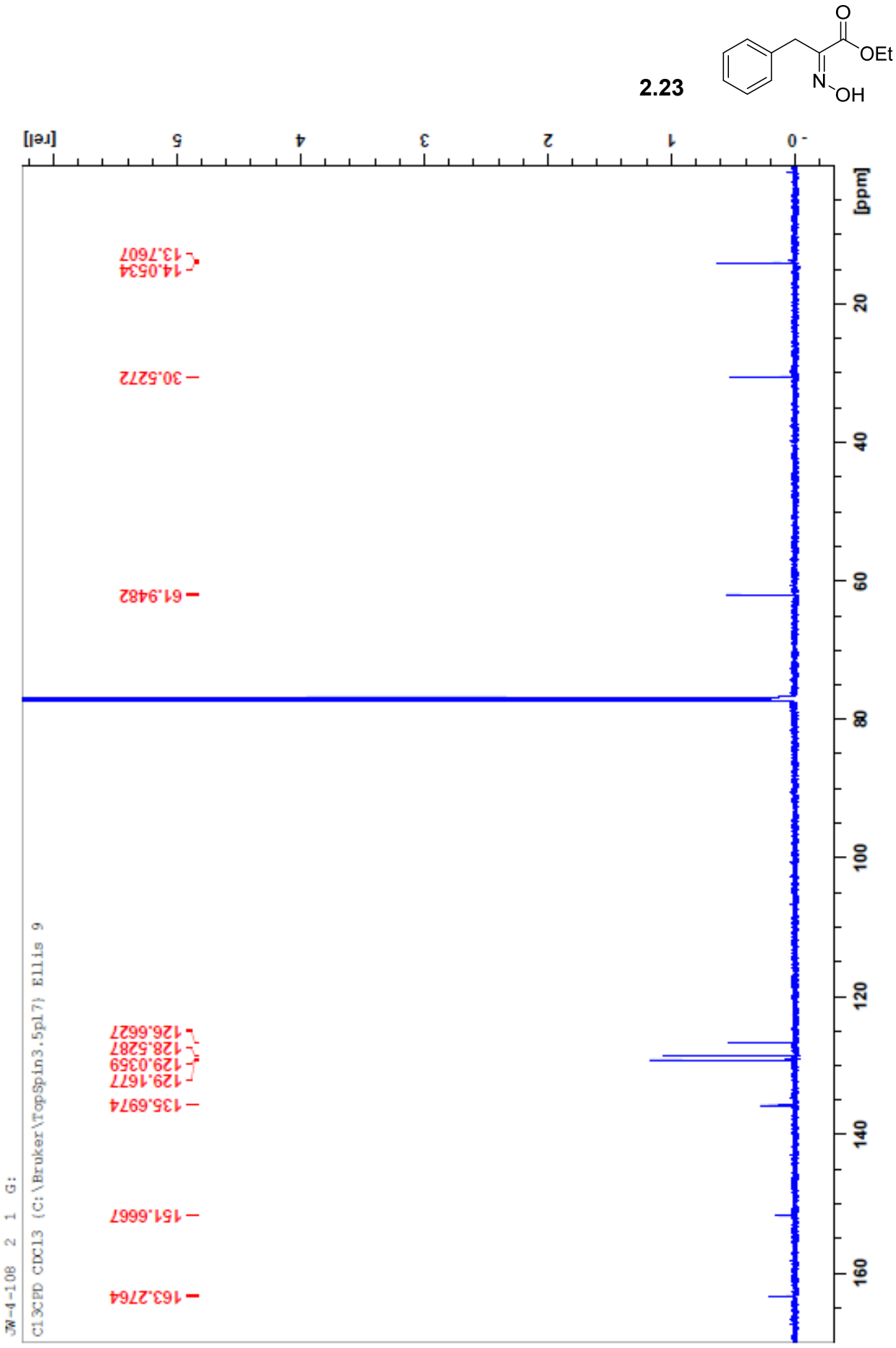
O
OEt
N
OH
[rel]
[ppm]
13.7607
14.0534
30.5272
61.9482
126.6627
128.5287
129.0359
129.1677
135.6974
151.6667
163.2764
JW-4-108 2 1 G:
C13CPD CDCl3 (C:\Bruker\TopSpin3.5pl7) Ellis 9

2.24

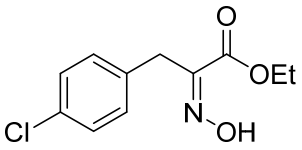
O
OEt
N
OH
Cl

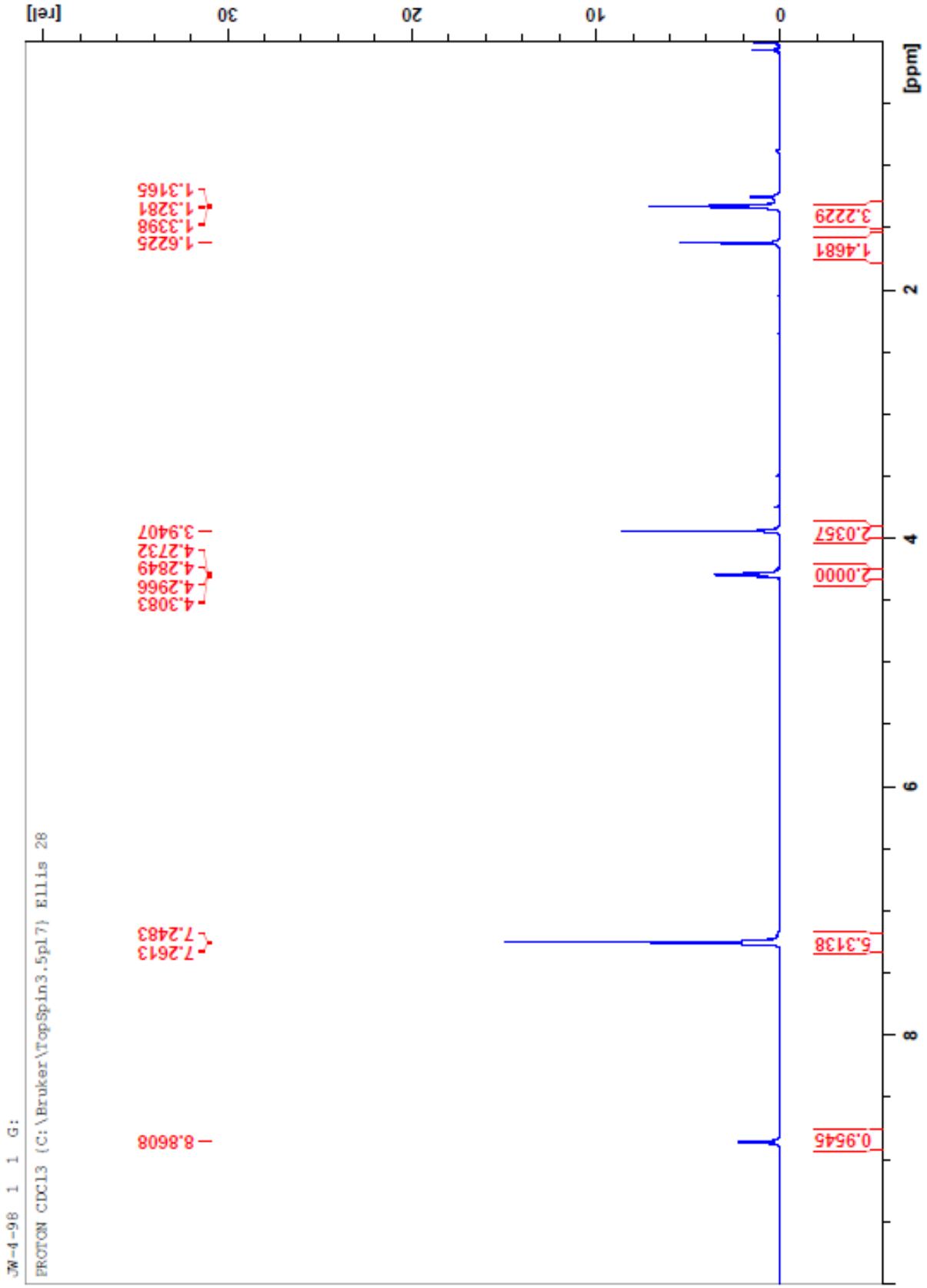
[rel]
30
20
10
0
[ppm]
2
4
6
8
1.3165
1.3281
1.3398
1.6225
3.9407
4.2732
4.2849
4.2966
4.3083
7.2613
7.2483
8.8608
3.2229
1.4681
2.0357
2.0000
5.3138
0.9545
JW-4-98 1 1 G:
PROTON CDCl3 (C:\Bruker\TopSpin3.5pl7) Ellis 28

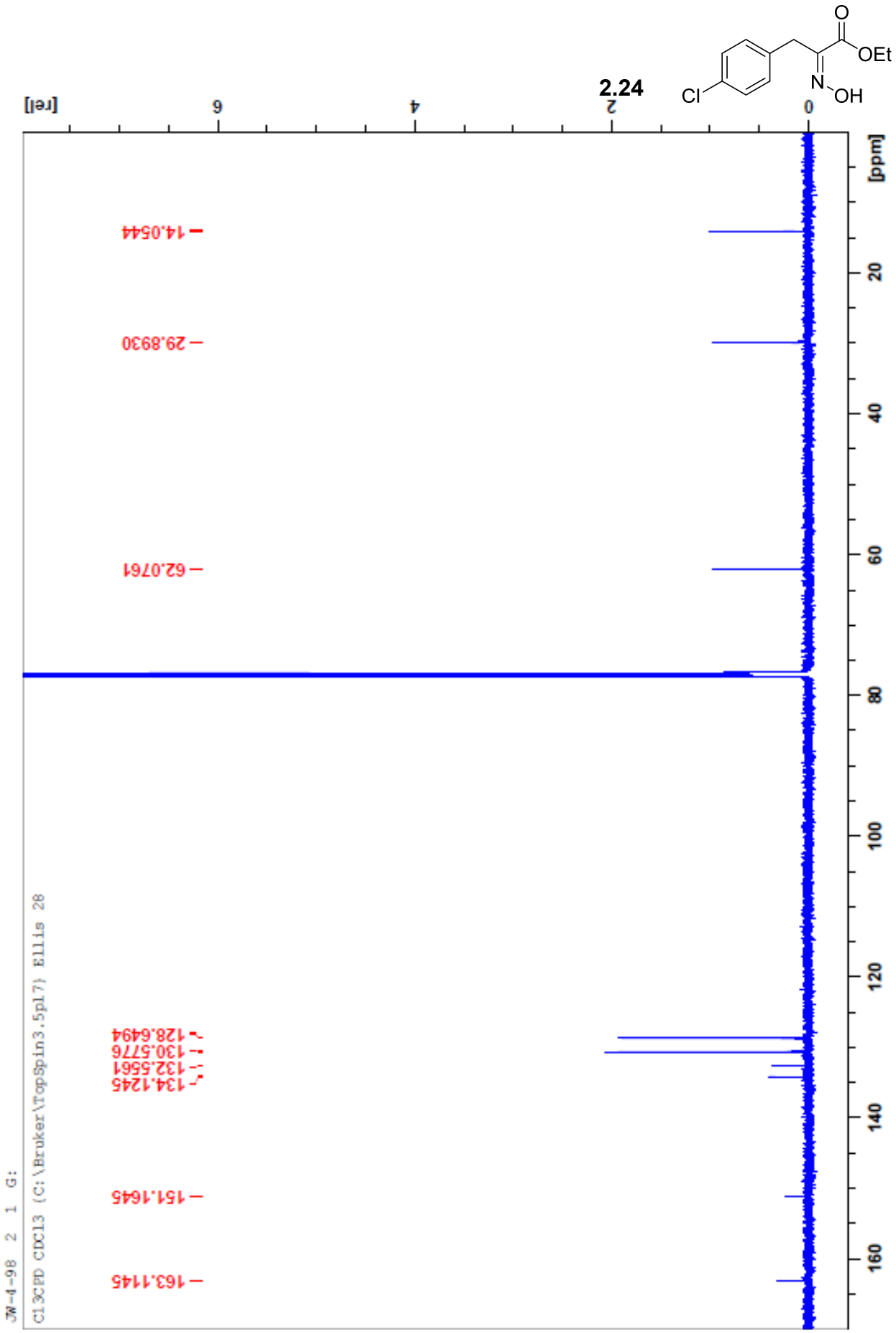
2.24
Cl
O
OEt
N
OH
[rel]
[ppm]
14.0544
29.8930
62.0761
128.6494
130.5776
132.5561
134.1245
151.1645
163.1145
JW-4-98 2 1 G:
C13CPD CDCl3 (C:\Bruker\TopSpin3.5pl7) Ellis 28

2.25

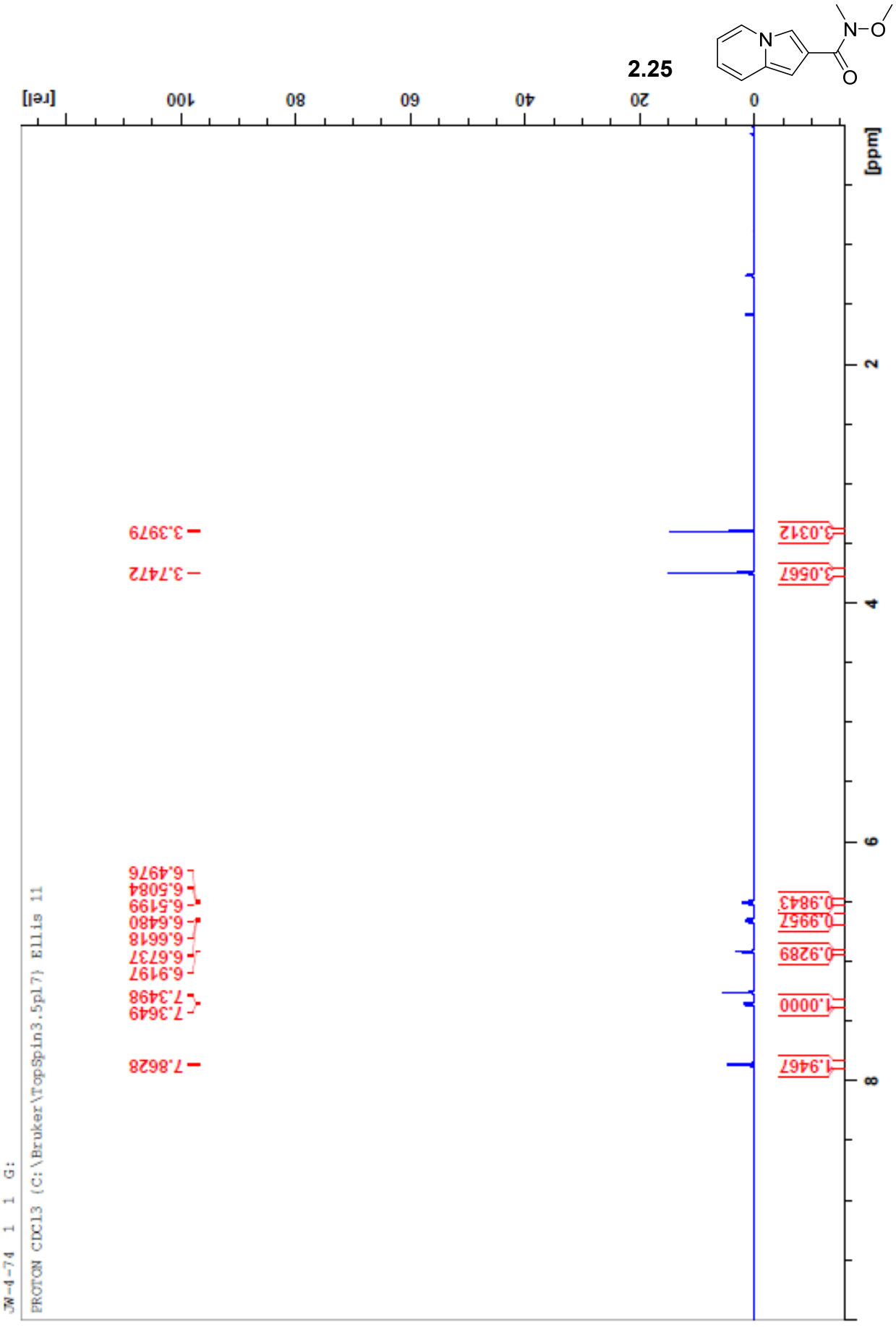
N
N–O
O
[rel]
100
80
60
40
20
0
[ppm]
2
4
6
8
3.3979
3.7472
6.4976
6.5084
6.5199
6.6480
6.6618
6.6737
6.9197
7.3498
7.3649
7.8628
3.0312
3.0567
0.9843
0.9957
0.9289
1.0000
1.9467
JW-4-74 1 1 G:
PROTON CDCl3 (C:\Bruker\TopSpin3.5pl7) Ellis 11

2.25

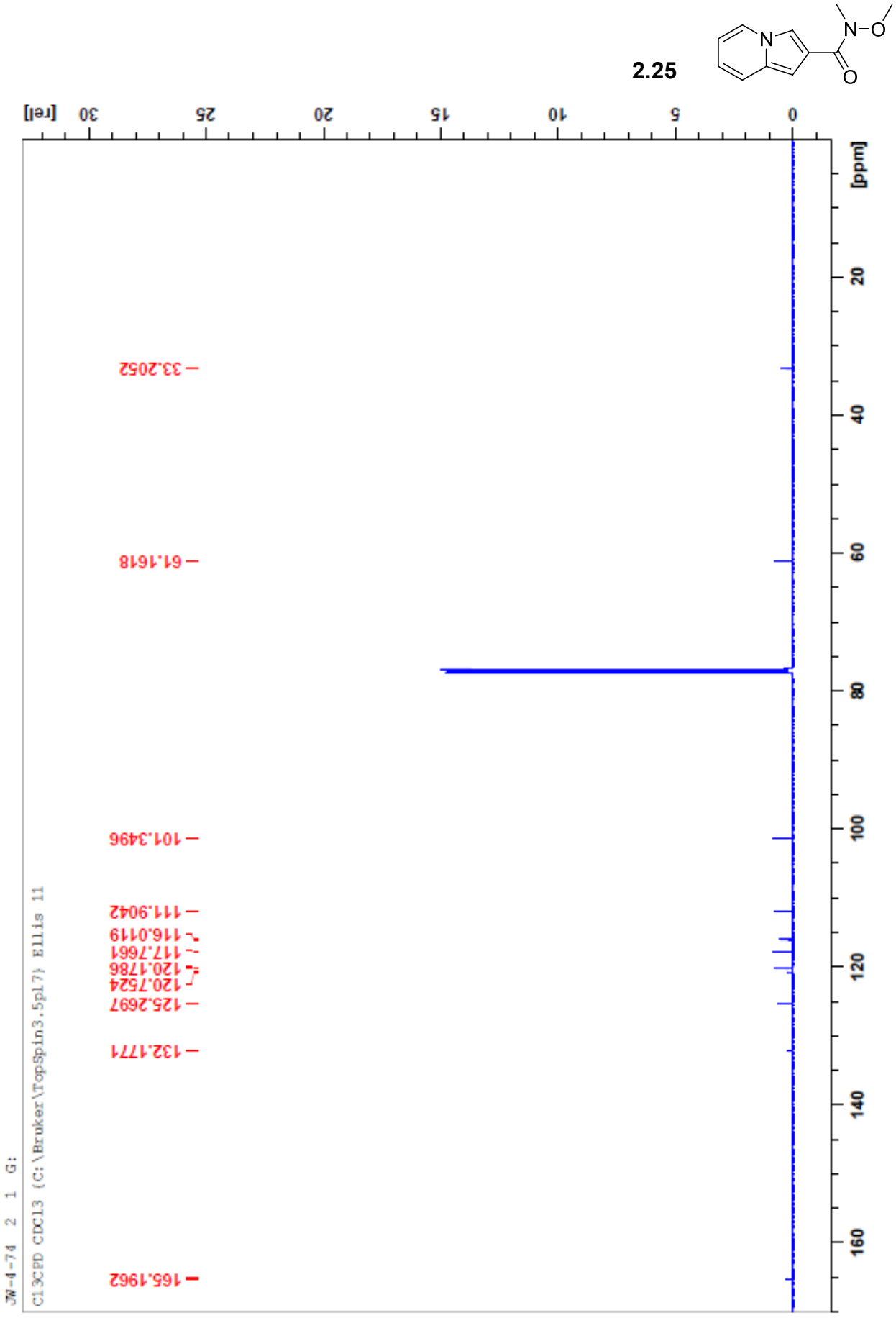
[rel]
30
25
20
15
10
5
0
[ppm]
20
40
60
80
100
120
140
160
33.2052
61.1618
101.3496
111.9042
116.0119
117.7661
120.1786
120.7524
125.2697
132.1771
165.1962
JW-4-74 2 1 G:
C13CPD CDCl3 (C:\Bruker\TopSpin3.5pl7) Ellis 11

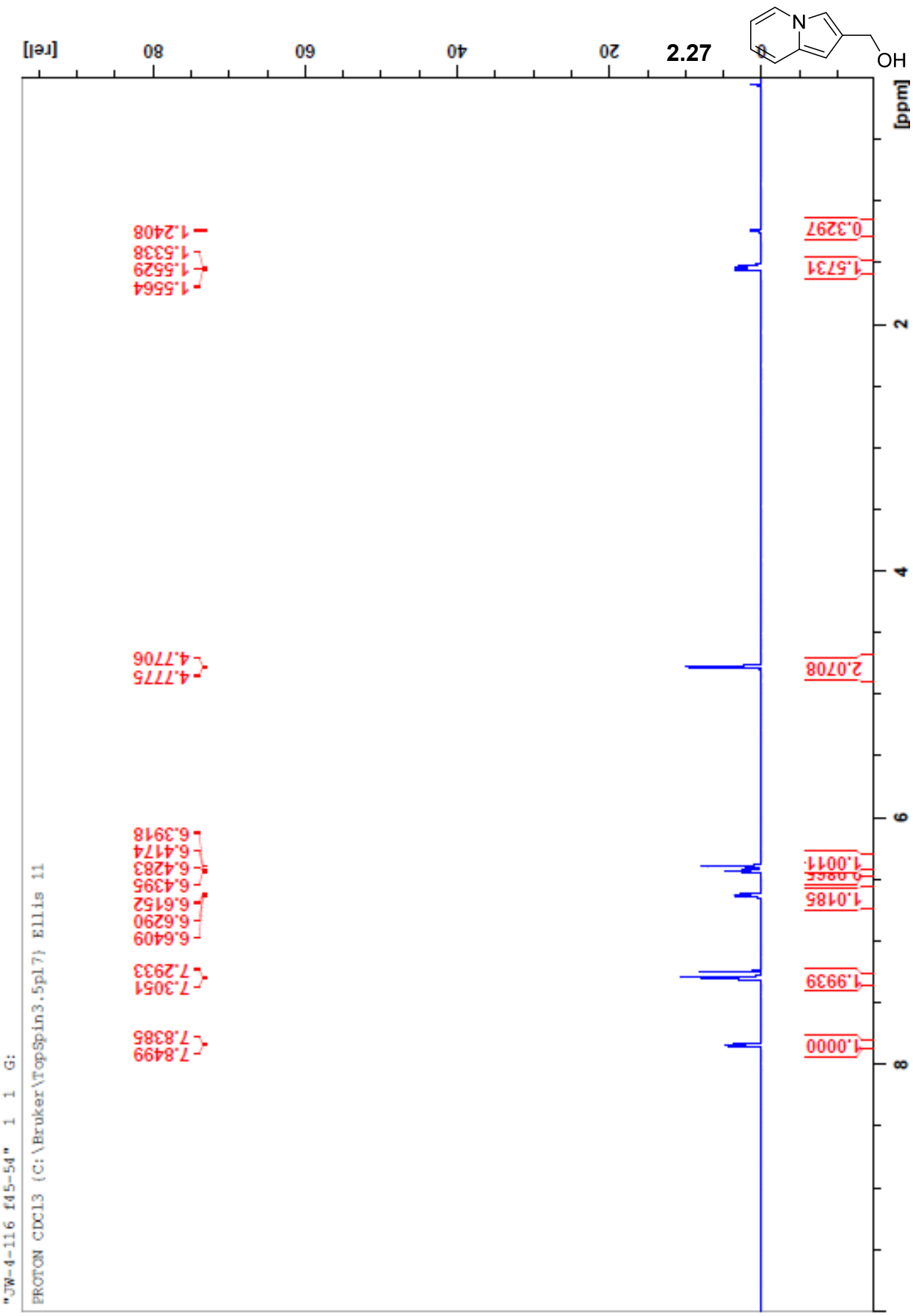
"JW-4-116 f45-54" 1 1 G:
PROTON CDCl3 (C:\Bruker\TopSpin3.5pl7) Ellis 11
[rel]
80
60
40
20
2.27
0
[ppm]
2
4
6
8
OH
N
1.2408
1.5338
1.5529
1.5564
4.7706
4.7775
6.3918
6.4174
6.4283
6.4395
6.6152
6.6290
6.6409
7.2933
7.3051
7.8385
7.8499
0.3297
1.5731
2.0708
1.0011
0.9856
1.0185
1.9939
1.0000

2.27

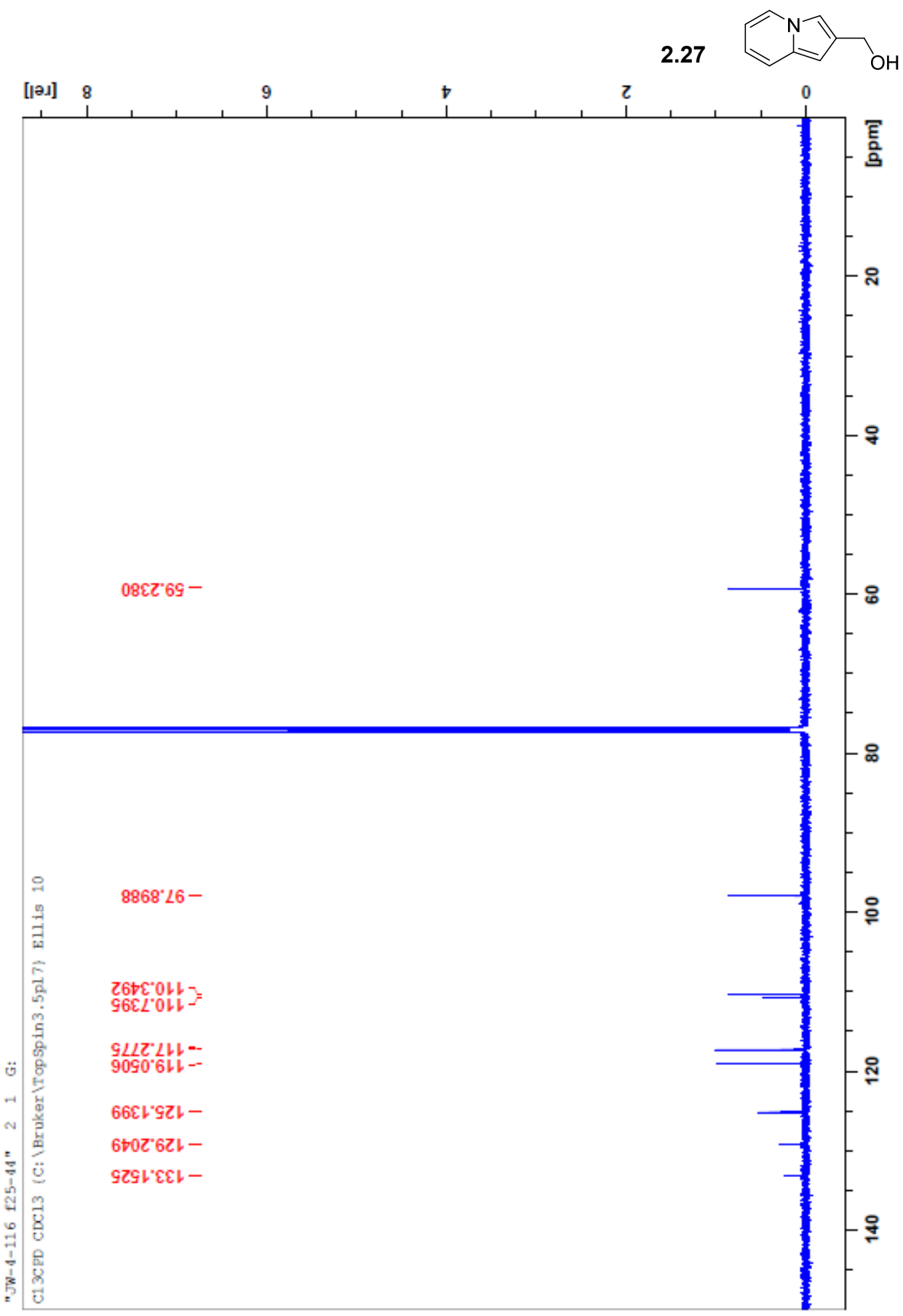
N
OH
[rel]
8
6
4
2
0
[ppm]
20
40
60
80
100
120
140
59.2380
97.8988
110.3492
110.7395
117.2775
119.0506
125.1399
129.2049
133.1525
"JW-4-116 f25-44" 2 1 G:
C13CPD CDCl3 (C:\Bruker\TopSpin3.5pl7) Ellis 10

2.26

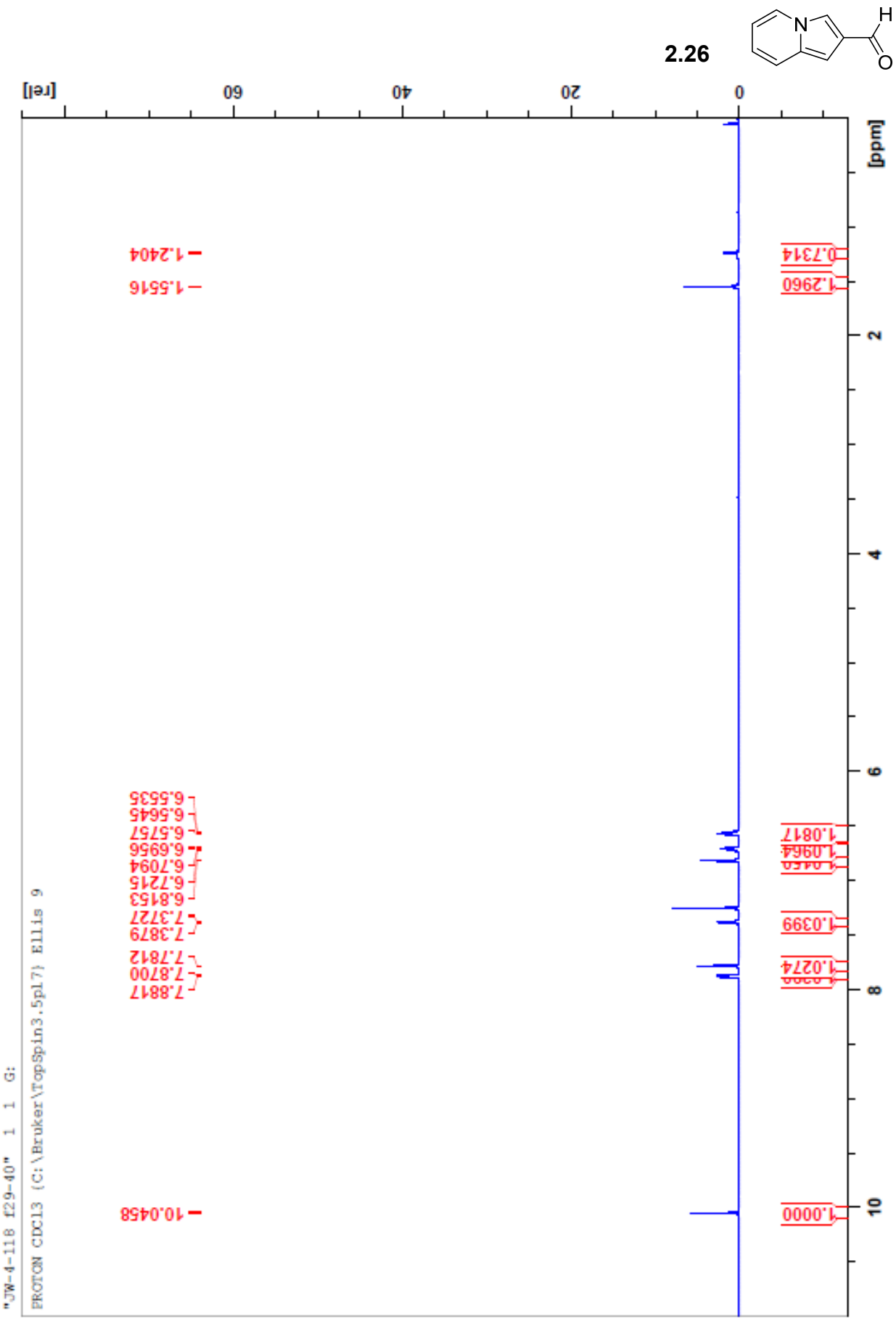
"JW-4-118 f29-40" 1 1 G:
PROTON CDCl3 (C:\Bruker\TopSpin3.5pl7) Ellis 9
[rel]
[ppm]
10.0458
7.8817
7.8700
7.7812
7.3879
7.3727
6.8153
6.7215
6.7094
6.6956
6.5757
6.5645
6.5535
1.5516
1.2404
1.0000
1.0399
1.0274
1.0817
1.0964
1.2960
0.7314

2.26

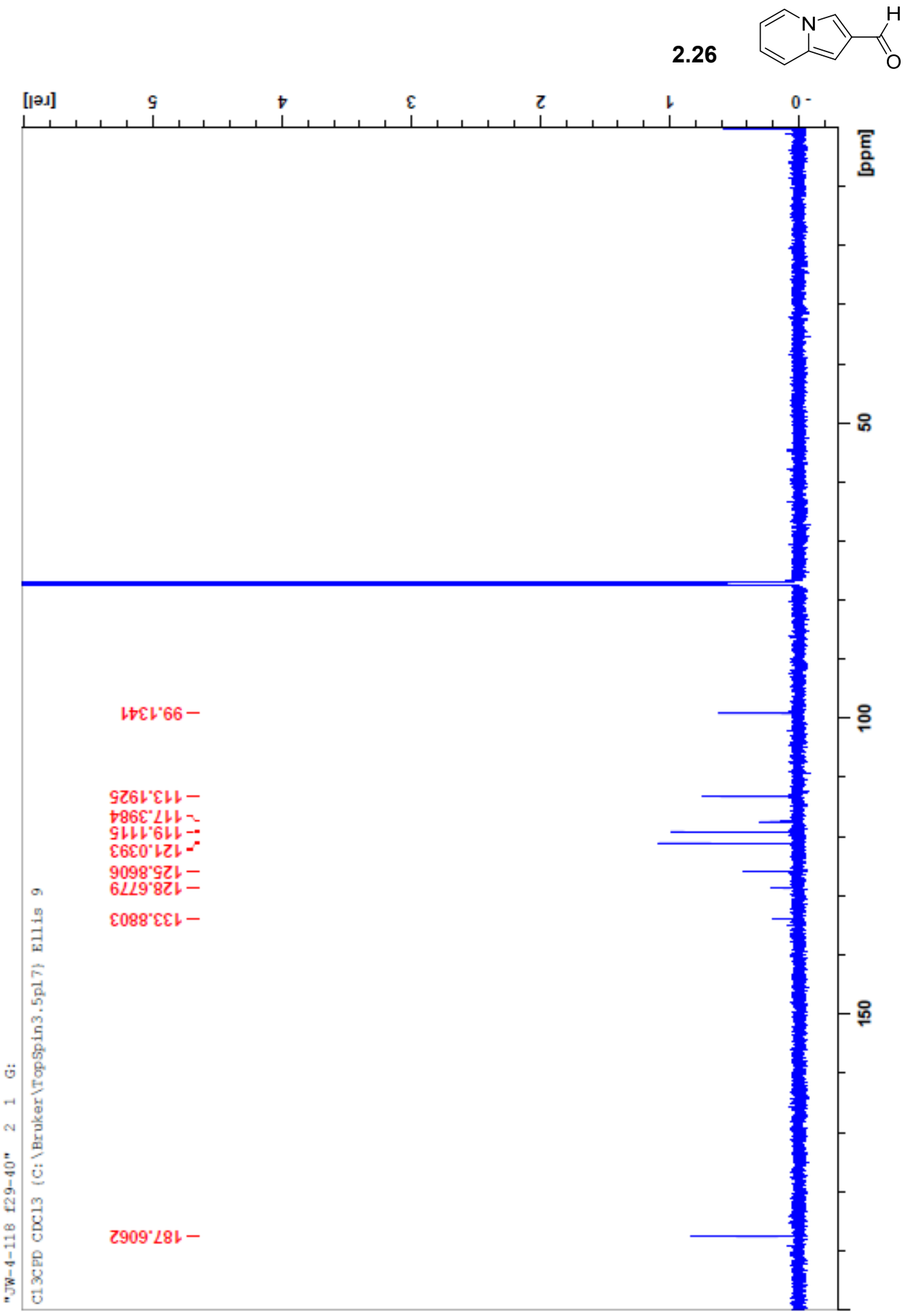
"JW-4-118 f29-40" 2 1 G:
C13CPD CDCl3 (C:\Bruker\TopSpin3.5pl7) Ellis 9
187.6062
133.8803
128.6779
125.8606
121.0393
119.1115
117.3984
113.1925
99.1341
[rel]
[ppm]

2.31

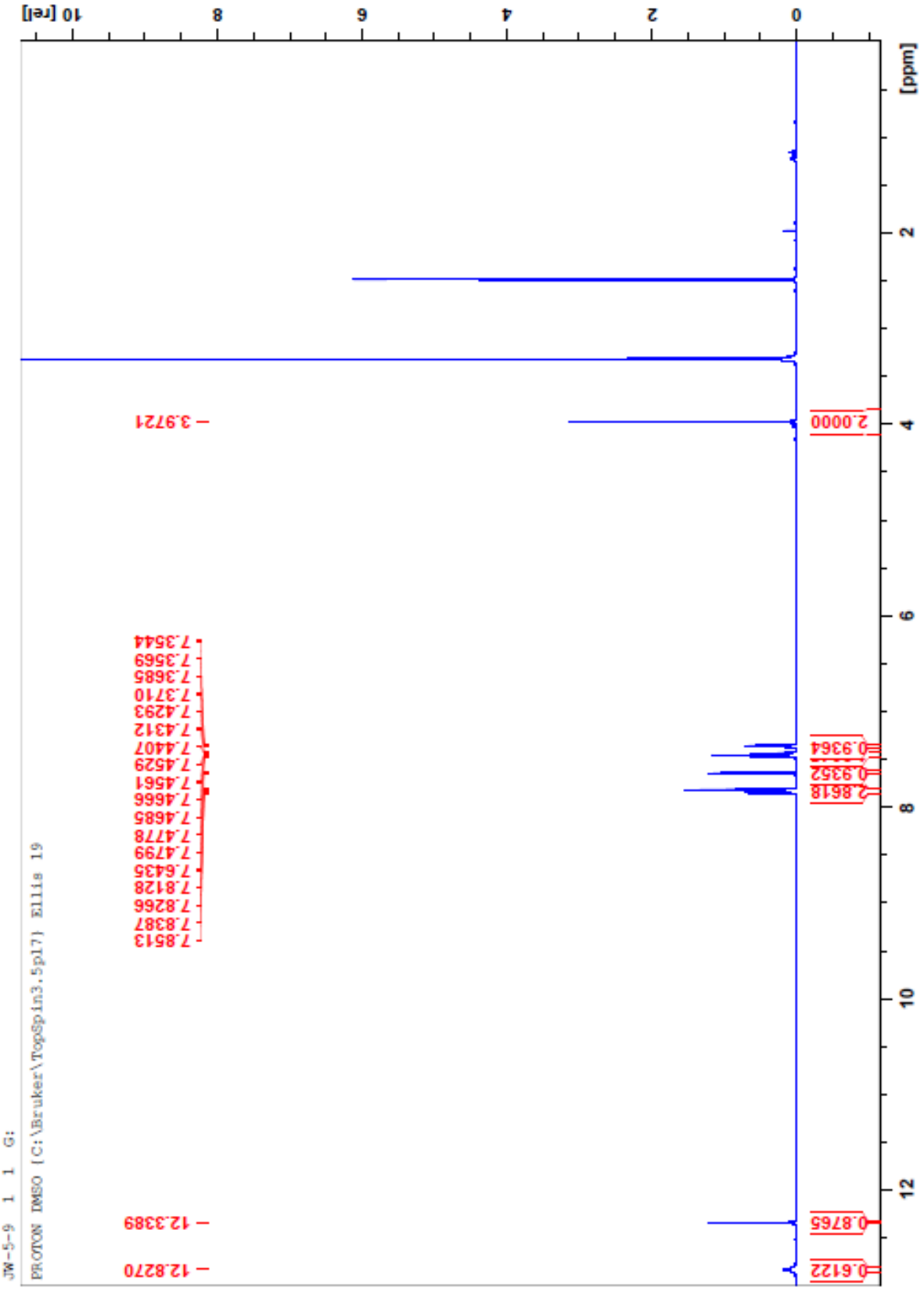
JW-5-9 1 1 G:
PROTON DMSO (C:\Bruker\TopSpin3.5pl7) Ellis 19
12.8270
12.3389
7.8513
7.8387
7.8266
7.8128
7.6435
7.4799
7.4778
7.4685
7.4666
7.4561
7.4529
7.4407
7.4312
7.4293
7.3710
7.3685
7.3569
7.3544
3.9721
0.8765
0.6122
2.0000
0.9364
0.9352
2.8618
[ppm]
[rel]

2.31

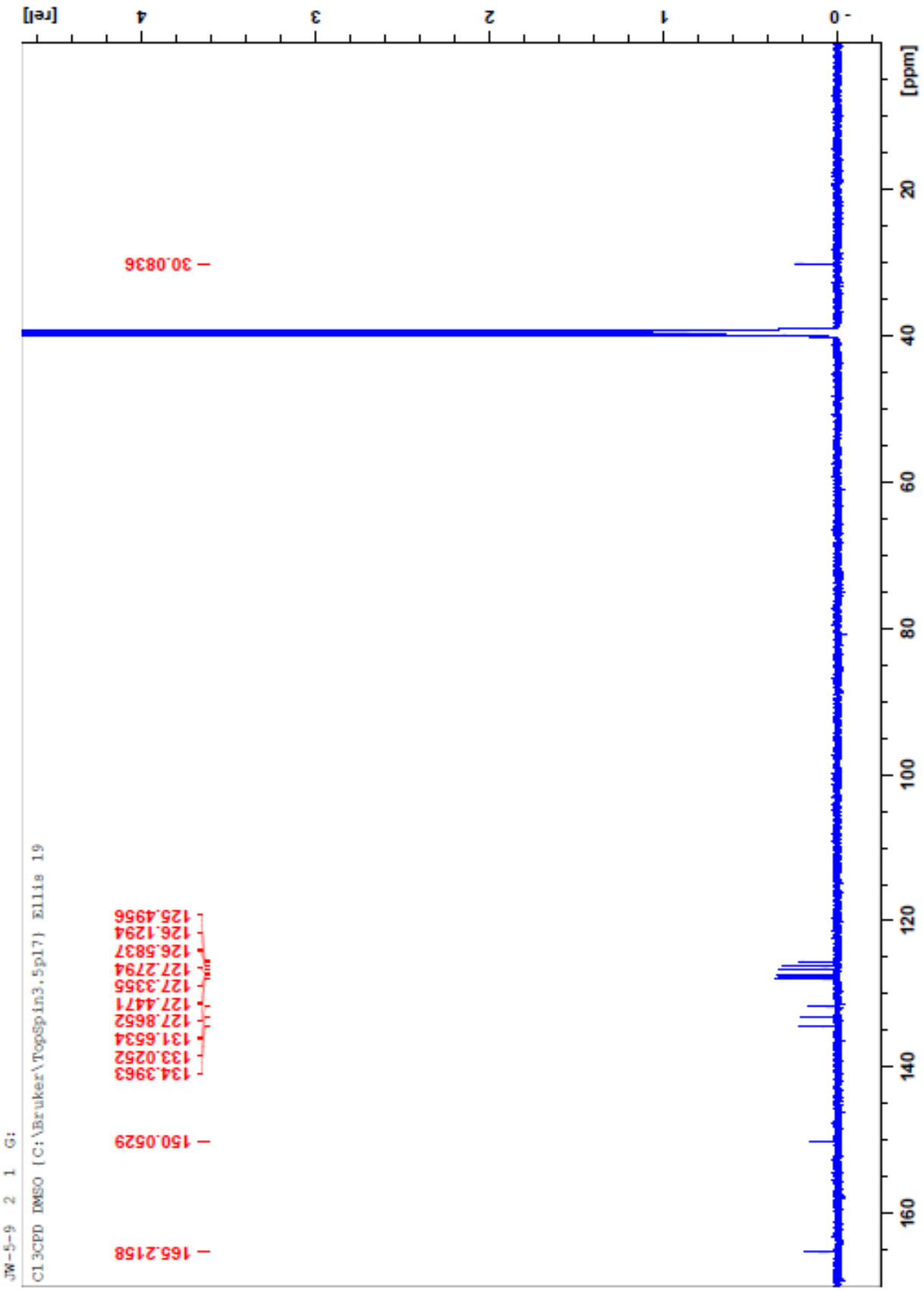
JW-5-9 2 1 G:
C13CPD DMSO (C:\Bruker\TopSpin3.5pl7) Ellis 19
165.2158
150.0529
134.3963
133.0252
131.6534
127.8652
127.4471
127.3355
127.2794
126.5837
126.1294
125.4956
30.0836
[rel]
[ppm]

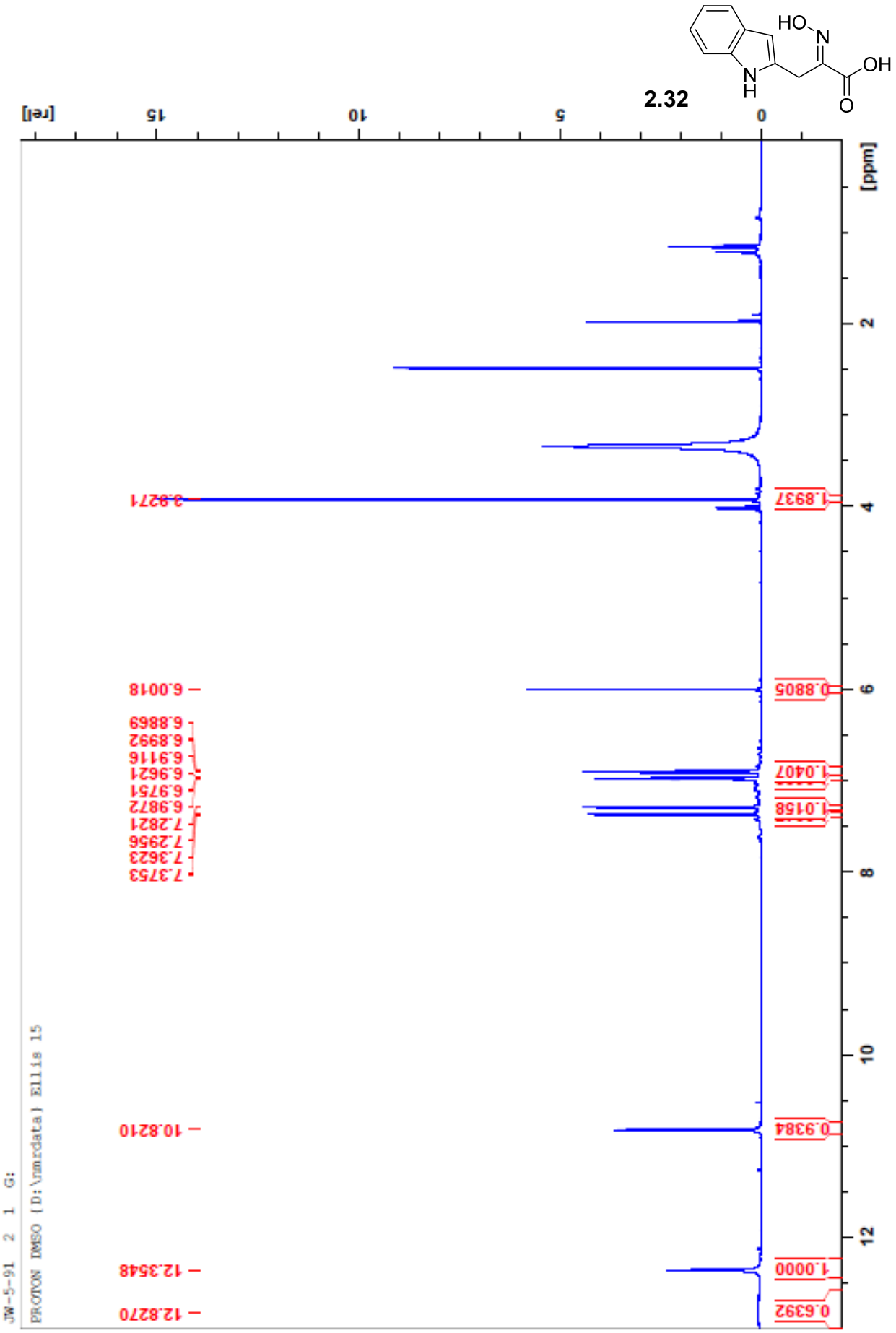
2.32
HO
N
OH
N
H
O
[rel]
15
10
5
0
[ppm]
2
4
6
8
10
12
3.8271
6.0018
6.8869
6.8992
6.9116
6.9621
6.9751
6.9872
7.2821
7.2956
7.3623
7.3753
10.8210
12.3548
12.8270
1.8937
0.8805
1.0407
1.0158
0.9384
1.0000
0.6392
JW-5-91 2 1 G:
PROTON DMSO (D:\nmrdata) Ellis 15

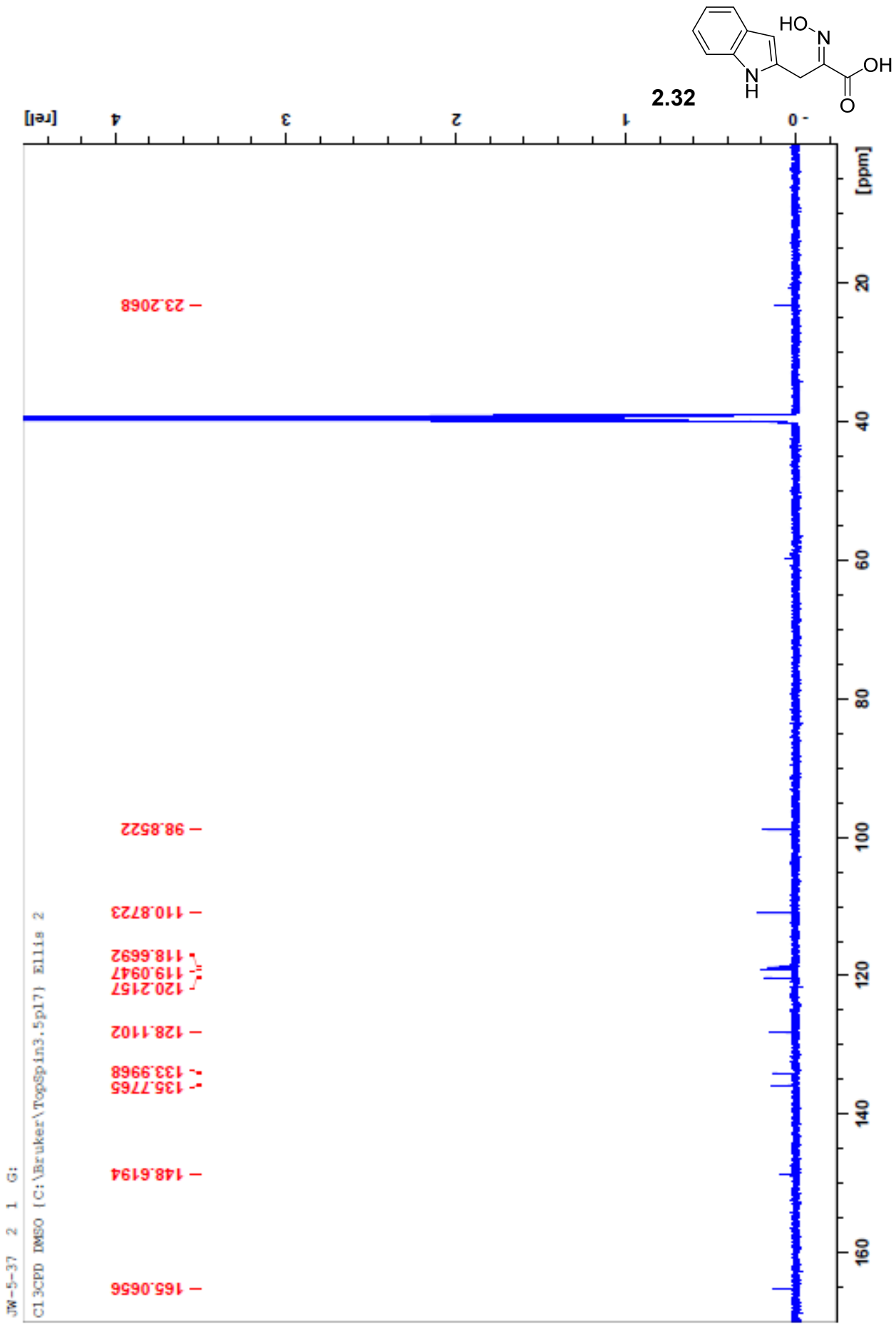
2.32
HO
N
OH
N
H
O
[rel]
[ppm]
23.2068
98.8522
110.8723
118.6692
119.0947
120.2157
128.1102
133.9968
135.7765
148.6194
165.0656
JW-5-37 2 1 G:
C13CPD DMSO (C:\Bruker\TopSpin3.5pl7) Ellis 2

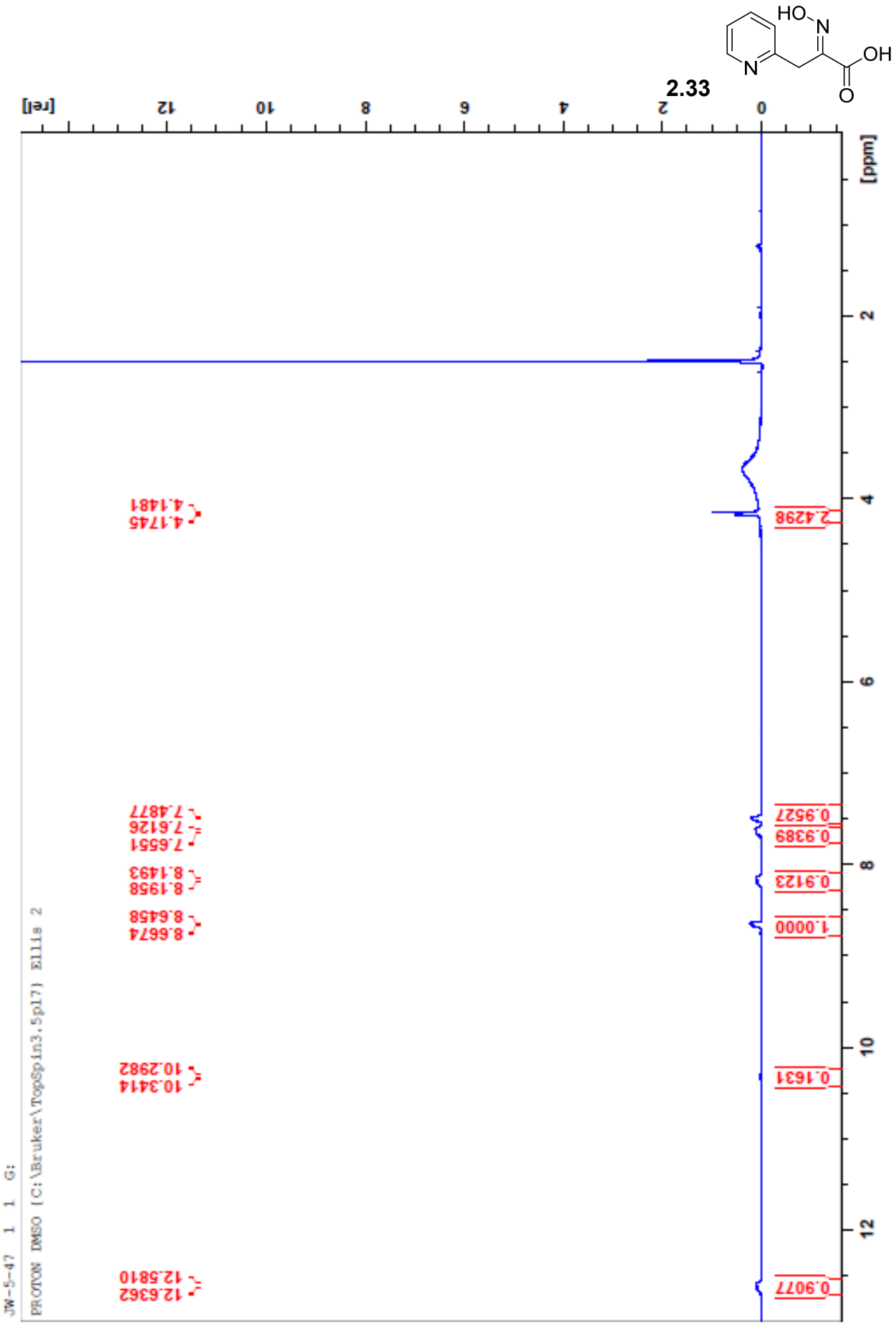
HO
N
N
OH
O
2.33
JW-5-47 1 1 G:
PROTON DMSO (C:\Bruker\TopSpin3.5pl7) Ellis 2
12.5810
12.5362
10.3414
10.2982
8.6574
8.6458
8.1958
8.1493
7.6551
7.6126
7.4877
4.1745
4.1481
0.9077
0.1631
1.0000
0.9123
0.9389
0.9527
2.4298
[ppm]

2.33

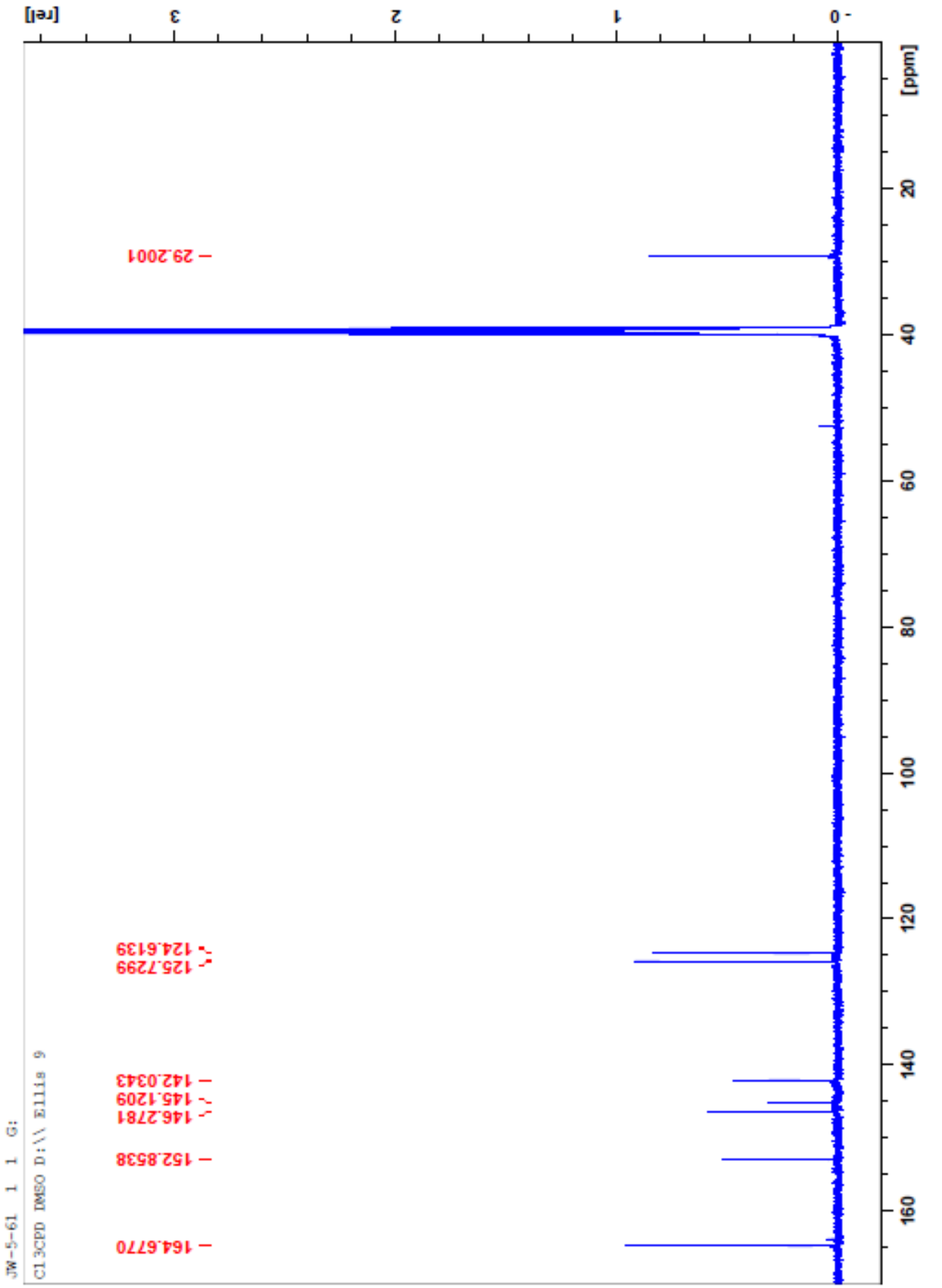
[rel]
3
2
1
0
[ppm]
20
40
60
80
100
120
140
160
29.2001
124.6139
125.7299
142.0343
145.1209
146.2781
152.8538
164.6770
JW-5-61 1 1 G:
C13CPD DMSO D:\\ E111a 9

2.34

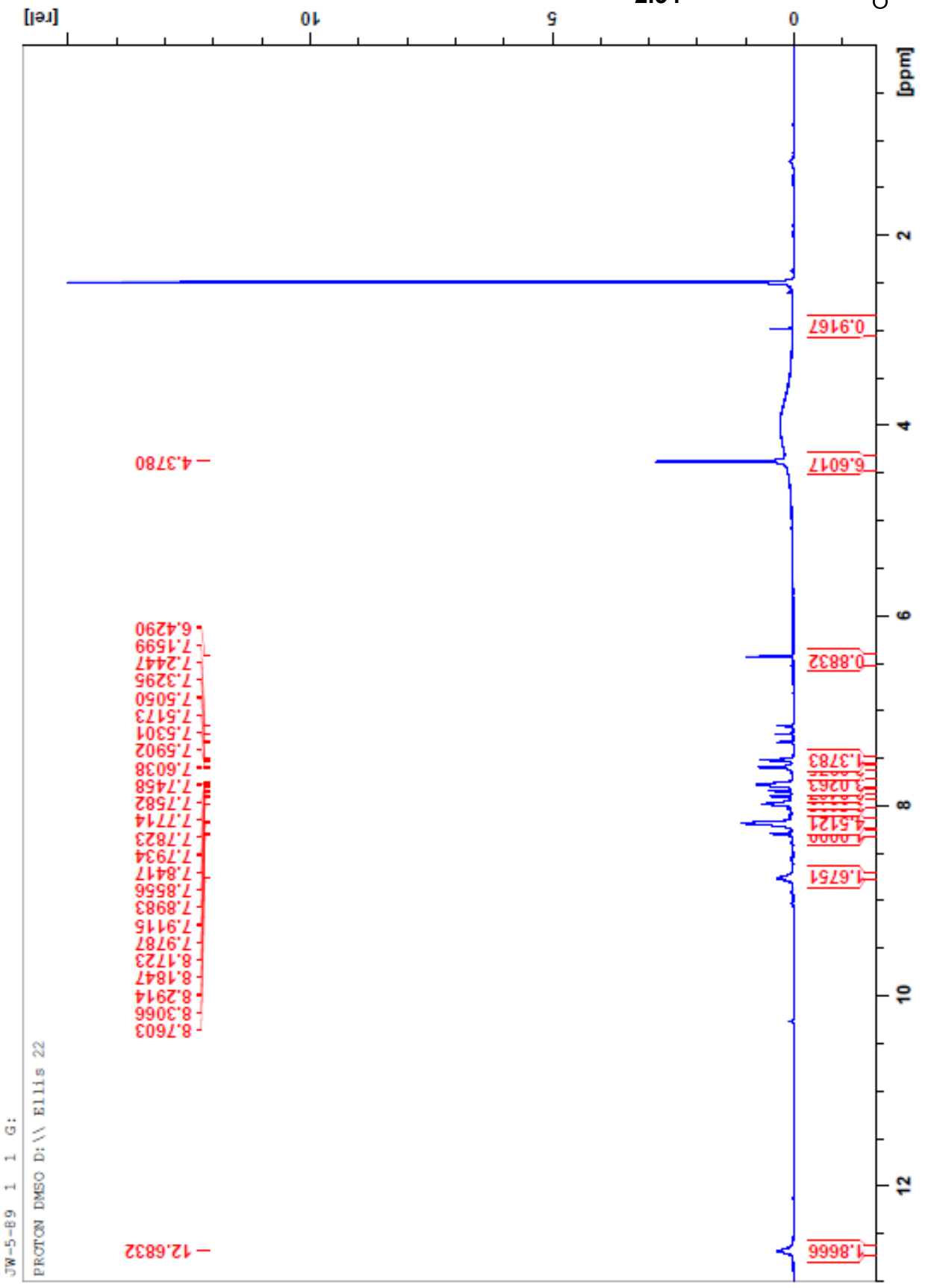
JW-5-89 1 1 G:
PROTON DMSO D:\\ Ellis 22
[rel]
[ppm]
12.6832
8.7603
8.3066
8.2914
8.1847
8.1723
7.9787
7.9115
7.8983
7.8556
7.8417
7.7934
7.7823
7.7714
7.7582
7.7458
7.6038
7.5902
7.5301
7.5173
7.5050
7.3295
7.2447
7.1599
6.4290
4.3780
1.8666
1.6751
1.3783
0.8832
6.6017
0.9167

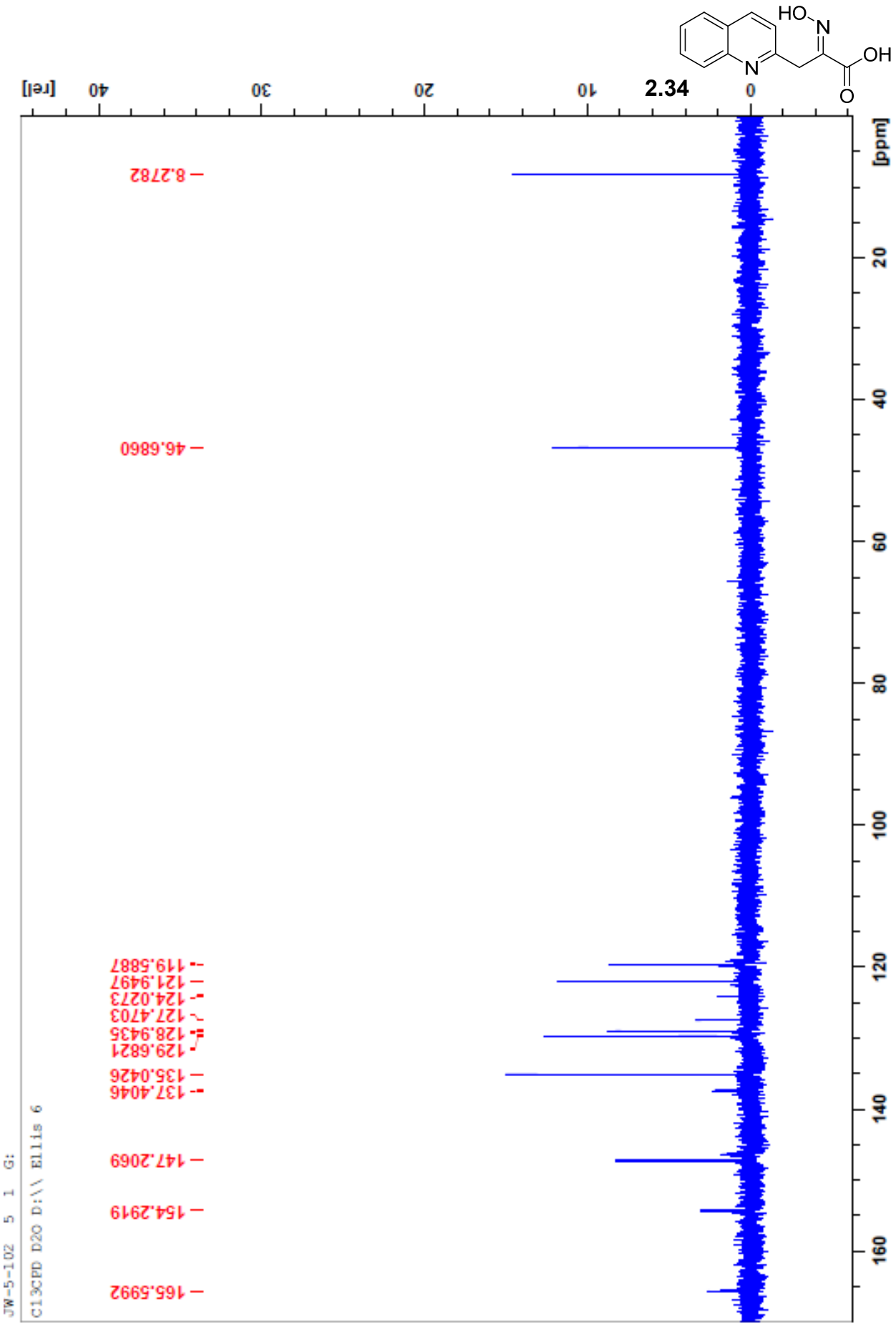
HO
N
OH
O
N
2.34
[rel]
40
30
20
10
0
[ppm]
20
40
60
80
100
120
140
160
8.2782
46.6860
119.5887
121.9497
124.0273
127.4703
128.9435
129.6821
135.0426
137.4046
147.2069
154.2919
165.5992
JW-5-102 5 1 G:
C13CPD D2O D:\\ Ellis 6

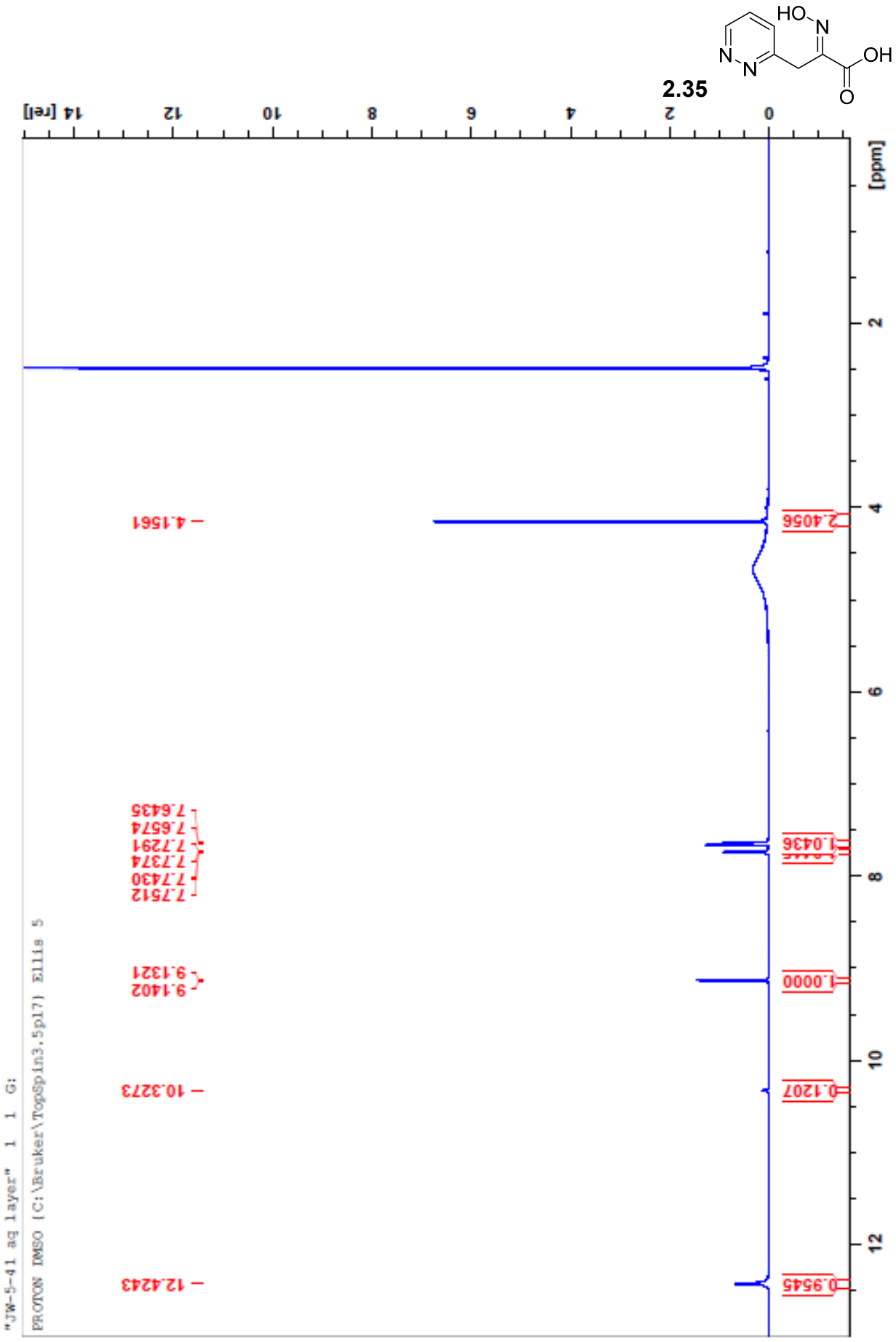
2.35
HO
N
N
N
OH
O
"JW-5-41 aq layer" 1 1 G:
PROTON DMSO (C:\Bruker\TopSpin3.5pl7) Ellis 5
12.4243
10.3273
9.1402
9.1321
7.7512
7.7430
7.7374
7.7291
7.6574
7.6435
4.1561
0.9545
0.1207
1.0000
1.0436
2.4056
[rel]
[ppm]

2.35

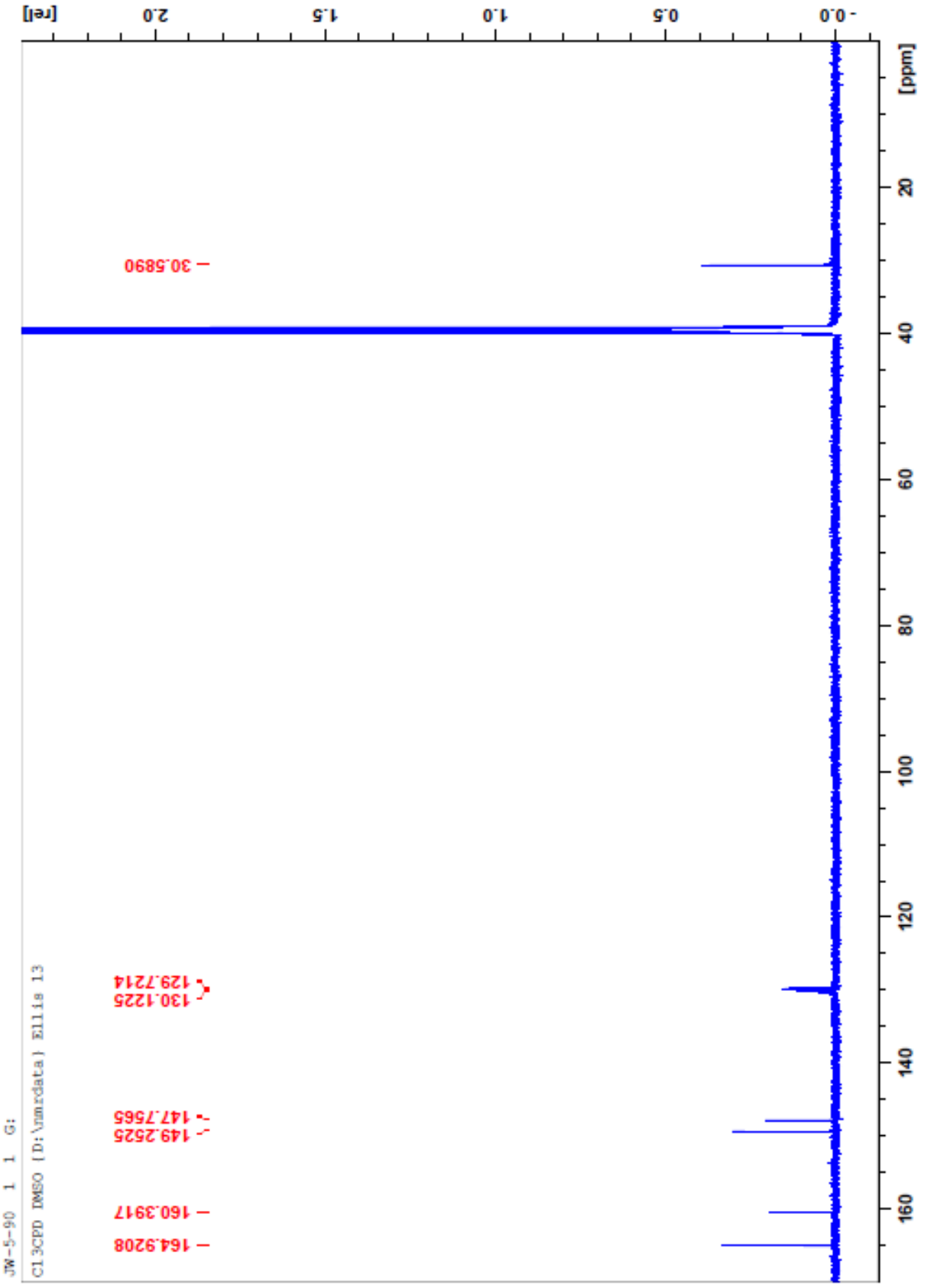
[rel]
2.0
1.5
1.0
0.5
0.0
[ppm]
20
40
60
80
100
120
140
160
30.5890
129.7214
130.1225
147.7565
149.2525
160.3917
164.9208
JW-5-90 1 1 G:
C13CPD DMSO [D:\nmrdata] Ellis 13

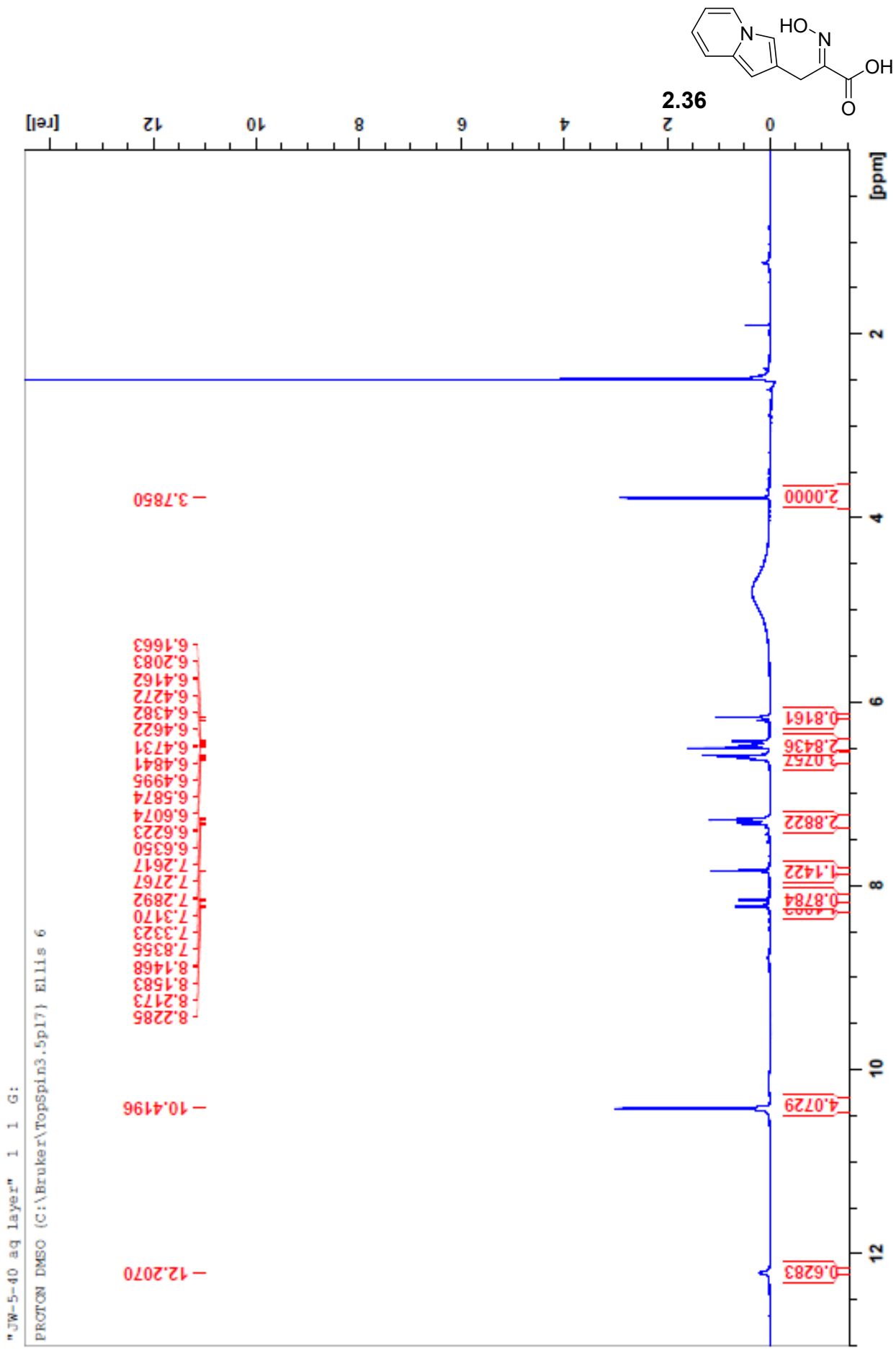
2.36
HO
N
N
OH
O
"JW-5-40 aq layer" 1 1 G:
PROTON DMSO (C:\Bruker\TopSpin3.5pl7) Ellis 6
[rel]
[ppm]
3.7850
10.4196
12.2070
8.2285
8.2173
8.1583
8.1468
7.8355
7.3323
7.3170
7.2892
7.2767
7.2617
6.6350
6.6223
6.6074
6.5874
6.4995
6.4841
6.4731
6.4622
6.4382
6.4272
6.4162
6.2083
6.1663
2.0000
0.8161
2.8436
3.0757
2.8822
1.1422
0.8784
4.0729
0.6283

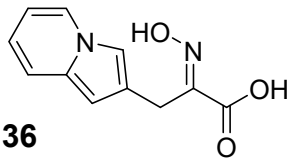
HO
N
N
OH
O

2.36

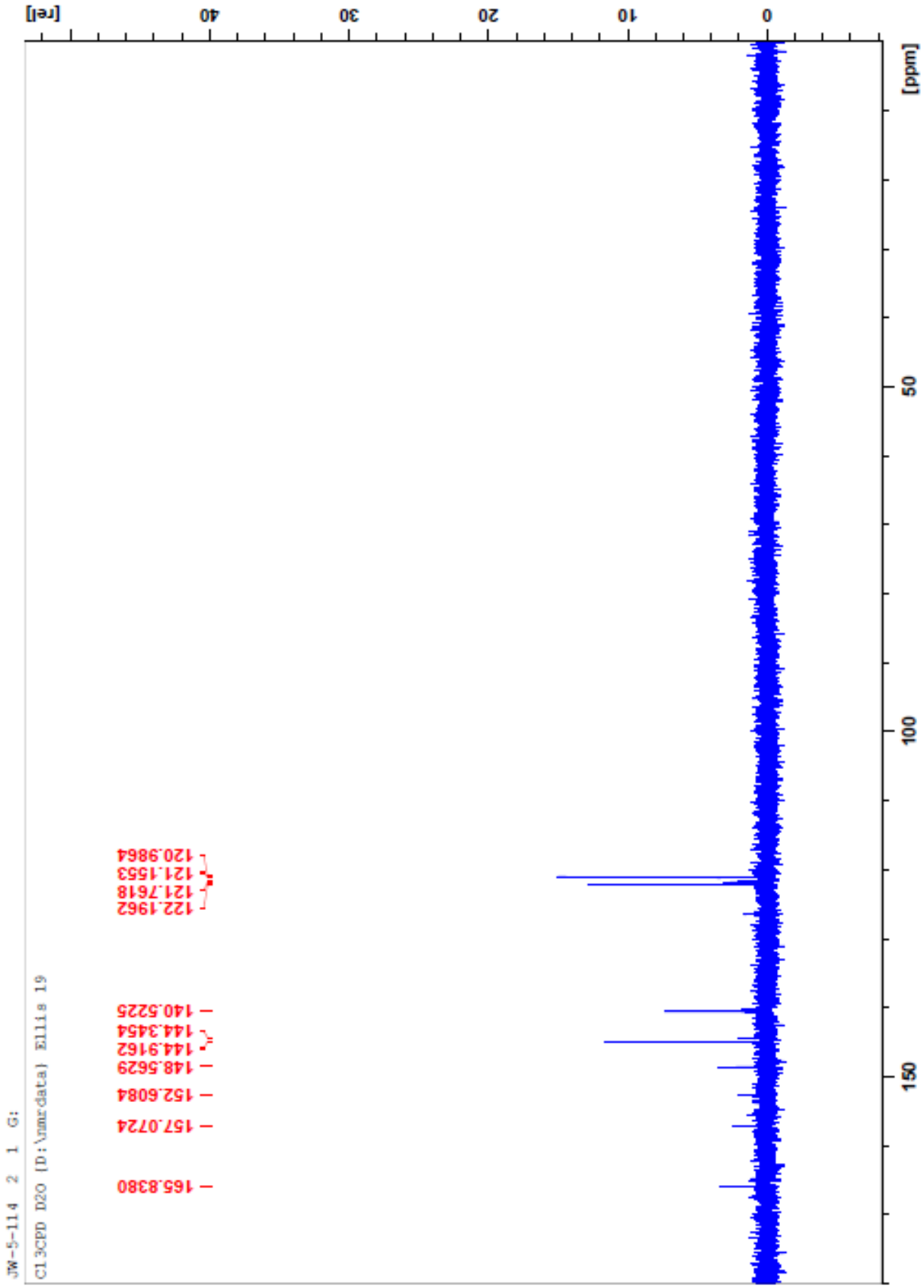
[rel]
40
30
20
10
0
[ppm]
50
100
150
120.9864
121.1553
121.7618
122.1962
140.5225
144.3454
144.9162
148.5629
152.6084
157.0724
165.8380
JW-5-114 2 1 G:
C13CPD D2O (D:\nmrdata) Ellis 19

2.37

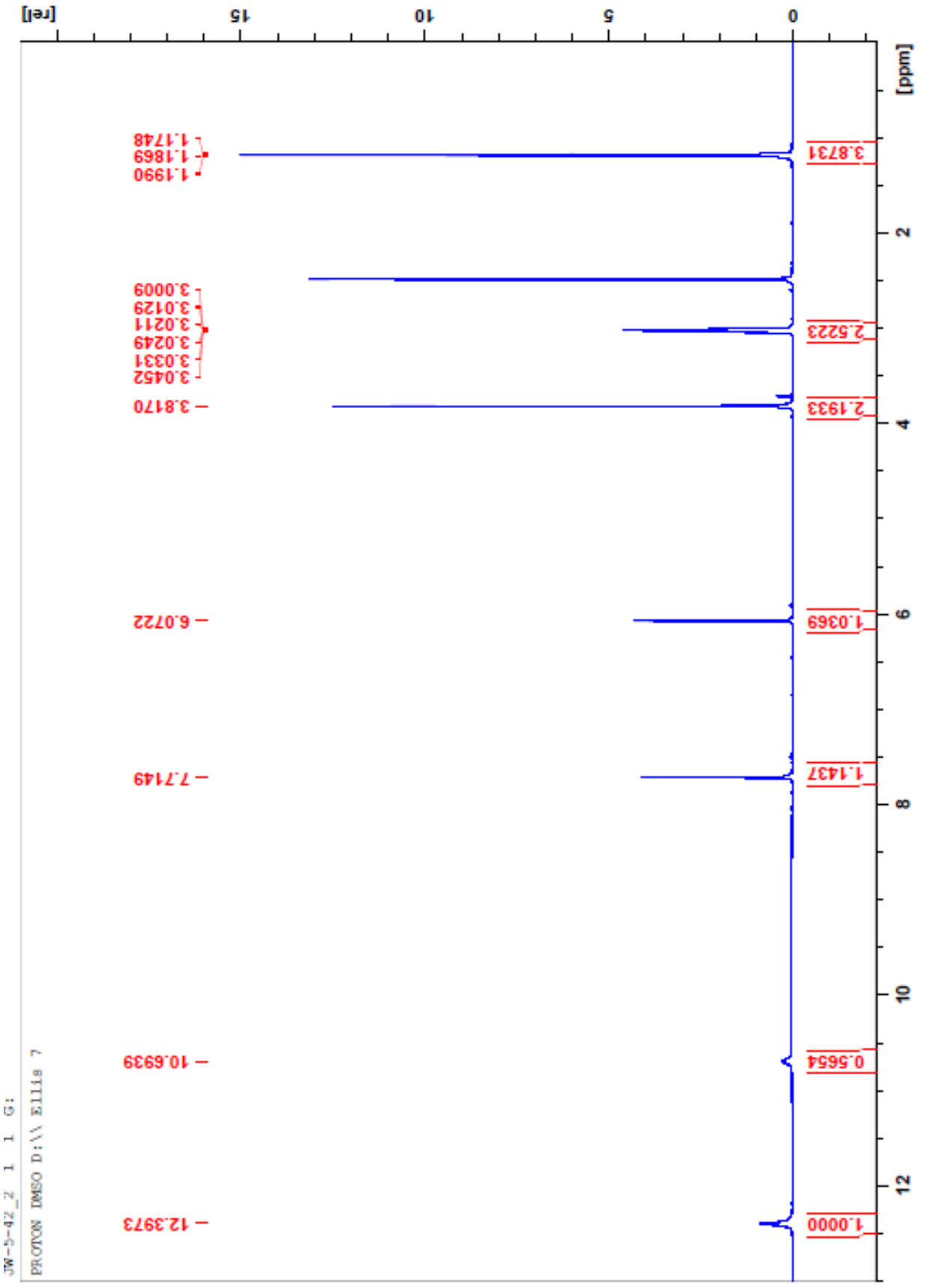
[rel]
15
10
5
0
[ppm]
2
4
6
8
10
12
1.1748
1.1869
1.1990
3.0009
3.0129
3.0211
3.0249
3.0331
3.0452
3.8170
6.0722
7.7149
10.6939
12.3973
3.8731
2.5223
2.1933
1.0369
1.1437
0.5654
1.0000
JW-5-42_2 1 1 G:
PROTON DMSO D:\\\ E111a 7

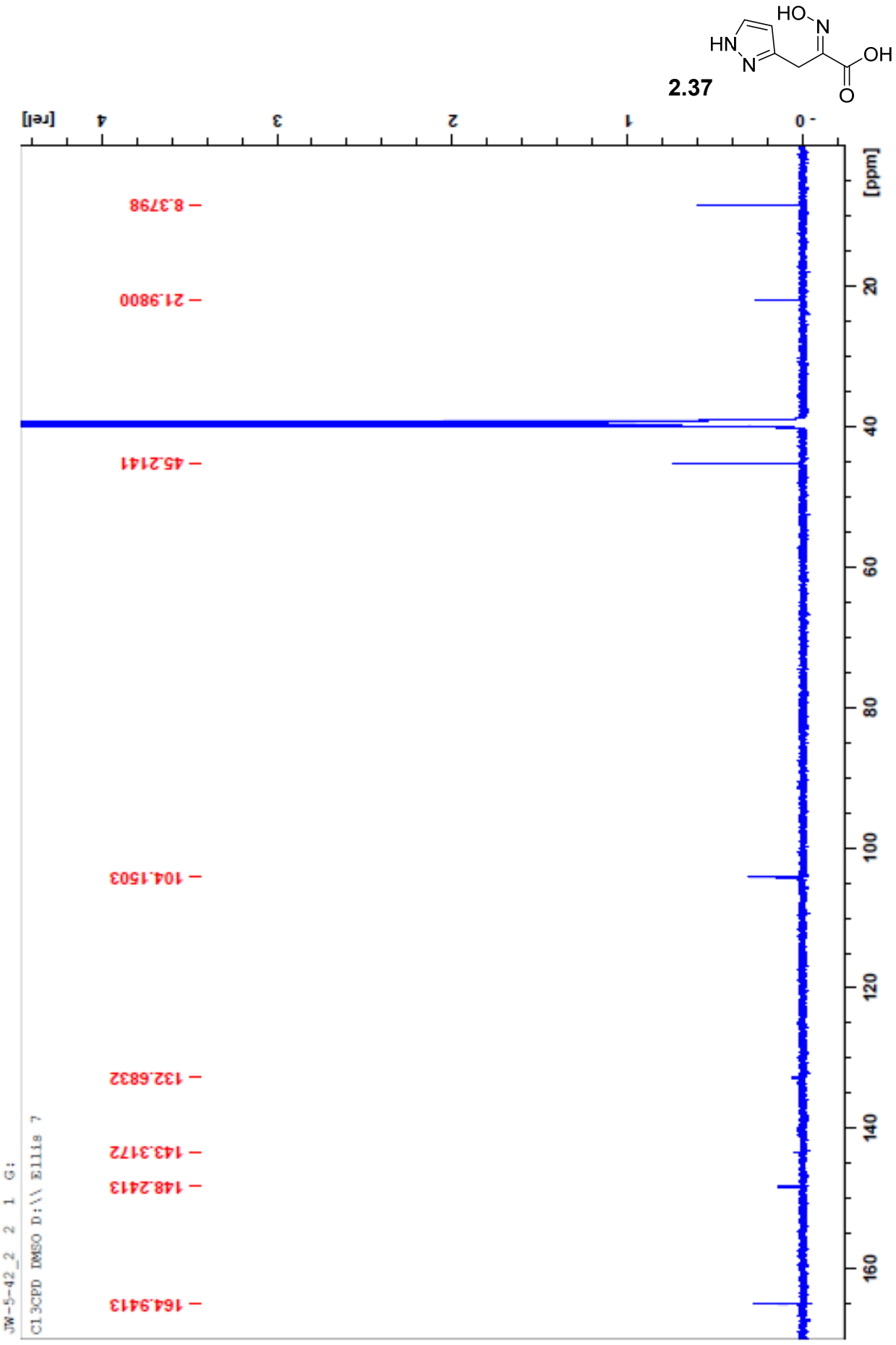
HO
N
HN
N
OH
O
2.37
[rel]
4
3
2
1
0
[ppm]
20
40
60
80
100
120
140
160
8.3798
21.9800
45.2141
104.1503
132.6832
143.3172
148.2413
164.9413
JW-5-42_2 2 1 G:
C13CPD DMSO D:\\ Ellis 7

2.38

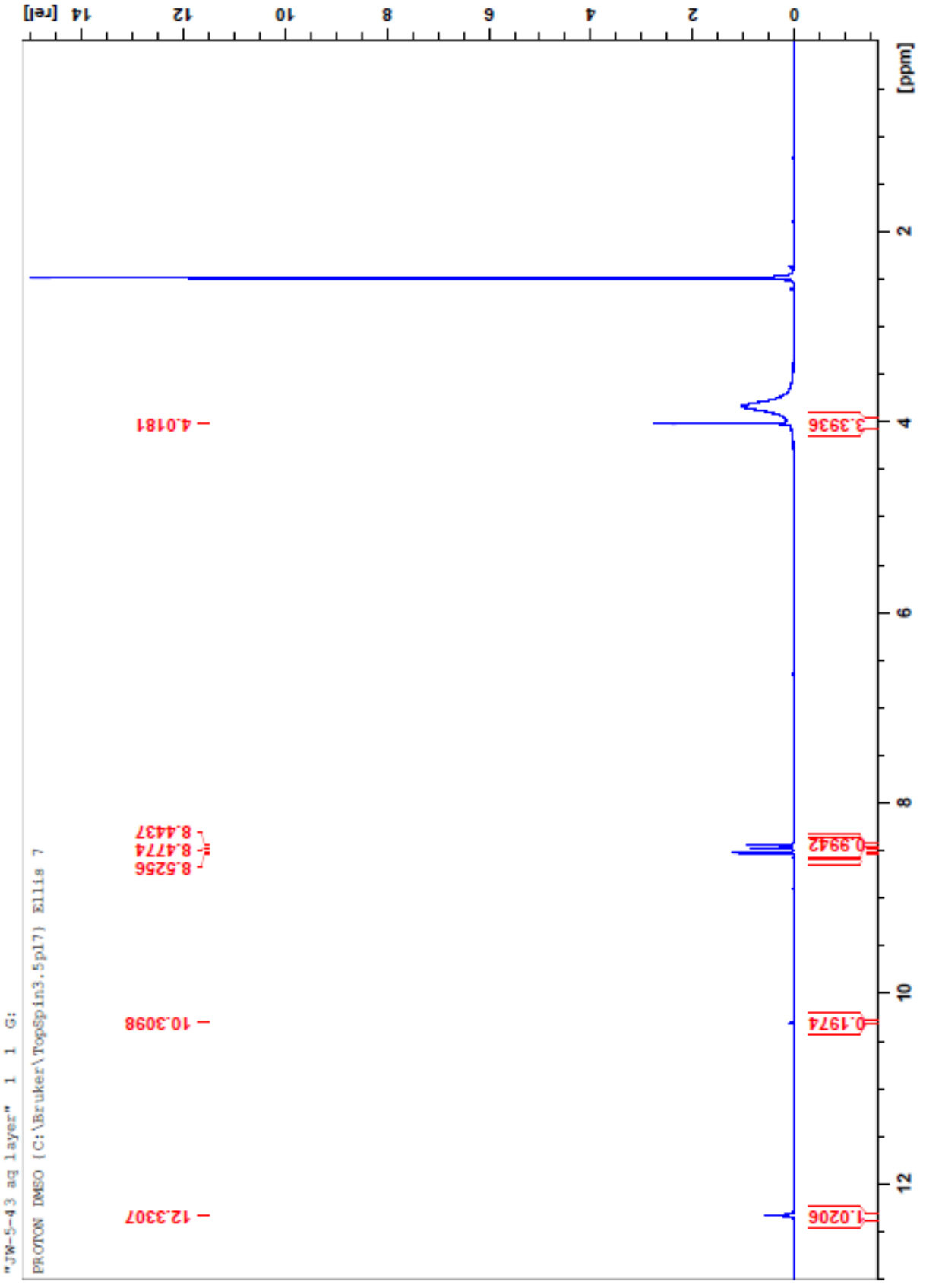
"JW-5-43 aq layer" 1 1 G:
PROTON DMSO (C:\Bruker\TopSpin3.5pl7) Ellis 7
12.3307
10.3098
8.5256
8.4774
8.4437
4.0181
1.0206
0.1974
0.9942
3.3936
[rel]
[ppm]

2.38

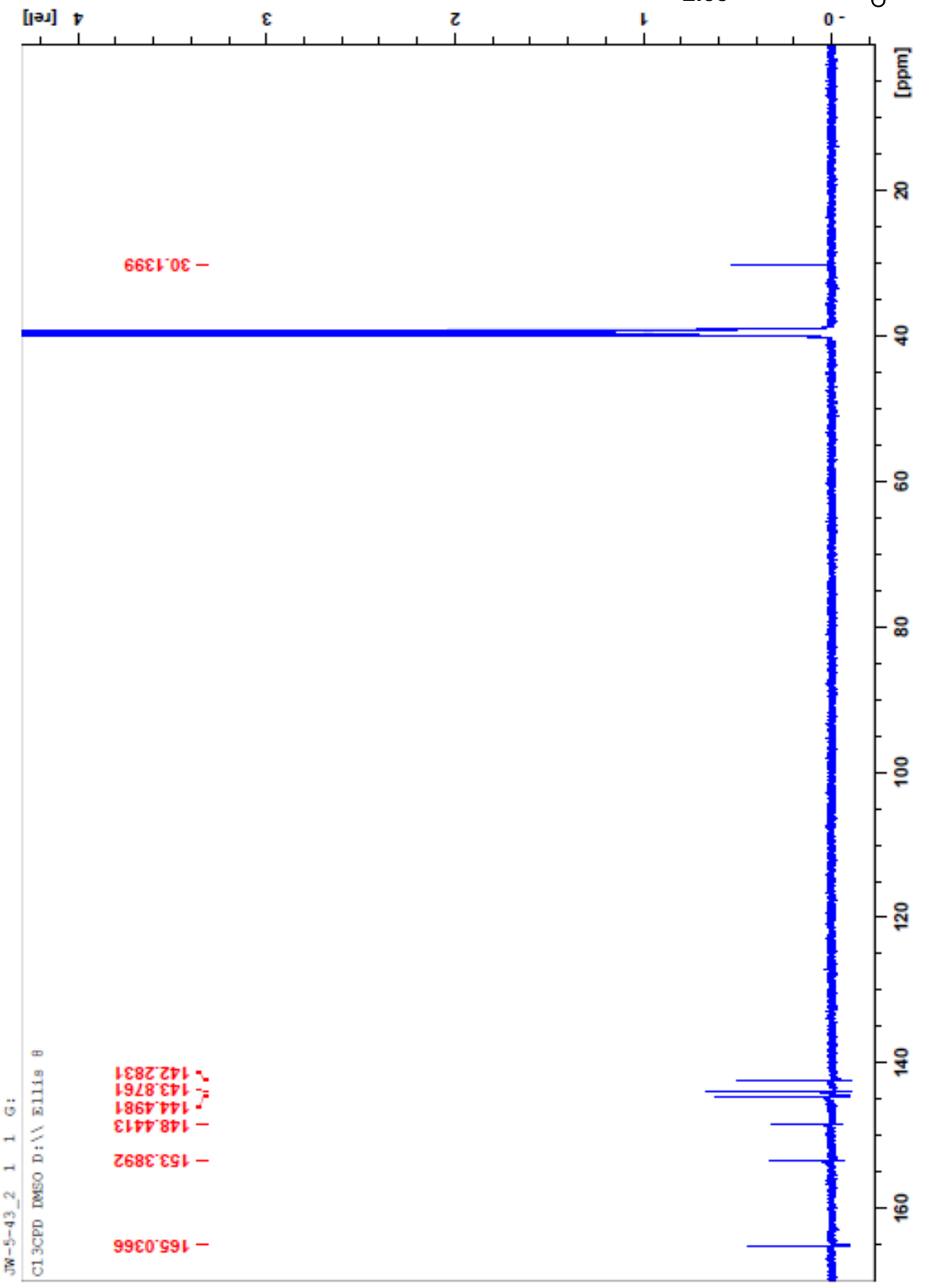
30.1399
142.2831
143.8761
144.4981
148.4413
153.3892
165.0366
JW-5-43_2 1 1 G:
C13CPD DMSO D:\\ Ellis 8
[rel]
[ppm]

2.39

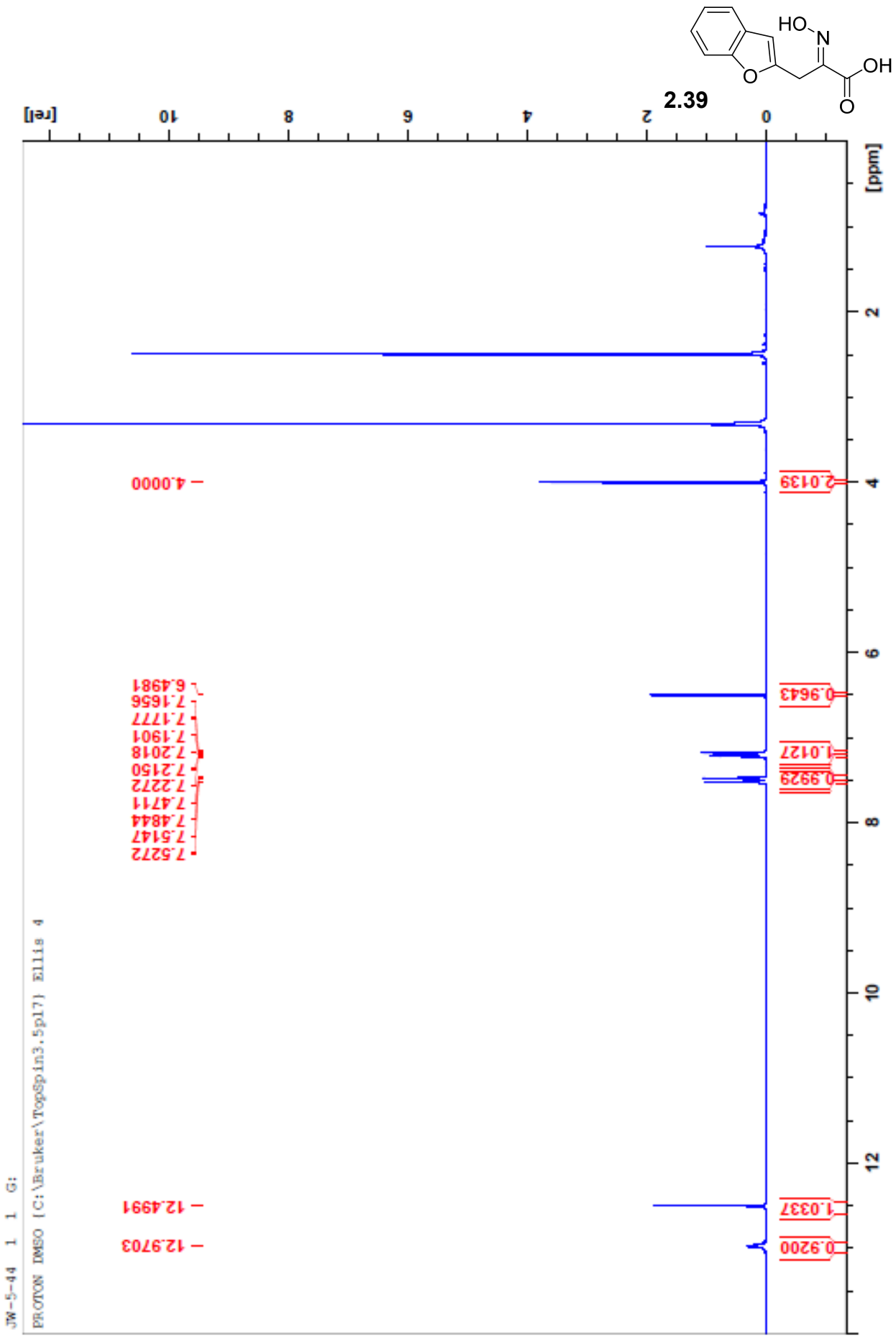
HO
N
OH
O
O
[rel]
10
8
6
4
2
0
[ppm]
2
4
6
8
10
12
4.0000
2.0139
0.9643
1.0127
0.9929
1.0337
0.9200
12.4991
12.9703
6.4981
7.1656
7.1777
7.1901
7.2018
7.2150
7.2272
7.4711
7.4844
7.5147
7.5272
JW-5-44 1 1 G:
PROTON DMSO (C:\Bruker\TopSpin3.5pl7) Ellis 4

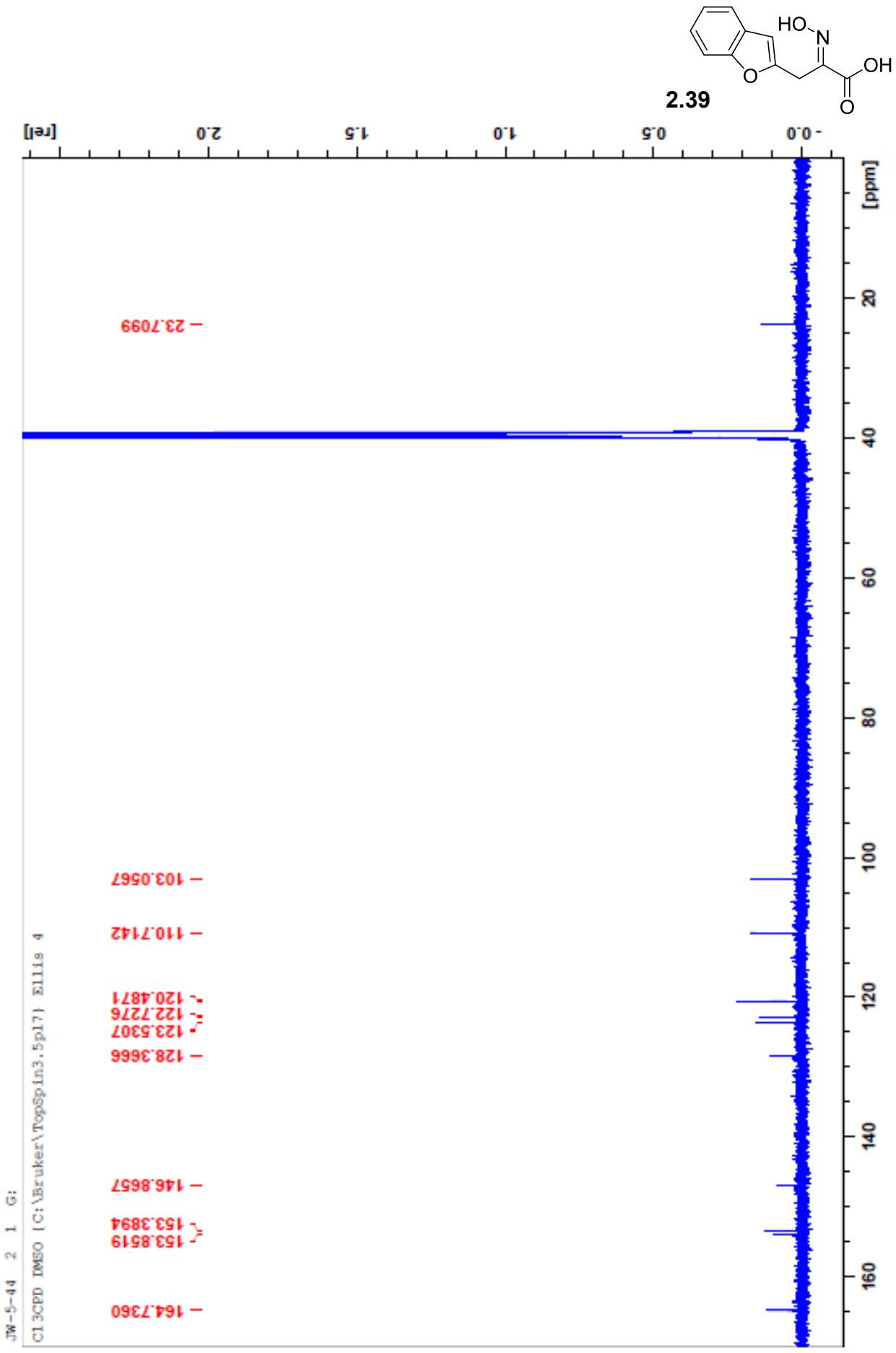
HO
N
OH
O
O
2.39
[rel]
2.0
1.5
1.0
0.5
0.0
[ppm]
20
40
60
80
100
120
140
160
23.7099
103.0567
110.7142
120.4871
122.7276
123.5307
128.3666
146.8657
153.3894
153.8519
164.7360
JW-5-44 2 1 G:
C13CPD DMSO (C:\Bruker\TopSpin3.5pl7) Ellis 4

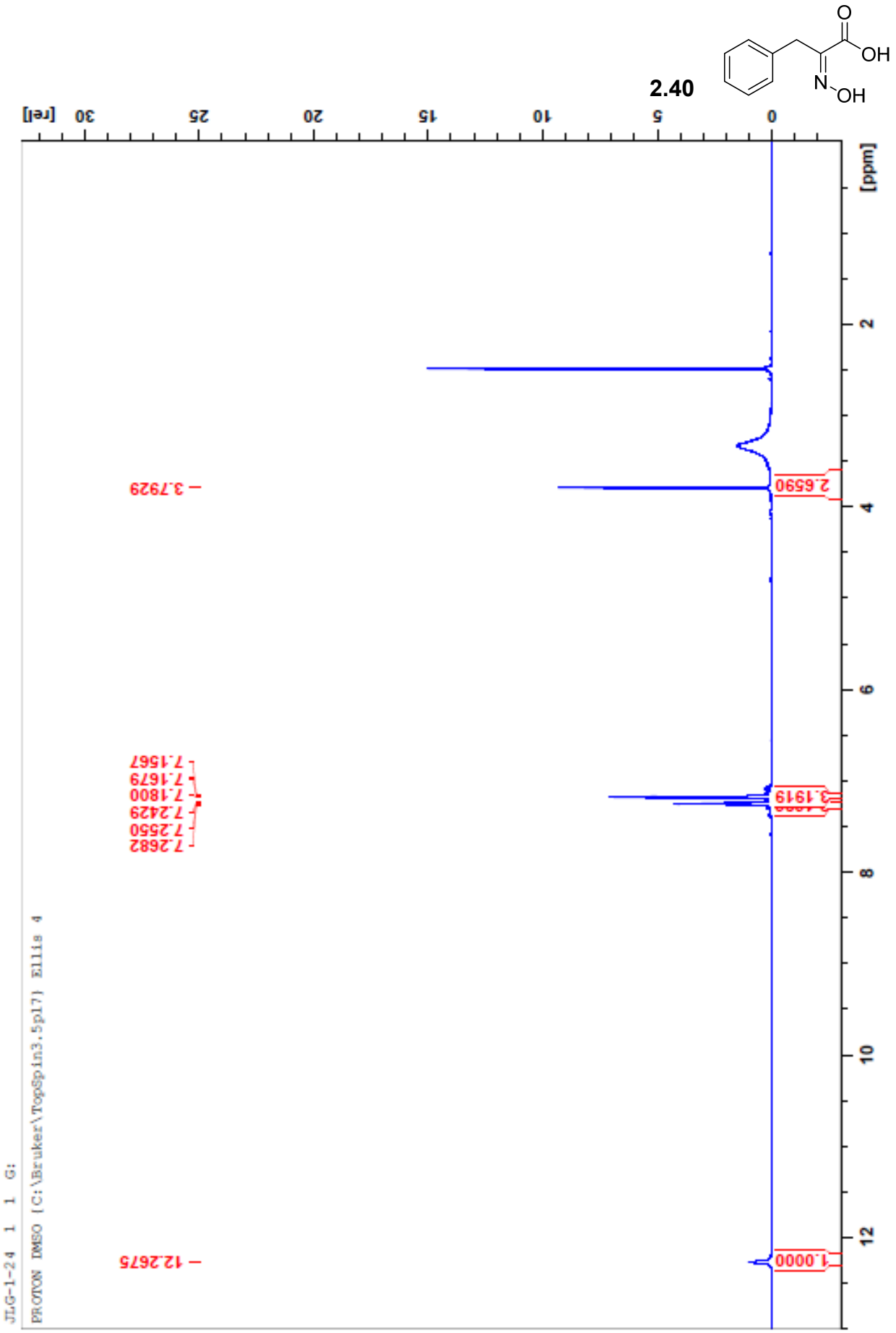
2.40
O
OH
N
OH
[rel]
30
25
20
15
10
5
0
[ppm]
2
4
6
8
10
12
3.7929
2.6590
7.2682
7.2550
7.2429
7.1800
7.1679
7.1567
3.1919
1.0000
12.2675
JLG-1-24 1 1 G:
PROTON DMSO (C:\Bruker\TopSpin3.5pl7) Ellis 4

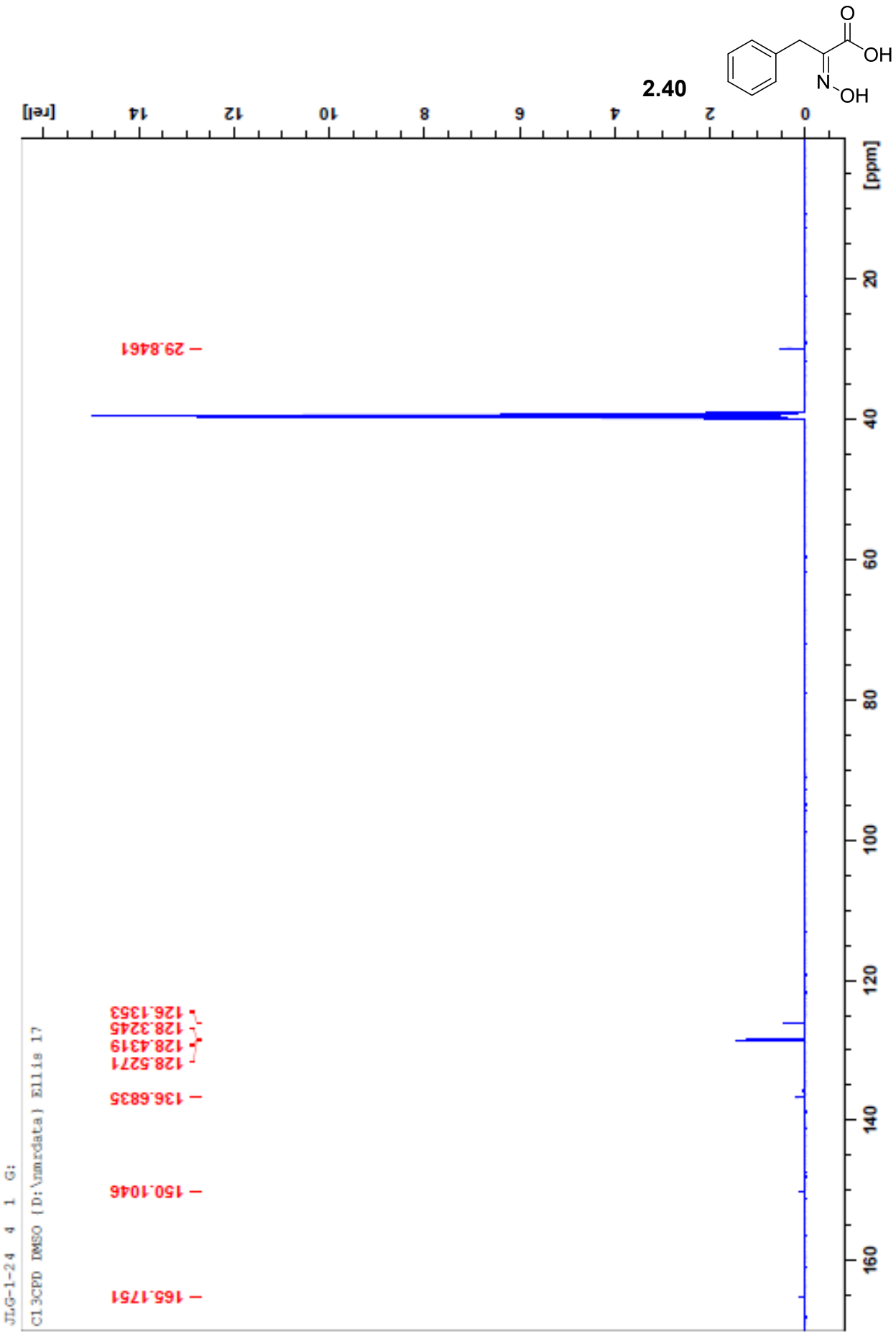
2.40
O
OH
N
OH
[rel]
0
2
4
6
8
10
12
14
[ppm]
20
40
60
80
100
120
140
160
29.8461
126.1353
128.3245
128.4319
128.5271
136.6835
150.1046
165.1751
JLG-1-24 4 1 G:
C13CPD DMSO (D:\nmrdata) Ellis 17

2.41

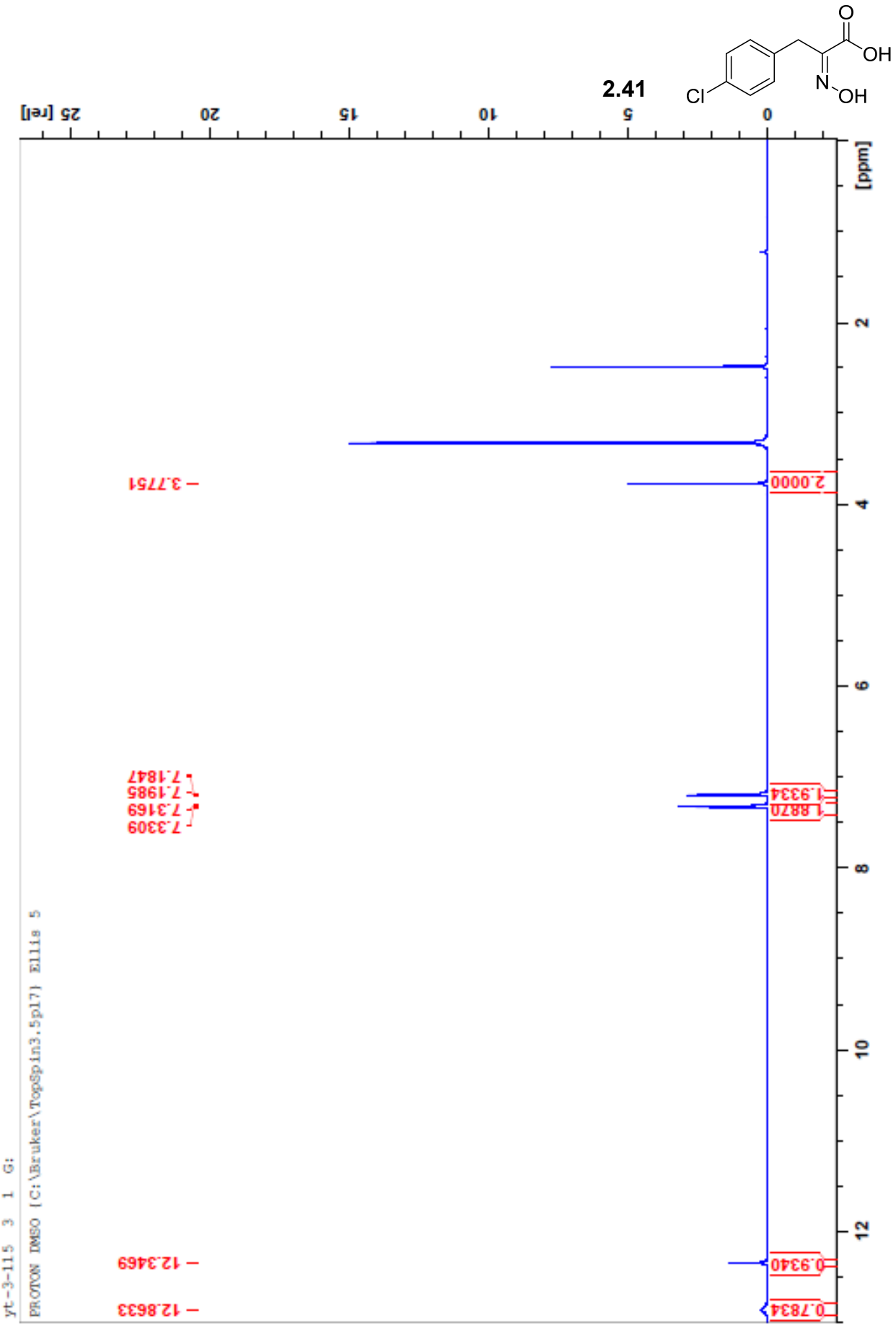
O
OH
N
OH
Cl
[ppm]
[rel]
yt-3-115 3 1 G:
PROTON DMSO [C:\Bruker\TopSpin3.5pl7] Ellis 5
12.8633
12.3469
7.3309
7.3169
7.1985
7.1847
3.7751
0.7834
0.9340
1.8820
1.9334
2.0000

2.41

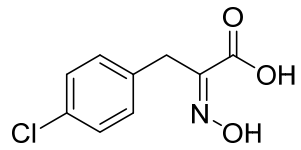
O
OH
N
OH
Cl

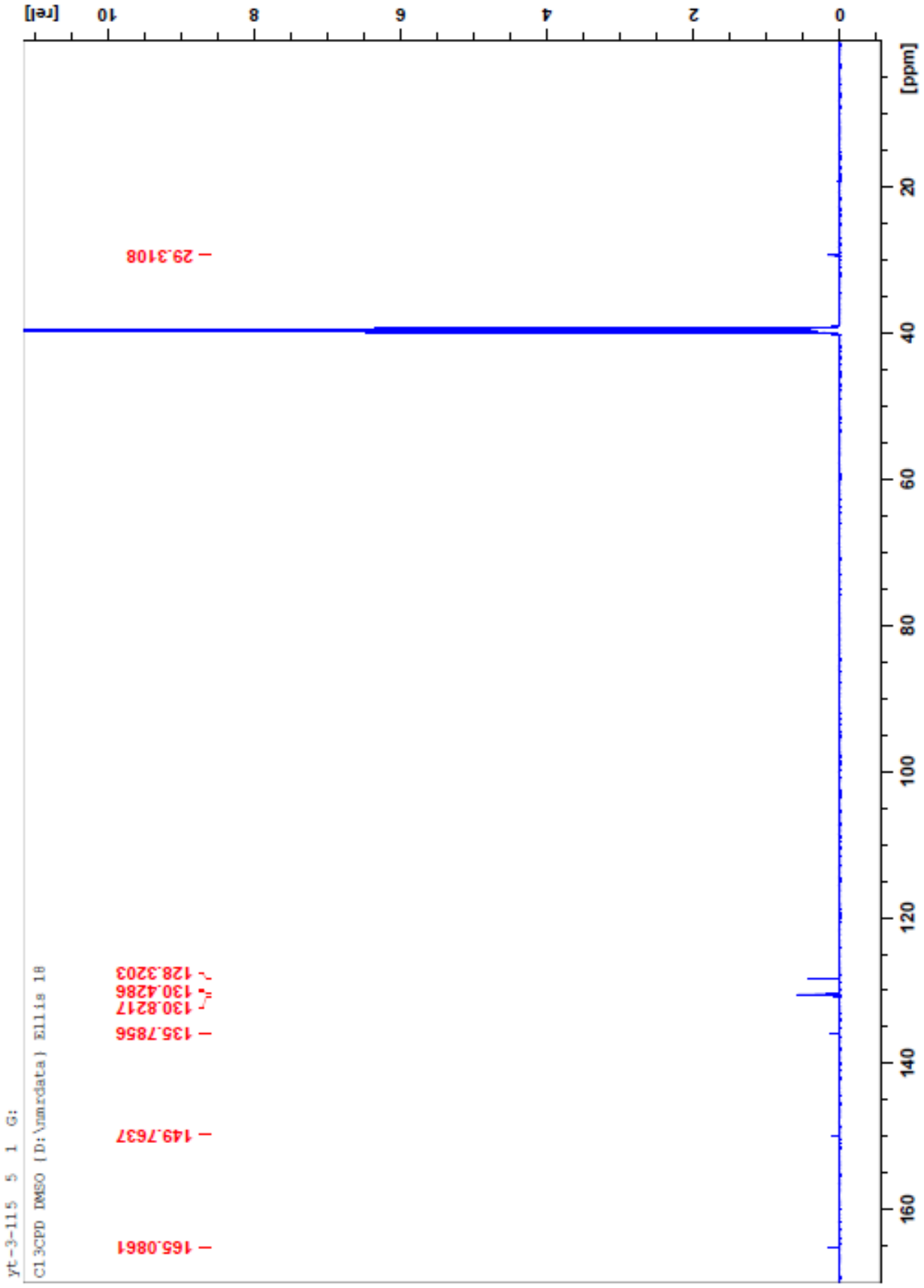
yt-3-115 5 1 G:
C13CPD DMSO (D:\nmrdata) Ellis 18
165.0861
149.7637
135.7856
130.8217
130.4286
128.3203
29.3108
[rel]
[ppm]

4.6


OH
H2N

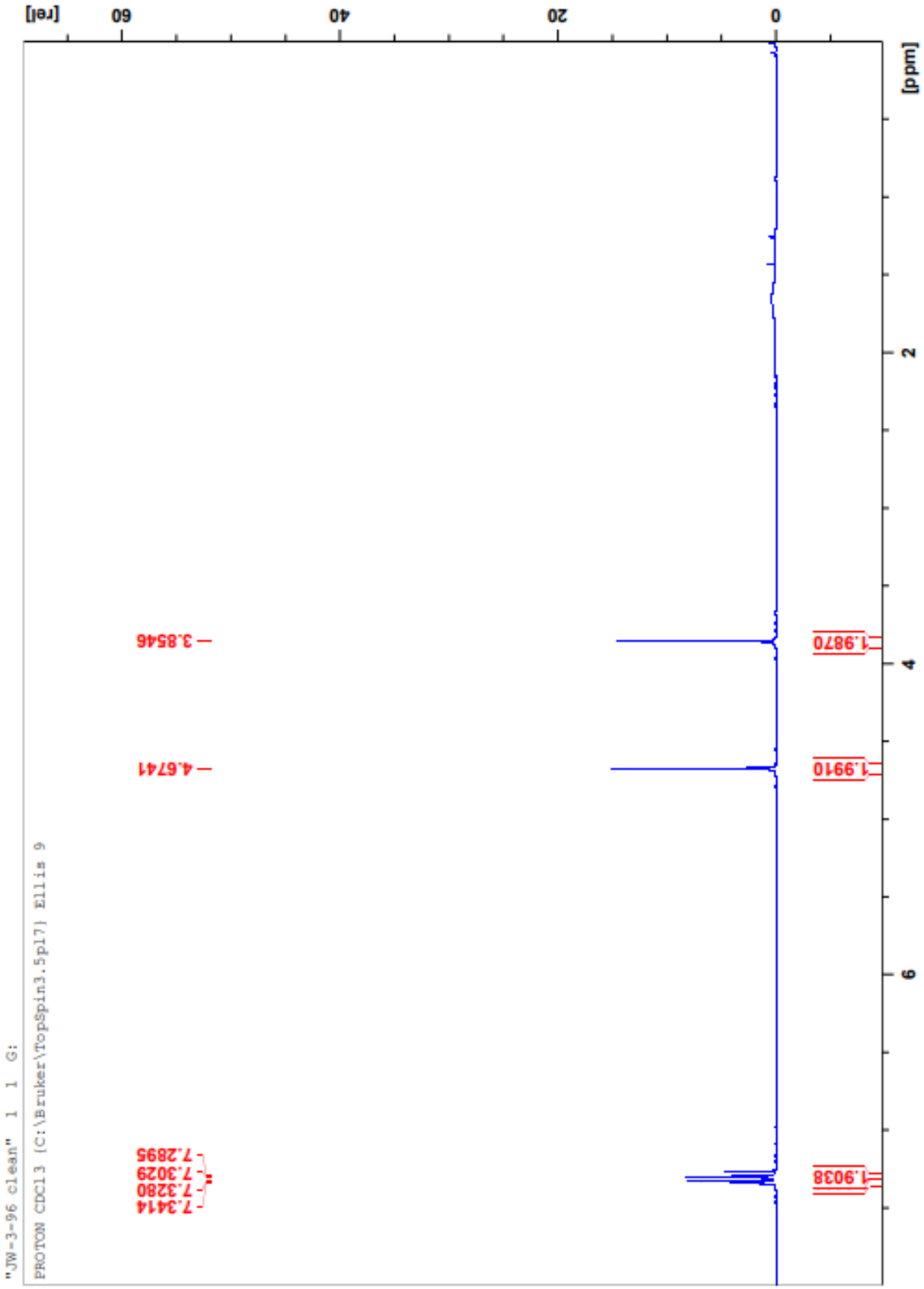
"JW-3-96 clean" 1 1 G:
PROTON CDCl3 (C:\Bruker\TopSpin3.5pl7) Ellis 9
7.2895
7.3029
7.3280
7.3414
4.6741
3.8546
1.9038
1.9910
1.9870
[rel]
60
40
20
0
[ppm]
6
4
2

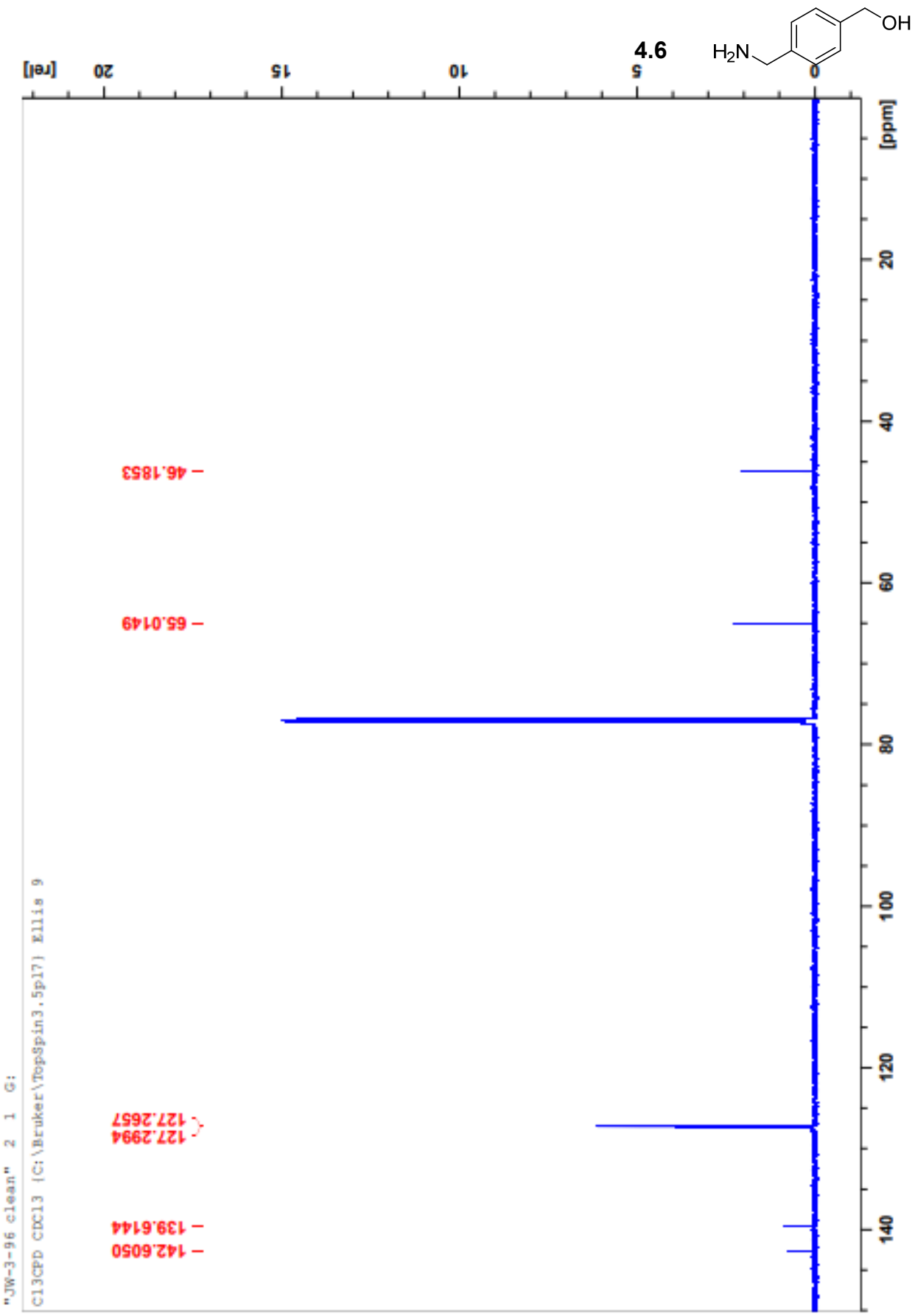
4.6
OH
H_2N
[rel]
20
15
10
5
0
[ppm]
20
40
60
80
100
120
140
46.1853
65.0149
127.2994
127.2657
139.6144
142.6050
"JW-3-96 clean" 2 1 G:
C13CPD CDCl3 (C:\Bruker\TopSpin3.5pl7) Ellis 9

4.16

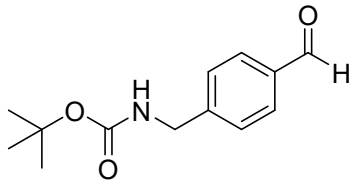
O
H
H
N
O
O

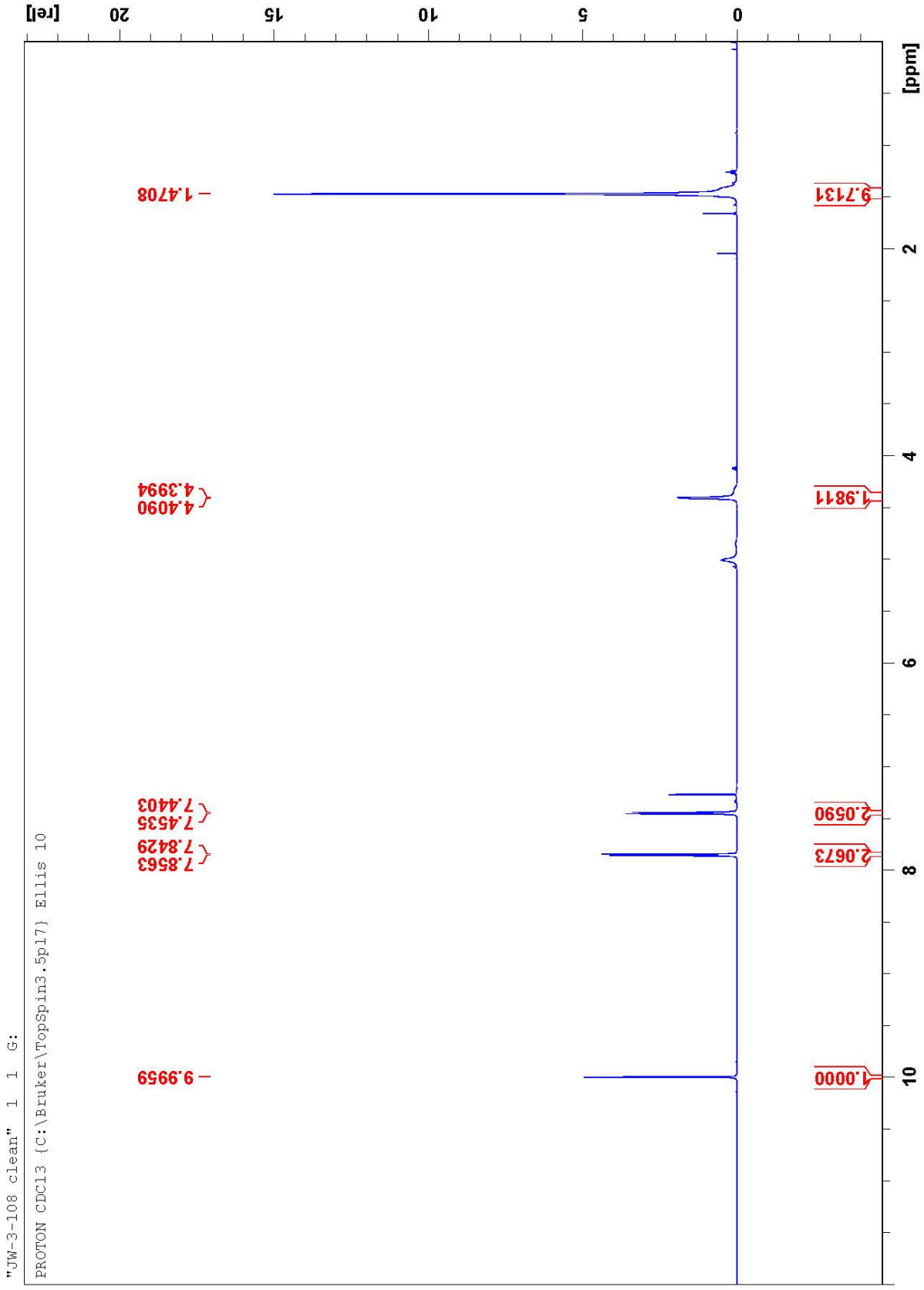
[rel]
20
15
10
5
0
[ppm]
2
4
6
8
10
9.7131
1.9811
2.0590
2.0673
1.0000
1.4708
4.4090
4.3994
7.4535
7.4403
7.8563
7.8429
9.9959
"JW-3-108 clean" 1 1 G:
PROTON CDCl3 {C:\Bruker\TopSpin3.5pl7} Ellis 10

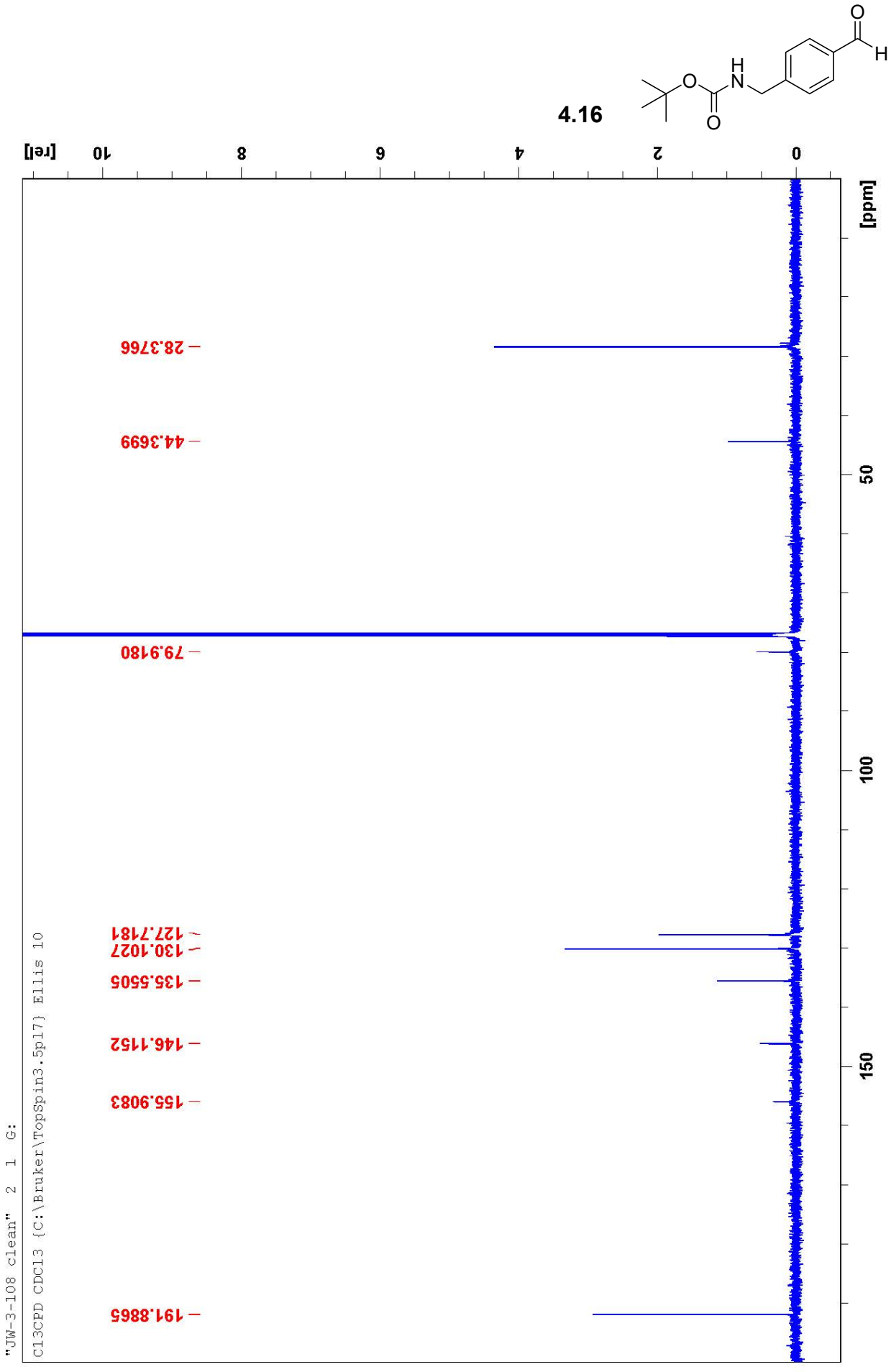
4.16
O
H
N
O
O
[rel]
0
2
4
6
8
10
[ppm]
50
100
150
28.3766
44.3699
79.9180
127.7181
130.1027
135.5505
146.1152
155.9083
191.8865
"JW-3-108 clean" 2 1 G:
C13CPD CDCl3 {C:\Bruker\TopSpin3.5pl7} Ellis 10

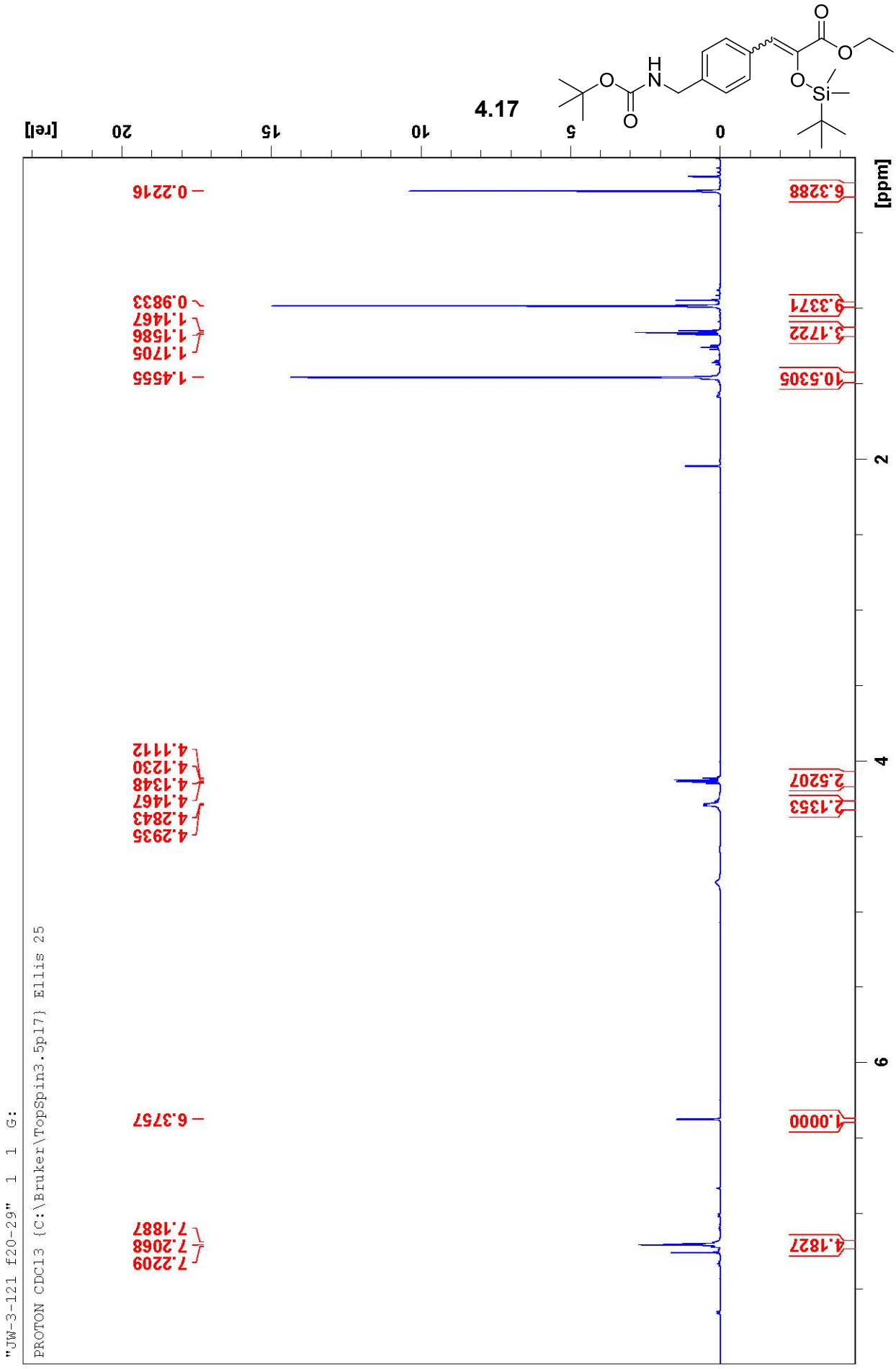
4.17
"JW-3-121 f20-29" 1 1 G:
PROTON CDCl3 {C:\Bruker\TopSpin3.5pl7} Ellis 25
[rel]
[ppm]
0.2216
0.9833
1.1467
1.1586
1.1705
1.4555
4.1112
4.1230
4.1348
4.1467
4.2843
4.2935
6.3757
7.2068
7.2209
7.1887
6.3288
9.3371
3.1722
10.5305
2.5207
2.1353
1.0000
4.1827

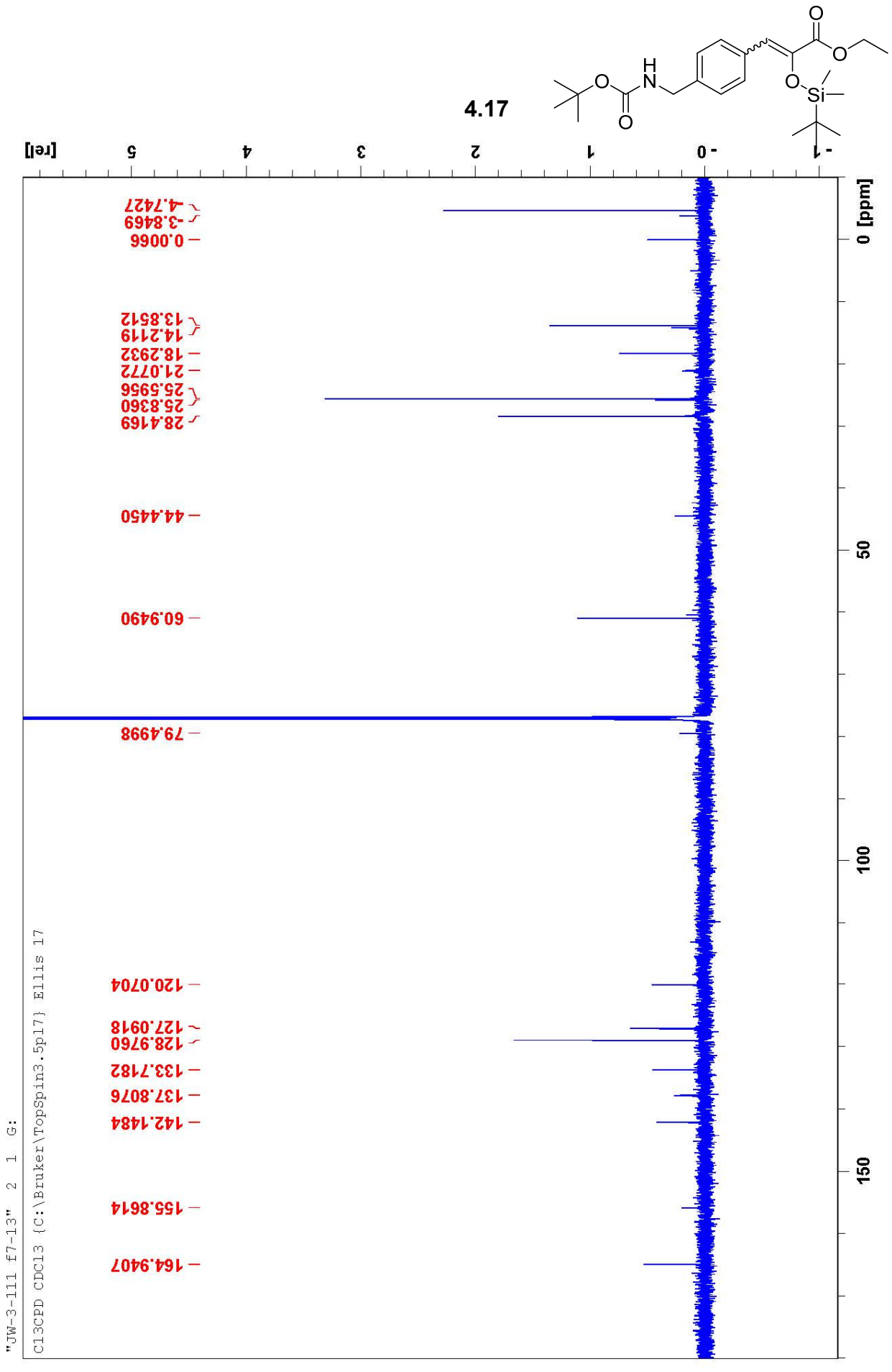
4.17
[rel]
5
4
3
2
1
0
-1
0 [ppm]
50
100
150
-4.7427
-3.8469
0.0066
13.8512
14.2119
18.2932
21.0772
25.5956
25.8360
28.4169
44.4450
60.9490
79.4998
120.0704
127.0918
128.9760
133.7182
137.8076
142.1484
155.8614
164.9407
"JW-3-111 f7-13" 2 1 G:
C13CPD CDCl3 {C:\Bruker\TopSpin3.5pl7} Ellis 17

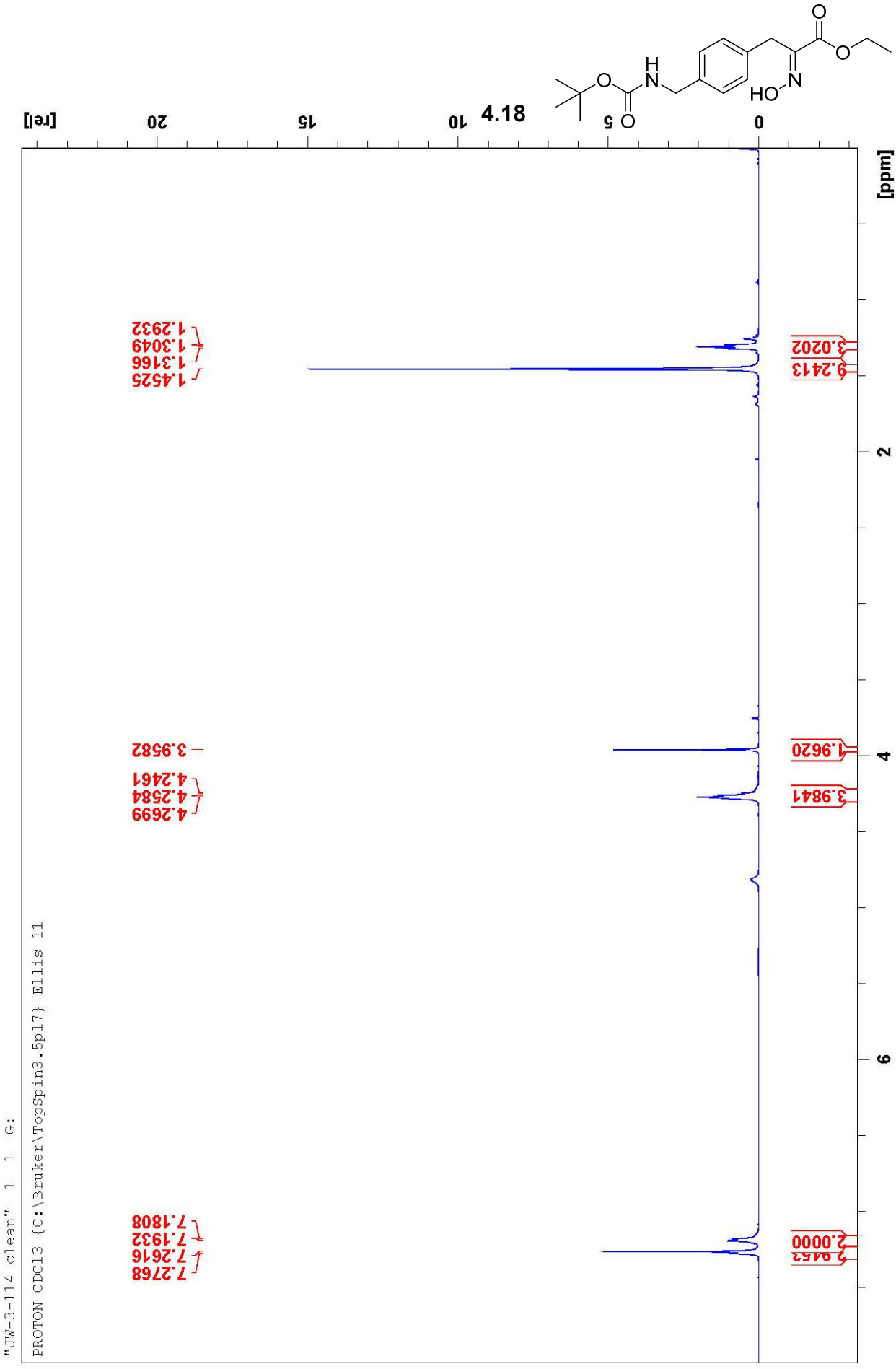
4.18
[rel]
20
15
10
5
0
[ppm]
6
4
2
1.2932
1.3049
1.3166
1.4525
3.0202
9.2413
3.9582
4.2461
4.2584
4.2699
1.9620
3.9841
7.1808
7.1932
7.2616
7.2768
2.0000
9.0452
"JW-3-114 clean" 1 1 G:
PROTON CDCl3 {C:\Bruker\TopSpin3.5pl7} Ellis 11

4.18

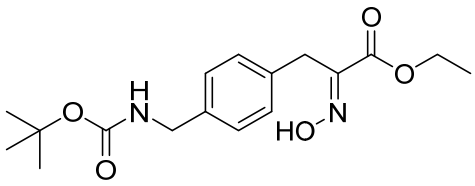
O
O
H
N
O
O
HO
N

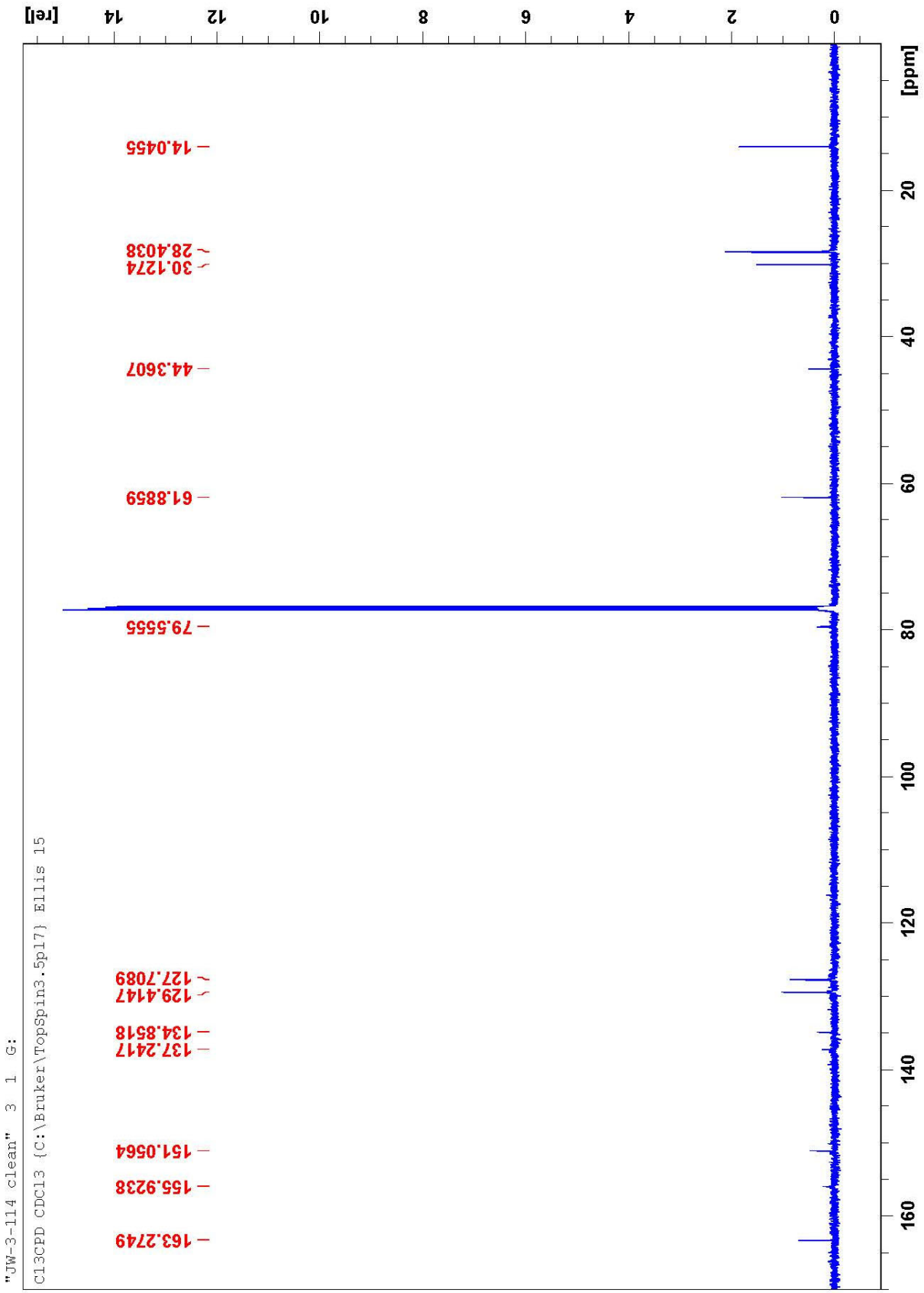
[rel]
14
12
10
8
6
4
2
0
[ppm]
20
40
60
80
100
120
140
160
14.0455
28.4038
30.1274
44.3607
61.8859
79.5555
127.7089
129.4147
134.8518
137.2417
151.0564
155.9238
163.2749
"JW-3-114 clean" 3 1 G:
C13CPD CDCl3 {C:\Bruker\TopSpin3.5pl7} Ellis 15

4.19

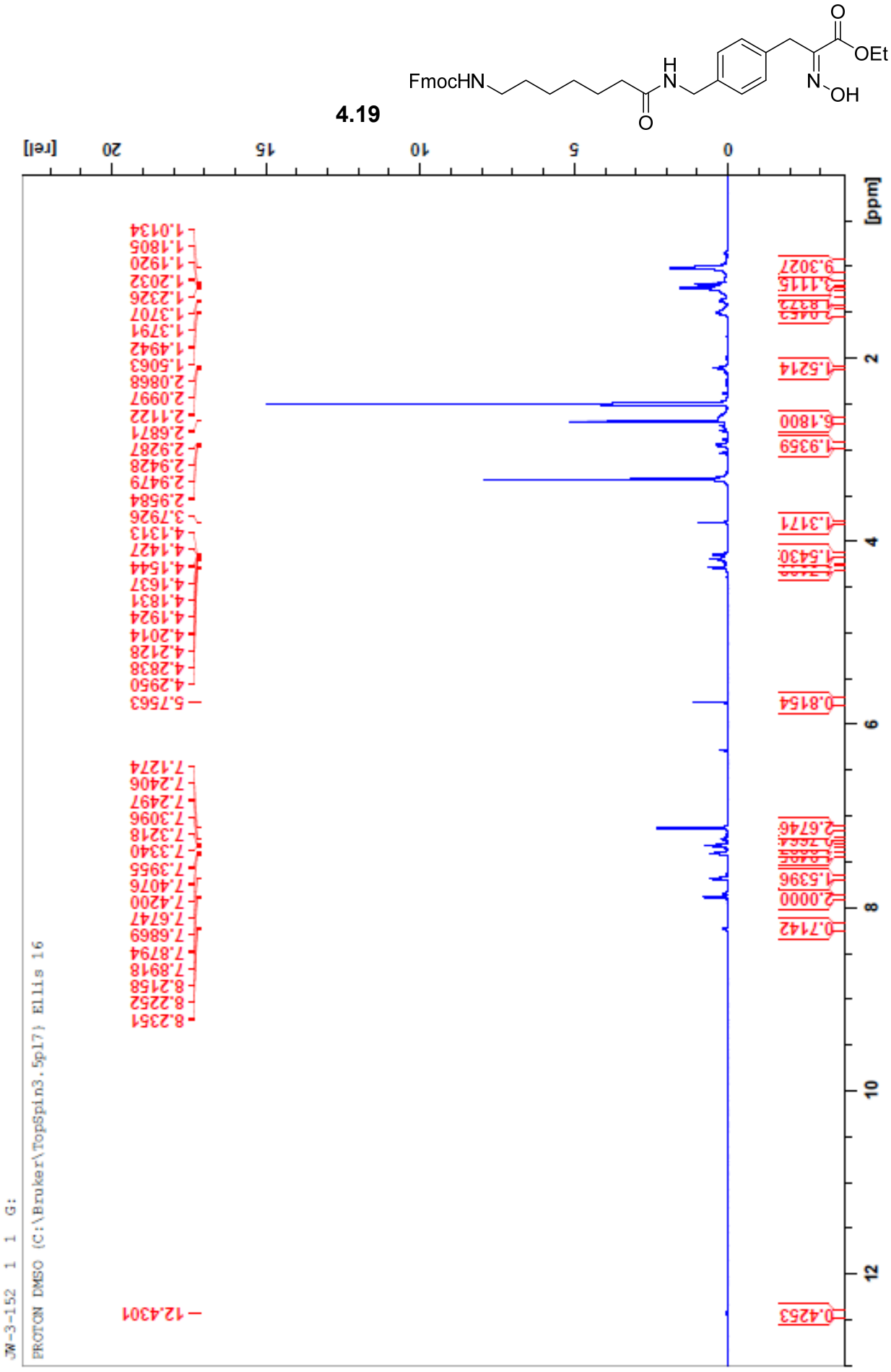
FmocHN
H
N
O
O
OEt
N
OH
[rel]
20
15
10
5
0
[ppm]
2
4
6
8
10
12
1.0134
1.1805
1.1920
1.2032
1.2326
1.3707
1.3791
1.4942
1.5063
2.0868
2.0997
2.1122
2.6871
2.9287
2.9428
2.9479
2.9584
3.7926
4.1313
4.1427
4.1544
4.1637
4.1831
4.1924
4.2014
4.2128
4.2838
4.2950
5.7563
7.1274
7.2406
7.2497
7.3096
7.3218
7.3340
7.3955
7.4076
7.4200
7.6747
7.6869
7.8794
7.8918
8.2158
8.2252
8.2354
12.4301
9.3027
3.4115
1.8227
1.0465
1.5214
6.1800
1.9359
1.3171
1.5430
0.8154
2.6746
1.5396
2.0000
0.7142
0.4253
JW-3-152 1 1 G:
PROTON DMSO (C:\Bruker\TopSpin3.5pl7) Ellis 16

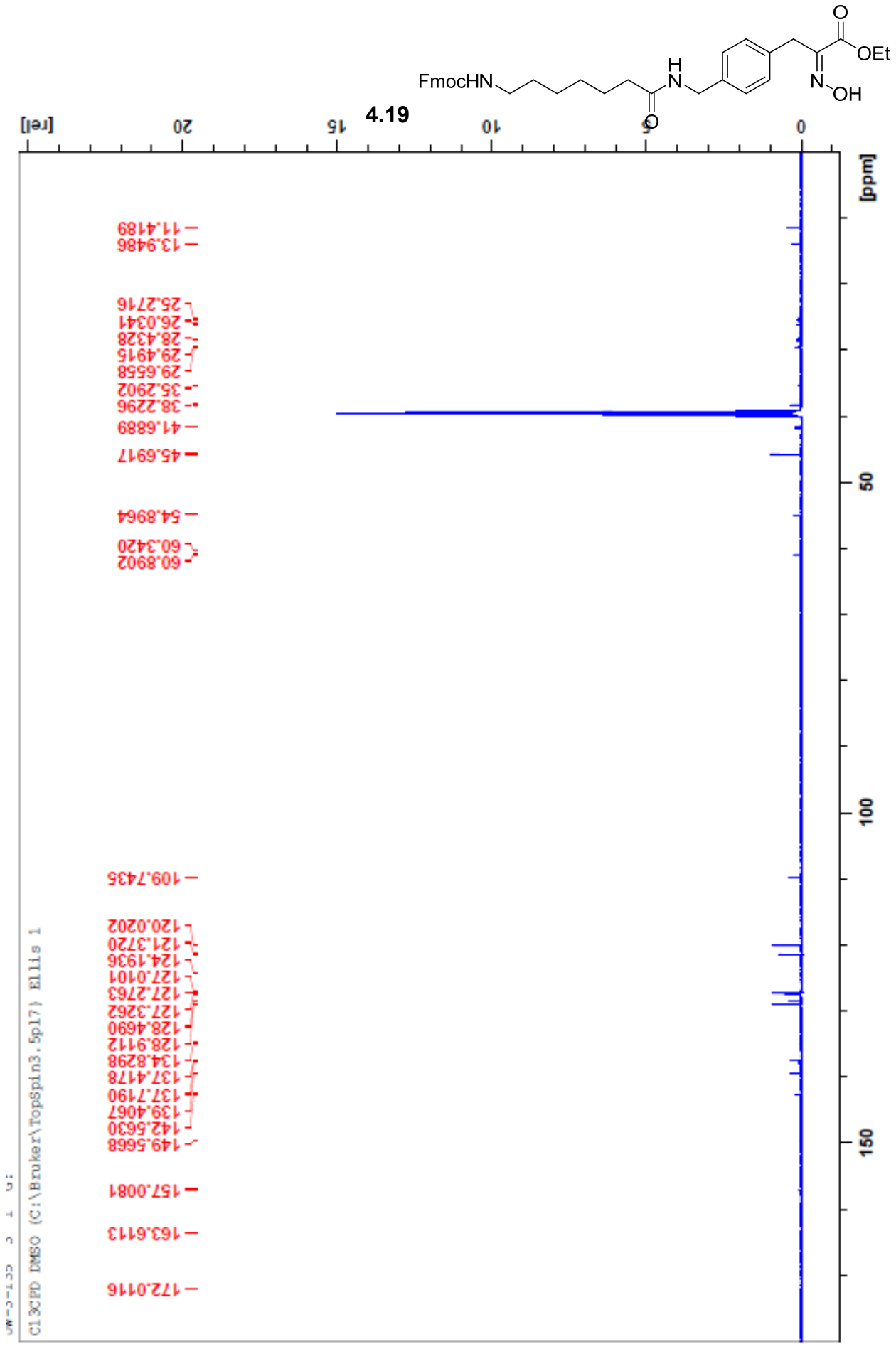
FmocHN
H
N
O
N
OH
OEt
4.19
[rel]
20
15
10
5
0
[ppm]
50
100
150
11.4189
13.9486
25.2716
26.0341
28.4328
29.4915
29.6558
35.2902
38.2296
41.6889
45.6917
54.8964
60.3420
60.8902
109.7435
120.0202
121.3720
124.1936
127.0101
127.2763
127.3262
128.4690
128.9112
134.8298
137.4178
137.7190
139.4067
142.5630
149.5668
157.0081
163.6113
172.0116
C13CPD DMSO (C:\Bruker\TopSpin3.5pl7) Ellis 1

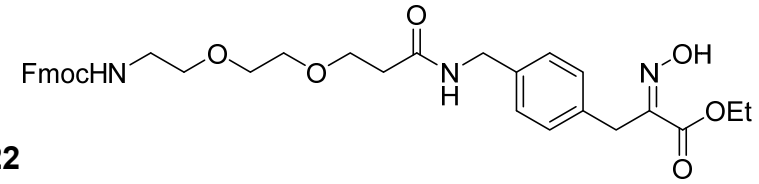
FmocHN
O
O
O
N
H
N
OH
OEt
O

4.22

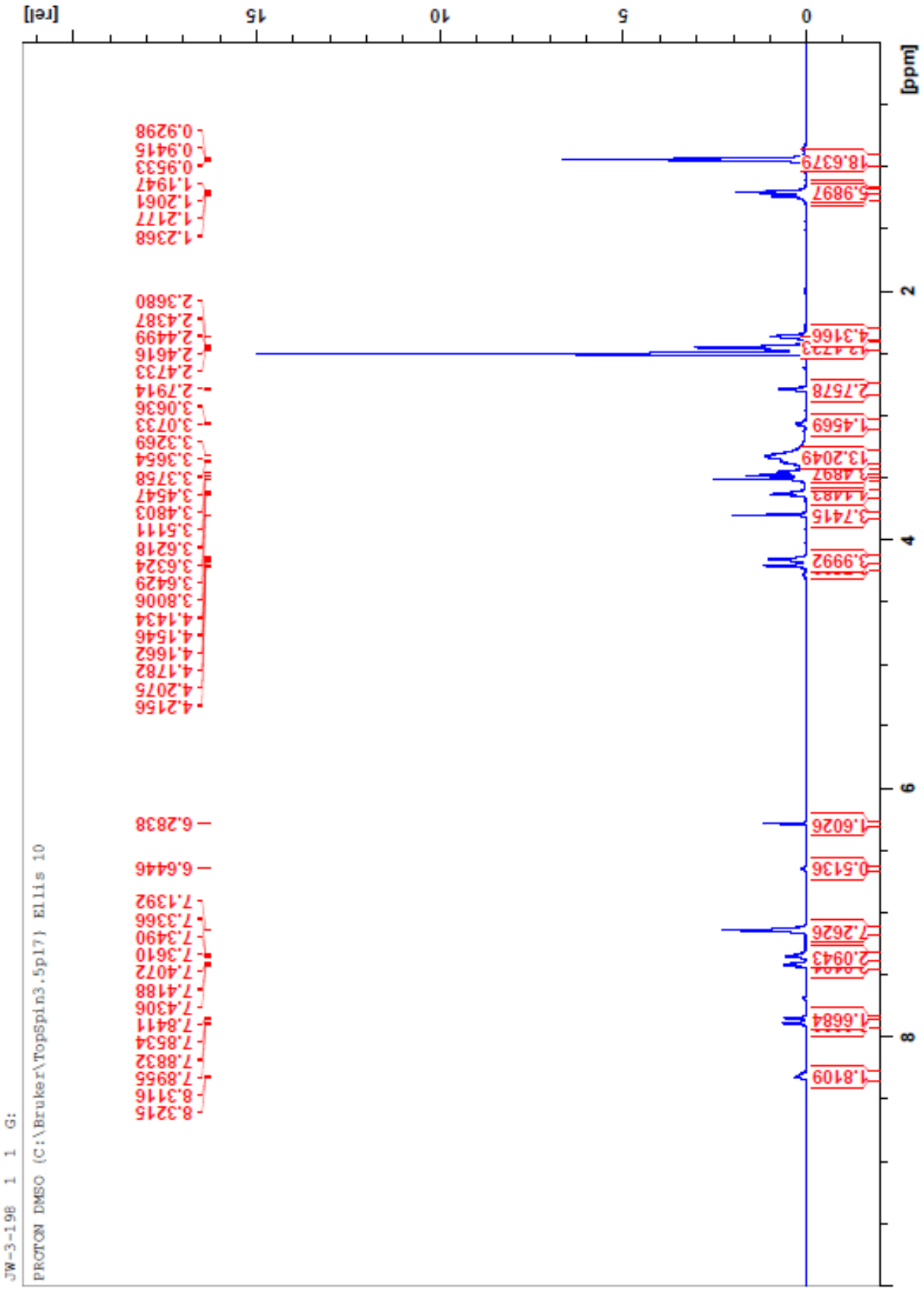
[rel]
15
10
5
0
[ppm]
2
4
6
8
18.6379
5.9897
4.3166
2.7578
1.4569
3.7415
3.9992
1.6026
0.5136
7.2626
2.0943
1.6684
1.8109
0.9298
0.9415
0.9533
1.1947
1.2061
1.2177
1.2368
2.3680
2.4387
2.4499
2.4616
2.4733
2.7914
3.0636
3.0733
3.3269
3.3654
3.3758
3.4547
3.4803
3.5111
3.6218
3.6324
3.6429
3.8006
4.1434
4.1546
4.1662
4.1782
4.2075
4.2156
6.2838
6.6446
7.1392
7.3366
7.3490
7.3610
7.4072
7.4188
7.4306
7.8411
7.8534
7.8832
7.8955
8.3116
8.3215
JW-3-198 1 1 G:
PROTON DMSO (C:\Bruker\TopSpin3.5pl7) Ellis 10

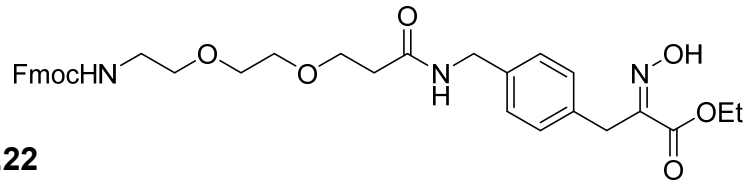
FmocHN
O
O
O
N
H
N
OH
OEt
O

4.22

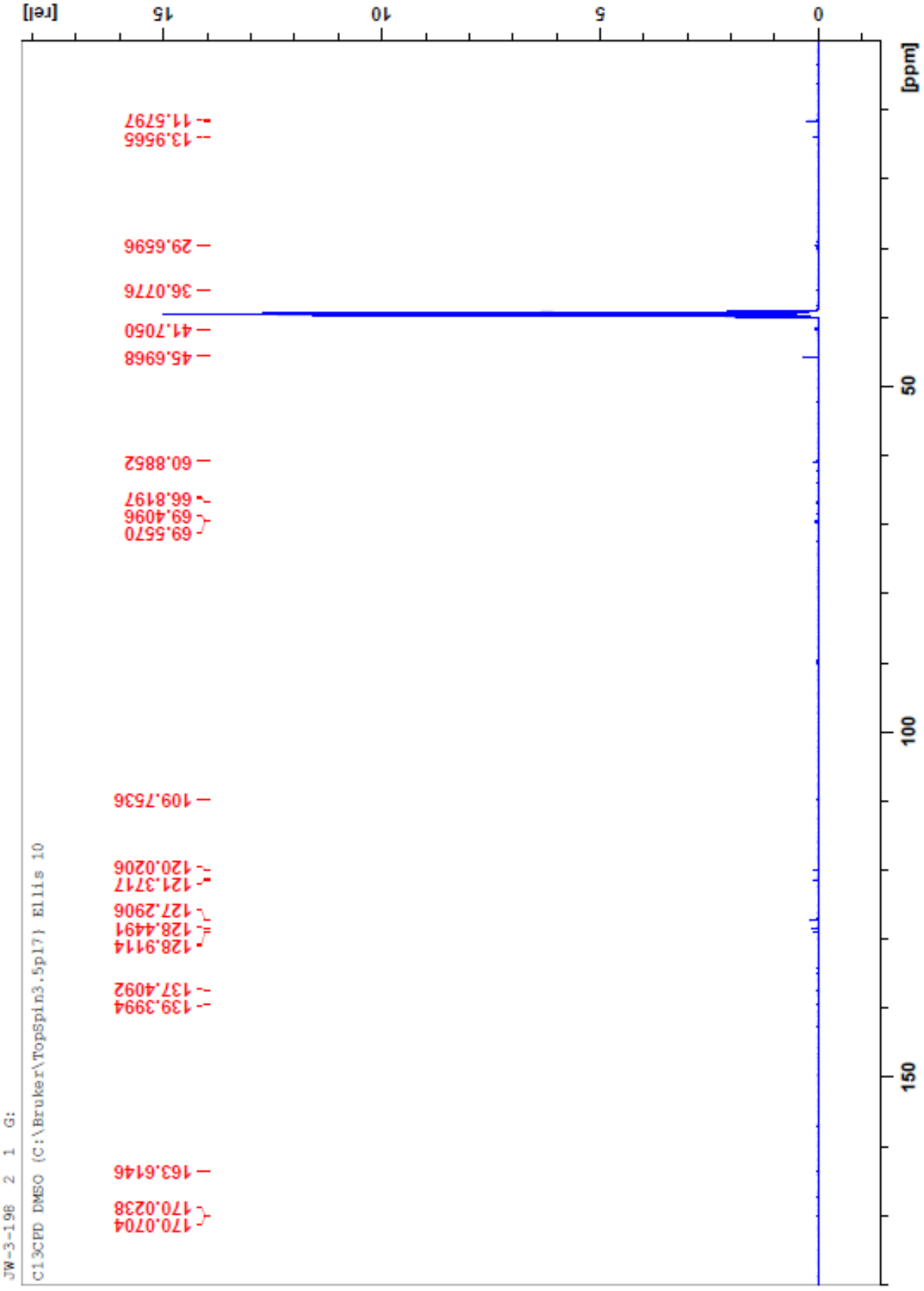
[rel]
15
10
5
0
[ppm]
50
100
150
11.5797
13.9565
29.6596
36.0776
41.7050
45.6968
60.8852
66.8197
69.4096
69.5570
109.7536
120.0206
121.3717
127.2906
128.4491
128.9114
137.4092
139.3994
163.6146
170.0238
170.0704
JW-3-198 2 1 G:
C13CPD DMSO (C:\Bruker\TopSpin3.5pl7) Ellis 10

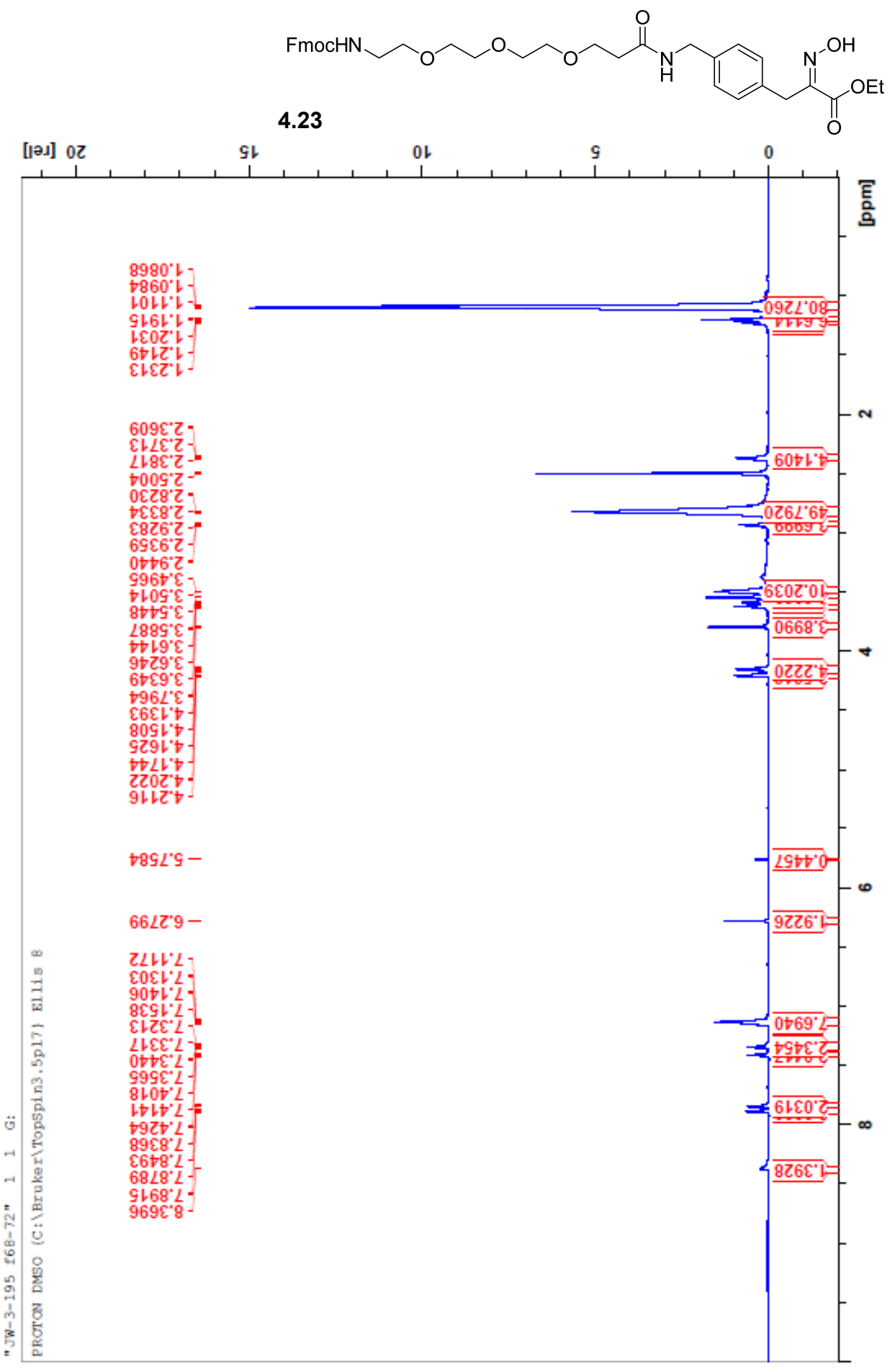
FmocHN
O
O
O
O
N
H
N
OH
OEt
O
4.23
[rel]
20
15
10
5
0
[ppm]
2
4
6
8
1.0868
1.0984
1.1101
1.1915
1.2031
1.2149
1.2313
2.3609
2.3713
2.3817
2.5004
2.8230
2.8334
2.9283
2.9359
2.9440
3.4965
3.5014
3.5448
3.5887
3.6144
3.6246
3.6349
3.7964
4.1393
4.1508
4.1625
4.1744
4.2022
4.2116
5.7584
6.2799
7.1172
7.1303
7.1406
7.1538
7.3213
7.3317
7.3440
7.3565
7.4018
7.4141
7.4264
7.8368
7.8493
7.8789
7.8915
8.3696
80.7260
4.1409
49.7920
10.2039
3.8990
4.2220
0.4457
1.9226
7.6940
2.3454
2.0319
1.3928
"JW-3-195 f68-72" 1 1 G:
PROTON DMSO (C:\Bruker\TopSpin3.5pl7) Ellis 8

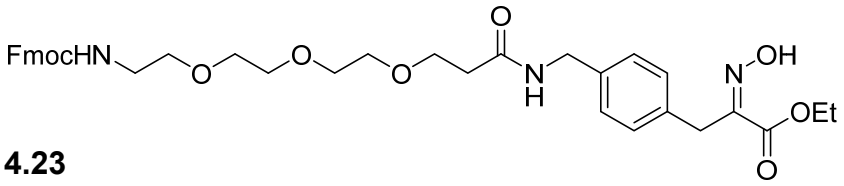
FmocHN
O
O
O
O
N
H
N
OH
OEt
O

4.23

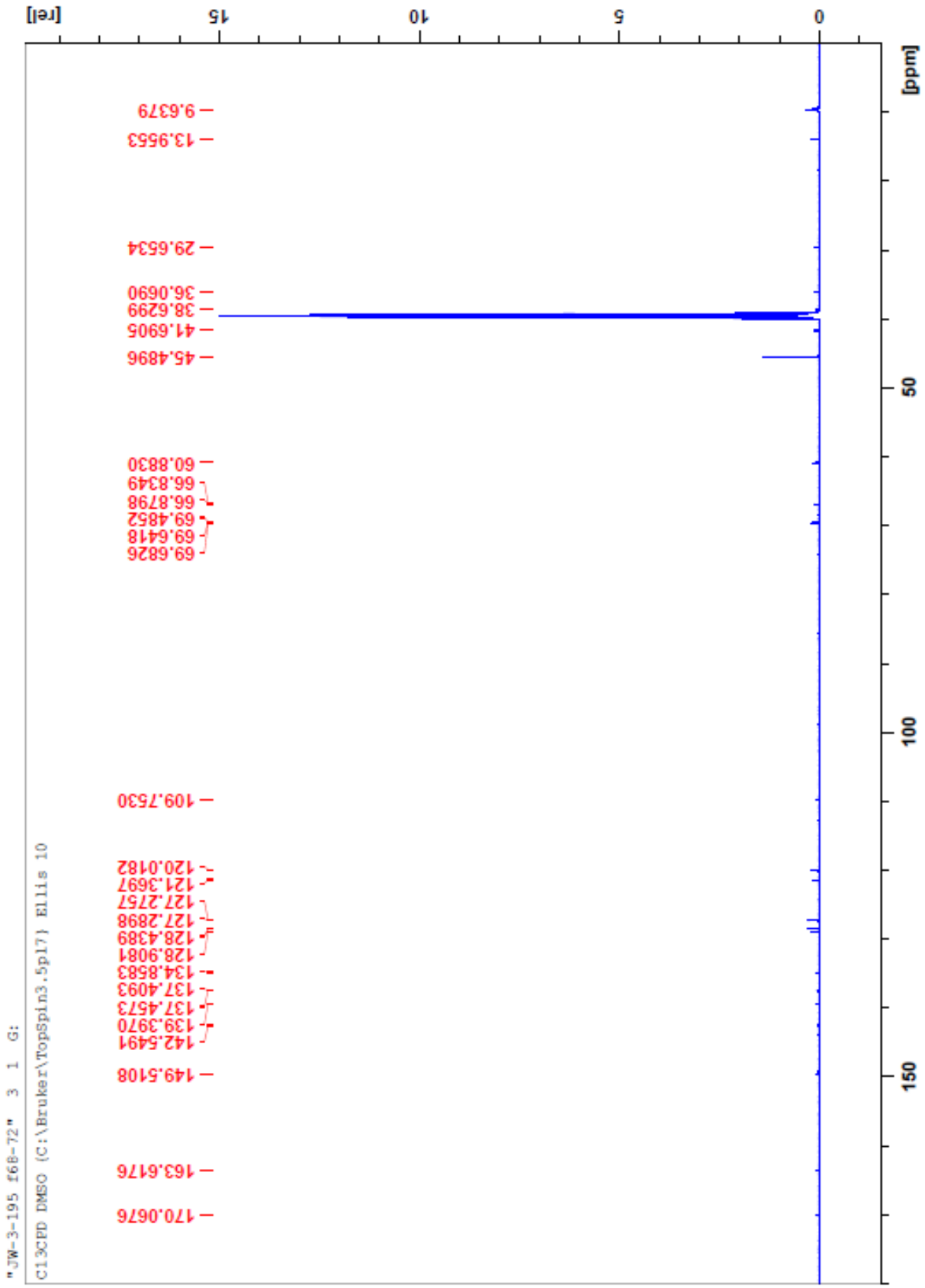
[rel]
15
10
5
0
[ppm]
50
100
150
9.6379
13.9553
29.6534
36.0690
38.6299
41.6905
45.4896
60.8830
66.8349
66.8798
69.4852
69.6418
69.6826
109.7530
120.0182
121.3697
127.2757
127.2898
128.4389
128.9081
134.8583
137.4093
137.4573
139.3970
142.5491
149.5108
163.6176
170.0676
"JW-3-195 f68-72" 3 1 G:
C13CPD DMSO (C:\Bruker\TopSpin3.5pl7) Ellis 10

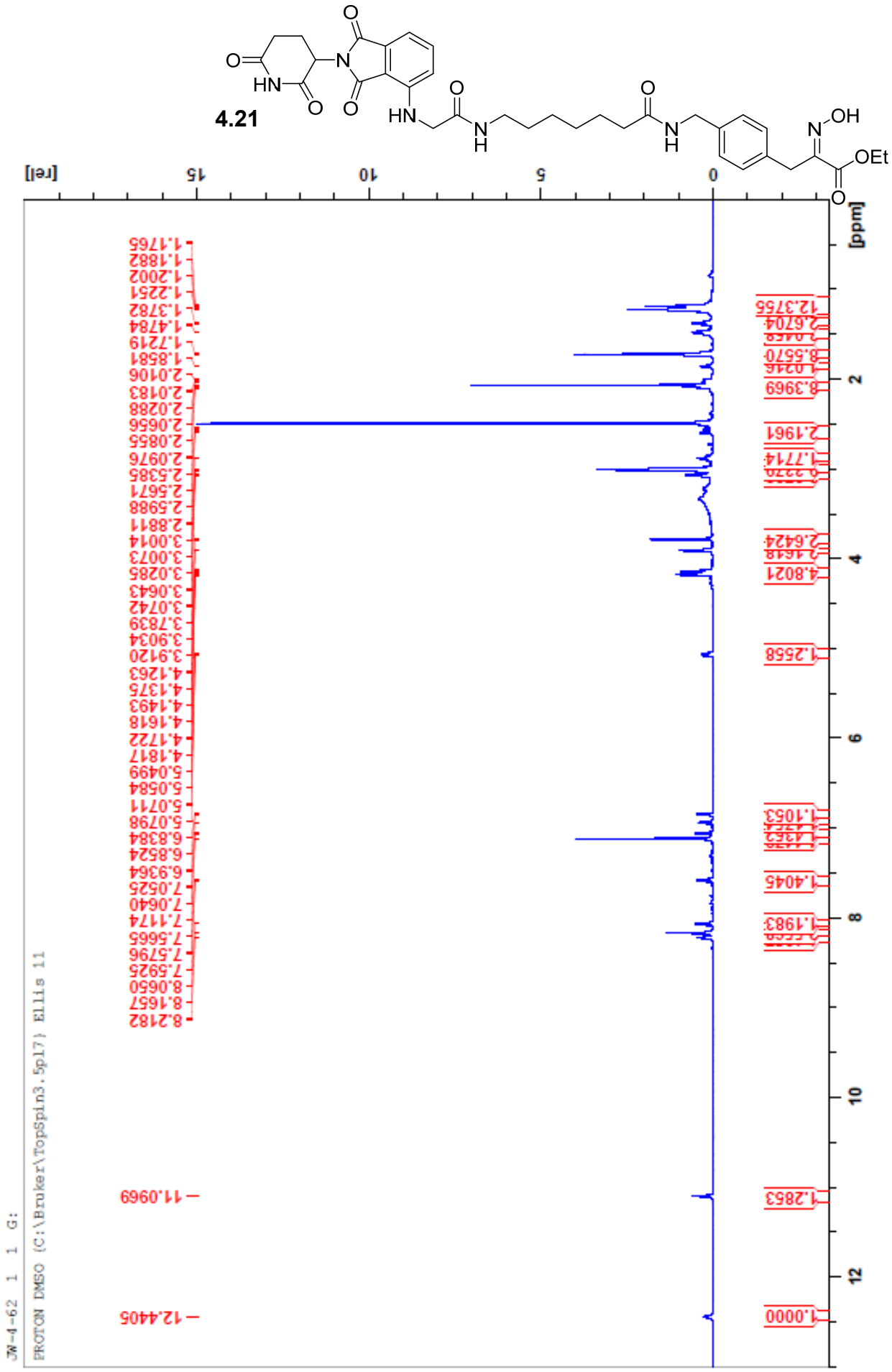
4.21
[rel]
15
10
5
0
[ppm]
2
4
6
8
10
12
JW-4-62 1 1 G:
PROTON DMSO (C:\Bruker\TopSpin3.5pl7) Ellis 11
1.1765
1.1882
1.2002
1.2251
1.3782
1.4784
1.7219
1.8581
2.0106
2.0183
2.0288
2.0656
2.0855
2.0976
2.5385
2.5671
2.5988
2.8811
3.0014
3.0073
3.0285
3.0643
3.0742
3.7839
3.9034
3.9120
4.1263
4.1375
4.1493
4.1618
4.1722
4.1817
5.0499
5.0584
5.0711
5.0798
6.8384
6.8524
6.9364
7.0525
7.0640
7.1174
7.5665
7.5796
7.5925
8.0650
8.1657
8.2182
11.0969
12.4405
12.3755
2.6704
8.5570
8.3969
2.1961
1.7714
2.6424
4.8021
1.2558
1.1053
1.4045
1.1983
1.2853
1.0000

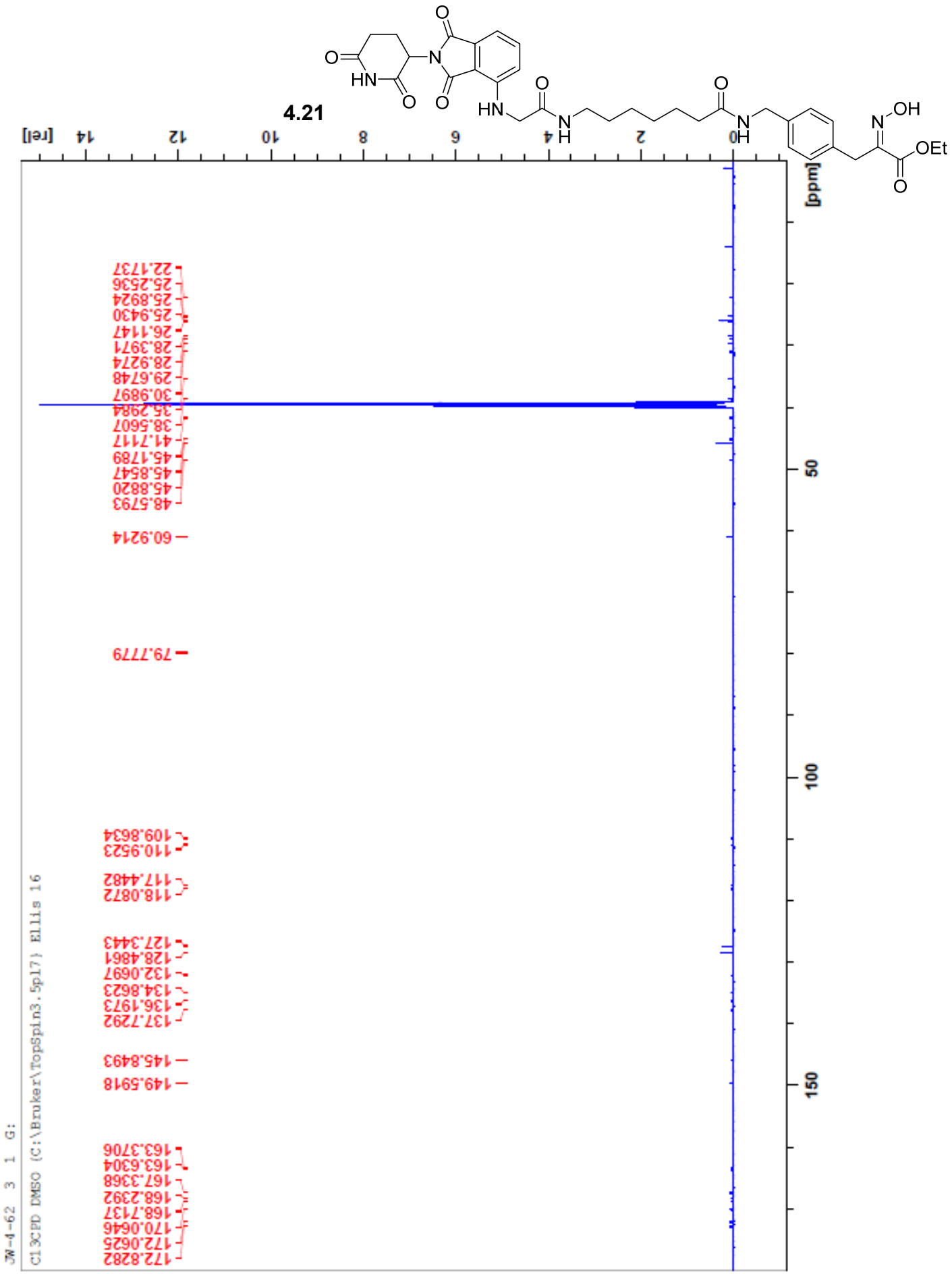
4.21
[rel]
[ppm]
JW-4-62 3 1 G:
C13CPD DMSO (C:\Bruker\TopSpin3.5pl7) Ellis 16

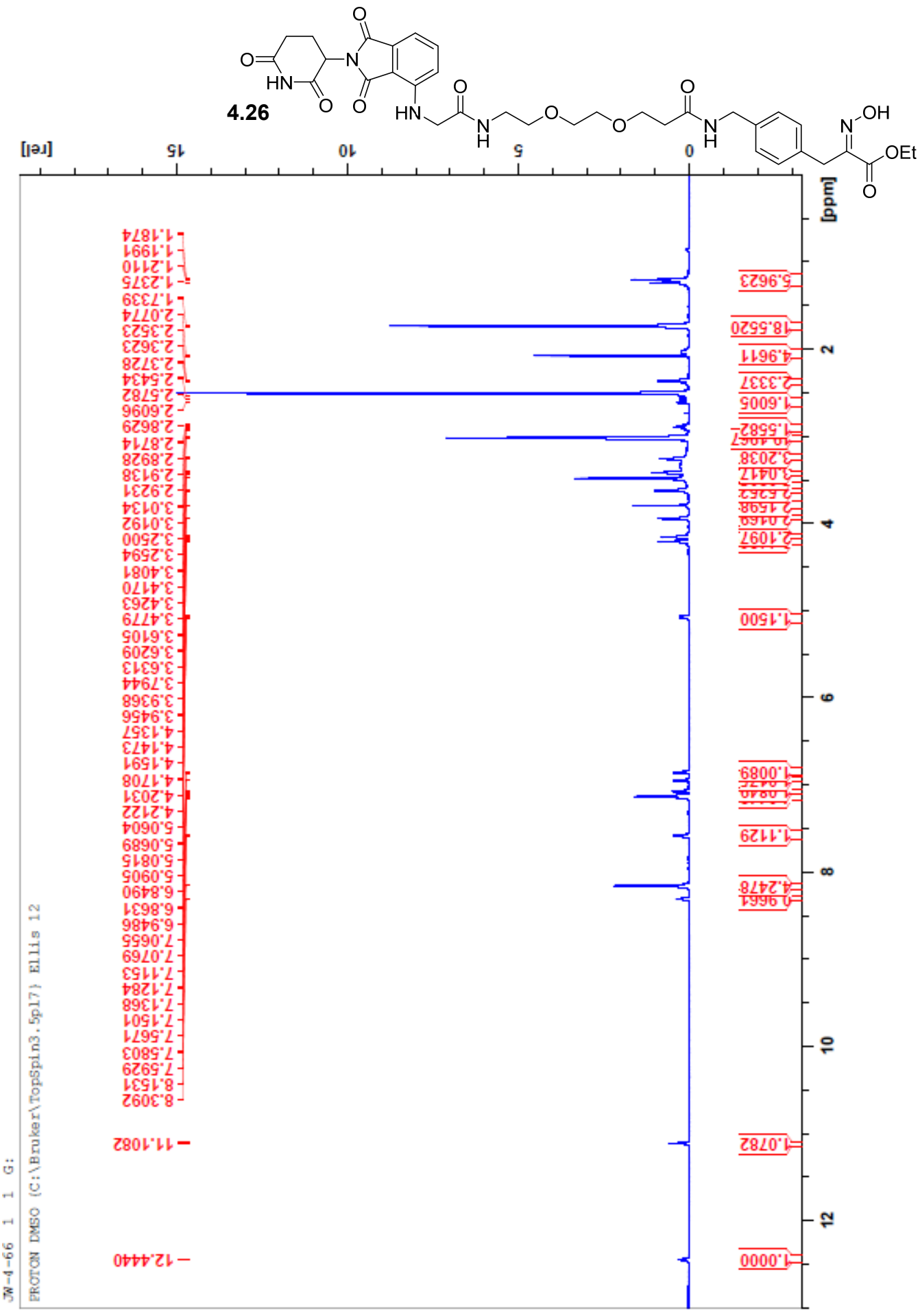
4.26
[rel]
15
10
5
0
[ppm]
2
4
6
8
10
12
JW-4-66 1 1 G:
PROTON DMSO (C:\Bruker\TopSpin3.5pl7) Ellis 12

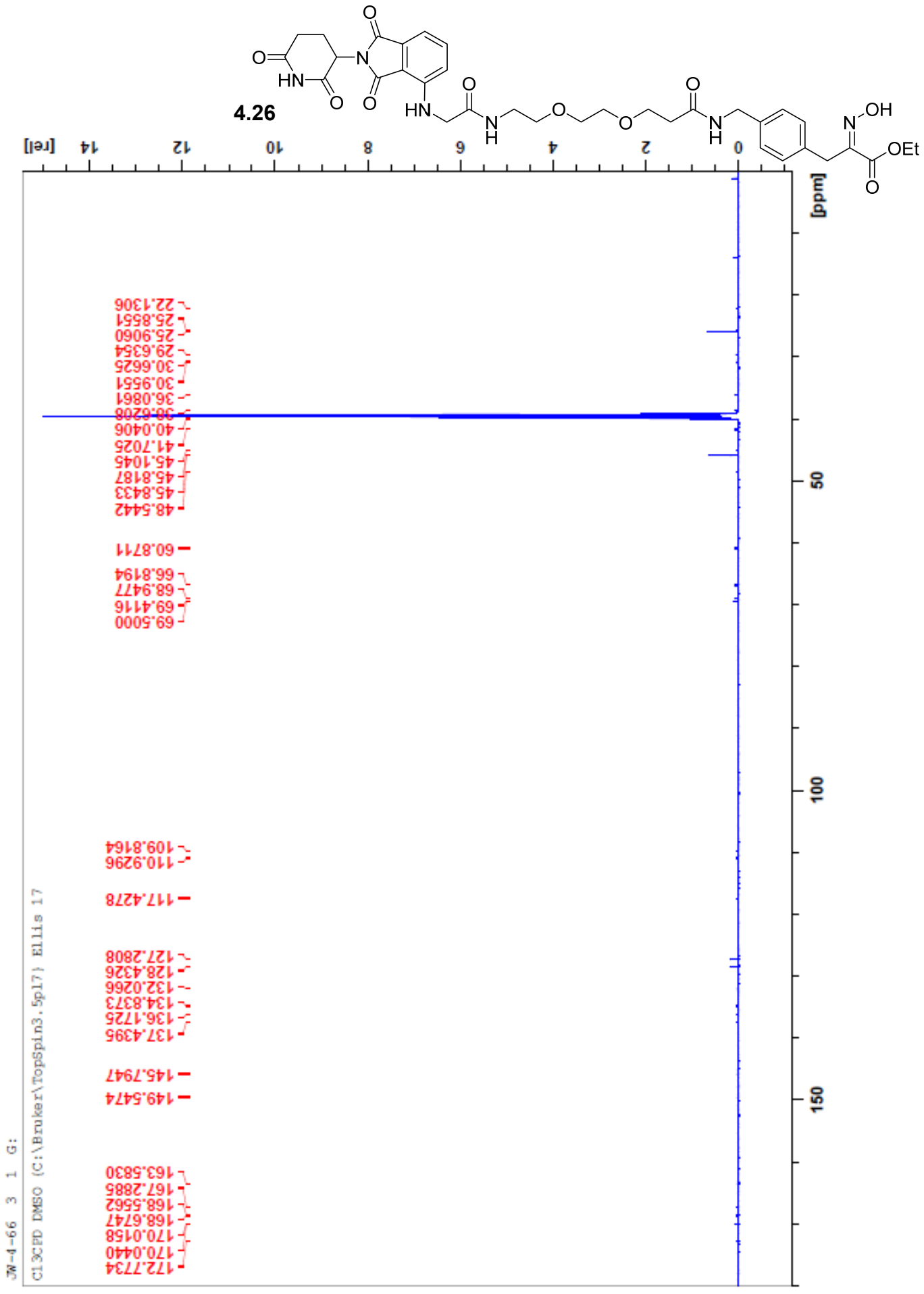
4.26
[rel]
[ppm]
JW-4-66 3 1 G:
C13CPD DMSO (C:\Bruker\TopSpin3.5pl7) Ellis 17

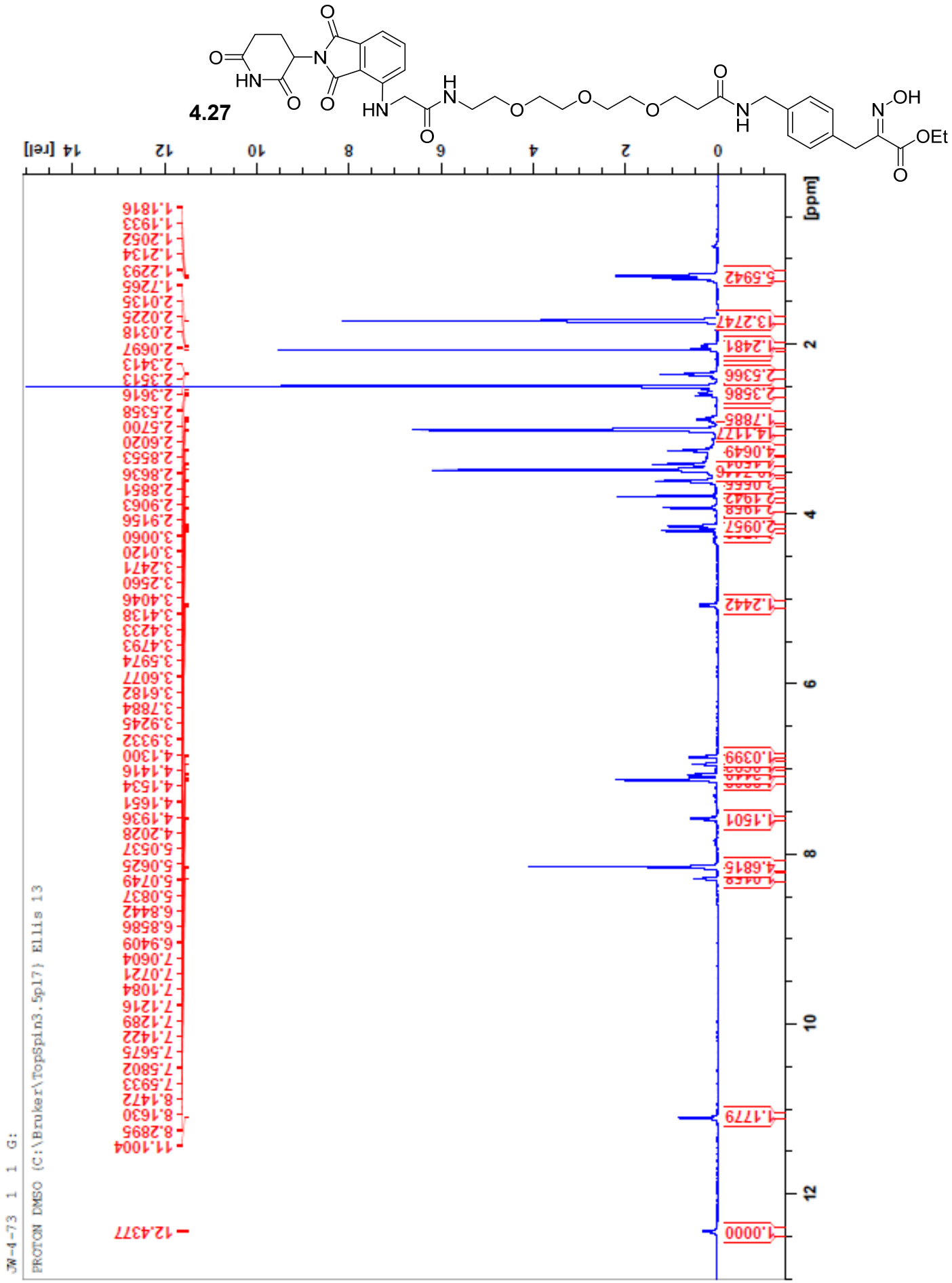
4.27
JW-4-73 1 1 G:
PROTON DMSO (C:\Bruker\TopSpin3.5pl7) Ellis 13
[rel]
[ppm]

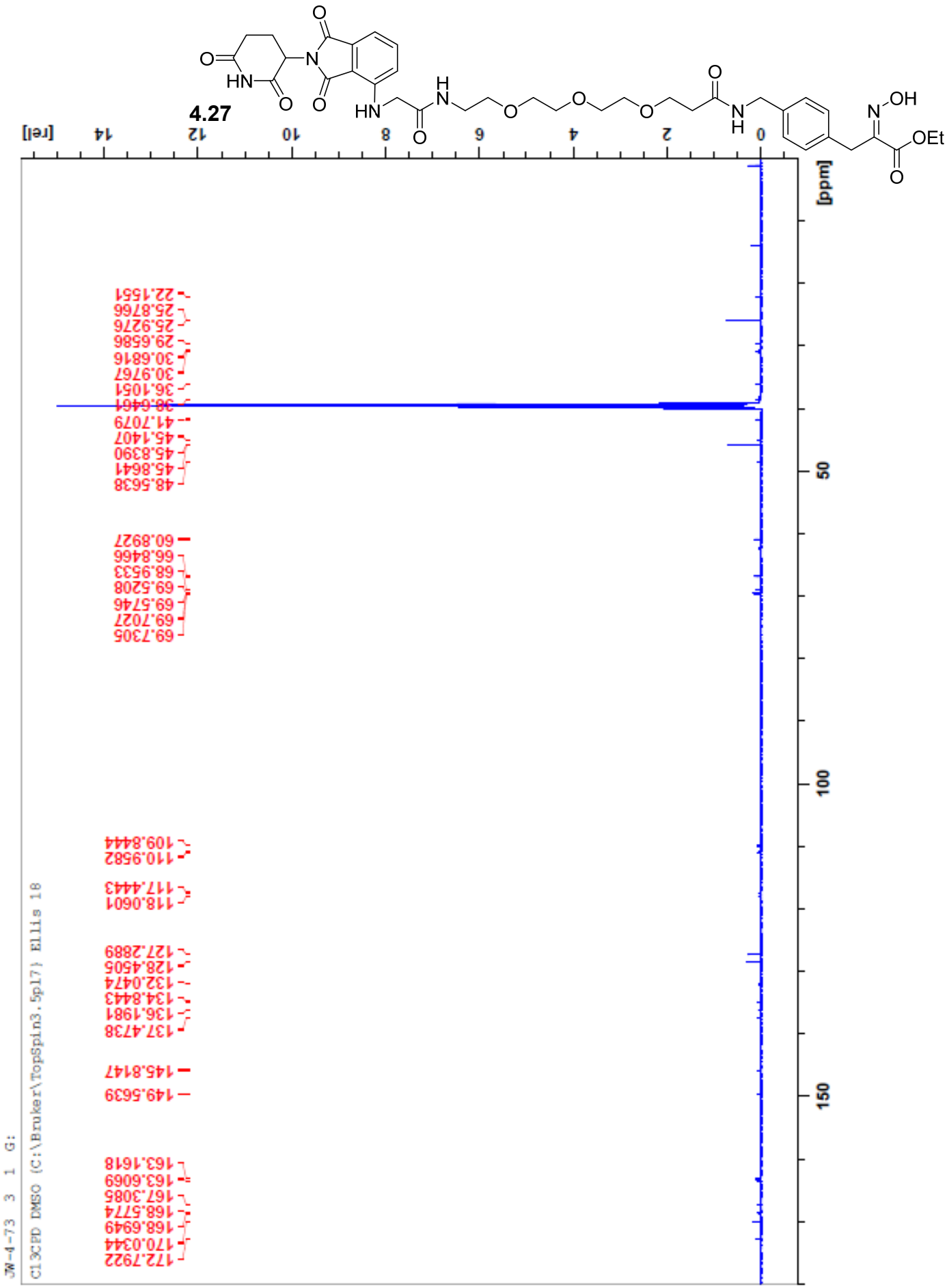
4.27
[rel]
[ppm]
JW-4-73 3 1 G:
C13CPD DMSO (C:\Bruker\TopSpin3.5pl7) Ellis 18

Vita

Jacqueline Louise West (née Gross) was born on January 1, 1993 in Valhalla, New York and is a citizen of the United States of America. She graduated from the University of North Carolina Wilmington in 2015 with a Bachelor of Science in Biology, and in 2018 with a Master of Science in Chemistry.